SYNTHESIS OF TETRAPHENYLETHYLENE AND NAPHTHALENE DIIMIDE DERIVATIVES FOR SELF-ASSEMBLIES AND SENSING APPLICATIONS

A THESIS SUBMITTED IN PARTIAL FULFILLMENT FOR THE DEGREE OF

DOCTOR OF PHILOSOPHY

IN THE SCHOOL OF CHEMICAL SCIENCES
GOA UNIVERSITY

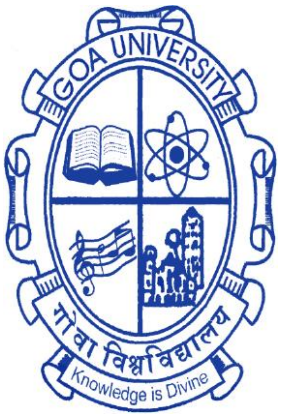

By

Mr. DINESH NAGNATH NADIMETLA

SCHOOL OF CHEMICAL SCIENCES
GOA UNIVERSITY
TALEIGAO PLATEAU, GOA

March 2023

SYNTHESIS OF TETRA PHENYLETHYLENE AND NAPHTHALENE DIIMIDE DERIVATIVES FOR SELF-ASSEMBLIES AND SENSING APPLICATIONS

A THESIS SUBMITTED IN PARTIAL FULFILLMENT FOR THE DEGREE OF

DOCTOR OF PHILOSOPHY

IN THE SCHOOL OF CHEMICAL SCIENCES
GOA UNIVERSITY

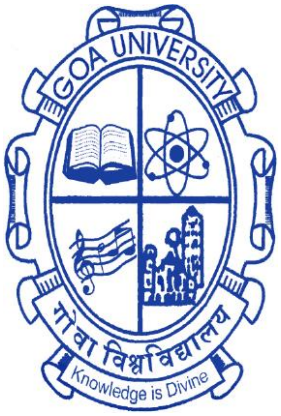

By

Mr. DINESH NAGNATH NADIMETLA

SCHOOL OF CHEMICAL SCIENCES
GOA UNIVERSITY
TALEIGAO PLATEAU, GOA

March 2023

DECLARATION

I, Mr. Dinesh Nagnath Nadimetla hereby declare that this thesis represents work which has been carried out by me and that it has not been submitted, either in part or full, to any other University or Institution for the award of any research degree.

Place: Taleigao Plateau
Date:

Mr. Dinesh Nagnath Nadimetla
Research Scholar,
School of Chemical Sciences,
Goa University, Goa

CERTIFICATE

I hereby certify that the above declaration of the candidate, Mr. Dinesh Nagnath Nadimetla is true and the work was carried out under my supervision.

Prof. S.V. Bhosale
Research Guide
School of Chemical Sciences
Goa University, Goa

ACKNOWLEDGEMENT

On the successful completion of my thesis, I feel happy and contended in writing this note of thanks to all the ones who have accompanied me through this worthy journey.

This long journey has remained a period of intense learning for me on a scientific as well as personal front. First and foremost, I would like to express my sincere gratitude and special appreciation to my Ph.D. supervisor **Prof. Sheshanath V. Bhosale** for his constant support and encouragement with a patient in my research work. I acknowledge his help and guidance to improve myself as an individual. He is a tremendous mentor and has guided my way through his intelligent ideas, expertise, and immense knowledge in the field. I am thankful for his advice during my whole tenure.

I extend my sincere thanks to my subject experts **Dr. Sandesh Bugde** and **Dr. Subhadeep Banerjee** for their timely assistance, and questioning during the DRC and for their valuable suggestions that helped me a lot of progress in my research work.

I express my kind gratitude to **Prof. H. Menon** (Vice-Chancellor, Goa University) and **Prof. V.S. Nadkarni** (Registrar, Goa University), **Prof. Varun Sahni** (Former Vice-Chancellor, Goa University) and **Prof. Y.V. Reddy** (Former Registrar, Goa University), for providing necessary support and permissions to conduct my research work. I am thankful to **Prof. V. M. S. Verenkar** (Dean, SCS, Goa University), **Dr. B. A. Shinkre** (Vice-Dean Research, SCS, Goa University), **Prof. S. N. Dhuri** (Vice-Dean Academics, SCS, Goa University) for providing all the necessary facilities for my research work. In addition, I am thankful to **Prof. B. R. Srinivasan** and **Prof. S. G. Tilve** for their constant motivation during my research work. And also, all the faculty members of the School of Chemical Sciences, **Prof. R. N. Shirsat, Dr. V. K. Mandrekar, Dr. R. E. Patre, Dr. D. G. Porob, Ms. S. V. Girkar, Dr. P. P. Morajkar, Dr. R. K. Kunkalekar**, **Dr. H. K. Kadam, Dr. P. S. Volvoikar, Dr. V. R. Chari, Dr. V. V. Gobre** and **Dr. Kedar Narvekar, Dr. Savita Kudolkar, Dr. Prachi Torney, Dr. Shrikant Naik, Dr, Diptesh Naik, Dr. Anjani Narvekar** for their timely help and constant support.

I would like to acknowledge my collaborators **Dr. Sidhanath V. Bhosale,** CSIR-IICT, Hyderabad, Telangana, India for their constant support and encouragement for research work. **Prof. Subi J. George,** JNCASR, Bengaluru, India for chiral assemblies study and **Dr. Subhajit Bandyopadhyay,** IISER Kolkata, India, for collaboration work, **Dr. Avinash Puyad** for DFT calculations. **Dr. P. K. Singh**, BARC-Mumbai, and **Dr. A. B. Rode**, RCB-

Faridabad, for sensing collaboration work. I also acknowledge our co-authors **Dr**. **Mousumi Samanta, Dr. Anushri Rananaware, Dr. Sk. Atiur Rahaman, Dr. Monochura Saha, Dr. Mohammad Al Kobaisi, Dr. Sunil Gaikwad, Dr. Sopan, Dr. Jotiram, Dr. Shailesh, Mr. Madan, Mr. Dnyneshwar, Mr. Saikat, and Ms. Pooja, for** their cooperation in analysis. I wish to thank **Mr. Madhusudan Lanjewar** for his guidance and help provided in SEM analysis. I express my thanks to **Mr. Kumar, Dr.Dattaprasad, and Ms. Jyoti** (BITS-Goa) for providing powder XRD and SEM data.

I am very thankful to The Council of Scientific and Industrial Research-University Grants Commission (**CSIR-UGC**), New Delhi for fellowship. This financial support has enabled me to complete my Ph.D. studies successfully.

I express my earnest gratitude to **Dr. Sandesh B. Dessai** (Librarian, Goa University), **Dr. V. Gopakumar** (Former Librarian, Goa University) and other library staff members, Goa University, for providing me with the required learning resources related to my research work. I sincerely appreciate the assistance of **Mr. Pravin Mishal**, **Mr. Vibhav Marshelkar** and **Mr. Nandkishor Bandekar** in regard to library matters.

I am thankful to all the non-teaching staff, **Mr. Yoganand Kholkar, Mr. Gaurav Kinlekar, Mr. Mehul Shirodkar, Mr. Prajyot Chari, Mr. Kiran Dabolkar, Mr. Kishor Govekar, Mr. Rayappa Harijan, Mr. Deepak Chari, Mr. Nikhil Pednekar, Mr. Kirtesh Sawant, Mr. Rudraunsh Mahale, Mrs. Shital Palkar, Mr. Jaidev, Mr. Harish** and **Mr. Raju** for their assistance. I extend my kind gratitude to the administrative staff of Goa University, especially to **Mr. Kalpesh Dhuri**, **Mrs. Sneha Haldankar**, **Mr. Agostinho Rodrigues**, **Mr. Sunil** and **Mr. Vijesh** for their appropriate help and cooperation.

I would like to acknowledge my friendly seniors and colleague's **Dr. Chandan Naik, Dr. Rahul Kerkar, Dr. Pratik Asogekar, Dr. Prayoti Gauns Dessai, Dr. Vishal Pawar, Dr. Apurva Narvekar, Dr. Megha Deshpande, Dr. Sudesh Morajkar, Dr. Pooja Bhargao, Dr. Kedar Narvekar, Dr. Sarvesh Harmalkar, Dr. Abhijeet Shetgaonkar, Dr. Shashank Mhaldar and Dr. Ketan Mandrekar. Ms. Neha Parsekar, Ms. Lima Rodrigues, Mr. Akshay Salkar, Dr. Amarja Naik, Ms. Luann D'souza, Ms. Seneca Costa, Ms. Mangala Sawal,** for their kind help during my university days and my juniors **Pritesh, Gayatri, Sanjali, Sonam, Nikita, LalitPrabha, Sarvesha, Siddhi, Samantha, Nitesh, Leo, Namrata** for their help during my research work.

This journey would have not been completed without the help and support of my wonderful lab mates. I express my gratitude to all my group members **Mr. Vishal More, Mr. Ratan Jadhav, Mr. Kerba More, Ms. Geeta Zalmi, Mr. Vilas Gawade, Mr. Harshad Mirgane,** and **Ms. Pooja Shreechippa,** for their timely help and support and making this journey knowledgeable and fun-filled.

"Home is where you are loved the most and act the worst." ― Marjorie Pay Hinckley

The final and the most awaited acknowledgments to my parents **Mr. Nagnath Nadimetla**, **Mrs. Renuka Nagnath Nadimetla**, and **Mrs. Vanita Nadimetla** for their countless blessings, unconditional love, support and encouragement. Sincere Gratitude to my grandmother **Mrs. Ratnabai Rangayya Nadimetla** and my grandfather Late **Mr.Rangayya B. Nadimetla** for their love and blessings. You all will always be remembered and have a special place in my heart. I thank my dear sisters **Mrs. Amruta Naresh Konda**, **Mrs. Rohini Ganesh Adam** and **Ms. Pooja Nadimetla** for their love and support. You are the world to me and I owe you all everything. Many thanks to my uncles **Mr. Gopal Nadimetla**, **Mr. Prakash Channa** and **Mr. Shridar Nadimetla**, and to my aunts **Mrs. Shanta Konda** and **Mrs. Sunita Gouda** for their support and love. Love to my dear cousins **Mr. Akshay Nadimetla**, **Ms. Monika Nadimetla**, **Ms. Akshada, Ms. Laxmi, Ms. Indrayani, Ms. Archana, Ms. Shalini, Ms. Komal, Ms. Kirthi,** and **Ms. Prithi**, thank you for being enthusiastic siblings. You are all inspiring people, thank you for being in my life.

I thank the almighty God for blessing me with a healthy life and for providing me with more than I could ever have imagined. You have surrounded me with people who always look out for me. You have given me family and friends who bless me every day with kind words and actions.

"Success is a journey, not a destination"
-Arthur Ashe

~Dinesh Nagnath Nadimetla

Dedicated
to my father Mr. Nagnath R. Nadimetla and my love Ms. Pooja

Table of Contents

List of Abbreviation

AcOH	-	Acetic acid
ACQ	-	Aggregation-caused quenching
AFM	-	Atomic Force microscopy
AIE	-	Aggregation-induced emission
ALP	-	Alkaline Phosphatase
BODIPY	-	Boron-Dipyrromethene
CD	-	Circular Dichroism
$CHCl_3$	-	Chloroform
CHEF	-	Chelation Enhanced Fluorescence
CISS	-	Chiral Induced Spin Selectivity
CPL	-	Circularly Polarized Luminescence
DBH	-	1,3-Dibromo-5,5-dimethylhydantoin
DCM	-	Dicholoromethane
DLS	-	Dynamic light scattering
DMAP	-	4-Dimethylaminopyridine
DME	-	Dimethoxy ethane
DMF	-	Dimethylformamide
DNA	-	Deoxyribonucleic acid
EDC	-	1-Ethyl-3-(3-dimethylaminopropyl)carbodiimide
ESI-MS	-	Electron spray ionization mass spectroscopy
ESIPT	-	Excited State Intramolecular Proton Transfer
FRET	-	Fluorescence resonance energy transfer
GuHCl	-	Guanidinium chloride
HNO_3	-	Nitric acid
HOBT	-	Hydroxybenzotriazole
HOMO	-	Highest Occupied Molecular Orbital
ICT	-	Intramolecular charge transfer
IR	-	Infrared
$KMnO_4$	-	Potassium Permanganate
LOD	-	Limit of detection
LUMO	-	Lowest unoccupied Molecular Orbital
MALDI	-	Matrix Assisted Laser Desorption/Ionisation
MCH	-	Methyl cyclohexane
MOF	-	Metal–organic frameworks
Na_2CO_3	-	Sodium carbonate
n-BuLi	-	n-Butyl lithium
NDA	-	1,4,5,8-naphthalenetetracarboxylic acid dianhydride
NDI	-	Naphthalenediimide
nM	-	Nano molar
NMR	-	Nuclear magnetic resonance

OFETs	-	Organic field-effect transistors
OLEDs	-	Organic light-emitting diodes
$Pd(PPh_3)_4$	-	Palladium-tetrakis(triphenylphosphine)
Pd/C	-	Palladium carbon
PDI	-	Perylenediimide
PET	-	Photo-induced electron transfer
PL	-	Photoluminescence
PPM	-	Parts per million
PTSA	-	p-toluene sulfonic acid
QA	-	Quinacridone
RDI	-	Rylenediimides
RNA	-	Ribonucleic acid
SEM	-	Scanning electron microscopy
TBA	-	Tetra butyl ammonium
TCSPC	-	Time-correlated single-photon counting
TEA	-	Tetra ethyl ammonium
TEM	-	Transmission electron microscopy
TFA	-	Trifluoro acetic acid
THF	-	Tetrahydrofuran
$TiCl_4$	-	Titanium (IV) chloride
TLC	-	Thin layer chromatography
TMS	-	Tetramethylsilane
TOF	-	Time of Flight
TPE	-	Tetraphenylethylene
TPE-BTA	-	N^1,N^3,N^5-tris(4-(1,2,2-triphenylvinyl)phenyl)benzene-1,3,5-tricarboxamide
UV-Vis	-	UV-Visible
XRD	-	X-ray diffraction
μM	-	Micro Molar

List of Schemes

List of Tables

List of Figures

Abstract

The designing small organic molecules with high-efficiency luminescence in the solid-state, for use in many areas such as chiral supramolecular assemblies,[1] sensing imaging applications,[2] organic light-emitting diodes,[3] and many more have attracted the attention of many researchers, Although small organic molecules have proved attractive due to their near-unity fluorescence (PL) quantum yield in dilute solution, current fluorescent materials suffer drawbacks due to aggregation caused quenching (ACQ), in aggregates and the solid-state, as a result of attractive dipole-dipole interactions and/or effective intermolecular π-π-stacking inter-actions, and thus cannot be used 'as is' for mechanochromic luminescent materials.[4] To overcome the ACQ effect in aggregated states new photoluminescent materials are required. Earlier work, by the Tang group, demonstrated the new phenomenon of aggregation-induced-emission (AIE).[5] However, designed and synthesized AIE-active molecules for chiral supramolecular assembly and sensing application. Detailed characterization studies such as Nuclear Magnetic Resonance(NMR) Infrared Spectroscopy(IR), CHN-Elemental analysis, High-Resolution Mass Spectroscopy(HRMS), Matrix-Assisted Laser Desorption/Ionization-Time Of Flight (MALDI-TOF) Mass spectrometry, Liquid Chromatography with mass spectrometry (LCMS), UV-Vis. Spectroscopy (UV-Vis.), Photoluminescence Spectrometer(PL), Scanning Electron Microscopy (SEM), Circular dichroism (CD), Powder X-ray Diffraction(XRD), Time-correlated single-photon counting (TCSPC), have been performed on synthesized molecules. The thesis, studied the solvent-induced assembly of tetraphenylethene derivative (TPE-BTA) and naphthalene diimide derivatives (NDI-R/S-BINOL). In addition, designed and synthesized TPE derivatives for C60 encapsulation and release, detection of fluoride anion, and copper (II) ion. In the sensing, study stoichiometry was calculated by using Job's Plot, and the binding and association constant was calculated by using Benesi-Hildebrand polt. and also using fluorescence intensity the Stern-Volmer (K_{SV}) quenching constant and limit of detection(LOD) were calculated. The exciting results obtained from all the above research have been briefly summarized in this synopsis.

Thesis objectives

The aim of the thsis objectuives are:

- Aim is to synthesize tetraphenylethylene (AIE-active) derivatives for hierarchical assembly

- Main purpose to prepare induction of chirality within the supramolecular assembly to naphthalene diimide (NDI) using R/S-BINOL chiral derivatives
- To prepare the azo-system bearing AIE-active TPE derivatives for encapsulation and release of fullerene derived by light
- To synthesize tetraphenylethylene urea derivative for fluoride ion sensing
- To synthesize TPE derivative bearing thiophenylbipyridine moiety for selective sensing of copper(II) ion

Thesis organization and results:

"SYNTHESIS OF TETRAPHENYLETHYLENE AND NAPHTHALENE DIIMIDE DERIVATIVES FOR SELF-ASSEMBLIES AND SENSING APPLICATIONS" is divided into five chapters as follows:

Chapter 1: Introduction and literature review
Section I: literature study on chiral self-assembly
Section II: literature study on sensing application
Chapter 2: Solvent-induced hierarchical self-assembly of tetraphenylethylene derivative
Chapter 3: Synthesis and characterization of naphthalene diimide derivative bearing BINOL moiety for chiral assembly
Chapter 4: Synthesis and characterization of tetraphenylethylene derivatives for sensing applications
Section I: Study of the azo-tetraphenylethylene molecule for encapsulation and release of C60
Section II: Study of tetraphenylethylene cyclic urea molecule for fluoride ion sensing
Section III: Study of tetraphenylethylene derivative bearing thiophenylbipyridine moiety for sensing of copper (II) ion
Chapter 5: Conclusions of the thesis

A brief highlight of each chapter is presented below:

Chapter 1: Introduction and literature review
Section I: literature study on chiral self-assembly

This chapter included a brief introduction to small organic molecules for chiral supramolecular assembly and sensing application in two sections. Section I described general approaches toward supramolecular chiral molecules the synthesis and self-assembly of an achiral molecule to contolled chiral supramolecular nanostructures with their photoluminescent properties, which may further can be used for sensitive, selective and rapid detection of analytes with a choice. Various small molecules were discussed for achiral to chiral along with induction of chirality and controlled chiral helical structures

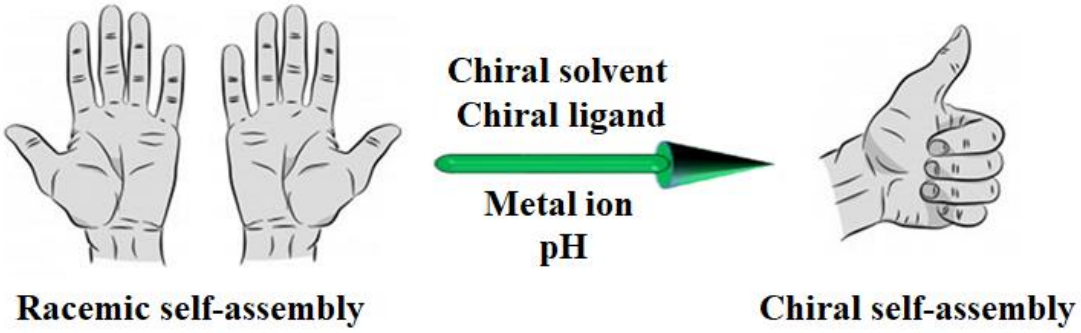

Figure 1. The schematic representation of chirality induced and controlled in organic molecules by varying solvent, ligand, metal ion, pH, etc.

in detail. The chirality of molecules is controlled and regulated by varying solvent,[6] pH,[7] metal ions,[8] and temperature[9] **(Fig. 1)**. Moreover, In section II, covered the sensing application of photoluminescent molecules. Recently most researchers attracted to use of the photoluminescent molecules such as TPE,[10–12] NDI,[13–15] Porphyrin,[16,17] Schiff's bases,[18] conjugate polymer,[19,20] various COFs, and MOFs[21,22] for various applications like chemosensors, host-guest, and biological probes.

***Section II**:* literature study on sensing application

This part focused on recently used photoluminescent molecules for chemosensors of anions, cations, and neutral guests.[23–25] Further, discussed a general mechanism involved in chemosensing. where the most common chemosensor has three parts binding site, spacer, and signaling unit. The signaling unit gets a response when the analyte bind at the binding site (**Fig. 2**). The maximum sensing mechanism involved the following mechanisms such as Photoinduced Electron Transfer(PET),[26] Fluorescence Resonance Energy

Transfer(FRET),[27] Intramolecular Charge Transfer(ICT),[28,29] Chelation Enhanced Fluorescence (CHEF),[30] and Excited State Intramolecular Proton Transfer(ESIPT)[31] etc.

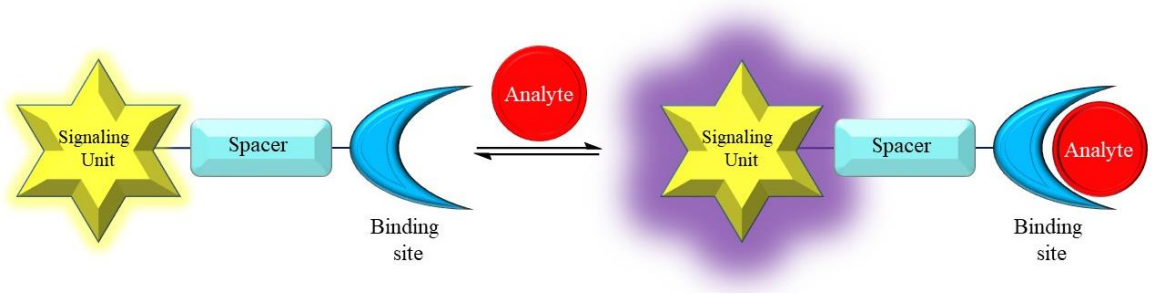

Figure 2. The schematic illustration of chemosensing mechanism.

Chapter 2: Solvent-induced hierarchical self-assembly of TPE-derivatives

As per literature the induction of chirality in self-assembly via achiral compounds, C_3-symmetrical molecules, π–conjugated molecules, and chiral molecules by using the sergeant-soldier method. In this case, synthesized C_3- symmetrical molecule having an amide functional group. Discussed the synthesis and characterization of a TPE-BTA. In this chapter, synthesis started McMurry reaction of benzophenone gives TPE **2** with 90% yield. After mono nitro-TPE **3** by using AcOH in HNO_3 at -5 ^oC for 15 Min. then followed by reduction of mono nitro TPE gives Mono amino TPE **(4)** with 93% yield. In the final step compound **4** reacted with 1,3,5-benzenetricarbonyl trichloride in presence of DMAP at room temperature giving TPE-BTA (88%). After synthesis of the TPE-BTA molecule, it was confirmed by IR, NMR, and Mass spectroscopy. Furthermore, mechanochormic, Aggregation induced emission, and solvatochromic study of TPE-BTA was carried out. Absorption spectra of TPE-BTA showed a band near 335 nm in THF and emission spectra (λ_{ex}=330) give a band at 490 nm. UV-Vis. and fluorescence study performed in various solvents, from the results the aggregation and self-assembly were observed in THF/Water and $CHCl_3$/MCH. The self-assembly study was carried out in $CHCl_3$/ MCH solvent system. The SEM images showed flower and helical structures in $CHCl_3$ and $CHCl_3$/MCH respectively, and also the cotton effect was observed in CD analysis.

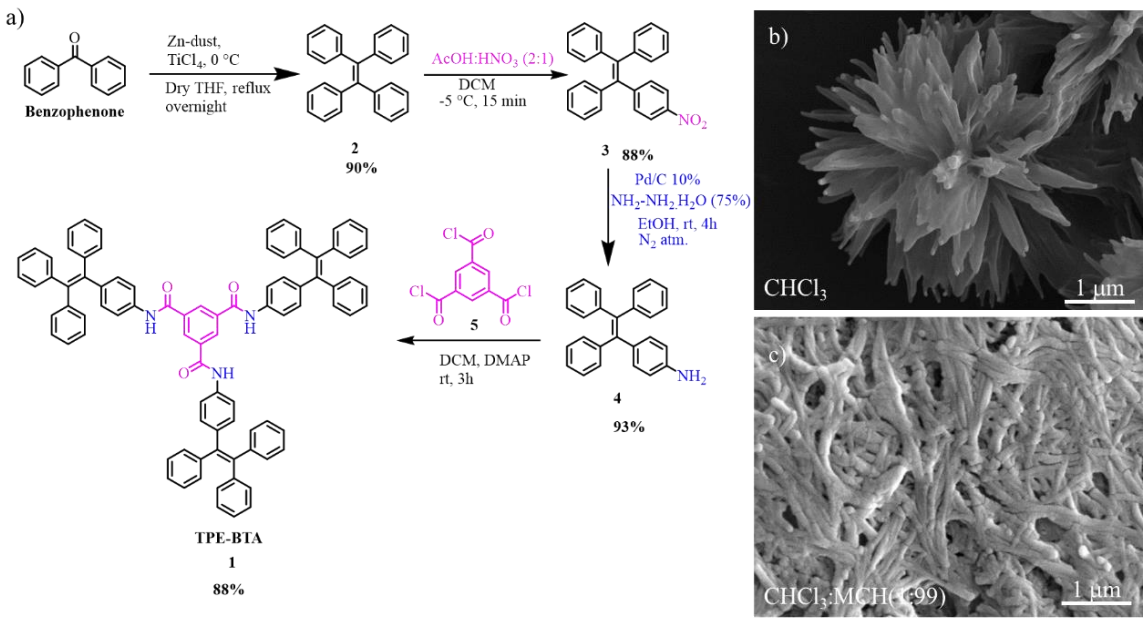

Figure 3. a) Synthetic route of TPE-BTA, b) & c) SEM images of TPE-BTA in $CHCl_3$ and $CHCl_3$/MCH(1:99) respectively.

Chapter 3: Synthesis and characterization of naphthalene diimide derivative bearing BINOL moiety for chiral assembly

Herein, designed and synthesized NDI-R/S-BINOL molecules (**Fig. 4**). The synthesis targeted molecules were we stated with bromination of naphthalene dianhydride(NDA) by using 1,3-dibromo-5,5-dimethyl hydantoin(DBH) gives 4-Br-naphthalene dianhydride(95%). Further, 4-Br-naphthalene dianhydride 4-Br-NDA converted into 4-Br-NDI(60%) treated with octyl amine in AcOH. In the final step, the targeted molecule NDI-R/S-BINOL (45%) was obtained from R/S-BINOL moiety reacted with 4-Br-NDI in presence of sodium hydride in dry DCM. The synthesized NDI-R/S-BINOL were confirmed by IR, NMR, and Mass spectroscopy. After successfully synthesized and characterized by various spectroscopic methods, then performed UV-Vis. and fluorescence study, both isomers NDI-R-BINOL and NDI-S-BINOL showed similar absorption spectra with two bands appearing at 310 nm and 425 nm. Solvatochromatic studied in various solvents such as Methanol, Acetonitrile, Tetrachloroethane, Tetrahydrofuran, Toluene, Methylcyclohexane, and the results possess that charge transfer band at near 680 nm. After that performed UV-Vis. and fluorescence study in tetrachloroethane(TCE) and methylcyclohexane(MCH) solvents. Finally, circular dichroism study of both molecules, where both the molecules showed an opposite cotton effect. NDI-R-BINOL exhibited a

positive cotton effect, on the other hand, NDI-S-BINOL showed a negative cotton effect in TCE: MCH solvent system.

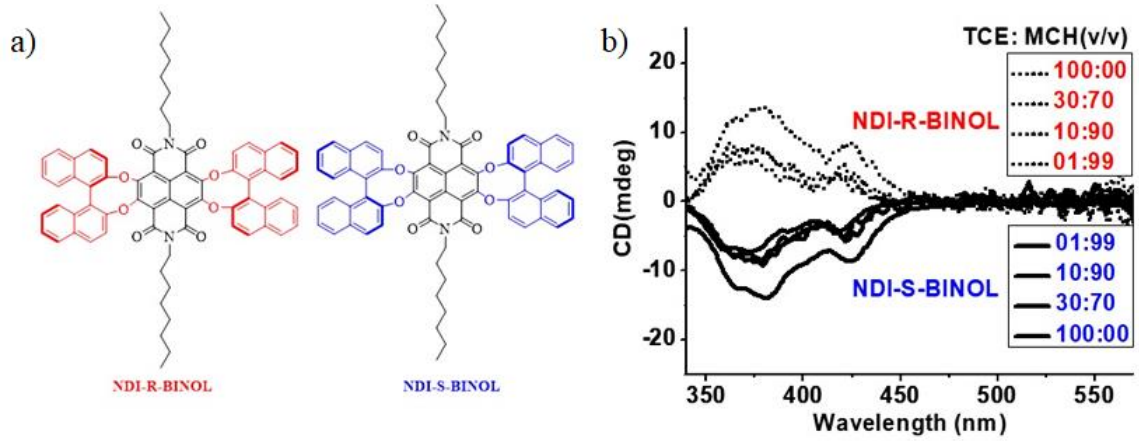

Figure 4. a), b) Structures and CD spectra of NDI-R/S-BINOL

Chapter 4: Synthesis and characterization of tetraphenylethylene derivatives for sensing applications

The recent year scientist interested in the development of photoluminescent dyes for sensing applications, due to they can use for naked-eye detection, and low-cost instrumentation, and also it will easy to utilize chemosensors in remotes area. This chapter focused on developing tetraphenylethylene derivates for sensing applications. This chapter-4 is distributed into three subsections (I-III) as follows:

***Section I**:* Study of the azo-tetraphenylethylene molecule for encapsulation and release of C60

In this section, a photoswitchable azobenzene-TPE **1** (host) was designed and successfully synthesized for encapsulation and release of C60 (guest) in presence of light (**Fig. 5**). The synthesis of the host azobenzene-TPE **1** molecule was prepared by a Suzuki reaction between reacting (4-(1,2,2-triphenylvinyl)phenyl)boronic acid with 1,2-bis(4-bromophenyl)diazene. The synthesized molecule **1** posses two forms E/Z. Further, the photoisomerization studies of synthesized azobenzene-TPE **1** upon exposure to UV light radiation it shown a forward reaction to form Z.**1** isomer form of the molecule, while E.**1** isomer formed through backward reaction by irradiating with visible light. In the photoisomerization, E.**1** isomer converted yellow color into Z.**1** isomer as an intense orange

color. And this phenomenon is also visualized by fluorescence and NMR spectroscopy. The fluorescence spectra of E.**1** isomer (λ_{ex} = 405nm) exhibited a broad band with peaks at 440 and 470 nm and a shoulder peak appears near at 550 nm. whereas Z.**1** isomer band at 480 nm with less intense. However, the light-triggered encapsulation of C60 in Z.**1** isomer were confirmed by various spectroscopic method. In the fluorescence spectra upon addition of 0 to 4 Equiv. of C60 in the Z.**1** isomer (6 μM, CS_2) intensity was decreased at 520 nm and a new peak at 725 nm was observed. Although the encapsulation study was executed with an E isomer no change was observed in fluorescence spectra. Moreover, the MALDI-TOF MS of Z.**1**.C60 shown perfectly matches the calculated isotopic pattern. And also a ^{13}C NMR of C60 displayed differences in the presence and absence of Z.**1** isomer. DFT calculation demonstrated clear interactions between the Z.**1** isomer and the C60. As one can see that TPE-based Z-form of **1** perfectly act as a recpeptor for C60 iluustrated in Figure 5a. Phenyl rings of molecule **1** gathered around to accommodate the C60 with a perfect shape complementarity to form the supramolecular assembly. finally, the light-triggered release of C60 from the Z form of molecule **1**, the Z.**1**.C60 irradiate with visible light, Z form converted into E form, while this conversation the C60 was released. This release of C60 was seen in UV-Vis., fluorescence spectra, and NMR spectra.

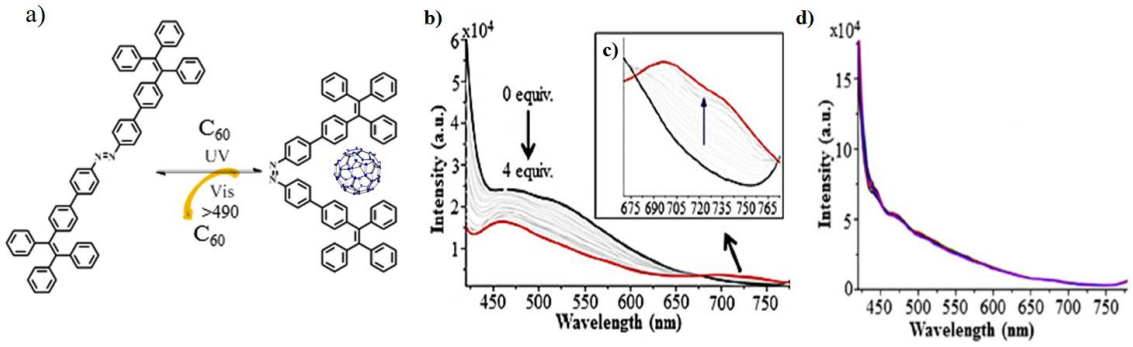

Figure 5. a) Structural illustration of host-guest complex and release of a guest and (**b** & **c**) shows the emission of the receptor **1** (6 μM) in *Z*-form with C60 , however, in *E*-form with C60 (0 to 24 μM) in CS_2 doesnot show the similar interactions (d).

***Section II**:* Study of tetraphenylethylene cyclic urea molecule for fluoride ion sensing

In this section, synthesized a tetraphenylethylene molecule bearing cyclic urea **1** a functional group **(Fig. 6**). The accidentally synthesized cyclic urea while preparing diamino-TPE for other purposes. All the synthesized derivatives was fully characterized by means of FT-IR, NMR and Mass spectroscopy. After confirmation, compound **1** showed color change while

the addition of fluoride ion. Further, the addition of other anions like AcO^-, NO_3^-, $H_2PO_4^-$, HSO_4^-, I^-, and Cl^- compound **1** not shown any color change. A receptor **1** (20 μM) in DMSO exhibited a very strong absorption band at 330 nm, while the addition of the F^- ion (as its tetrabutylammonium fluoride salt) band shifted to 385 nm with a new peak observed at 290 nm. However, with the addition of other anions in receptor **1,** no significant changes were observed. In the fluorescence study, receptor **1** (20 μM) displayed a strong band at 445 nm (λ_{ex} = 330 nm), whereas intensity was decreased by the addition of fluoride ion. Addition of other anions no changes observed in fluorescence intensity.

Moreover, ^{1}H NMR of receptor **1** was recorded in DMSO-d_6, and the urea two N-H protons appeared at 10.52 and 10.61 ppm. Further addition of F^- ions(5 Equiv.) gives the complete disappearance of N-H proton. While more addition, the hydrogen bifluoride ion complex was formed, which resulted in a new broad peak at 16.46 ppm

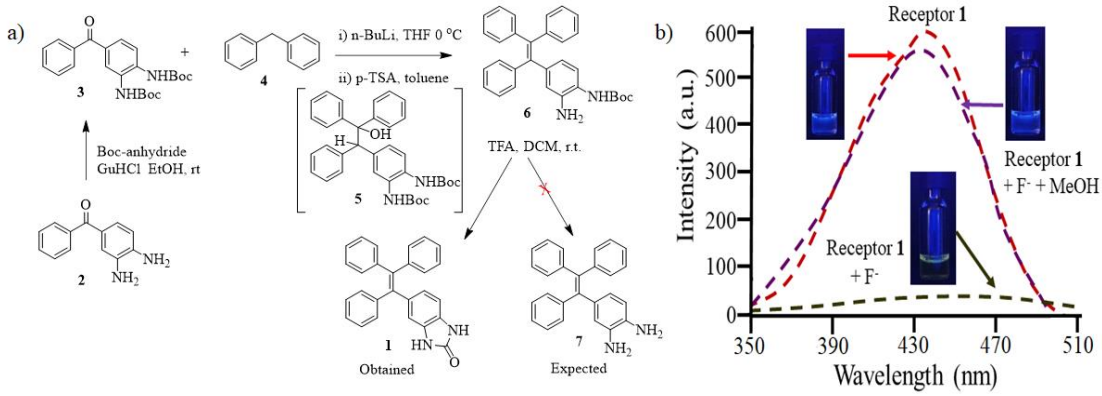

Figure 6. a) Synthetic route of TPE-cyclic urea **1**, b) Fluorescence emission spectra of **1** (30 μM, λ_{ex} = 330 nm), after the addition of F^- (10 equiv.) and addition of methanol to complex **1**-F^- in DMSO,

Section III: Study of tetraphenylethylene derivative bearing thiophenylbipyridine moiety for sensing of copper (II) ion

In this section, synthesized and characterized TPE-based molecule **1** bearing thiophenylbipyridine moiety as a binding site. Whereas, multistep reaction performed to synthesis of the receptor 6-(thiophene-2-yl)-4-(5-(4-(1,2,2-triphenylvinyl)phenyl)thiophen-2-yl)-2,2'-bipyridine **1** reaction between compound **8** and pyridine salt **9** in presence of ammonium acetate (**Fig.7**). The synthesized molecules were confirmed by IR, NMR, Mass spectroscopy, and elemental analysis. Molecule **1** has shown an efficient highly selective and sensitive to the detection of Cu^{2+} ion in acetonitrile. The sensing study of receptor **1** for different metal ions was studied via colorimetric, UV-Vis absorption, fluorescence

emission, and ^{1}H NMR titration. Photoinduced Electron Transfer "Off-on" involved in sensing mechanism of **1** towards Cu^{2+} ion. While receptor **1** coordinated with Cu^{2+} ions, the electron-donating nature of TPE- moiety was boosted, and a significant decrease in absorption peak intensity was observed, which facilitates the colorimetric detection of Cu^{2+} with the naked eye and complexation of Cu^{2+} ion with **1** resulted in a fluorescence quenching via **1** a PET '*turn-off*' sensor for Cu^{2+}.

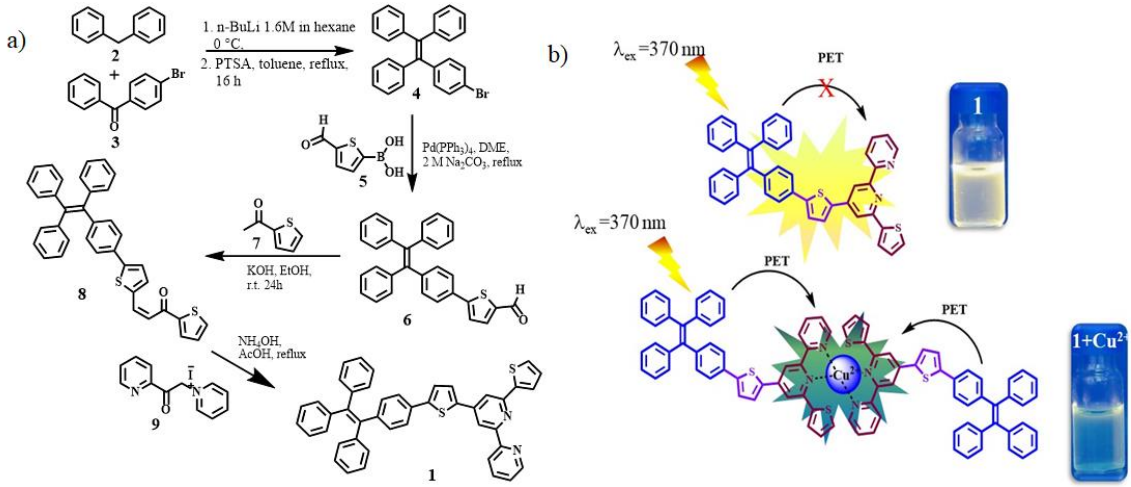

Figure 7. a) Synthetic route of receptor **1** b) Sensing mechanism of **1** towards Cu^{2+} ion.

Chapter 5: Conclusions of the thesis

Designed, synthesized, and characterized C_3-symmetrical TPE-BTA molecules for chiral assembly, synthesized C_3- symmetrical molecule having an amide functional group. synthesized molecules confirmed by IR, NMR, and Mass spectroscopy. Furthermore, a mechanochormic study of TPE-BTA resulted from a molecule that exhibited similar fluorescence properties in various states. Aggregation-induced emission behavior was observed in THF/water and $CHCl_3$/MCH. TPE-BTA has shown aggregation in 99% H_2O in THF and 99% MCH in $CHCl_3$ solvent system. A solvatochromic study of TPE-BTA was carried out in various rations of THF/water and $CHCl_3$/MCH solvent system. Absorption and emission study performed in various solvents, from results the aggregation and self-assembly were observed in THF/Water and $CHCl_3$/MCH. Flower-like and helical structures in $CHCl_3$ and $CHCl_3$/MCH were observed in SEM. Circular dichroism shows the cotton effect. From obtaining results conclude that inducing chirality in an achiral molecule by treating with various solvents.

Designed, synthesized, and characterized NDI-R/S-BINOL molecules. The synthesized NDI-R/S-BINOL were confirmed by IR, NMR, and Mass spectroscopy. Further investigated absorption and emission spectra, both isomers NDI-R-BINOL and NDI-S-BINOL showed similar absorption spectra with two bands appearing at 310 nm and 425 nm. Solvatochromatic effect shown NDI-R/S-BINOL in various solvents such as Methanol, Acetonitrile, Tetrachloroethane, Tetrahydrofuran, Toluene, Methylcyclohexane, and the results posses that charge transfer band at near 670 nm. Moreover, the self-assembly of NDI-R/S-BINOL was performed by using UV-Vis. and fluorescence study in tetrachloroethane(TCE) and methylcyclohexane(MCH) solvents. Circular dichroism study of both molecules were both the molecules shown perfectly mirror image to each other. NDI-R/S-BINOL exhibited positive and negative cotton effects, respectively in TCE: MCH solvent system. The obtained results concluded that chiral BINOL molecules were induced and controlled chirality in planar, achiral NDI molecule.

A TPE-based azobenzene photoswitchable molecule has been synthesized and characterized by IR, NMR, and Mass spectroscopic techniques. The structural conversion of the structure upon E→Z photoisomerization of compound **1** offers the possibility of the formation of a complementary cavity (host) for the housing of the C60 guest molecule. Various spectroscopic techniques investigated a host-guest interaction with both the *E* and the *Z* isomers of **1** and the C60 molecule. Whereas, It was observed that the ***Z*-1.C60** association (4.02×10^4 M^{-1}) was prominent as compared to the isomer ***E*-1.C60** (1.76×10^3 M^{-1}). Job's plot revealed stoichiometry of host-guest was 1:1. The ***Z*-1.C60** association was shown reversed by the irradiation with visible light that converts the ***Z*-1** form to the ***E*-1** form, and resulted in releasing of C60. Therfore, this one of the first eample which demonstrated of the stimuli-responsive host system that may be used for light-induced association and dissociation of a C60 molecule.

The tetraphenylethylene cyclic-urea-based receptor **1** was synthesized and characterized by various spectroscopic techniques. Receptor **1** was displayed to be highly selective and sensitive for the detection of fluoride anions. The recognition of fluorides anion over other anions, such as CN^-, AcO^-, NO_3^-, $H_2PO_4^-$, OH^-, ClO_4^-, SCN^-, HSO_4^-, I^- and Cl^- was confirmed by UV-Vis absorption spectroscopy, a decrease in fluorescence and strip-based sensing. In the ^1H NMR spectrum, the disappearance of the N_2H proton resonances in the cyclic urea was attributed to the formation of a hydrogen bonding complex of fluoride ion

with urea i. e. HF_2^-. The stoichiometry of the receptor was calculated from Job's plot and it showed 1:2. And a limit of detection(LOD) calculated by using formula $3\delta/S$, of receptor LOD was 30μM. Remarkably, reversible anion sensing was confirmed upon addition of methanol to the complex of **1**-F^-. Moreover, a strip test to detect F^- anions by receptor **1** was also developed. Thus, this work gives an idea to the development of these types of cyclic urea derivatives for real practical applications in sensing as well as for the preparation of fluorescence devices in a solid state.

Designed, synthesized, and characterized new AIE-active receptor **1** and studied mechanochromic properties of receptor **1.** Receptor **1** displayed various quantum yields in different solvents. Receptor **1** shows colorimetric, naked eyes, and fluorescent sensing of Cu^{2+} metal ions. The association constant of **1** with Cu^{2+} is shown to be $2.34x10^{-5}$ M. Job's plot investigated a stoichiometry of receptor **1** with Cu^{2+} shown 2:1 and limit of detection (LOD) found as low as 7.93 nM. The highly selective for the Cu^{2+} metal ions over other metal anions, such as Zn^{2+}, Pb^{2+}, Mg^{2+}, Mn^{2+}, Al3+, Hg^{2+}, Co^{2+}, Ba^{2+}, Ni^{2+}, Fe^{3+}, Cd^{2+}, $Ag^{+,}$ and K^+, was studied by UV-Vis absorption and fluorescence emission spectroscopy, and paper strip-based sensing. The binding constant prompted us to explore chromophore **1** as a paper strip sensor for Cu^{2+} to develop kits for real-world practical application Overall, the outcome of this thesis led to the development of chiral assemblies from achiral molecules and chemosensors from AIE-active molecules.

References:

(1) Feng, H. T.; Liu, C.; Li, Q.; Zhang, H.; Lam, J. W. Y.; Tang, B. Z. Structure, Assembly, and Function of (Latent)-Chiral AIEgens. *ACS Mater. Lett.* **2019**, *1* (1), 192–202. https://doi.org/10.1021/acsmaterialslett.9b00116.

(2) Mao, L.; Liu, Y.; Yang, S.; Li, Y.; Zhang, X.; Wei, Y. Recent Advances and Progress of Fluorescent Bio-/Chemosensors Based on Aggregation-Induced Emission Molecules. *Dye. Pigment.* **2019**, *162*, 611–623. https://doi.org/10.1016/j.dyepig.2018.10.045.

(3) Cekaviciute, M.; Petrauskaite, A.; Nasiri, S.; Simokaitiene, J.; Volyniuk, D.; Sych, G.; Budreckiene, R.; Grazulevicius, J. V. Towards Blue AIE/AIEE: Synthesis and Applications in OLEDs of Tetra-/Triphenylethenyl Substituted 9,9-Dimethylacridine Derivatives. *Molecules* **2020**, *25* (3). https://doi.org/10.3390/molecules25030445.

(4) Huang, Y.; Xing, J.; Gong, Q.; Chen, L.; Liu, G.; Zhang, H.; Chen, Z.; Zhang, Q.; Yao, C.; Wang, Z. Molecular Barriers. *Nat. Commun.* **2019**, No. 1219, 1–9. https://doi.org/10.1038/s41467-018-08092-y.

(5) Luo, J.; Xie, Z.; Xie, Z.; Lam, J. W. Y.; Cheng, L.; Chen, H.; Qiu, C.; Kwok, H. S.; Zhan, X.; Liu, Y.; Zhu, D.; Tang, B. Z. Aggregation-Induced Emission of 1-Methyl-1,2,3,4,5-Pentaphenylsilole. *Chem. Commun.* **2001**, *18*, 1740–1741. https://doi.org/10.1039/b105159h.

(6) Takaishi, K.; Iwachido, K.; Ema, T. Solvent-Induced Sign Inversion of Circularly Polarized Luminescence: Control of Excimer Chirality by Hydrogen Bonding. *J. Am. Chem. Soc.* **2020**, *142* (4), 1774–1779. https://doi.org/10.1021/jacs.9b13184.

(7) Lazzari, F.; Alexander, B. D.; Dalgliesh, R. M.; Alongi, J.; Ranucci, E.; Ferruti, P.; Griffiths, P. C. PH-Dependent Chiral Recognition of d- and l-Arginine Derived Polyamidoamino Acids by Self-Assembled Sodium Deoxycholate. *Polymers (Basel).* **2020**, *12* (4). https://doi.org/10.3390/POLYM12040900.

(8) Wang, F.; Feng, C. L. Metal-Ion-Mediated Supramolecular Chirality of l-Phenylalanine Based Hydrogels. *Angew. Chemie - Int. Ed.* **2018**, *57* (20), 5655–5659. https://doi.org/10.1002/anie.201800251.

(9) Hu, J.; Xie, Y.; Zhang, H.; He, C.; Zhang, Q.; Zou, G. Chiral Induction, Modulation and Locking in Porphyrin Based Supramolecular Assemblies with Circularly Polarized Light. *Chem. Commun.* **2019**, *55* (34), 4953–4956. https://doi.org/10.1039/c9cc01613a.

(10) Qiao, W. G.; Xiong, J. Bin; Yuan, Y. X.; Zhang, H. C.; Yang, D.; Liu, M.; Zheng, Y. S. Chiroptical Property of TPE Triangular Macrocycle Crown Ethers from Propeller-like Chirality Induced by Chiral Acids. *J. Mater. Chem. C* **2018**, *6* (13), 3427–3434. https://doi.org/10.1039/c7tc05759h.

(11) Anuradha; La, D. D.; Al Kobaisi, M.; Gupta, A.; Bhosale, S. V. Chiral Assembly of AIE-Active Achiral Molecules: An Odd Effect in Self-Assembly. *Chem. - A Eur. J.* **2017**, *23* (16), 3950–3956. https://doi.org/10.1002/chem.201605458.

(12) Hu, M.; Feng, H. T.; Yuan, Y. X.; Zheng, Y. S.; Tang, B. Z. Chiral AIEgens – Chiral Recognition, CPL Materials and Other Chiral Applications. *Coord. Chem. Rev.* **2020**, *416*, 213329. https://doi.org/10.1016/j.ccr.2020.213329.

(13) Shaikh, D. B.; Bhosale, R. S.; La, D. D.; Al Kobaisi, M.; Bhosale, S. V.; Bhosale, S. V. Chiral Supramolecular Assemblies from an Achiral Naphthalene Diimide Bearing a Urea Moiety. *Chem. - An Asian J.* **2018**, *13* (21), 3268–3273. https://doi.org/10.1002/asia.201801115.

(14) Nandre, K. P.; Bhosale, S. V.; Krishna, K. V. S. R.; Gupta, A.; Bhosale, S. V. A Phosphonic Acid Appended Naphthalene Diimide Motif for Self-Assembly into Tunable Nanostructures through Molecular Recognition with Arginine in Water. *Chem. Commun.* **2013**, *49* (48), 5444–5446. https://doi.org/10.1039/c3cc41259h.

(15) Wagalgave, S. M.; Padghan, S. D.; Burud, M. D.; Kobaisi, M. Al; La, D. D.; Bhosale, R. S.; Bhosale, S. V.; Bhosale, S. V. Supramolecular Super-Helix Formation via Self-Assembly of Naphthalene Diimide Functionalised with Bile Acid Derivatives. *Sci.*

Rep. **2019**, *9* (1), 1–9. https://doi.org/10.1038/s41598-019-49235-5.

(16) Rananaware, A.; La, D. D.; Al Kobaisi, M.; Bhosale, R. S.; Bhosale, S. V. Controlled Chiral Supramolecular Assemblies of Water Soluble Achiral Porphyrins Induced by Chiral Counterions. *Chem. Commun.* **2016**, *52* (67), 10253–10256. https://doi.org/10.1039/c6cc04427a.

(17) Li, Y.; Duan, P.; Liu, M. Solvent-Regulated Self-Assembly of an Achiral Donor–Acceptor Complex in Confined Chiral Nanotubes: Chirality Transfer, Inversion and Amplification. *Chem. - A Eur. J.* **2017**, *23* (34), 8225–8231. https://doi.org/10.1002/chem.201700613.

(18) Muppidi, V. K.; Das, S.; Raghavaiah, P.; Pal, S. Copper(II) Complexes with Chiral Reduced Schiff Bases: Helical Self-Assembly via Intermolecular C-H···O Interactions. *Inorg. Chem. Commun.* **2007**, *10* (2), 234–238. https://doi.org/10.1016/j.inoche.2006.10.011.

(19) Rubio-Magnieto, J.; Thomas, A.; Richeter, S.; Mehdi, A.; Dubois, P.; Lazzaroni, R.; Clément, S.; Surin, M. Chirality in DNA–π-Conjugated Polymer Supramolecular Structures: Insights into the Self-Assembly. *Chem. Commun.* **2013**, *49* (48), 5483–5485. https://doi.org/10.1039/c3cc42108b.

(20) Ikai, T.; Shimizu, S.; Awata, S.; Shinohara, K. I. Chiral Amplification in π-Conjugated Helical Polymers with Circularly Polarized Luminescence. *Macromolecules* **2018**, *51* (6), 2328–2334. https://doi.org/10.1021/acs.macromol.8b00229.

(21) Han, X.; Zhang, J.; Huang, J.; Wu, X.; Yuan, D. Chiral Induction in Covalent Organic Frameworks. *Nat. Commun.* No. 2018, 1–10. https://doi.org/10.1038/s41467-018-03689-9.

(22) Deng, G.; Teo, B. K.; Zheng, N. Assembly of Chiral Cluster-Based Metal-Organic Frameworks and the Chirality Memory Effect during Their Disassembly. *J. Am. Chem. Soc.* **2021**, *143* (27), 10214–10220. https://doi.org/10.1021/jacs.1c03251.

(23) Patil, N. S.; Dhake, R. B.; Ahamed, M. I.; Fegade, U. A Mini Review on Organic Chemosensors for Cation Recognition (2013-19). *J. Fluoresc.* **2020**, *30* (6), 1295–1330. https://doi.org/10.1007/s10895-020-02554-7.

(24) Wu, D.; Sedgwick, A. C.; Gunnlaugsson, T.; Akkaya, E. U.; Yoon, J.; James, T. D. Fluorescent Chemosensors: The Past, Present and Future. *Chem. Soc. Rev.* **2017**, *46* (23), 7105–7123. https://doi.org/10.1039/c7cs00240h.

(25) Upadhyay, S.; Singh, A.; Sinha, R.; Omer, S.; Negi, K. Colorimetric Chemosensors for D-Metal Ions: A Review in the Past, Present and Future Prospect. *J. Mol. Struct.* **2019**, *1193*, 89–102. https://doi.org/10.1016/j.molstruc.2019.05.007.

(26) Dadashi-Silab, S.; Doran, S.; Yagci, Y. Photoinduced Electron Transfer Reactions for Macromolecular Syntheses. *Chem. Rev.* **2016**, *116* (17), 10212–10275.

https://doi.org/10.1021/acs.chemrev.5b00586.

(27) Wu, L.; Huang, C.; Emery, B. P.; Sedgwick, A. C.; Bull, S. D.; He, X. P.; Tian, H.; Yoon, J.; Sessler, J. L.; James, T. D. Förster Resonance Energy Transfer (FRET)-Based Small-Molecule Sensors and Imaging Agents. *Chem. Soc. Rev.* **2020**, *49* (15), 5110–5139. https://doi.org/10.1039/c9cs00318e.

(28) Wang, X.; Li, T.; Ma, C. A Novel ICT-Based Chemosensor for F- and Its Application in Real Samples and Bioimaging. *J. Hazard. Mater.* **2021**, *413* (August 2020), 125384. https://doi.org/10.1016/j.jhazmat.2021.125384.

(29) Wu, J.; Liu, W.; Ge, J.; Zhang, H.; Wang, P. New Sensing Mechanisms for Design of Fluorescent Chemosensors Emerging in Recent Years. *Chem. Soc. Rev.* **2011**, *40* (7), 3483–3495. https://doi.org/10.1039/c0cs00224k.

(30) Liu, S.; Wang, Y. M.; Han, J. Fluorescent Chemosensors for Copper(II) Ion: Structure, Mechanism and Application. *J. Photochem. Photobiol. C Photochem. Rev.* **2017**, *32*, 78–103. https://doi.org/10.1016/j.jphotochemrev.2017.06.002.

(31) Goswami, S.; Maity, S.; Maity, A. C.; Das, A. K.; Pakhira, B.; Khanra, K.; Bhattacharyya, N.; Sarkar, S. ESIPT Based Hg2+ and Fluoride Chemosensor for Sensitive and Selective “turn on” Red Signal and Cell Imaging. *RSC Adv.* **2015**, *5* (8), 5735–5740. https://doi.org/10.1039/c4ra07838a.

Chapter I

Introduction and literature review

Chapter 1

Jean-Marie Lehn introduced supramolecular chemistry in the 1970. The term supramolecular chemistry was defined as "the chemistry of the intermolecular bond, covering the structures and functions of the entities formed by the association of two or more chemical species" by J. M. Lehn.[1–4] Supramolecular chemistry is a multidisciplinary field, which involves biological -systems inspired by nature, building blocks generated from supramolecular synthons in organic and inorganic chemistry, and the study of properties that come in under physical chemistry. Currently, studying all kinds of intermolecular non-covalent bond formation in engineered molecular systems referred to as supramolecular chemistry, which also includes dynamic covalent chemistry. Donald J. Cram, Jean-Marie Lehn, and Charles J. Pedersen received the Nobel Prize in Chemistry (1987)[5] for their contributions to this field, particularly in the host-guest binding molecules, and Bernard L. Feringa, Sir J. Fraser Stoddart, and Jean-Pierre Sauvage received it in 2016 for their contributions to the development of molecular machines.[6]

Organic supramolecular chemistry involves non-covalent bonding such as hydrophobic interaction, electrostatic interaction, hydrogen bond interaction, van der Waals interaction, cation $-\pi$ interaction, $\pi-\pi$ stacking. Generally, the bottom-up approach was utilized for building a superstructure in supramolecular chemistry. Design a molecule with different electronic functions group for self-assembly into the supramolecular superstructure.[7–9] Due to the wide range of applications, researchers are interested in working in supramolecular chemistry. This thesis mainly focuses on self-assembly and sensing application.

In this chapter, two sections briefly introduced small organic compounds for chiral supramolecular assembly and sensing applications. Synthesis and self-assembly of an achiral molecule to controlled chiral supramolecular nanostructures with their photo luminescent features were discussed in Section I. These structures may also be employed for sensitive, selective, and efficient detection of analytes with a range of options. Tiny compounds for achiral-to-chiral conversion, chirality induction, and controlled chiral helical architectures were discussed. Section II, concentrated on recently developed chemosensors for anions, cations, and neutral visitors using photo luminescent molecules. Besides, a generic mechanism underlying chemo sensing was discussed. The most classic chemosensor consists of three components: a binding site, a spacer, and a signaling unit. When the analyte binds at the binding site, the signaling unit responds.

Section I: literature study on chiral self-assembly

1.1 Introduction

1.1.1 Origin of Chirality

Chirality, which regulates the handedness of biochemical reactions and primarily directs biological structures to choose a specific chirality at the beginning and amplification of bio-molecular chirality, determines the origins of life and evolution. Chirality is one of nature's most amazing phenomena.[10,11] It is unclear how, at various biological structural levels, natural processes transform molecular chirality into selective left- or right-handed homochirality in animals.[12] One of the most beautiful examples of chiral self-assembly in natural systems is the tobacco mosaic virus (TMV). TMV is made up of a single type of protein, which is typically arranged into a right-handed nucleoprotein helix and interconnected by an RNA string.[13] The capacity to destabilize the capsid structure once inside the host cell is the greatest trait of self-assembled TMV viruses. Usually, anionic amino acid residues, such as glutamate (Glu) residues, are crucial in causing the TMV capsid superstructure's chirality to collapse.[14] To replicate the shape and operation of bio molecular chirality within biological systems, various efforts have been made to create chirality in dynamic supramolecular assembly.[15–17] However, it failed to replicate the intrinsic intricacy of even the most basic biological system that is similar to TMV. However, one instance of artificial supramolecular helicity that is connected to the discussion of chirality propagation is of the highest importance.[18] The complexity of chirality-directed biological processes may be realistically modelled by changing the dynamic helicity in response to physical and chemical stimuli.[19–22]

In order to regulate the chirality of superstructures, a variety of triggers have been used, including stirring,[23] magnetic fields,[24] redox forces,[25] solvophobicity,[26] pH,[27] and light.[28–30]

1.1.2 Chiral nanoscience and nanotechnology

Exciting developments in study are being made towards the advancement of materials and devices that specifically profit from molecular chirality, which is a prerequisite for chiral nanotechnology.[28] Chiral molecules play an advantageous part in nano-science and technology. Nanoscience is described as the study of molecules at the nano level, which is typically 1 to 100 nm.[15] It is impossible to superimpose a chiral item on its mirror copy. Keys, palms, screws, blades, and other objects are examples. The right and left hands of an individual are nearly similar, but inverted (**Fig. 1**) Despite being mirror pictures, they cannot be superimposed on one another. Because gloves from the left hand cannot be used on the right hand, it is simple to understand why the left and right hands cannot be superimposed

(**Fig. 1a**). There are molecules with left- and right-handed shapes and chirality throughout the biological universe and in all living entities (**Fig. 1b**). Enantiomers are the terms used to refer to a chiral molecule's two possible configurations. Asymmetric carbon centers or supramolecular structures that create chain helicity are two important requirements for a molecule to be chiral. The majority of chiral biomolecules and polymers found in nature include proteins, nucleic acids, and carbohydrates.

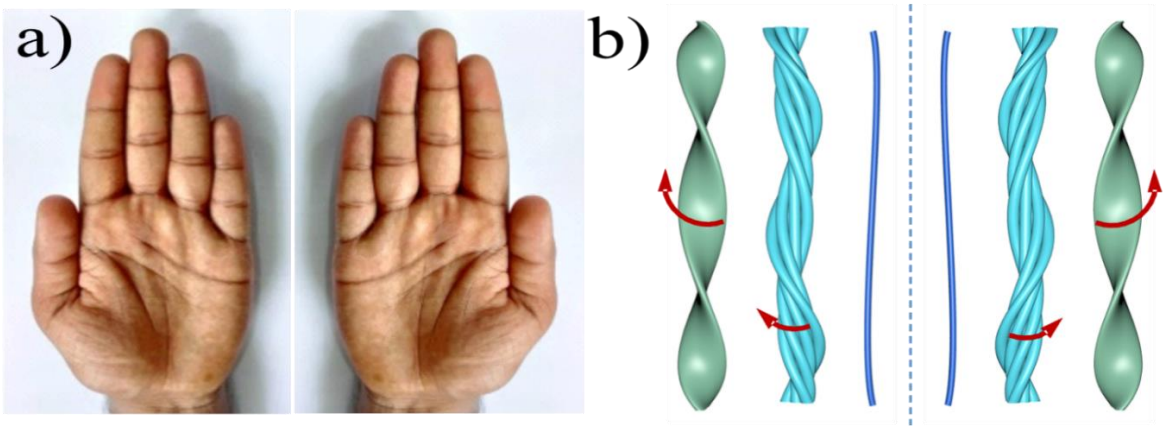

Figure 1.1: Non-superimposable mirror images a) left and right hand of person b) left and right-handed supramolecular helical fibers.

Since the "machinery of life" evolved over a long period of time, the genesis of the current study, we do not understand how or why certain biological systems have dominated over others. The key elements and compounds of these systems have been successfully isolated and studied by chemists, but we are still a long way from being able to assemble and recreate these supramolecular biological systems in the lab and use them for practical purposes, particularly drug delivery in targeted cells. In nano- and biotechnology, a supramolecular self-assembled chiral structure is essential.[13-30] Researchers have created chiral devices that are multi-stimulus sensitive. CPL (Circularly Polarized Luminescence), one of the created chiral systems, has applications in many technological fields, including quantum computing, 3D displays, and bio-responsive sensing.[31]

For the creation of molecular logic gates and memory devices, various research groups have created optical and molecular switches. Naaman and colleagues have looked into the possibility of using the CISS (Chiral Induced Spin Selectivity) phenomenon to influence the course of electrochemical processes.[32] The polymer P3HT was combined with a chiral helicene molecule as an additive to create organic photovoltaic devices, which Josee *et al.* found to have a fivefold better power conversion efficacy.[33] According to Shang and

colleagues, the pendant chirality of perylenediimides in self-assembled crystalline nanowires impacted the efficacy of organic solar systems.[34]

Building a supramolecular system capable of performing constantly autonomous movements will pave the way for the subsequent generation of bio-inspired mechanical systems. Supramolecular synthesis can be constructed using both bottom-up and top-down methods. In living systems, the formation of spatio-temporal structures with dissipative structures is driven by hierarchical molecular coordination. Building such self-organized functioning things using artificial means is still challenging. The regulation of helicity in man-made supramolecular ensembles is, however, without a question, of paramount importance because it is closely related to the discussion of chirality transmission[18] and has significant mechanistic ramifications for the life sciences. Notably, groups of non-covalent interactions control the biomolecular self-assembly in nature. Non-covalent interactions are inherently dynamic, and because of this and the fact that they can be influenced by physical and chemical triggers, it is theoretically possible to replicate the intricacy of chirality-directed biological self-assembly.[23–27,29]

Scientists have made significant progress in controlling chirality with exterior stimuli that imitate naturally chiral objects in order to show the chirality phenomenon using smaller organic molecules. Since small-molecule chirality has always intrigued scientists and offers a mentally taxing exercise for selective chemical synthesis and catalysis, it has attracted their attention. Small-molecule chirality has not typically been a crucial component for the creation of novel materials for popular technological uses, despite the important biological antecedent. Thus, new methods for designing novel materials that take into consideration chirality are now developing through the use of small molecules, which is resulting in new usefulness in technological uses. Another problem with evolved tiny molecules is that they emit less light when they aggregate into supramolecular chiral helical structures. The synthesis of achiral molecules and their self-assembly into active chiral molecules are addressed in this section along with the investigation of controlled supramolecular chiral nanostructures with their photo-luminescent properties for the quick, sensitive, and targeted detection of desired analytes. Numerous small compounds have been thoroughly explored for conversion from achiral to chiral, as well as chirality induction and regulated chiral helical shapes. Lastly, we will investigate the tetraphenylethylene (TPE) conjugates' photo-responsive helicity characteristics. Despite the enormous possibilities that small-molecule chirality has brought to certain systems, many of these instances are still in the early stages of technological development. The transition from proof-of-concept to practical uses

requires a lot of effort. Small molecules, which have benefits over other systems and can produce such material through straightforward synthetic methods, can be used to resolve this. In the end, we think that methodical and thorough work is required to take advantage of small-molecule chirality and their application in technical advancement.

1.2 Induction of chirality

The development of life and the chiral amplification found in nature are both closely linked to the inductions of chirality in supramolecular structures through hierarchical self-assembly of achiral compounds, as well as the regulation of their handedness. There are not many instances that show how chirality in amphiphiles, homo-chiral molecules, C3-symmetrical molecules, π-conjugated molecules, or a combination of chiral and achiral molecules is transmitted to the handedness of the self-assembled helical structure to produce twisted fibers.

1.3 Controlled chiral structures

The system having non-covalent bonding in molecules, chiral, achiral molecules, solvent, temperature, pH, or chemical compounds are just a few examples of the variables that can control and transmit chirality. Chiral handedness can also be specifically controlled by adjusting the odd or even number of carbons in side chains, and chirality in achiral molecules can be controlled by adjusting carbon chains via amide linkage to tetraphenylethylene[26,35] The chirality of achiral compounds could also be controlled by varying the ratios of different liquids.[36] Chirality is induced and controlled in the self-assembly of achiral molecules by optically active compounds.[37,38] When chiral solvents were added in tiny amounts during assembly, helical shapes of the assembly were produced. When the chiral solvent was removed, the self-assembly still maintained its chirality.

1.3.1 Achiral molecules to controlled chiral supramolecular helical superstructure

Understanding the function chirality performs in these systems requires the design and synthesis of achiral organic functional molecules that can assemble into chiral with specific handedness in the absence of chiral substances. In this regard, Anuradha *et al.*[26] reported the self-assembly-based tuning of an achiral molecule to a right-handed chiral superstructure. The authors began with the achiral aggregation induced emission (AIE) active TPE molecule, which was carrying four long alkyl chains **2** (**Scheme 1.1**) via amide linkage to

tetraamino-TPE. Which was induces and controls chirality by Circular Dichroism was used to validate the chirality of the formed structures after scanning electron microscopy (SEM) pictures showed the formation of a right-handed helical structure self-assembly (CD). The formation of a right-handed chiral superstructure is supported by both techniques. Surprisingly, neither CD activity nor any chiral helical structures were produced by the oligoethylene-substituted TPE via amide **3** (**Scheme 1.1**) bond that was examined.

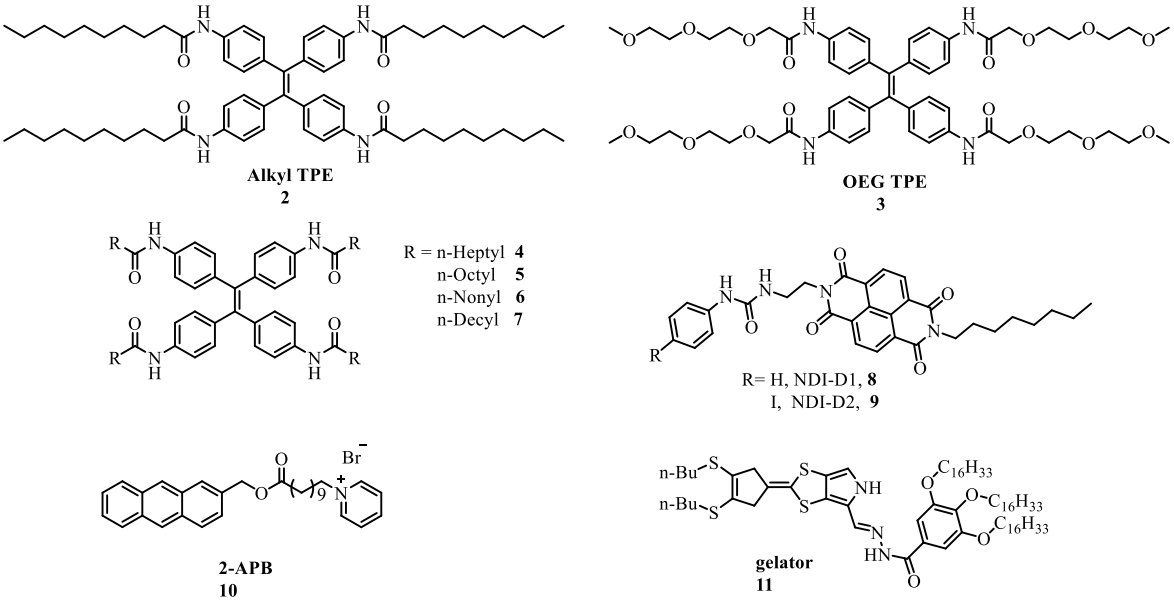

Scheme 1.1: Previously reported achiral molecules to controlled chiral supramolecular helical superstructure achiral molecules.

TPE's naturally occurring propeller-like structure enables the creation of chiral assemblies upon interaction of an amide linkage with a long alkyl chain via hydrogen bonding with a hydrophilic as well as the development of an amide linkage with a hydrophobic alkyl chain. The same group invented the first chiral self-assembling molecule, a tetra phenyl ethylene (TPE) molecule with four alkyl chains and an amide bond. The alkyl chains have different methyl groups, such as C7, C8, C9, and C10. It's interesting to note that the helical structure of supramolecular assembly was controlled by using odd and even numbers of carbon atoms in alkyl groups. Right handed helical structure was obtained from structures bearing an even number of carbon atoms in the alkyl group, whereas left handed superstructure is obtained in odd numbers, typically: C7-TPE and C9-TPE (anticlockwise twist), C8-TPE and C10-TPE (clockwise twist), respectively(**Fig. 1.3)**.

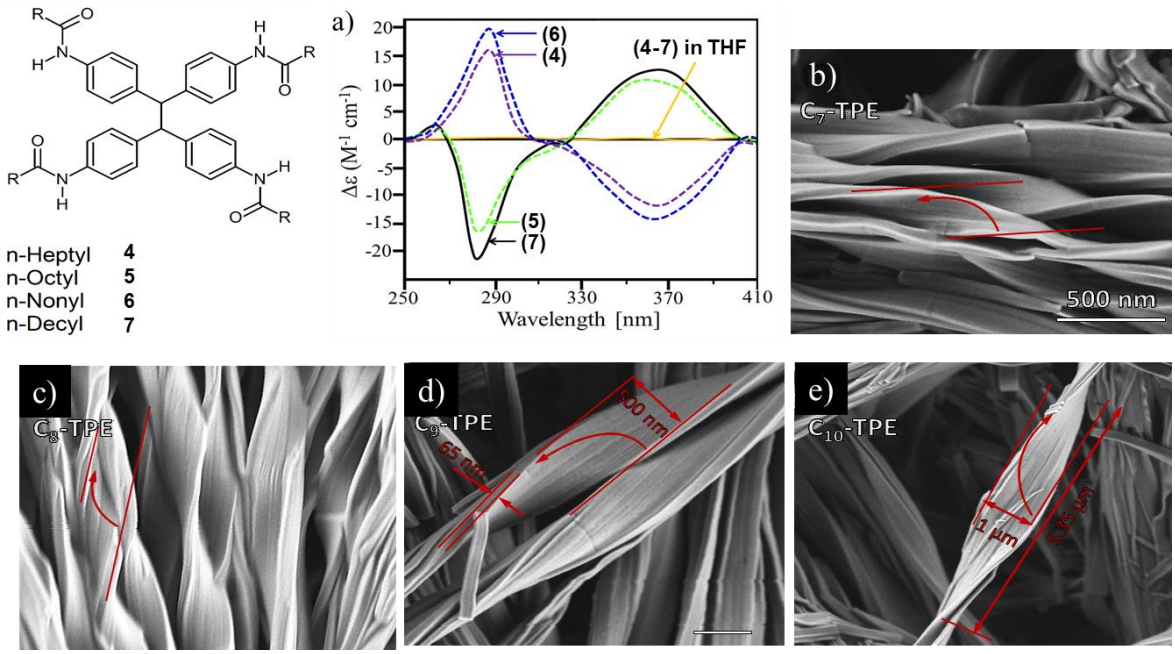

Figure 1.2: TPE (4-7) derivatives used for this study, a) CD spectra of 4-7 in THF and in MeCN/THF. SEM visualisation of twisted superstructures of 4-7 deposited on silicon wafers from MeCN/THF (9:1 v/v) by solvent evaporation. b) C7-TPE 4 (anticlockwise twist), c) C8-TPE 5 (clockwise twist), d) C9-TPE 6 (anticlockwise twist) and e) C10-TPE 7 (clockwise twist).

Shaikh *et al.*[39] developed and produced the urea-functionalized achiral naphthalenediimide (NDI) compounds NDI-D1 **8** and NDI-D2 **9** (**Scheme 1.1**). In Methanol:THF (40:60) solution, NDI-D1 creates chiral ribbons with the other two molecules. The hydrogen bonding between urea groups, the stacking of the NDI aromatic centre and the van der Waal's contacts between the long alkyl chains all contributed to the formation of the chiral ribbons in compound **8**. CD and SEM studies verified the existence of chiral structures. While Molecule **9** does not form any chiral assemblies, as demonstrated by the CD spectrum's lack of optical activity, it does produce nano-belt structures that can be seen in SEM pictures. Nano-belt shapes might be justified by the non-covalent contact between iodine and hydrogen.

The transformation of the achiral pyridinium derivative **2-APB; 10** (**Scheme 1.1**) into chiral supramolecular structures was reported by Wang and his team.[40] In molecule **10**, a hydrocarbon chain connects the hydrophilic pyridinium units and the hydrophobic anthracene units. The formation of Left/Right-handed helical structures with widths ranging

from 20 to 100 nm and near hundred micrometres was observed in the initial chiral supramolecular assemblies made from **10** and potassium iodide (KI) in water. Additionally, upon using pseudo-anion of similar radii such as (OCN, SCN, SeCN), the formation of Left/Right-handed helical structures with widths ranging from 20 to 100 nm and near hundred. Bingzhu and his team[36] looked into the water-controlled helicity of supramolecular nanofibers made of an achiral monopyrrolotetrathiafulvalene (**MPTTF; 11**) (**Scheme 1.1**) variant. In purified DMF, the clustering of **11** results in the formation of left- (M) and right- (P) helical structures. It was discovered that all fibres were transformed into right-handed helical structures upon the addition of a tiny quantity of water. Atomic force microscopy (AFM) images and CD spectra verified the existence of solution-based chiral structures. Due to hydrogen bonding, π–π-stacking, and σ–σ interaction within the molecules, this regulated and forced chirality was possible.

1.3.2 C_3-symmetrical molecules

In this type of C3-symmetrical molecules, building elements are benzene substituted at positions 1, 3, and 5 with amide or urea bonds, tricarboxylic acids, triamines, or any other functional groups to create chiral nano-assemblies. Due to steric hindrance caused by substituents on the central aromatic core and polar groups that form hydrogen bonds during stacking, the C3-symmetrical molecules resemble blades and cause chirality in the assemblage. In some instances, chirality is produced or controlled using chiral or achiral liquids.

Sun and his[41] team used an achiral molecule via hydrogen bonding to show light-controlled supramolecular construction. One melamine core **M** (**Fig. 1.3**) and three-photo addressable azobenzene **A** (**Fig. 1.3**) units were combined by hydrogen bonding to form a supercoil that self-assembled. Hydrogen bonds create a structure that looks like a turbine. Azo group-containing structures are light sensitive and readily change from one shape to another in the presence of light. Transmission electron microscopy (TEM), atomic force microscopy (AFM), CD spectroscopy, and X-ray diffraction (XRD) methods used to assess the crystallinity of the generated assemblies all served to corroborate the assembly formation (**Fig. 1.3**).

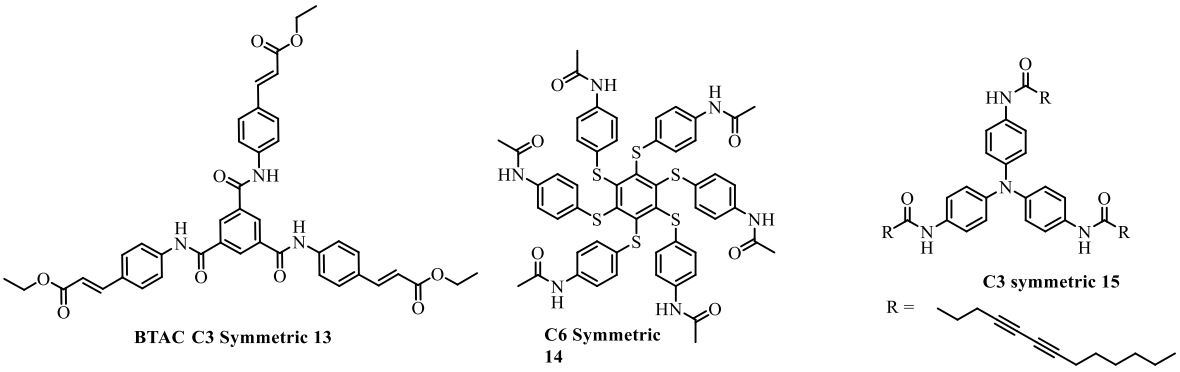

Scheme 1.2: C3 and C6 symmetric molecules.

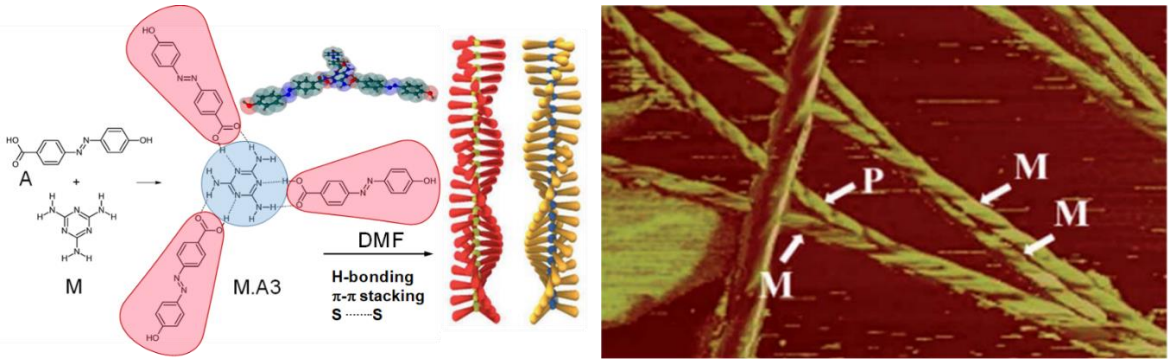

Figure 1.3: AFM images of the self-assembled helixes and supercoils with identified handedness and the schematic depiction of the M•A3 complex are shown.

Another technique described by Wua *et al.*[41] includes adjusting the self-assembly of achiral to chiral molecules, which also produce dual fluorescence-phosphorescence. The C6-symmetric achiral molecule BTAC **14** (**Scheme 1.2**) has a low molecular weight and six amide bonds that form numerous, powerful intermolecular hydrogen bonds that cause self-assemblies to form in the DMF solvent. The chiral twists growing over time in this report was an interesting finding. Additionally, authors investigated the nature of assembly in various water concentrations, and it was found that as the water concentration rises, the molecules aggregate tightly and exhibit an increase in chiral twisting. According to Kim *et al.*[42] supramolecular chirality in achiral molecules can be induced and regulated by light. Compound **15** (**Scheme 1.2**) was made by using EDC, HOBT, and trimethylamine in an amide coupling process with triphenylamine and diacetylene moieties. Furthermore, they used R/L CPL to regulate supramolecular chirality while studying the self-assembly of 15 in a chlorinated solvent under the exposure of visible and UV light.

In order to organize achiral Au nanoparticles in supramolecular construction, Jung *et al.*[43] used helical nanofiber frameworks. First, a gelator **16** (benzene-1,3,5-tricarboxamide)

derivative was used to synthesize a chiral supramolecular helical structure (**Fig. 1.4**). Then, to control the helical nature of the gel, chiral components (D/L form) that co-assemble with gelator **16** form a left/right handed helical structure were added. Additionally, helically templated gold nanoparticle superstructures were seen after the inclusion of Au (I) nanoparticle in components **17** or **18** and exposure to Ultraviolet light. UV-irradiation regulates the size of the Au nanoparticles on the spiral framework over time (**Fig. 1.4**).

According to Shen *et al.*, π–π- Stacking induced supramolecular gel to develop. Additionally, it was proposed that stacking could disrupt the C3-symmetric achiral molecule's symmetry in solvents, resulting in chiral construction with right and left handedness. Organogels 1,3,5-tricarboxylate **19–22** (**Fig. 1.5**) substituted with methyl cinnamate were produced in a variety of organic solvents, specifically cyclohexane, where symmetry breaking gel was produced. Helix-like structures of the assembly were also produced with the addition of small amounts of chiral solvents like (R) or (S)-terpinen-4-ol. Self-assembly also maintains its chirality after the elimination of the chiral fluid.[37]

1.3.3 Chiral molecules controlled chirality of achiral building blocks

By using this technique, chirality is transmitted from a chiral molecule to an achiral molecule and transformed into chiral self-assembly. A key factor in the development of chirality is the interplay between achiral and chiral molecules. The transmission of chirality between chiral and achiral compounds depends heavily on non-covalent bonds such as hydrogen bonds, van der Waals forces, host-guest interactions, electrostatic interactions, and hydrophobic interactions. In some circumstances, chiral surroundings or places can also give achiral components chirality. This could be accomplished through the straightforward synthesis of useful achiral molecules, which when combined with chiral molecules that are readily accessible on the market could result in useful supramolecular chiral assemblies. Amino acids are a major source of widely available chiral molecules, and they can affect the chirality of achiral molecules by acting in combination with long alkyl chains that contain chiral amino acids. Additionally, the benefits of using excellent gelators can be investigated.

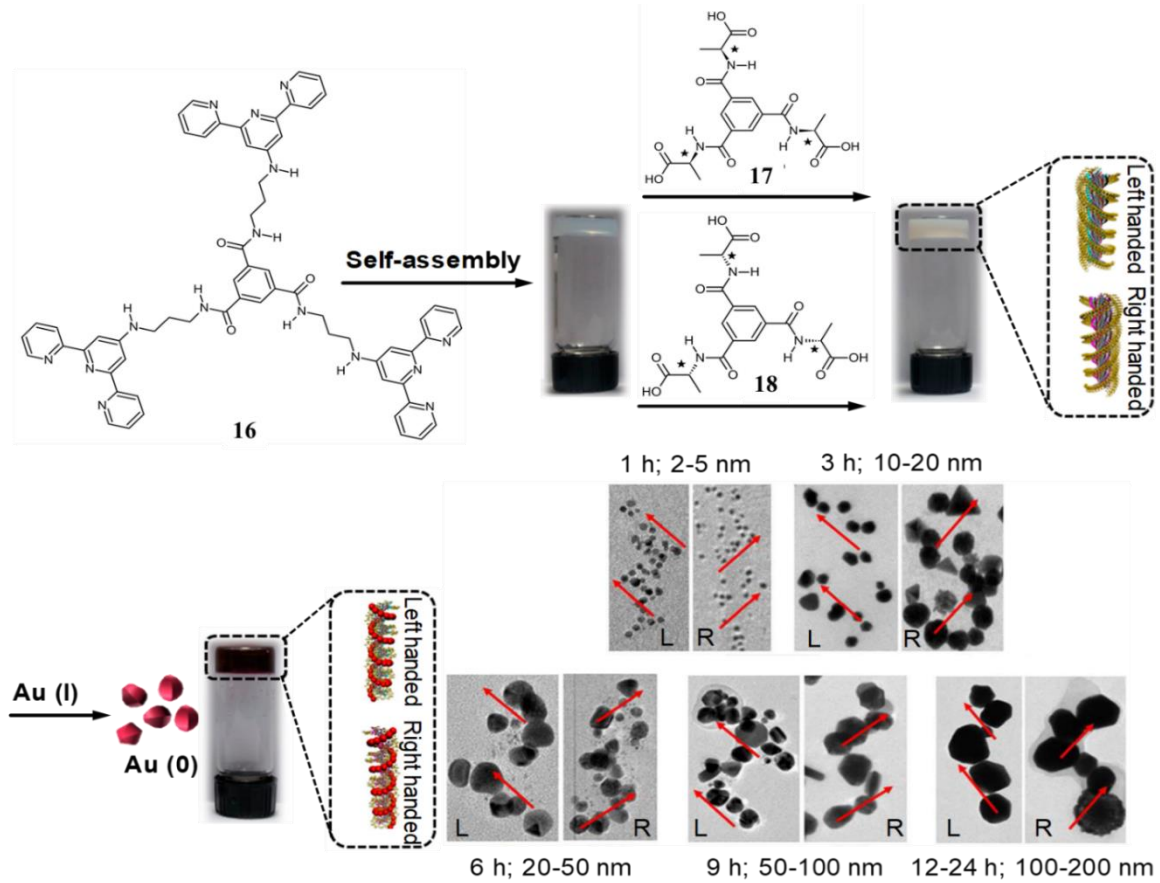

Figure 1.4: Gelator **16** as well as chiral elements **17** (D-form) and **18** (L-form). TEM pictures of the gold nanoparticle superstructures formed on the helical nanofiber template using hydrogel 16 containing 1 equivalent of **17** (D-form) or 1 equivalent of **18** (L-form) for varying UV-irradiation periods.

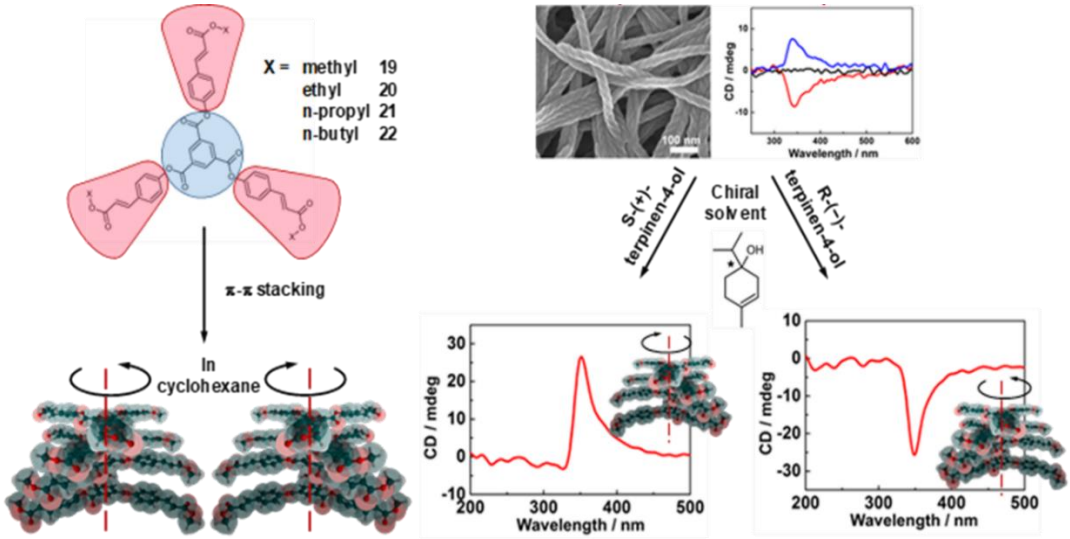

Figure 1.5: The add-remove chiral solvents method and the supramolecular chirality memory provide a graphic representation of symmetry breakdown in cyclohexane and the molecular structure of the achiral C3-symmetric (**19–22**) derivatives.

A naphthalene diimide compound with phosphonic acid groups **23** (**Scheme 1.3**) was previously developed by our group.[44] In water at pH 9, phos-NDI bonded to arginine produces spherical clusters and nano-belts. L-arginine and D-arginine together with phos-NDI produce nano-belts and globular clusters, respectively. We examined the absorption and CD spectra of **23** molecules of D/L-arginine at various values. Understanding how proteins construct particular self-assemblies on various surfaces may be gained from research on NDI-arginine nanoparticles. By using chiral amino acids in water, the Bhosale group reported regulated chiral supramolecular assemblages of achiral porphyrins. First, they created the chiral supramolecular assemblage using water-soluble chiral amino acids D/L-arginine (D/L-Arg) and octaphosphonate-tetraphenylporphyrin **24** (**Scheme 1.3**). Using CD, SEM, and TEM pictures, it was possible to clearly see how the chirality in the system was caused by chiral D- and L-arginine to produce contorted ribbons of right- and left-handed helical structure in water, respectively. The phosphate groups' association with D/L-arginine via hydrogen bonds and the π–π interaction is crucial for the development of chiral self-assembly.[45]

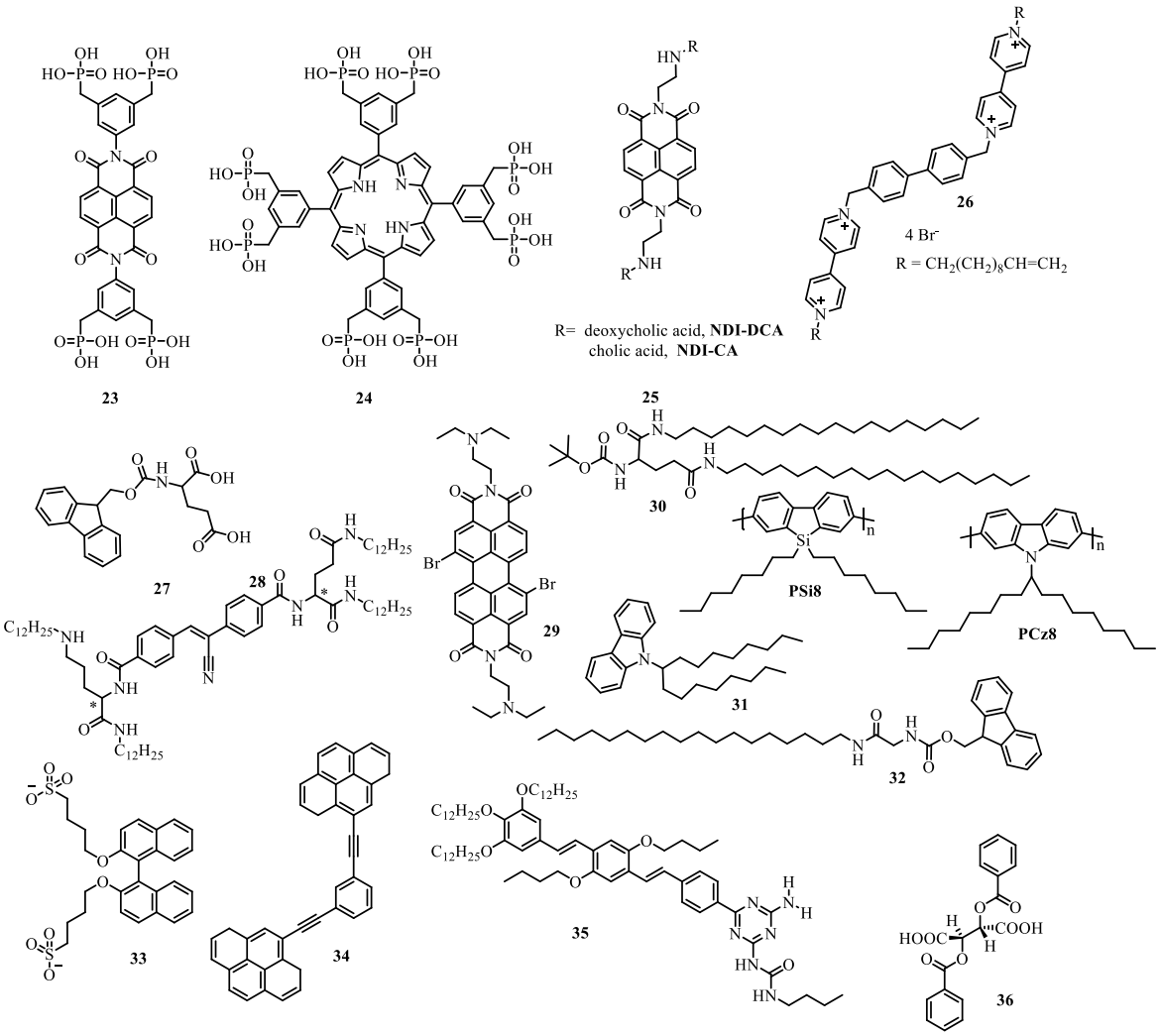

Scheme 1.3: Previously reported structures for chiral assembly.

In the interest of producing chiral molecules **25** that self-assembled into right-handed helical structures, Wagalgave *et al.*[46] combined an achiral NDI core molecule with bile acid derivatives linked by amide links (**Fig. 1.6**). The highly orderly spiral structures, according to the authors, transformed into super-structures through solvophobic effect, hydrogen bonding, and π- interaction. THF-H_2O solvents can produce helical shapes, and the same solvents were used to compare various ratios of fluorescence and absorbance. Helical structures were visible in SEM and TEM images, and CD spectra verified the creation of chiral assemblies. This research may aid in understanding the bio-molecular mechanisms and relationships that occur in DNA and protein.

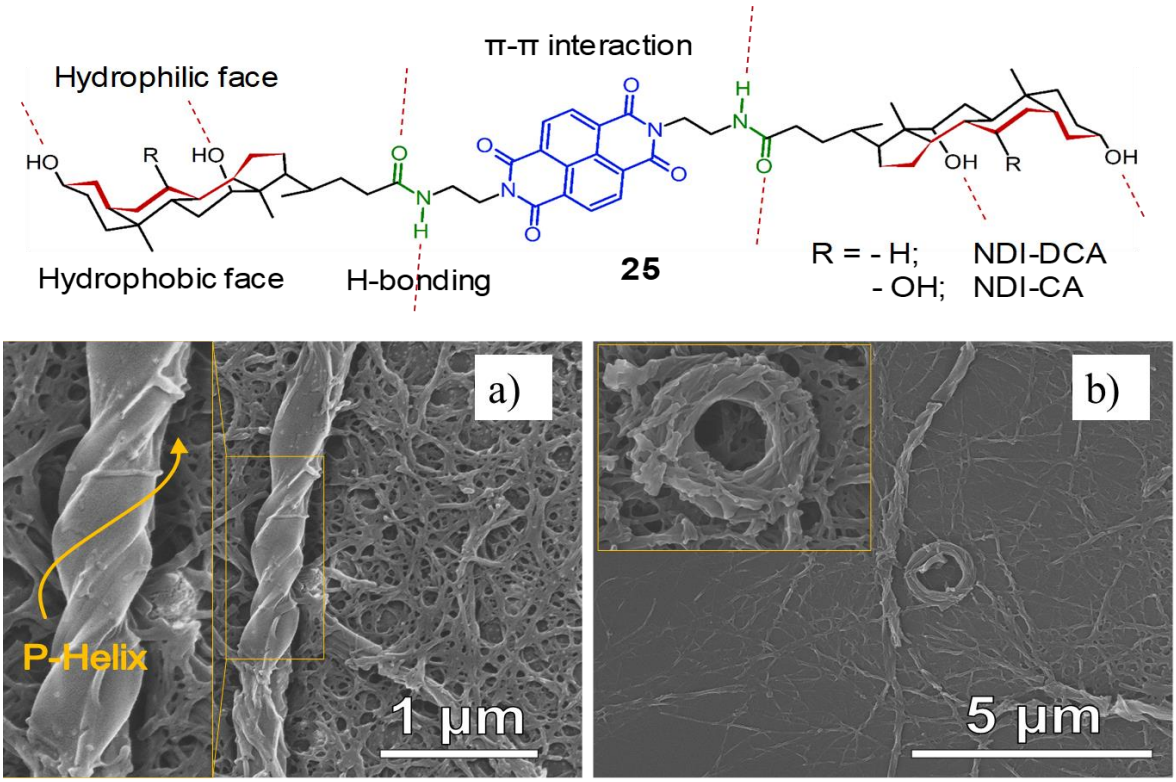

Figure 1.6: Chemical structures of the prepared NDIs with head groups of face amphiphilic cholic acid **25.** SEM images of **25**: a) helical structures from 70% water in THF solution and b) self-assembled rings from 75% water in THF solution.

The chiral memory effect is achieved with macroscopic enantiomerically pure helical and controlled handedness supramolecular strands, according to Olson and his team[47] who are working on supramolecular helical chemistry. Tryptophan (Trp), a natural amino acid, has the capacity to donate electrons when assembled into chiral helix structures, and bis-bipyridinium derivatives **26** (**Scheme 1.3**) function as electron acceptors. Racemic Trp was found to combine with **26** to create equivalent quantities of racemic M (left handed) and P (right handed) helical fibres. Further, M helical fibres were seen when enantiomerically pure L-Trp was used as the source, whereas D-Trp primarily produced P helical fibres. Additionally, fiber-fiber bundling was seen in large, enantiomerically pure helices as a result of numerous smaller helices merging. Melatonin and DAN-DEG, when used to substitute D/L Trp further, both demonstrated a powerful a π-electron donor and the preservation of an enantiomerically pure helical fibre. SEM pictures of pure enantiomerically helical achiral donors being formed. The function of the achiral molecule in multicomponent chiral self-assembly is described by Deng *et al.*[48] In the beginning, authors could create self-assembly using purines A or G and (Fmoc)-protected glutamic acid **27** (**Scheme 1.3**). AFM pictures M-helical structures are produced by Fmoc-L-Glu **27/A**, whereas P-helical structures are

produced by **27/A**. In supramolecular assembly, chirality is transferred from chiral to achiral molecules as evidenced by the formation of spiral structures. It's interesting to note that thioflavinT (ThT) addition resulted in both chirality transfer and (CPL) circular polarised luminescence.

Yang *et al*., described the synthesis of chiral nano-helix assembly, which is based on an achiral acceptor termed 9,10-bis(phenylethynyl)anthracene **28** (**Scheme 1.3**) and a chiral donor named N,N'-bis(dodecyl)-L(D)-amine-glutamic diamide, a stilbene that is cyano-substituted and is in charge. They first produced a chiral nano-helix through the gelation of the donor, which exhibits supramolecular chirality and CPL. Next, they combined the donor gelator with an achiral **28** acceptor to create a D-A composite nano-helix through hydrogen bonding, π-π interaction, and electrostatics. They noticed that not only was energy transferred, but that the circularly polarised fluorescence was also amplified, and they came to the conclusion that this was a novel.[49] In ethanol and toluene, respectively, Duan *et al*.[50] prepared co-gel assemblies of chiral N,N'-bis(octadecyl)-L/Boc-glutamic diamide-D (LBG/DBG) with achiral perylene bisimide **29** (**Scheme 1.3**). Although the aforementioned components were capable of producing strong CD signals that corresponded to PBI in ethanol, faint fluorescence was seen and no CPL signal was found. It's interesting to note that both a powerful fluorescence and a CPL signature could be seen in an acidic environment. In contrast, adding ammonia produces both CPL signs and no release. These structures then exhibit active and passive luminescence in an acidic and basic atmosphere, respectively. Yang and colleagues created a universal method for co-gelating achiral chain polymers to produce helix nano-assemblies. The nano-assemblies are made up of amphiphilic L- or D-glutamide gelator **30** and two achiral main chain polymers **PCz8** and **Psi8** (**Scheme 1.3**). CD spectroscopy and SEM analysis both supported the finding that macroscopic supramolecular chirality for polymers was only seen during the creation of co-gels with gelator. The standout feature of the formed structures was supramolecular chirality that persisted after the gelator was removed.[51]

In a different study, Cao *et al*.[52] explained how the introduction of a low amount of chiral molecules, temperature, and solvent in the self-assembly formation was investigated to transform achiral amino acid derivatives **32**(**Scheme 1.3**) into dendritic chiral nano-twist. A glycine-based achiral molecule was intended to self-assemble, and gelation in an organic solvent was used to achieve this. This self-assembly produces a variety of nanostructures, either at room temperature with a greater concentration or at a lower temperature with a lower concentration. With time, the nanofibers evolved into branching micro-belts. While

microbelts are produced at ambient temperature, nanofibers are formed at low temperatures (-15 °C). The authors were able to regulate the left and right helical shape by adding a small quantity of pure enantiomer (L-FAC18 and D-FAC18). Micro-belts can be further diluted with liquids to produce left and right helical nanofibers. Cheng and group[53] reported chiral binaphthayl sulphonates **33** (**Scheme 1.3**) and bipyrene-based pyridinium **34** as the source of helical nano-rods of supramolecular assembly (**BNS-BPP**) (**Scheme 1.3**). The chirality was transferred from chiral **33** to chiral **34** with the help of π–π and electrostatic interaction, forming the chiral supramolecular assemblage of **33.34**. R/S-BNS was used to create the M/P helical nonorods, which regulated the self-assembly of BPP through layering. In addition to robust CD signals in MeOH: H_2O (1:1) and SEM images with M/P helical Nano-rods at 500nm, the helical nano-rods generate red-coloured CPL signals. Asymmetric noncovalent manufacturing of self-assembled one-dimensional stacks, twisty stacks of achiral oligo(p-phenylenevinylene)ureidotriazine **35** (**Scheme 1.3**) monomers, was reported by George *et al*.[38] The chiral supplementary dibenzoyl tartaric acid **36** (**Scheme 1.3**) D- or L-TA molecules engage with the orthogonal two-point ion pair in the achiral **35** to give it chirality. Curiously, **35** still exhibited chiral memory after the chiral auxiliary was deleted. Guo *et al*.[54] described the self-assembly of the achiral nucleobase thymine with chiral and achiral oligo-(p-phenylenevinylene) compounds **37-39** (**Scheme 1.4**) to reduce surface chirality in multicomponent systems. A chiral OPV created clockwise (CW) and anticlockwise (CCW) rosettes in 1-octanol via hydrogen bonding, whereas an achiral OPV produced both. CW and CCW rosettes were produced by S/R chiral OPV, respectively. Additionally, writers noticed that enantiopure OPV and achiral thymine work together to create supramolecular distreoisomers. At the liquid-solid interface, chiral supramolecular monolayers were shown to develop by Xu *et al*.[55] using achiral oligo(p-phenylene vinylene) OPV4T **40-47**(**Scheme 1.4**) and achiral/chiral solvents. In this study, chiral solvents, sergeant-and-soldiers, and pure enantiomers were used for the production and enhancement of chirality in achiral building blocks. The construction of supramolecular monolayers at the liquid-solid boundaries was observed using these techniques. It was a simple way to prepare chiral

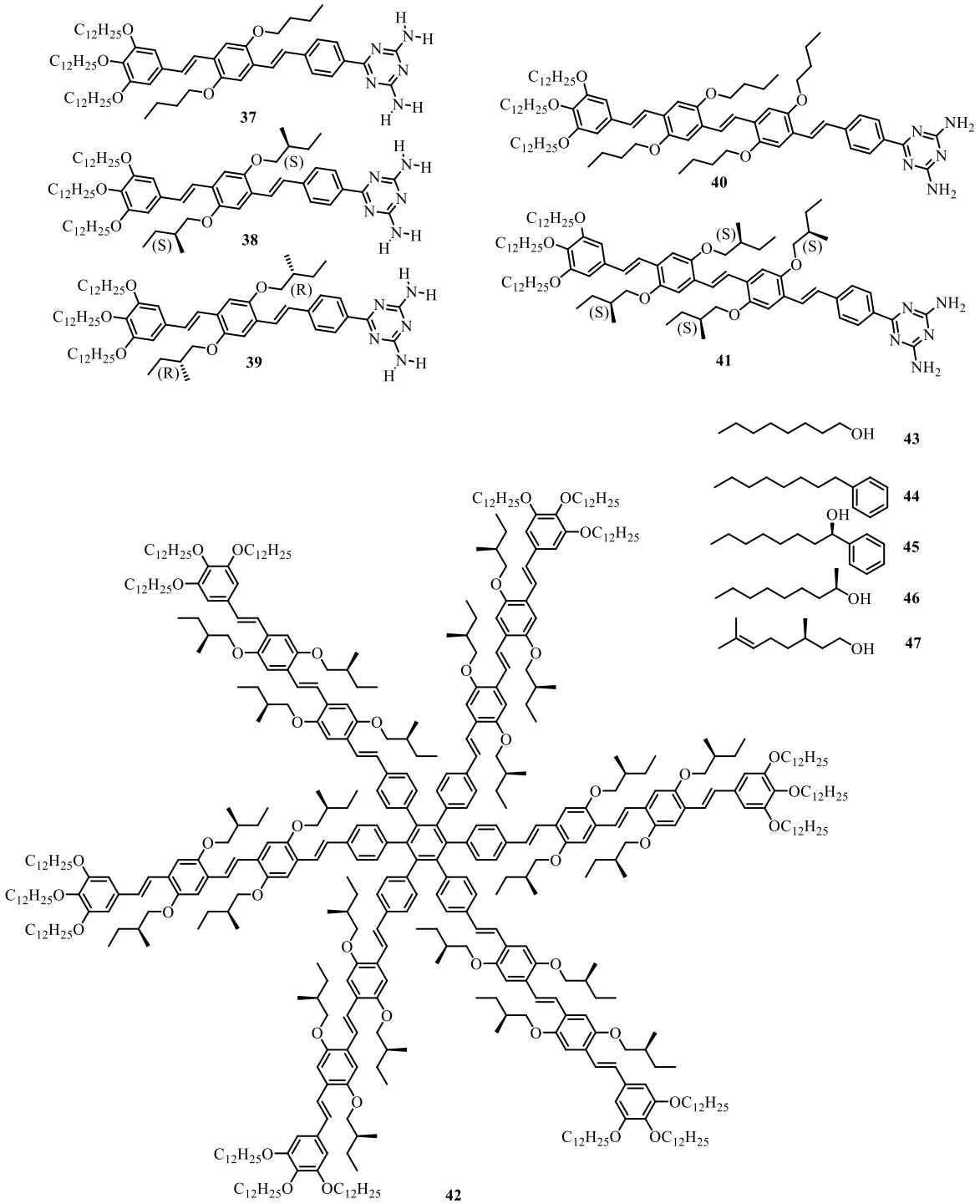

Scheme. 1.4: Chiral molecules used for chiral assembly

surfaces using achiral construction elements. As massive sergeants, chiral molecules transform achiral molecules into chiral monolayers. Supramolecular manufacturing of materials on surfaces involves first applying chiral molecules to the surface, removing extra material, and adding a second component that forms building blocks without interfering with supramolecular assembly. This method demonstrates to be very practical for chirality

induction in achiral molecules **40** (**Scheme 1.4**) and their uses in chiral resolution and asymmetric catalysis. Co-assembled supramolecular chirality calix[4]arene derivatives were reported to have undergone chirality transfer and reversal by Park *et al*.[56] By combining achiral bipyridine parallels (**48 & 49**) with a calix[4]arene-based building block, supramolecular chiral nanostructure can be formed (**Fig. 1.7**). The achiral bypyridine derivatives' chirality was transferred by calix[4]arene derivatives (3D and 3L; **50**). A curious difference between 3D and 3L was observed, with 3D having a **48** form (right handed) P-helical structure and 3L having a 2 form (left handed) M-helical structure. Additionally, inverting a 2D sheet into a coiled tubular construction by adding bipyridine to 0.2 to 0.6 equivalents of 3D or 3L is another method. Chirality inversion is greatly influenced by the amount of glycine molecules present in an achiral building block. Additionally, the reversal of chirality is influenced by the hydrogen bonds between achiral and chiral compounds.

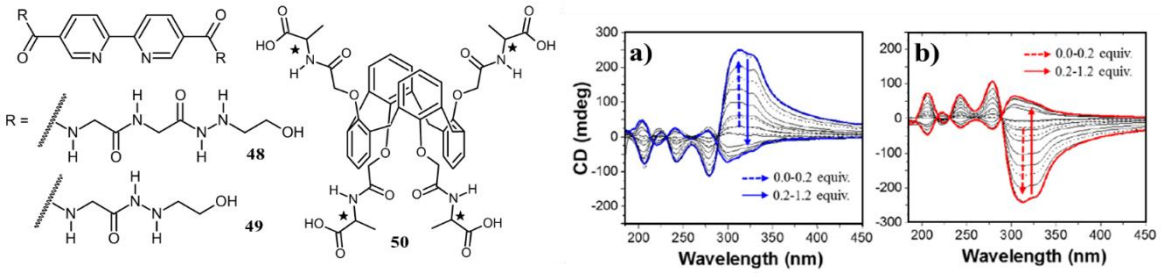

Figure 1.7: Chemical structures of glycine-appended bipyridine derivatives **48**, **49** and alanine appended calix[4]arene 3D, 3L **50**. CD spectra of a) co-hydrogel 1D (1+3D) b) 1L (1 + 3L)

Wang *et al*.[57] used the phenylalanine-glycine **51** chirality produced by bipyridines (**52 and 53**) derivatives to study the regulation of chirality in supramolecular assembly. Initial synthetic bipyridines (DPa) 1,2-di(pyridin-4-yl)ethane, (DPe) (E)-1,2-di(pyridin-4-yl)ethane, and (left-handed LPPG and right-handed DPPG) did not produce the chiral nanostructure. Additionally, when the bipyridine was used as (DPb) 1,4-di(pyridin-4-yl)benzene with (**Fig. 1.8**). Additionally, it was discovered that a shift in the stoichiometry of bipyridine (DPb; **53**) resulted in the chirality of the co-assembly being inverted. When the ratio is adjusted to PPG/DPb=1:2, one other pyridyl of DPb binds only with one end of PPG and forms co-assembly due to π–π stacking and hydrogen bonding in the molecule. The strong hydrogen bonds between pyridine-carboxylic acid result in co-assembly of PPG/DPb = 1:1. By altering the stoichiometry of the compound used in synthesis, the

technique described in this paper can be used to initiate and control chirality. By adjusting the stoichiometry, the works may aid in the study of living and self-assembling aggregates.

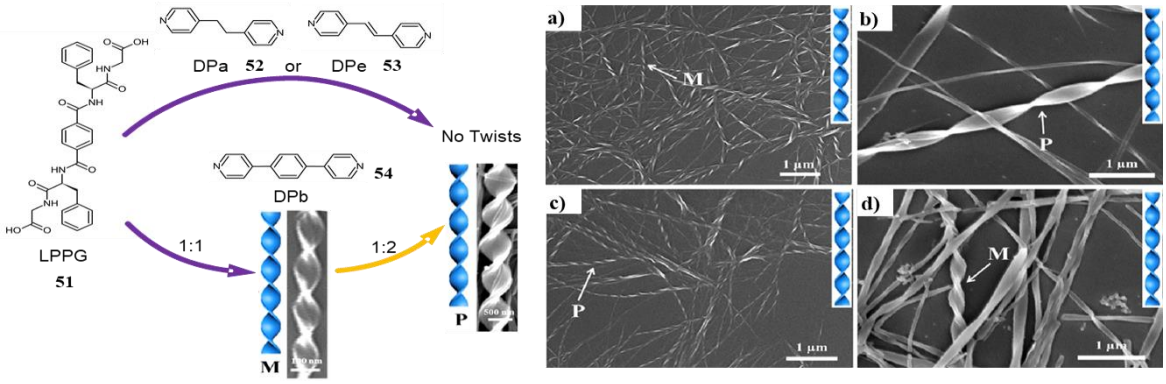

Figure 1.8: Molecular structures of LPPG **51** and bipyridines (DPx), and schematic illustration of nanostructures co-assembled from LPPG **51** with achiral bipyridines (DPa **52**, DPe **53** and DPb **54**) at different ratios. SEM images a), d) M and b), c) P denote left- and right handed chiral nanostructures, respectively.

A technique for reversing the helicity of supramolecular hydrogels caused by achiral substituents was described by Liu and colleagues.[58] From phenylalanine-based gelators **55-58** (**Fig. 1.9**), which displayed chirality reversal through the change of acid to ester functionalities, hydrogels self-assemblies were created. By using SEM, CD, diffraction, and molecular dynamics computations, these inversions of helicity were verified. This study is unique in that it shows how achiral substituents can cause chirality to reverse. The same group[59] created two-component hydrogels with supramolecular chirality using phenylalanine-based enantiomers **59** (**Fig. 1.9**) and achiral bis(pyridinyl) compounds **61** and **62** (**Fig. 1.9**). It was discovered that hydrogels had spiral fibrous shapes. The switch from H to J-aggregation of bis(pyridinyl) compounds caused the helix to invert (**Fig. 1.9**). CD, SEM, FTIR, and a solitary XRD set of data verified the chirality inversion. In LCHF, the helix P and M were produced by switching the bis(pyridinyl) DPDS and E-DPAz derivatives from H to J aggregation, respectively, whereas in DCHF, the helix P and M were produced by J and H aggregation of the above derivatives.

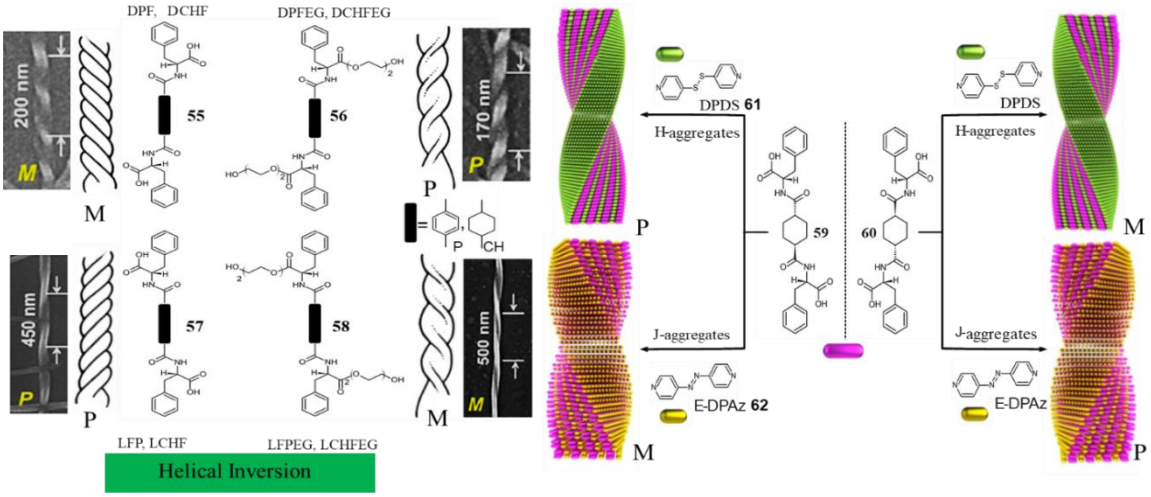

Figure 1.9: SEM images of helical fibers obtained from xerogels and schematic illustration of formation of helical fibers.

1.3.4 π–conjugated molecules

In the area of research, a π-conjugated molecule in supramolecular chirality of self-assembled systems holds a significant place. There are many reasons why π-conjugated molecules are used in field effect transistors (FETs), light emitting diodes (LEDs), solar cells, and other electrical devices. They also have high absorption in the UV-Vis region, which makes it simple to characterise them during CD analysis. Left-handed helix polyanthracene nanofibers were produced by the self-assembly of achiral anthracene monomer, according to Han *et al.*[60] Dehydrocyclization at locations 4, 8, and 16 of the benzene ring of the anthracene monomer in the presence of inert $FeCl_3$ was used to explain the creation of polyanthracene (**Scheme. 1.5**). Left-handed helical strands were produced using the liquid evaporation process. This kind of research provides insight into the transformation of achiral compounds into chiral helical shapes. SEM pictures supported the idea that more condensed material produces dense helical formations.

1.3.5 Amphiphiles

Molecules that contain both hydrophobic and hydrophilic groups are known as amphiphilic substances. The non-polar hydrophobic group is referred to as the tail, and the polar hydrophilic group as the head. In water or an organic fluid, amphiphilic molecules self-assemble to form a range of structures, including micelles, micro emulsions, and vesicles. Chiral hierarchies could create helices, cylinders, ribbons, fibres, and more. According to Barclay *et al.*[61] chiral self-assembly of the amphiphilic molecules **66** and **67** (**Scheme. 1.5**),

which have a glutamic acid (Glu) head group linked to a diphenyldiazenyl (Azo) group by an 11-carbon alkoxy chain and a variable length alkyl chain at the termination, was studied. Originally, a number of amphiphiles were investigated, and it was found that D,L-10-Azo-11-Glu produces nanotubes in TEM images. The intentional production of single enantiomers by authors L-10-Azo-11-Glu and D-10-Azo-11-Glu resulted in chiral aggregations that can be seen in TEM pictures and CD spectra.

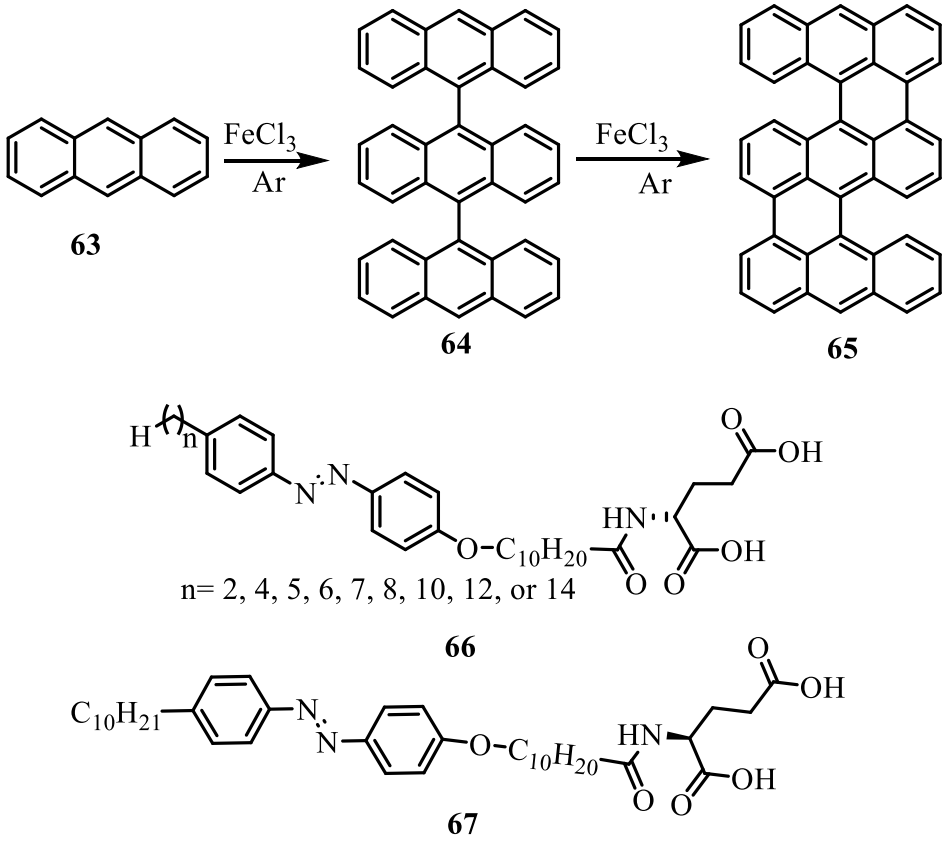

Scheme 1.5: π-conjugated and amphiphiles structures for chiral assembly.

1.4 Regulation of chirality of achiral molecules

In achiral molecule building elements, chirality can be controlled by altering the solvent, pH, temperature, or metal particle. The self-assembly constructed differently in polar and non-polar solvents that controls the supramolecular system's chirality molecules ability to switch between inter-electron transfers on and off can be used to tune the chirality of a system by altering pH in conjunction with protonation or deprotonation in the system.[62] Various temperatures can adjust the chirality of self-assembly, as well as the reversal of different metal ions and the chirality of supramolecular systems.

1.4.1 Solvents

Because of specific interactions between the solvent and the solute, solvents play a

significant role in the self-assembly processes and may have a significant effect on self-assembly. Basic characteristics of the fluid include its solubility, polarity, and volatility. This can help the total supramolecular assembly acquire particular chirality. The chiral structures from naphthalenediimide-tetraphenylethylene with alanine **68** and **69** were reported by Goskulwad *et al.*[63] (**Fig. 1.10**). The chirality of alanine is what causes helicity to be induced in NDI-Ala-TPE self-assemblies. In THF: H_2O at a 40:60 solvent ratio, L/D-alanine produces Left/Right (M/P) handed helix structures, respectively. Since specific clusters were seen when the solvent ratio was changed to 20:80, it can be concluded that solvent ratio is crucial for chiral self-assembly. CD spectra and SEM pictures verified the presence of helical structures (**Fig. 1.10**). Due to the n-type characteristics produced by the NDI core and TPE-based structure, this form of helical structure may be helpful as models for helical crystallisation and optoelectronic devices. The supramolecular self-assemblies of NDI-TPE conjugates with l-alanine **68** and d-alanine **69** were also examined (**Fig. 1.10**). One end of the NDI was connected to chiral arginine, and the other end was connected to a lengthy alkyl chain. Different liquid ratios of THF and H_2O were used to discuss the self-assemblies of **68** and **69**. Microbelts are created by mixing THF and water in a ratio of 40:60, whereas granular microsphere supramolecular formations are created by mixing THF and water in a ratio of 20:80. 10% THF in water; derivatives **68** and **69** create microspheres and belt-like structures, respectively. Using circular dichroism and SEM, the solvophobic impact on the self-assemblies of **68** and **69** was investigated.[64]

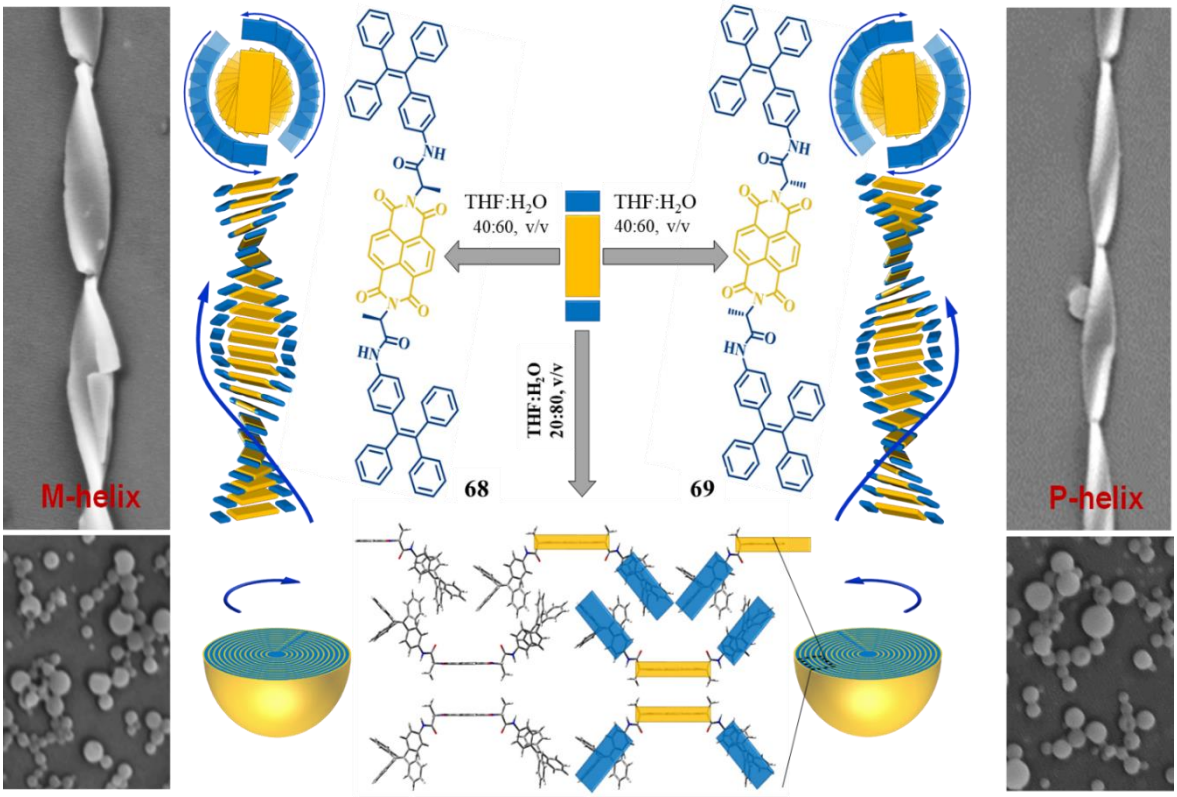

Figure 1.10: NDI-(L-Ala-TPE)2 **68** and NDI-(D-Ala-TPE)2 **69** self-assembly from helical ribbon and nanoparticles as a function of solvophobic effect when adjusted by THF water ratio is shown schematically on the left and right, respectively.

According to Han *et al.*[65] in polar liquids, achiral trigonal molecules **70** (**Fig. 1.11**) were used to build luminous supramolecular nanostructures. Three sterically crowded aromatic rings were directly linked via azo groups to a central benzene centre in C3-symmetric molecules that were created (**Fig. 1.11**). Electron microscopy and X-ray diffractograms backed the hypothesis that π–π stacking and hydrogen bonding contacts led to the self-assembly of an achiral azo-benzene. Interestingly, various aggregation forms (from adhesive helical nanoparticles to crystalline bands and sticks) were produced with various liquids. These arrays have demonstrated the ability to change their helicity and fluorescence strength in reaction to heat and light, making them better candidates for use as artificial light- or heat-based monitors in the future.

The supramolecular assemblage of 1,3-dihydroxyl functionalized naphthalene diimide **71-76** (**Scheme 1.6**) compounds was described by Ghosh *et al.*[66] Tetra-chloroethylene (TCE) causes R-NDI and S-NDI to consolidate, forming ladder-like H-bonded chains with a left-handed and a right-handed helix, respectively. R- and S-isomers in a 1:1 ratio did not gel in

TCE, but the substance did separate out of the examined liquids. Additionally, the precipitated substance yielded unfavourable CD findings. Flash photolysis time-resolved microwave conductivity was used to evaluate the charge-carrier transport properties of supramolecular structures (FP-TRMC).

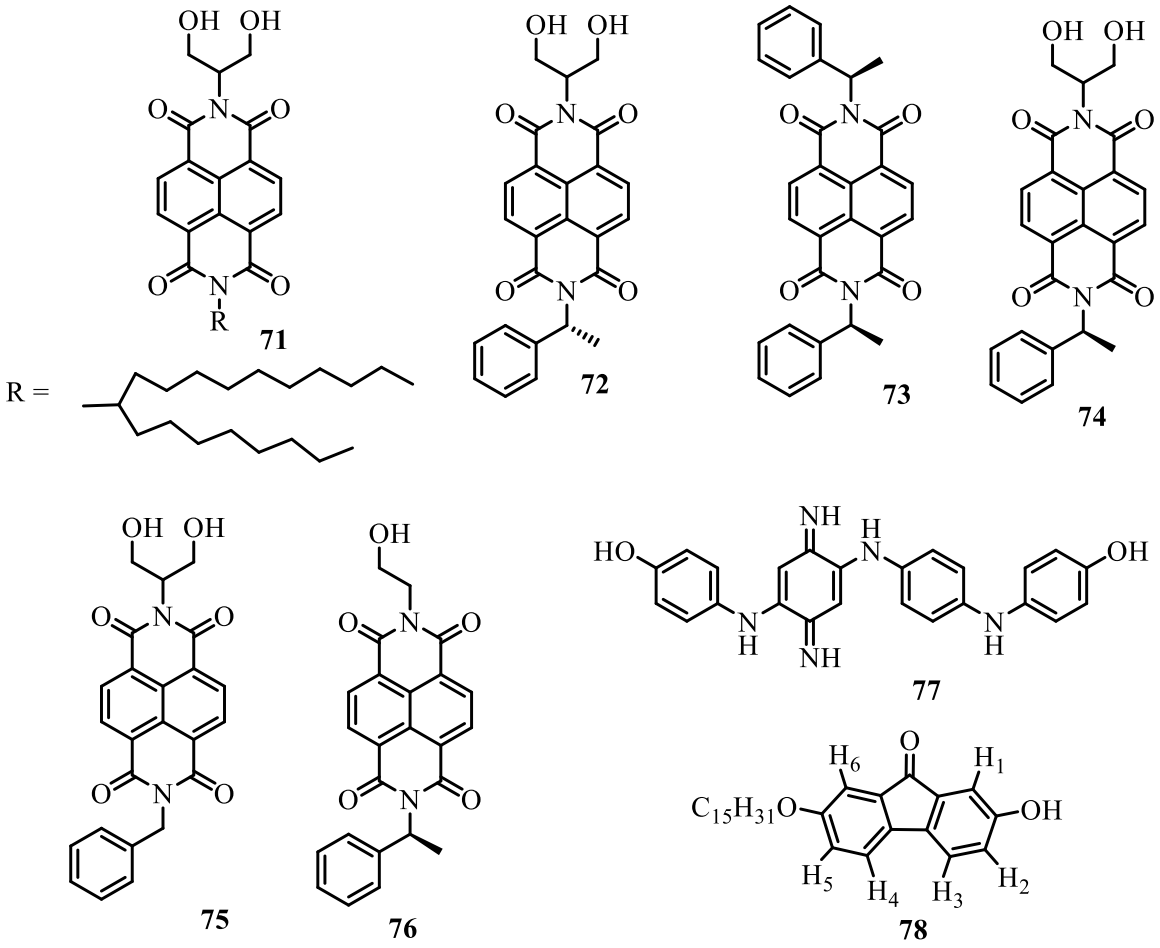

Scheme 1.6: Solvent induced and controlled previously reported molecules for chiral superstructures.

A solvent-controlled supramolecular chirality of achiral conjugated oligoaniline compounds was reported by Zhou *et al*. **77** (**Scheme 1.6**). In a 35% i-propanol/water solvent system, self-assembly was created, and in a 40% i-propanol/water solvent system, contorted nanoribbons with nearly equal amounts of left- and right-handed nanoribbons were created. The method produced fewer left-handed ribbons when the solvent proportion was increased from 40% to 45%, while producing more right-handed ribbons. An essential factor in the formation of chiral self-assembly is the hydrogen bonding between the solvent and achiral molecules, which regulated the chirality and π–π stacking in the oligo aniline derivatives. The positive and negative cotton effects seen in CD spectra verified the right and left twist ribbons creation.[66] The Deng group[67] revealed that achiral molecules can self-assemble

through hydrogen bonding to produce chiral diversity. A variety of solvent systems was used to study the morphologies of (2-hydroxyl-7-pentadecyloxy-9-fluorenone) **78** (**Scheme 1.6**). Initially, varying ratios of mixed solvent (1-octanoic/ 1-octanol, 1/1, *v/v*) were used, and distinct patterns were observed. The alternative pattern was achieved by further adjusting the solvents volume ratio from (1-octanoic/ 1-octanol = 2/1 to 5/1, *v/v*), in which two Nano patterns were observed, one with a clockwise rotation and the other with an anticlockwise rotation linked to a particular molecular orientation. A chiral assemblage was also produced by switching the fluid systems from 1-octanoic acid/1-octanol, which is 6/1 to 10/1. The arrangement of molecules at the liquid/solid boundary is altered by numerous intermolecular hydrogen bonds, resulting in chiral polymorphic nanostructures. Li *et al.*[68] created chiral nanotwists and nanotube structures using their self-assembled system components gelator **81**, C60 **79**, and TPP **80** (**Fig. 1.11**). When doped into the polymer, achiral donor **80** and acceptor guests **79** showed solvent-regulated self-assembly **81**. In DMSO solvent, chiral gelator self-assembles into chiral nanotubes; in toluene solvent, it creates nanotwists. For the first time, the chirality transmission was just controlled by the liquids.

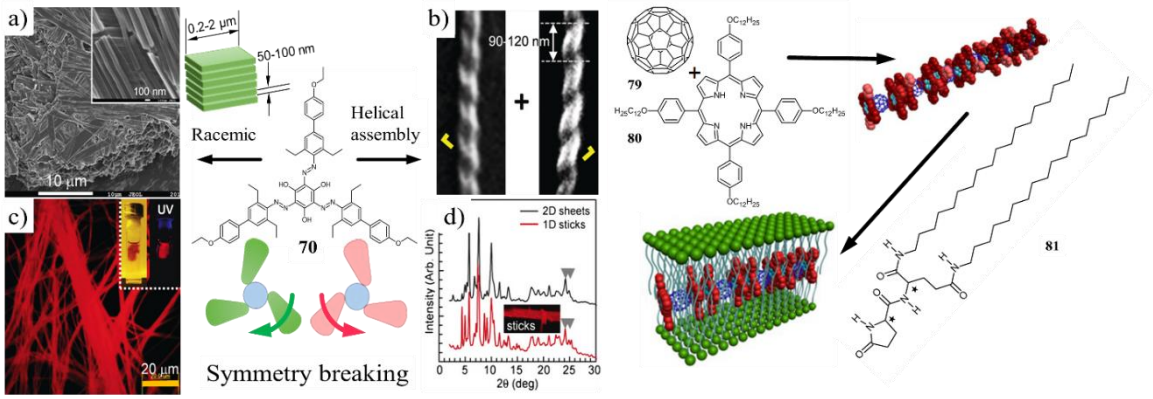

Figure 1.11: Schematic representation of formation chiral assembly.

A sequence of pyrene sandwiches were created by the Takaishi and Ema groups[69] in collaboration, using axially chiral 1,1-binaphthyls. They also looked into the solvent-dependent sign reversal of circularly polarised luminescence (CPL). Their research showed that the hydroxyl-containing molecule (R,R)-3 generates (-)- and (+)-CPL in nonpolar and polar solvents, respectively, with g_{lum} values of -0.012 and +0.012. This flipping behaviour is brought on by the reversal of excimer chirality, which results from intermolecular hydrogen bonding present or absent, respectively. The aforementioned discovery may thus be helpful for the creation of CPL sensing in supramolecular chemistry in the future.

Recently, we described the creation of naphthalenediimide (NDI) amphiphiles with tartaric acid hydroxyl groups that are either acylated or deacylated.[70] Further, we investigated solvent-triggered hierarchical self-assembly of both structures. It's interesting to note that in a solvent system of 30:70 *v/v* THF/MCH, NDI bearing acylated derivative produces biomimetic hairy caterpillar-like superstructures, whereas long helical ribbons are produced in a solvent system of 90:10 *v/v* MCH. Because of the formation of excimers, this derivative shows aggregation-induced emission properties in higher MCH in THF; however, NDI bearing deacylated amphiphile exhibits the complete opposite phenomenon, i.e., aggregation-cause quenching (ACQ) effect and self-assembly of deacylated NDI produces sheets-like microstructures. So, it is evident from this study that solvophobic contact plays a significant part in self-assembling structures.

1.4.2 pH

By altering pH, achiral molecules can be made chiral, which can be used to influence the shape of a self-assembling supramolecular system. Goskulwad *et al.*[71] created the NDI-L-Glu molecule, which combines anionic amino acid L-glutamic acid (L-Glu) as an attachment with π-conjugated naphthalenediimide (NDI) as a central component. The planar, aromatic, and π -conjugated nature of the NDI molecule allows for a variety of uses, including good n-type conductivity, stability, and the capacity to self-assemble into supramolecular structures. L-Glu is a key component of protein agglomeration in biological processes; it causes sickle cell anaemia in people by switching glutamate for valine in the β-globin chain of haemoglobin in blood cells. This study describes how NDI-L-Glu self-assembles into a chiral helical structure with a mixture of left- and right-handed helices at neutral pH. It's interesting to note that when the pH changes from neutral to acidic, the helicity tunes towards left handedness, while at basic conditions, the right helical structures are visible in TEM analysis (**Fig. 1.12**). Synthesized NDI-L-Glu supramolecular self-assembly even exhibits temperature-dependent helical shape switching.

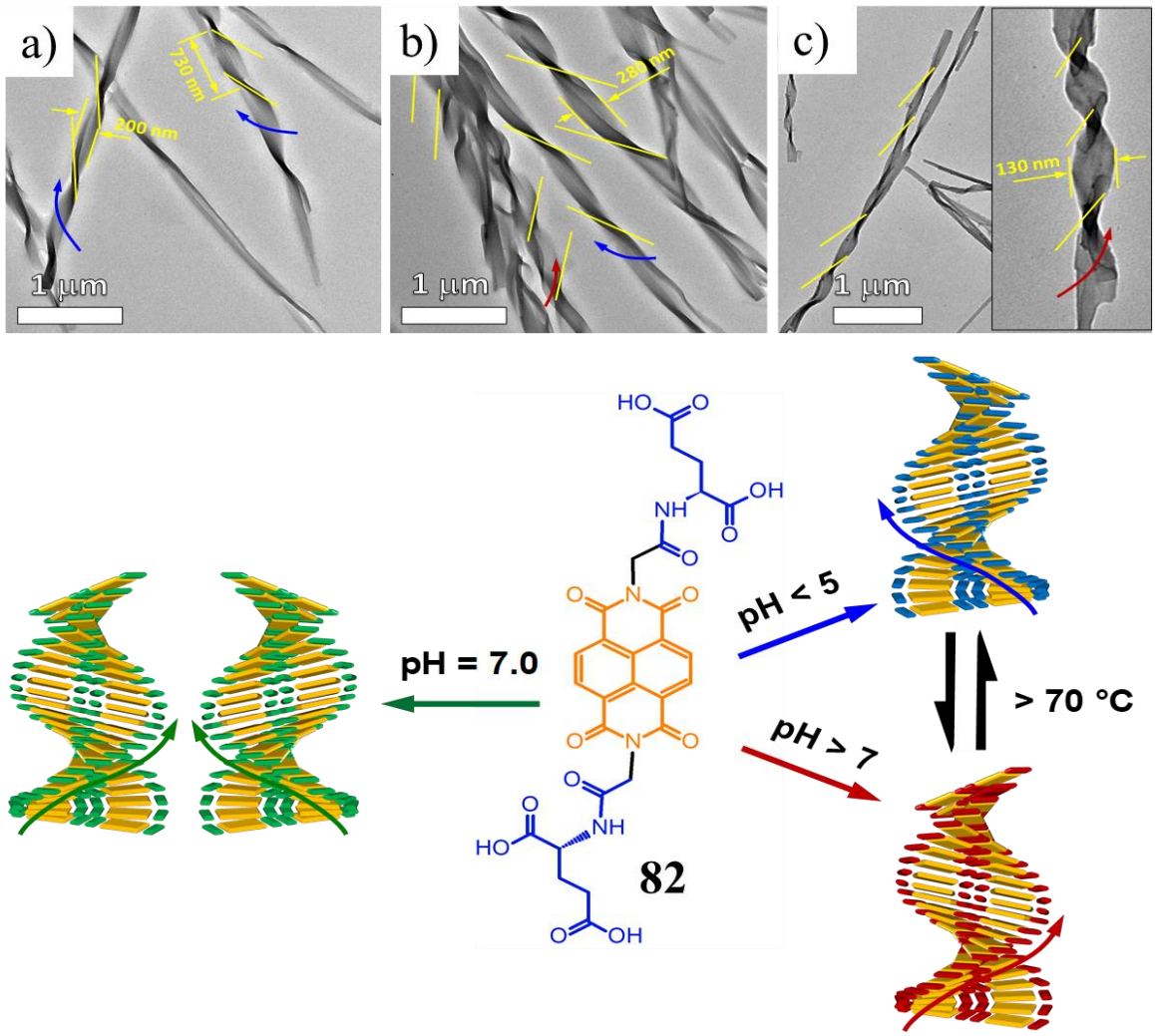

Figure 1.12: TEM imaging to visualise different pH-dependent self-assemblies. Helix shape shown schematically at different pH levels.

Chiral nanotubes made from a commercially advantageous achiral anthraquinone derivative were reported by Aydogan *et al*.[72] In ethanolamine, it has been found that achiral molecules self-assemble into chiral nanotubes by disrupting their symmetry. And when it was discovered that certain assemblies were pH sensitive, the pH was changed in order to regulate the nanotubes' structure. Additionally, NaOH was replaced by ethanolamine in these assemblies, resulting in a combination of helix, tube, and ribbon. Adams group created dipeptides with low molecular weight in water and demonstrated that by adjusting pH, a single dipeptide can be tuned to produce potential enantiomers, diastereomers, and racemates.[73] By adjusting pH, Parquette and colleagues' synthesized coumarin-tetrapeptide compound generates chiral nanotubes and nanoribbons that experience interconversion.[74] This study unequivocally shows that the change from nanotubes to nanoribbon nanostructures was accompanied by an M-P helical inversion, which is a two-step process.

First, coumarin-tetrapeptide conjugate produces nanoribbons through β-sheet and π–π interactions; second, with a slight drop in pH, nanoribbons wound into helical ribbons and simultaneously developed into smooth nanotubes. This study is the first to show that minor pH variations can adjust the chiral supramolecular structures. This finding sheds light on how to regulate chiral nanomaterials made from optically active small peptides and may help with the creation of biomedical or optoelectronic devices in the future. The co-assembly of phenylalanine gelator and achiral cationic polyacrylamide led to the creation of chiral supramolecular superstructures, according to research by the Feng group.[75] Additionally, they noted that even small pH changes have a significant impact on the chirality of nanostructures. For instance, at pH 7, co-assembled hydrogels containing L-enantiomers provide right-handed structures; however, at pH > 7, handedness of supramolecular structures changes to left-handed nanostructures. This work provides useful information on how to regulate chirality in biological systems by merely changing biochemical cues, such as pH, and it may be crucial for future research on living systems. Thus, it is evident that chirality in supramolecular helical superstructures can be adjusted and regulated by adjusting pH.

1.4.3 Temperature

The chirality of supramolecular achiral molecules that self-assemble also depends on temperature; at different temperatures, the chirality is inverted or an achiral sheet is formed. According to Cheng *et al*.[76] temperature has a significant impact on the tuning of achiral to chiral self-assembly at the liquid-solid interface. Chiral 2D nanostructures were designed to form achiral molecules, and at certain temperatures, R and S flower-like structures were observed for the 1 and 2 systems, respectively, at 55 and 60 °C. In scanning tunnelling microscopy STM, the additional chiral fluid was particularly interesting because octanol only produced one R and S flower. Hu *et al*.[77] described achiral porphyrin-derived chiral supramolecular structures in a different study. They discovered that at the beginning of CPL irradiation, porphyrin form regulated handedness of supramolecular structures that are enantioselective and curiously, the chiral structures can be eliminated to the beginning by simple heating. As a result, this occurrence is very intriguing for both heating-induced symmetry breakdown as well as adjusting the achiral porphyrin to chiral supramolecular assemblies. The fabrication of new chiral conducting nanostructures for use in chiral catalysis and optoelectronics may therefore have a bright future in this research. When

temperature, glucose levels, light intensity, and pH levels are altered, phenylboronic acid-capped gold nanorods (PBA-Au NRs) reversibly self-assemble under the guidance of a supramolecular glycopeptide mimic template. They use four cues in this first study to direct reversible supramolecular nanostructures.[78]

1.4.4 Metal

On the basis of how metal ions coordinate to related functional groups of molecules during assembly, metal ions can now also induce or regulate the chirality of supramolecular structures. Two achiral molecules, phthalocyanine (Pc1), which contains eight short alkoxy chains, and cerium double-decker phthalocyanine (Ce(Pc1)2), which contains tetrapyrrole macrocycle rings, were used in Wang *et al.*[79] study on achiral assembly changed to chiral assembly. Phthalocynine was created by π–π interaction and was a good building block. This report stated that interest was moving towards the creation of achiral double-decker phthalocynine (sandwich-type) with metal ions. At room temperature, these achiral double-decker phthalocynines were transformed into optically active supramolecular assemblies by interference of air-water and atmospheric pressure on Pc1 and Ce(Pc1)2 (**Fig. 1.13**). In supramolecular systems, Wang *et al.*[80] described chirality of chiral hydrogel under metal ion regulation. In this study, supramolecular hydrogelators are developed by the coordination of the L-phenylalanine derivatives **85** and **86** with metal ions. Coordination with various metal ions has the potential to invert the supramolecular chirality of the gelator structure. The hydrogen bonds between the amide groups in the metal ion align with the carbonyl group of the amide group already control the chirality of the hydrogel's supramolecular system.

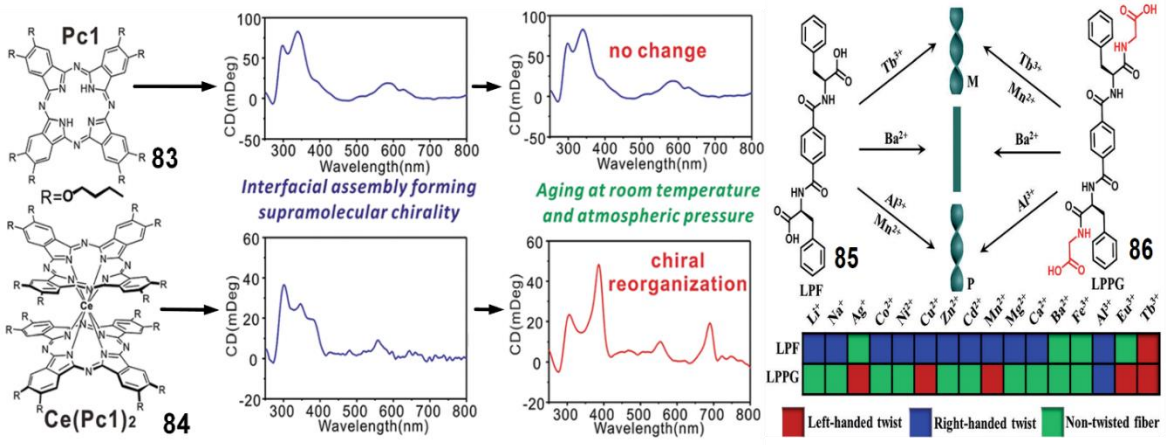

Figure 1.13: Formation of chiral assemblies by changing temperature and inducing metal ion.

In order to investigate for the first time kinetically controlled chiral supramolecular polymerization formed through multiple steps with coordination structural change, Choi *et al.*[81] synthesised a number of bipyridine-based ligands with hydrazine and D- or L-alanine moieties at the alkyl chain groups. Future research on metal-coordinated materials with improved functional characteristics for supramolecular systems and an improved grasp of the chiral assembly process in intricate biological systems may both benefit from their discoveries. In addition to being transmitted to supramolecular self-assembled structures, these control and induction of chirality in supramolecular self-assembly by modulating internal (natural) or external stimulation are also greatly enhanced when combined with a self-organization process. which specifically incorporates one enantiomer or achiral molecule into the particular handedness in helical superstructures that are typically guided by various stimuli like temperature, CPL, solvent, pH, light, glucose, metal, etc.

1.5 Conclusion

In supramolecular chemistry, the study of chirality in self-assembly is one of the most fascinating and fortunate topics. The process of creating supramolecular structures that contain chiral and achiral molecules is dependent on a number of variables, including solvent, temperature, pH, light, and chemical compounds. Asymmetry breaking has been used to transform achiral molecules into supramolecular chiral self-assemblies. Despite this, new supramolecular structures can be created. Typically, chiral supramolecular frameworks are easily constructed in nature using achiral compounds. Additionally, it is more cost-effective to create chiral supramolecular frameworks using achiral molecules than chiral molecules. Because of the majority-rule principle and the sergeant-and-soldier principle, supramolecular chirality from achiral molecules also demonstrates some characteristics, such as chiral memories in assemblages. In self-assembled systems, supramolecular chirality has been shown to be advantageous for chiral molecular identification, chiral detection, asymmetric catalysis, CPL, and chiroptical switching. Supramolecular assemblies are linked to structural regulation, intermolecular interactions, function development, chiral recognition, and many other characteristics. The ability to tune molecules into numerous distinct chiral systems in a cooperative or syndetic manner and be studied is not well understood in biological systems. Ultimately, groundbreaking ideas from organic

supramolecular chemistry, nanosciences, materials science, biology, medicine, and medical science should be incorporated into study on supramolecular chirality.

It's important to remember that controlling helicity with achiral molecules may give full control over how supramolecular chirality is assessed using a variety of stimuli, including light, temperature, fluid, pH, metal, etc. Therefore, we think that chiral catalysis, chiral recognition, chiral sensing, chiral discriminations, and other chiral uses may be made possible in the future by tuning achiral to chiral supramolecular helical superstructures.

References

(1) Williams, G. T.; Haynes, C. J. E.; Fares, M.; Caltagirone, C.; Hiscock, J. R.; Gale, P. A. Advances in Applied Supramolecular Technologies. *Chem. Soc. Rev.* **2021**, *50* (4), 2737–2763. https://doi.org/10.1039/d0cs00948b.

(2) Spectroscopic Study of the Benzene-s-Trinitrobenzene Molecular Complex1. **1952**, *1221*, 8–10.

(3) Topps, J. .; Elliott, R. C. © 1965 Nature Publishing Group. *Nat. Publ. Gr.* **1965**, *205* (5007), 498–499.

(4) Patrick, C. R.; Prosser, G. S. 1960 Nature 1021 Prosser. *Nature* **1960**, No. 4742, 4742.

(5) The Nobel Prize in Chemistry 1987. NobelPrize.org. Nobel Prize Outreach AB 2023. Tue. 28 Feb 2023. https://www.nobelprize.org/prizes/chemistry/1987/summary/.

(6) The Nobel Prize in Chemistry 2016. NobelPrize.org. Nobel Prize Outreach AB 2023. Tue. 28 Feb 2023. https://www.nobelprize.org/prizes/chemistry/2016/summary/.

(7) Lehn, J. M. Cryptates: The Chemistry of Macropolycyclic Inclusion Complexes. *Acc. Chem. Res.* **1978**, *11* (2), 49–57. https://doi.org/10.1021/ar50122a001.

(8) Ariga K.; Kunitake T. *Supramolecular Chemistry – Fundamentals and Applications*; 2006.

(9) J.-M. Lehn. Supramolecular Chemistry-Scope and Perspectives Molecules, Supermolecules, and Molecular Devices (Nobel Lecture). *Angew. Chemie Int. Ed. English* **1988**, *27* (1), 89–112.

(10) Luisi, P. L. From Chemical Origins to Synthetic Biology.

(11) Bonner, W. A. The Origin and Amplification of Biomolecular Chirality. *Orig. Life Evol. Biosph.* **1991**, *21* (2), 59–111. https://doi.org/10.1007/BF01809580.

(12) Palmans, A. R. A.; Meijer, E. W. Amplification of Chirality in Dynamic

Supramolecular Aggregates. *Angew. Chemie - Int. Ed.* **2007**, *46* (47), 8948–8968. https://doi.org/10.1002/anie.200701285.

(13) Fraenkel-Conrat, H.; Williams, R. C. Reconstitution of Active Tobacco Mosaic Virus From Its Inactive Protein and Nucleic Acid Components. *Proc. Natl. Acad. Sci.* **1955**, *41* (10), 690–698. https://doi.org/10.1073/pnas.41.10.690.

(14) Wang, H.; Planchart, A.; Stubbs, G. Caspar Carboxylates: The Structural Basis of Tobamovirus Disassembly. *Biophys. J.* **1998**, *74* (1), 633–638. https://doi.org/10.1016/S0006-3495(98)77822-1.

(15) Percec, V.; Percec, V.; Glodde, M.; Glodde, M.; Bera, T. K.; Bera, T. K.; Miura, Y.; Miura, Y.; Shiyanovskaya, I.; Shiyanovskaya, I.; Singer, K. D.; Singer, K. D.; Balagurusamy, V. S. K.; Balagurusamy, V. S. K.; Heiney, P. A.; Heiney, P. A.; Schnell, I.; Schnell, I.; Rapp, A.; Rapp, A.; Spiess, H.-W.; Spiess, H.-W.; Hudson, S. D.; Hudson, S. D.; Duan, H.; Duan, H. Self-Organization of Supramolecular Helical Dendrimers into Complex Electronic Materials. *Nature* **2002**, *419* (6905), 384–387.

(16) Rudick, J. G.; Percec, V. Induced Helical Backbone Conformations of Self-Organizable Dendronized Polymers. *Acc. Chem. Res.* **2008**, *41* (12), 1641–1652. https://doi.org/10.1021/ar800086w.

(17) Yashima, E.; Ousaka, N.; Taura, D.; Shimomura, K.; Ikai, T.; Maeda, K. Supramolecular Helical Systems: Helical Assemblies of Small Molecules, Foldamers, and Polymers with Chiral Amplification and Their Functions. *Chem. Rev.* **2016**, *116* (22), 13752–13990. https://doi.org/10.1021/acs.chemrev.6b00354.

(18) Michinobu, T.; Shinoda, S.; Nakanishi, T.; Hill, J. P.; Fujii, K.; Player, T. N.; Tsukube, H.; Ariga, K. Mechanical Control of Enantioselectivity of Amino Acid Recognition by Cholesterol-Armed Cyclen Monolayer at the Air-Water Interface. *J. Am. Chem. Soc.* **2006**, *128* (45), 14478–14479. https://doi.org/10.1021/ja066429t.

(19) Shimomura, K.; Ikai, T.; Kanoh, S.; Yashima, E.; Maeda, K. Switchable Enantioseparation Based on Macromolecular Memory of a Helical Polyacetylene in the Solid State. *Nat. Chem.* **2014**, *6* (5), 429–434. https://doi.org/10.1038/nchem.1916.

(20) Bailey, J.; Chrysostomou, A.; Hough, J. H.; Gledhill, T. M.; McCall, A.; Clark, S.; Ménard, F.; Tamura, M. Circular Polarization in Star-Formation Regions: Implications for Biomolecular Homochirality. *Science (80-.).* **1998**, *281* (5377), 672–674. https://doi.org/10.1126/science.281.5377.672.

(21) Mason, S. F. Origins of Biomolecular Handedness. *Nature* **1984**, *311* (5981), 19–23.

https://doi.org/10.1038/311019a0.

(22) Kondepudi, D. K.; Nelson, G. W. Weak Neutral Currents and the Origin of Biomolecular Chirality. **2008**, 11–16. https://doi.org/10.1063/1.51237.

(23) Avalos, M.; Babiano, R.; Cintas, P.; Jiménez, J. L.; Palacios, J. C.; Barron, L. D. Absolute Asymmetric Synthesis under Physical Fields: Facts and Fictions. *Chem. Rev.* **1998**, *98* (7), 2391–2404. https://doi.org/10.1021/cr970096o.

(24) Rikken, G. L. J. A.; Raupach, E. <Nature 2000 Rikken.Pdf>. **2000**, *405* (June).

(25) Ohta, E.; Sato, H.; Ando, S.; Kosaka, A.; Fukushima, T.; Hashizume, D.; Yamasaki, M.; Hasegawa, K.; Muraoka, A.; Ushiyama, H.; Yamashita, K.; Aida, T. Redox-Responsive Molecular Helices with Highly Condensed π-Clouds. *Nat. Chem.* **2011**, *3* (1), 68–73. https://doi.org/10.1038/nchem.900.

(26) Anuradha; La, D. D.; Al Kobaisi, M.; Bhosale, S. V. Right Handed Chiral Superstructures from Achiral Molecules: Self-Assembly with a Twist. *Sci. Rep.* **2015**, *5* (August), 1–11. https://doi.org/10.1038/srep15652.

(27) Cho, J. Il; Tanaka, M.; Sato, S.; Kinbara, K.; Aida, T. Oligo(4-Aminopiperidine-4-Carboxylic Acid): An Unusual Basic Oligopeptide with an Acid-Induced Helical Conformation. *J. Am. Chem. Soc.* **2010**, *132* (38), 13176–13178. https://doi.org/10.1021/ja106118w.

(28) Ariga, K.; Hill, J. P.; Lee, M. V.; Vinu, A.; Charvet, R.; Acharya, S. Challenges and Breakthroughs in Recent Research on Self-Assembly. *Sci. Technol. Adv. Mater.* **2008**, *9* (1). https://doi.org/10.1088/1468-6996/9/1/014109.

(29) Bisoyi, H. K.; Li, Q. Light-Directing Chiral Liquid Crystal Nanostructures: From 1D to 3D. *Acc. Chem. Res.* **2014**, *47* (10), 3184–3195. https://doi.org/10.1021/ar500249k.

(30) Huck, N. P. M.; Jager, W. F.; Lange, B. De; Feringa, B. L. Dynamic Control and Amplification of Molecular Chirality by Circular Polarized Light Author (s): Nina P . M . Huck , Wolter F . Jager , Ben de Lange , Ben L . Feringa Published by : American Association for the Advancement of Science Stable URL : Http:/. **2009**, *273* (5282), 1686–1688.

(31) Van Leeuwen, T.; Heideman, G. H.; Zhao, D.; Wezenberg, S. J.; Feringa, B. L. In Situ Control of Polymer Helicity with a Non-Covalently Bound Photoresponsive Molecular Motor Dopant. *Chem. Commun.* **2017**, *53* (48), 6393–6396. https://doi.org/10.1039/c7cc03188b.

(32) Mtangi, W.; Kiran, V.; Fontanesi, C.; Naaman, R. Role of the Electron Spin

Polarization in Water Splitting. *J. Phys. Chem. Lett.* **2015**, *6* (24), 4916–4922. https://doi.org/10.1021/acs.jpclett.5b02419.

(33) Josse, P.; Favereau, L.; Shen, C.; Dabos-Seignon, S.; Blanchard, P.; Cabanetos, C.; Crassous, J. Enantiopure versus Racemic Naphthalimide End-Capped Helicenic Non-Fullerene Electron Acceptors: Impact on Organic Photovoltaics Performance. *Chem. - A Eur. J.* **2017**, *23* (26), 6277–6281. https://doi.org/10.1002/chem.201701066.

(34) Shang, X.; Song, I.; Ohtsu, H.; Lee, Y. H.; Zhao, T.; Kojima, T.; Jung, J. H.; Kawano, M.; Oh, J. H. Supramolecular Nanostructures of Chiral Perylene Diimides with Amplified Chirality for High-Performance Chiroptical Sensing. *Adv. Mater.* **2017**, *29* (21), 1–7. https://doi.org/10.1002/adma.201605828.

(35) Anuradha; La, D. D.; Al Kobaisi, M.; Gupta, A.; Bhosale, S. V. Chiral Assembly of AIE-Active Achiral Molecules: An Odd Effect in Self-Assembly. *Chem. - A Eur. J.* **2017**, *23* (16), 3950–3956. https://doi.org/10.1002/chem.201605458.

(36) Liu, Y.; Jia, Y.; Zhu, E.; Liu, L.; Qiao, Y.; Che, G.; Yin, B. Supramolecular Helical Nanofibers Formed by an Achiral Monopyrrolotetrathiafulvalene Derivative: Water-Triggered Gelation and Chiral Evolution. *New J. Chem.* **2017**, *41* (19), 11060–11068. https://doi.org/10.1039/c7nj02215h.

(37) Shen, Z.; Jiang, Y.; Wang, T.; Liu, M. Symmetry Breaking in the Supramolecular Gels of an Achiral Gelator Exclusively Driven by π-π Stacking. *J. Am. Chem. Soc.* **2015**, *137* (51), 16109–16115. https://doi.org/10.1021/jacs.5b10496.

(38) George, S. J.; De Bruijn, R.; Tomović, Ž̂eljko; Van Averbeke, B.; Beljonne, D.; Lazzaroni, R.; Schenning, A. P. H. J.; Meijer, E. W. Asymmetric Noncovalent Synthesis of Self-Assembled One-Dimensional Stacks by a Chiral Supramolecular Auxiliary Approach. *J. Am. Chem. Soc.* **2012**, *134* (42), 17789–17796. https://doi.org/10.1021/ja3086005.

(39) Shaikh, D. B.; Bhosale, R. S.; La, D. D.; Al Kobaisi, M.; Bhosale, S. V.; Bhosale, S. V. Chiral Supramolecular Assemblies from an Achiral Naphthalene Diimide Bearing a Urea Moiety. *Chem. - An Asian J.* **2018**, *13* (21), 3268–3273. https://doi.org/10.1002/asia.201801115.

(40) Hu, J.; Gao, L.; Zhu, Y.; Wang, P.; Lin, Y.; Sun, Z.; Yang, S.; Wang, Q. Chiral Assemblies from an Achiral Pyridinium-Tailored Anthracene. *Chem. - A Eur. J.* **2017**, *23* (6), 1422–1426. https://doi.org/10.1002/chem.201604730.

(41) Wang, Y.; Zhou, D.; Li, H.; Li, R.; Zhong, Y.; Sun, X.; Sun, X. Hydrogen-Bonded

Supercoil Self-Assembly from Achiral Molecular Components with Light-Driven Supramolecular Chirality. *J. Mater. Chem. C* **2014**, *2* (31), 6402–6409. https://doi.org/10.1039/c4tc00649f.

(42) Kim, J.; Lee, J.; Kim, W. Y.; Kim, H.; Lee, S.; Lee, H. C.; Lee, Y. S.; Seo, M.; Kim, S. Y. Induction and Control of Supramolecular Chirality by Light in Self-Assembled Helical Nanostructures. *Nat. Commun.* **2015**, *6*, 1–8. https://doi.org/10.1038/ncomms7959.

(43) Jung, S. H.; Jeon, J.; Kim, H.; Jaworski, J.; Jung, J. H. Chiral Arrangement of Achiral Au Nanoparticles by Supramolecular Assembly of Helical Nanofiber Templates. *J. Am. Chem. Soc.* **2014**, *136* (17), 6446–6452. https://doi.org/10.1021/ja5018199.

(44) Nandre, K. P.; Bhosale, S. V.; Krishna, K. V. S. R.; Gupta, A.; Bhosale, S. V. A Phosphonic Acid Appended Naphthalene Diimide Motif for Self-Assembly into Tunable Nanostructures through Molecular Recognition with Arginine in Water. *Chem. Commun.* **2013**, *49* (48), 5444–5446. https://doi.org/10.1039/c3cc41259h.

(45) Rananaware, A.; Samanta, M.; Bhosale, R. S.; Kobaisi, M. Al; Roy, B.; Bheemireddy, V.; Bhosale, S. V.; Bandyopadhyay, S.; Bhosale, S. V. Photomodulation of Fluoride Ion Binding through Anion-φ Interactions Using a Photoswitchable Azobenzene System. *Sci. Rep.* **2016**, *6* (March), 1–10. https://doi.org/10.1038/srep22928.

(46) Wagalgave, S. M.; Padghan, S. D.; Burud, M. D.; Kobaisi, M. Al; La, D. D.; Bhosale, R. S.; Bhosale, S. V.; Bhosale, S. V. Supramolecular Super-Helix Formation via Self-Assembly of Naphthalene Diimide Functionalised with Bile Acid Derivatives. *Sci. Rep.* **2019**, *9* (1), 1–9. https://doi.org/10.1038/s41598-019-49235-5.

(47) Yuan, T.; Sun, Z.; Mu, A. U.; Zeng, M.; Kalin, A. J.; Cheng, Z.; Olson, M. A.; Fang, L. Cover Feature: Assembly and Chiral Memory Effects of Dynamic Macroscopic Supramolecular Helices (Chem. Eur. J. 62/2018). *Chem. - A Eur. J.* **2018**, *24* (62), 16453–16453. https://doi.org/10.1002/chem.201804589.

(48) Deng, M.; Zhang, L.; Jiang, Y.; Liu, M. Role of Achiral Nucleobases in Multicomponent Chiral Self-Assembly: Purine-Triggered Helix and Chirality Transfer. *Angew. Chemie - Int. Ed.* **2016**, *55* (48), 15062–15066. https://doi.org/10.1002/anie.201608638.

(49) Yang, D.; Duan, P.; Zhang, L.; Liu, M. Chirality and Energy Transfer Amplified Circularly Polarized Luminescence in Composite Nanohelix. *Nat. Commun.* **2017**, *8* (11), 1–9. https://doi.org/10.1038/ncomms15727.

(50) Han, D.; Han, J.; Huo, S.; Qu, Z.; Jiao, T.; Liu, M.; Duan, P. Proton Triggered Circularly Polarized Luminescence in Orthogonal- and Co-Assemblies of Chiral Gelators with Achiral Perylene Bisimide. *Chem. Commun.* **2018**, *54* (44), 5630–5633. https://doi.org/10.1039/c8cc02777c.

(51) Yang, D.; Zhao, Y.; Lv, K.; Wang, X.; Zhang, W.; Zhang, L.; Liu, M. A Strategy for Tuning Achiral Main-Chain Polymers into Helical Assemblies and Chiral Memory Systems. *Soft Matter* **2016**, *12* (4), 1170–1175. https://doi.org/10.1039/c5sm02547h.

(52) Cao, H.; Yuan, Q.; Zhu, X.; Zhao, Y. P.; Liu, M. Hierarchical Self-Assembly of Achiral Amino Acid Derivatives into Dendritic Chiral Nanotwists. *Langmuir* **2012**, *28* (43), 15410–15417. https://doi.org/10.1021/la303263g.

(53) Wang, Y.; Li, X.; Li, F.; Sun, W. Y.; Zhu, C.; Cheng, Y. Strong Circularly Polarized Luminescence Induced from Chiral Supramolecular Assembly of Helical Nanorods. *Chem. Commun.* **2017**, *53* (54), 7505–7508. https://doi.org/10.1039/c7cc04363e.

(54) Guo, Z.; De Cat, I.; Van Averbeke, B.; Lin, J.; Wang, G.; Xu, H.; Lazzaroni, R.; Beljonne, D.; Schenning, A. P. H. J.; De Feyter, S. Affecting Surface Chirality via Multicomponent Adsorption of Chiral and Achiral Molecules. *Chem. Commun.* **2014**, *50* (80), 11903–11906. https://doi.org/10.1039/c4cc04393f.

(55) Xu, H.; Ghijsens, E.; George, S. J.; Wolffs, M.; Tomovič, Ž.; Schenning, A. P. H. J.; De Feyter, S. Chiral Induction and Amplification in Supramolecular Systems at the Liquid-Solid Interface. *ChemPhysChem* **2013**, *14* (8), 1583–1590. https://doi.org/10.1002/cphc.201300212.

(56) Choi, H.; Cho, K. J.; Seo, H.; Ahn, J.; Liu, J.; Lee, S. S.; Kim, H.; Feng, C.; Jung, J. H. Transfer and Dynamic Inversion of Coassembled Supramolecular Chirality through 2D-Sheet to Rolled-Up Tubular Structure. *J. Am. Chem. Soc.* **2017**, *139* (49), 17711–17714. https://doi.org/10.1021/jacs.7b09760.

(57) Wang, F.; Feng, C. L. Stoichiometry-Controlled Inversion of Supramolecular Chirality in Nanostructures Co-Assembled with Bipyridines. *Chem. - A Eur. J.* **2018**, *24* (7), 1509–1513. https://doi.org/10.1002/chem.201704431.

(58) Liu, G.; Li, X.; Sheng, J.; Li, P. Z.; Ong, W. K.; Phua, S. Z. F.; Ågren, H.; Zhu, L.; Zhao, Y. Helicity Inversion of Supramolecular Hydrogels Induced by Achiral Substituents. *ACS Nano* **2017**, *11* (12), 11880–11889. https://doi.org/10.1021/acsnano.7b06097.

(59) Liu, G.; Sheng, J.; Wu, H.; Yang, C.; Yang, G.; Li, Y.; Ganguly, R.; Zhu, L.; Zhao, Y. Controlling Supramolecular Chirality of Two-Component Hydrogels by J- and H-

Aggregation of Building Blocks. *J. Am. Chem. Soc.* **2018**, *140* (20), 6467–6473. https://doi.org/10.1021/jacs.8b03309.

(60) Han, B.; Shen, F.; Su, H.; Zhang, X.; Shen, Y.; Zhang, T. Self-Assembly of Achiral Monomer into Left-Handed Helical Polyanthracene Nanofibers. *Mater. Express* **2016**, *6* (1), 88–92. https://doi.org/10.1166/mex.2016.1274.

(61) Barclay, T. G.; Constantopoulos, K.; Zhang, W.; Fujiki, M.; Petrovsky, N.; Matisons, J. G. Chiral Self-Assembly of Designed Amphiphiles: Influences on Aggregate Morphology. *Langmuir* **2013**, *29* (32), 10001–10010. https://doi.org/10.1021/la401987y.

(62) Zhang, L.; Qin, L.; Wang, X.; Cao, H.; Liu, M. Supramolecular Chirality in Self-Assembled Soft Materials: Regulation of Chiral Nanostructures and Chiral Functions. *Adv. Mater.* **2014**, *26* (40), 6959–6964. https://doi.org/10.1002/adma.201305422.

(63) Goskulwad, S. P.; Kobaisi, M. Al; La, D. D.; Bhosale, R. S.; Ratanlal, M.; Bhosale, S. V.; Bhosale, S. V. Supramolecular Chiral Helical Ribbons of Tetraphenylethylene-Appended Naphthalenediimide Controlled by Solvent and Induced by l- and d-Alanine Spacers. *Chem. - An Asian J.* **2018**, *13* (24), 3947–3953. https://doi.org/10.1002/asia.201801421.

(64) Goskulwad, S. P.; More, V. G.; Kobaisi, M. Al; Bhosale, R. S.; La, D. D.; Antolasic, F.; Bhosale, S. V.; Bhosale, S. V. Solvent-Induced Self-Assembly of Naphthalenediimide Conjugated to Tetraphenylethene through D- and L-Alanine. *ChemistrySelect* **2019**, *4* (9), 2626–2633. https://doi.org/10.1002/slct.201900087.

(65) Han, M.; Cho, S. J.; Norikane, Y.; Shimizu, M.; Seki, T. Assembly of an Achiral Chromophore into Light-Responsive Helical Nanostructures in the Absence of Chiral Components. *Chem. - A Eur. J.* **2016**, *22* (12), 3971–3975. https://doi.org/10.1002/chem.201600227.

(66) Ghosh, G.; Paul, M.; Sakurai, T.; Matsuda, W.; Seki, S.; Ghosh, S. Supramolecular Chirality Issues in Unorthodox Naphthalene Diimide Gelators. *Chem. - A Eur. J.* **2018**, *24* (8), 1938–1946. https://doi.org/10.1002/chem.201704825.

(67) Miao, K.; Hu, Y.; Xu, L.; Dong, M.; Wu, J.; Miao, X.; Deng, W. Chiral Polymorphism in the Self-Assemblies of Achiral Molecules Induced by Multiple Hydrogen Bonds. *Phys. Chem. Chem. Phys.* **2018**, *20* (16), 11160–11173. https://doi.org/10.1039/c8cp00591e.

(68) Li, Y.; Duan, P.; Liu, M. Solvent-Regulated Self-Assembly of an Achiral Donor–

Acceptor Complex in Confined Chiral Nanotubes: Chirality Transfer, Inversion and Amplification. *Chem. - A Eur. J.* **2017**, *23* (34), 8225–8231. https://doi.org/10.1002/chem.201700613.

(69) Takaishi, K.; Iwachido, K.; Ema, T. Solvent-Induced Sign Inversion of Circularly Polarized Luminescence: Control of Excimer Chirality by Hydrogen Bonding. *J. Am. Chem. Soc.* **2020**, *142* (4), 1774–1779. https://doi.org/10.1021/jacs.9b13184.

(70) Shejul, D. A.; Wagalgave, S. M.; Jadhav, R. W.; Kobaisi, M. Al; La, D. D.; Jones, L. A.; Bhosale, R. S.; Bhosale, S. V.; Bhosale, S. V. Aggregation-Induced Emission Characteristics and Solvent Triggered Hierarchical Self-Assembled Chiral Superstructures of Naphthalenediimide Amphiphiles. *New J. Chem.* **2020**, *44* (4), 1615–1623. https://doi.org/10.1039/c9nj05137f.

(71) Goskulwad, S.; La, D. D.; Kobaisi, M. Al; Bhosale, S. V.; Bansal, V.; Vinu, A.; Ariga, K.; Bhosale, S. V. Dynamic Multistimuli-Responsive Reversible Chiral Transformation in Supramolecular Helices. *Sci. Rep.* **2018**, *8* (1), 1–11. https://doi.org/10.1038/s41598-018-29152-9.

(72) Unsal, H.; Aydogan, N. Formation of Chiral Nanotubes by the Novel Anthraquinone Containing-Achiral Molecule. *J. Colloid Interface Sci.* **2013**, *394* (1), 301–311. https://doi.org/10.1016/j.jcis.2012.12.023.

(73) McAulay, K.; Dietrich, B.; Su, H.; Scott, M. T.; Rogers, S.; Al-Hilaly, Y. K.; Cui, H.; Serpell, L. C.; Seddon, A. M.; Draper, E. R.; Adams, D. J. Using Chirality to Influence Supramolecular Gelation. *Chem. Sci.* **2019**, *10* (33), 7801–7806. https://doi.org/10.1039/c9sc02239b.

(74) Mason, M. L.; Lalisse, R. F.; Finnegan, T. J.; Hadad, C. M.; Modarelli, D. A.; Parquette, J. R. PH-Controlled Chiral Packing and Self-Assembly of a Coumarin Tetrapeptide. *Langmuir* **2019**, *35* (38), 12460–12468. https://doi.org/10.1021/acs.langmuir.9b01939.

(75) Kousar, A.; Liu, J.; Mehwish, N.; Wang, F.; Dang-i, A. Y.; Feng, C. PH-Regulated Supramolecular Chirality of Phenylalanine-Based Hydrogels. *Mater. Today Chem.* **2019**, *11*, 217–224. https://doi.org/10.1016/j.mtchem.2018.11.005.

(76) Cheng, L.; Li, Y.; Zhang, C. Y.; Gong, Z. L.; Fang, Q.; Zhong, Y. W.; Tu, B.; Zeng, Q.; Wang, C. Temperature-Triggered Chiral Self-Assembly of Achiral Molecules at the Liquid-Solid Interface. *ACS Appl. Mater. Interfaces* **2016**, *8* (46), 32004–32010. https://doi.org/10.1021/acsami.6b10883.

(77) Hu, J.; Xie, Y.; Zhang, H.; He, C.; Zhang, Q.; Zou, G. Chiral Induction, Modulation

and Locking in Porphyrin Based Supramolecular Assemblies with Circularly Polarized Light. *Chem. Commun.* **2019**, *55* (34), 4953–4956. https://doi.org/10.1039/c9cc01613a.

(78) Chen, L.; Zheng, J.; Feng, J.; Qian, Q.; Zhou, Y. Reversible Modulation of Plasmonic Chiral Signals of Achiral Gold Nanorods Using a Chiral Supramolecular Template. *Chem. Commun.* **2019**, *55* (76), 11378–11381. https://doi.org/10.1039/c9cc06050b.

(79) Wang, X.; Liu, C.; Jiang, Y.; Wang, C.; Wang, T.; Bai, M.; Jiang, J. Room Temperature Chiral Reorganization of Interfacial Assembly of Achiral Double-Decker Phthalocyanine. *Phys. Chem. Chem. Phys.* **2018**, *20* (10), 7223–7229. https://doi.org/10.1039/c7cp08647d.

(80) Wang, F.; Feng, C.-L. Metal-Ion-Mediated Supramolecular Chirality of l -Phenylalanine Based Hydrogels . *Angew. Chemie* **2018**, *130* (20), 5757–5761. https://doi.org/10.1002/ange.201800251.

(81) Choi, H.; Heo, S.; Lee, S.; Kim, K. Y.; Lim, J. H.; Jung, S. H.; Lee, S. S.; Miyake, H.; Lee, J. Y.; Jung, J. H. Kinetically Controlled Ag+-Coordinated Chiral Supramolecular Polymerization Accompanying a Helical Inversion. *Chem. Sci.* **2020**, *11* (3), 721–730. https://doi.org/10.1039/c9sc04958d.

Section II: literature study on sensing application

1.6 Introduction

Chemosensors for anions and cations detections are widely used in medicine, environmental science, biology, and chemistry, among other fields. The subfield of supramolecular chemistry that this is has been studied for more than 150 years. It concerns chemosensors that distinguish between and find anions and cations using optical or electrical signals. Currently, a wide range of reliable chemosensors is in place to find both anions and cations. Chemosensors can also be used to create sensory devices, remove anions and cations, and divide them. Chemosensors can identify poisonous cations like mercury as well as anions like fluorine and cyanide. Chemosensors are now a popular subfield of supramolecular chemistry as an outcome. This part concentrates on the use of optical chemosensors for anions and cations detection using colorimetric and fluorometric methods.[1]

A "molecule of abiotic origin that indicates the existence of matter or energy" is how Czarnick describes the chemosensor.[2] Additionally, chemosensors are molecular receptors that have the ability to detect, accurately engage with, and produce a detectable signal in reaction to an analyte. Electric or optical signals are both acceptable. It comprises of a signalling portion and a sensing portion. Both discrimination and binding effectiveness are the responsibility of the detection group. The signaling component is responsible for transforming information into a signal that can be detected.

Chemosensors have received a lot of attention recently due to their photophysical characteristics that are sensitive to the environment. Optical signal changes can reveal information about chemistry factors like pH and analyte concentration.[3] To detect heavy metal ions, chemosensors are intensively investigated.[4,5] Colorimetric and fluorometric chemosensors are two categories of optical chemosensors. The benefit of colorimetric receptors is that they can easily notice changes in color with the naked eye, simplifying the procedure. The ratio between the intensities of two emissions, on the other hand, makes fluorometric chemosensors more preferred for ratiometric responses and enables correction of the sensor's analysis concentration as well as the effects of the environment, such as temperature and orientation.[6] Chemosensors that are sensitive towards particular hazardous ions are in high demand right now. Researchers have created chromophores that are selective to a particular anion or cation because some anions and cations are harmful to both people and animals.[7–9] Many heavy metal ions are prohibited by various international

organizations due to their toxicity and lack of biodegradability, which causes them to accumulate in the ecosystem.[10,11]

For many uses and in many different areas of science, medicine, politics, and security, the capacity to identify a wide range of analytes under a wide range of real-world situations is essential. In overall, scientists have had great success developing detection techniques for small organic molecules,[12–14] anions,[15-26] and cations,[27-47] biological macromolecules including peptides[48-58] and oligonucleotides,[59] and whole cells[60] and organisms, including bacteria[61,62] and fungi.[63,64] Notable successes include the use of these systems for the detection of explosive compounds.[65–70]

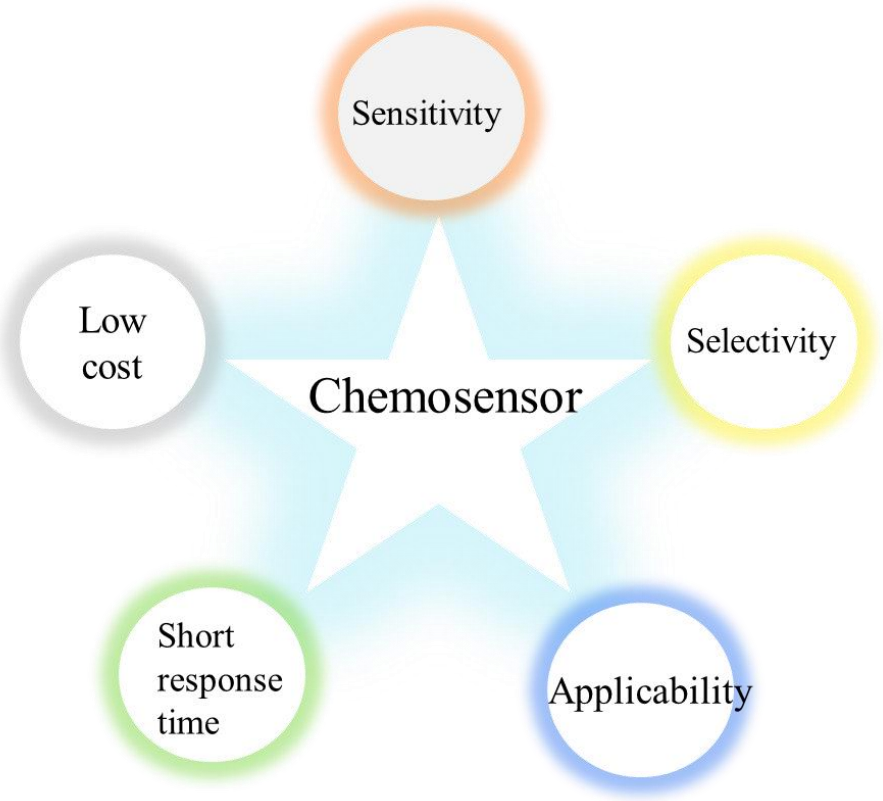

Figure 1.14: These aspects makes an ideal chemosensor: Sensitivity, Selectivity, Applicability, Short response time, and Low cost to synthesis

Scientists and researchers are currently working to create chemosensors that can be used to analyse environmental and commercial sample data. Due to their high sensitivity, high selectivity, faster response time, high spatial and temporal resolution, low cost, and ease of use even in remote areas, fluorometric chemosensors have drawn growing interest in the detection of selective anion or cation.

1.7 Optical chemosensors

Investigation methods that measure light strength include optical instruments. Upon substance (guest) attachment to the receptor (host), they alter the photophysical characteristics of the receptor. These modifications are identified using UV-Visible and fluorescence spectroscopy devices, depending on the sort of sensor. Colorimetric, fluorometric, and luminous chemosensors are the three main categories of chemosensors.

1.7.1 Colorimetric chemosensors

The color change that takes place after the receptor binds with a particular substance is known as a colorimetric chemosensor. The sensing element of the chemosensor changes color after engaging the receptor and analyte. Since it is possible to collect both qualitative and quantifiable data using colorimetric chemosensors, there has been a lot of interest in this technology.[71–75]

1.7.2 Fluorometric chemosensors.

Fluorescence is one of the most useful responding techniques for optical sensing. Due to their sensitivity, selectivity, fast reaction time, on-site and real-time detection, simple performance, flexibility, and low molar estimate of the analyte, fluorescence chemosensors have generated a great deal of interest. Fluorometric chemosensors experience a shift in fluorescence activity when the analyte binds to the receptor.[76] Goppelsroder first reported the synthesis of a highly luminous morin chelate as the first fluorescent chemosensor for detecting aluminium ions in 1867. The colorimetric sensors can only identify concentrations at micromolar levels, while the fluorescent chemosensor provides for detection at the picomolar scale.

The benefits of the fluorometric chemosensor are primarily attributable to the proportionality of the light emission to the analyte content. In comparison, the fraction of intensities recorded before and after the beam travels through the sample in absorbance tests indicates a relationship between the analyte concentration and the absorbance. The detection and signalling molecules, which are shown in **Figure 1.15**, are the fundamental components of fluorescent chemosensors. As a result, a fluorophore that converts the recognition into a photophysical signal (such as spectra, fluorescence quantum yield, and lifetime) is coupled to a receptor (ionophore) to produce a fluorescent chemosensor. The attachment of a specific analyte to the receptor, which results in a fluorescence signal and either an increase or a quenching of fluorescence, can change the photophysical characteristics. Turn-on

chemosensor is a term for the increased light intensity that results from the analyte's attachment to the receptor.[77,78] While the chemosensors turn-off happens because of the analyte binding to the fluorophore and a decrease in fluorescent intensity quenching. There are two types of fluorescent chemosensors, depending on how fluorescence and receptor are connected: combined and separated model The fluorophore is linked to the receptor by a spacer and signalling molecules that block conjugations in the separated model's proposed architecture. The fluorescence and receptor are conjugatively linked to one another in the integrated model; in this model, the receptor is a component of the fluorophore's -electron system.[79,80]

This section concentrated on newly developed chemosensors for anions, cations, and neutral guests using photo-luminescent molecules. Moreover, a general process underlying chemosensing was addressed. The most typical chemosensor consists of a binding site, a spacer, and a signaling unit in three sections. When the substance binds at the binding spot, the signaling unit responds (**Fig. 1.15**). Intramolecular Charge Transfer (ICT), Chelation Enhanced Fluorescence (CHEF), Photo-induced Electron Transfer (PET), Fluorescence Resonance Energy Transfer (FRET), Excited State Intramolecular Proton Transfer (ESIPT), Aggregation Induced Emission (AIE), and others were all involved in the maximum sensing mechanism.

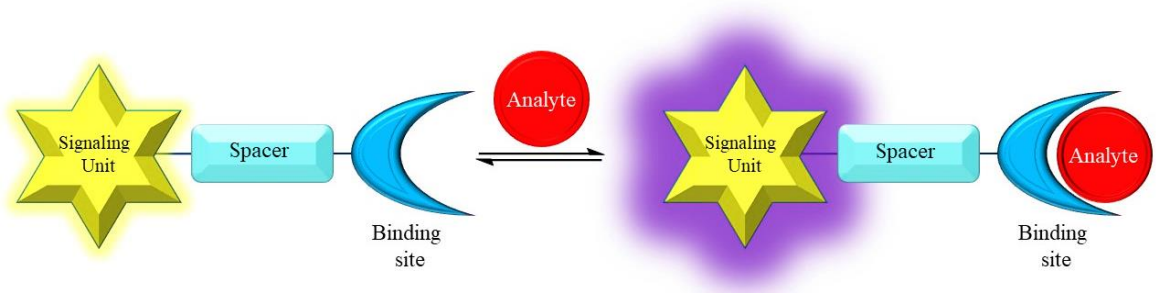

Figure 1.15: The graphic representation of chemo sensing mechanism.

1.8 Mechanism of Chemosensors

Essentially, a Jablonski diagram is an energy outline with energy on a vertical line. Although the energy levels can be expressed numerically, most of these diagrams only represent the energy levels schematically. Columns are used to organize the remainder of the diagram. Typically, each column corresponds to a particular spin number for a given species. The energy levels within the same spin multiplicity are sometimes divided into separate sections in schematics. Horizontal lines in each section denote the eigenstates of that specific

chemical. Horizontal lines in bold type indicate the boundaries of electronic energy levels. There are various vibronic energy states within each electronic energy state, and these vibronic states can be combined with the electronic state.

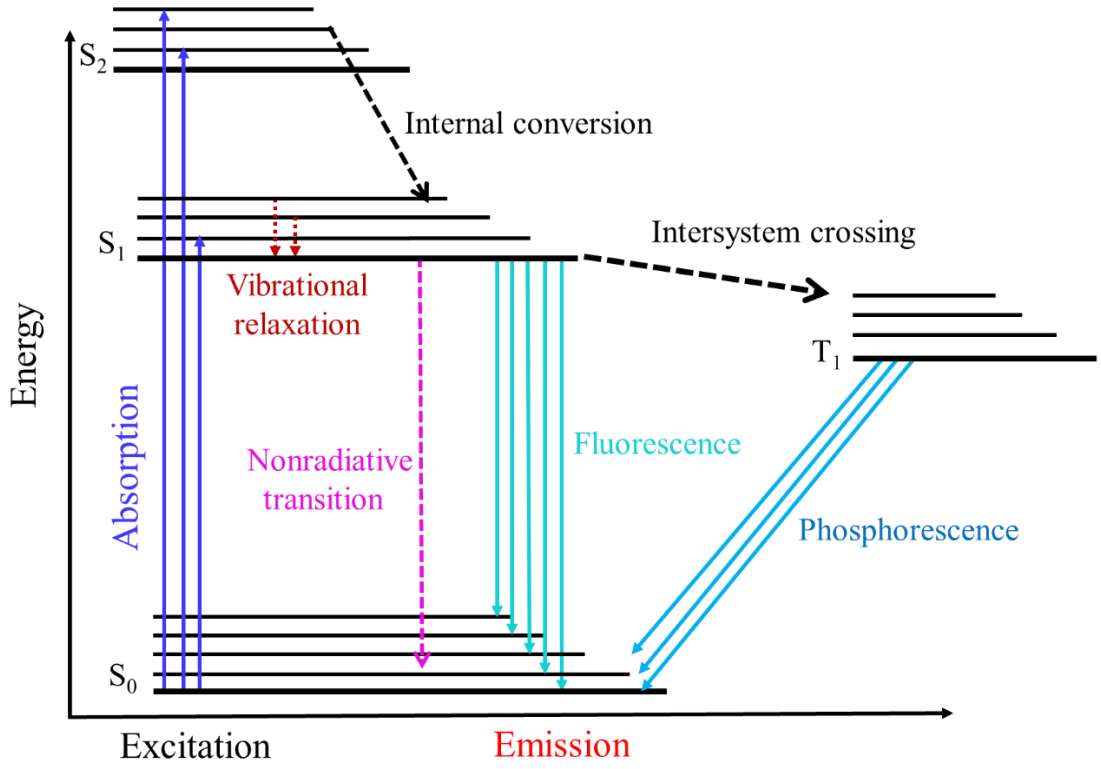

Figure 1.16: Jablonski diagram

Due to the enormous number of potential vibrations in a molecule, typically only fractions of these vibrational eigenstates are represented. Rotational energy levels can be further split into each of these vibrational energy states, but standard Jablonski diagrams skip these intricate levels of detail. The difference in energy decreases steadily as electronic energy levels rise, ultimately transforming into a continuum that can be studied using classical mechanics. The intersection of vibronic energy levels also grows as the electrical energy levels get closer together.[81–83]

1.8.1 Photo-induced electron transfer

A photo-induced electron transfer (PET) triggers the fluorescence quenching; the normal state recovers when a non-luminescent process occurs after the PET process. Based on the molecular orbital theory, the PET procedure might be able to describe the "on-off" toggling of fluorescent chemosensors. The fluorescent chemosensors based on PET have a fluorophore- spacer- receptor as their fundamental structure. This model has a gap between

the fluorescence and the receptor, which electrically isolates the fluorophore and receptor from the -electron systems as a result. Reductive PET and oxidative PET are the two subtypes of the PET procedure, respectively, based on the electron acceptor or donor connections to the fluorescence and receptor[84] **Figure 1.17** shows the fluorescent chemosensors construction. Because the electron transfer process from the quinoline moiety (the electron acceptor) to the imine nitrogen (the electron donor) has been stopped, the fluorescence enhancement was suppressed when Fe^{2+} ion was added to the probe solution. Because of the PET process being stopped after the complex between the probe and metal ion formed, the electron shift from the HOMO to LUMO level took place in a non-radioactive route, which caused the fluorescence to become quenched**. (Scheme 1.7**)

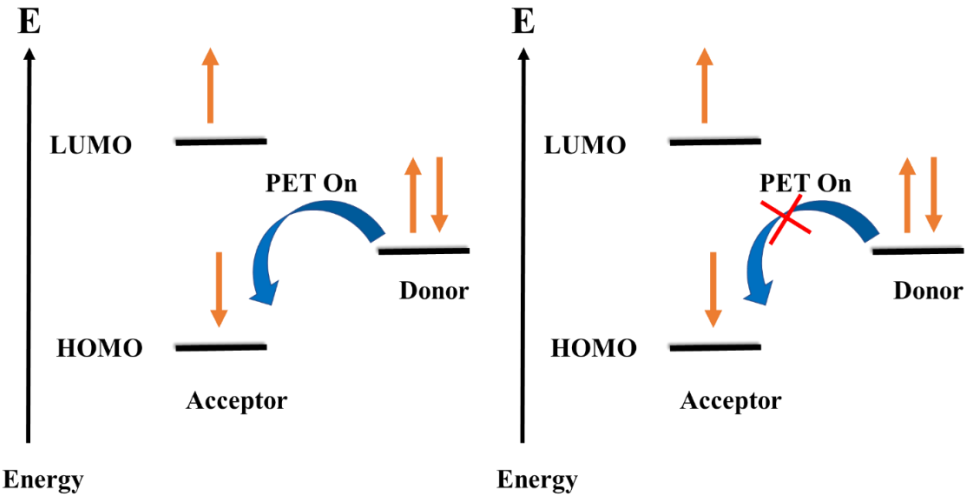

Figure 1.17: Schematic presentation of molecular orbital diagram of the photo-induced electron transfer process (PET).

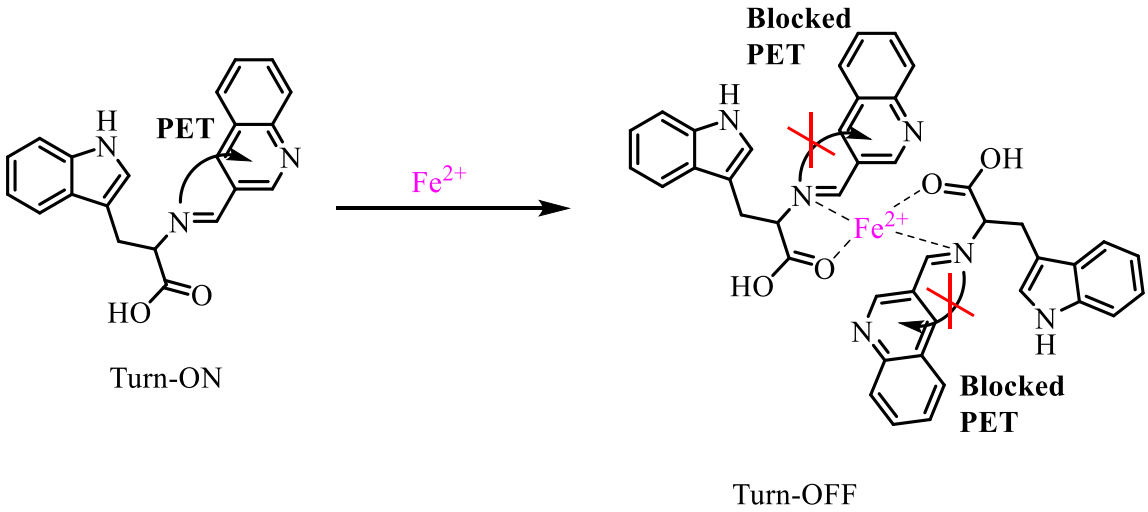

Scheme 1.7: Detection of Fe^{2+} ion, which involves PET mechanism

1.8.2 Intramolecular charge transfer

Intramolecular charge transfer (ICT) for Valeur *et al*. first introduced cation detection. ICT is described as an energized state in which the conjugation of an electron-donating unit (like $-NH_2$, $-N(CH_3)_2$, or $-OCH_3$) to an electron-accepting unit (like >C=O, -CN) in one molecule is shown to rise a "pushpull" π- electron system which has been extensively used for cation sensing.[1] When the electron donor reacts with the analyte, lowering the electron-donating character, a blue change in the absorption band is seen. However, an evolved ICT causes a red shift because of the analyte's reaction with the electron acceptor portion (**Figure 1.18**). Additionally, changes in the quantum yields and fluorescence lifetimes are seen. Numerous fluorescent imaging molecules have so far been produced by the ICT method by altering the fluorophores' ability to function as an electron donor, electron acceptor, or as a π-conjugate in order to combine with the target analyte. Based on the spectrum results, **Scheme 1.8** illustrates the ICT-based fluorescence "switch-on" process. The weak fluorescence emission at 415 nm is caused by ICT, which happens when a lone pair of electrons from the pyridine ring's "N" position and a free rotation of the -C = N- (imine) moiety occur in the Schiff base chemosensor L1. The imine free rotation is constrained and the ligand becomes totally rigid during the creation of the chemosensor L1+Bi^{3+} complex, which enhances the fluorescence while constricting the ICT process.[85]

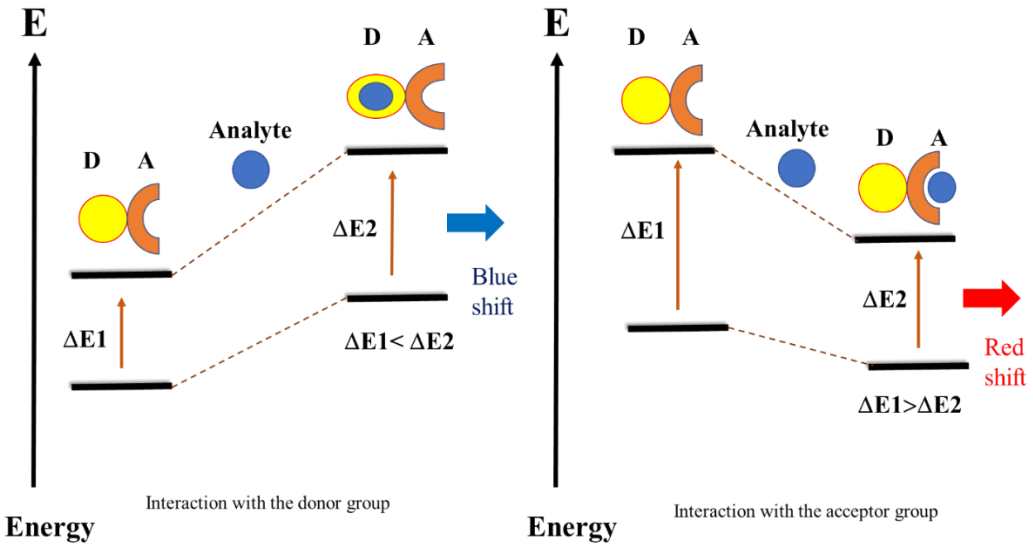

Figure 1.18 Schematic illustration of ICT mechanism

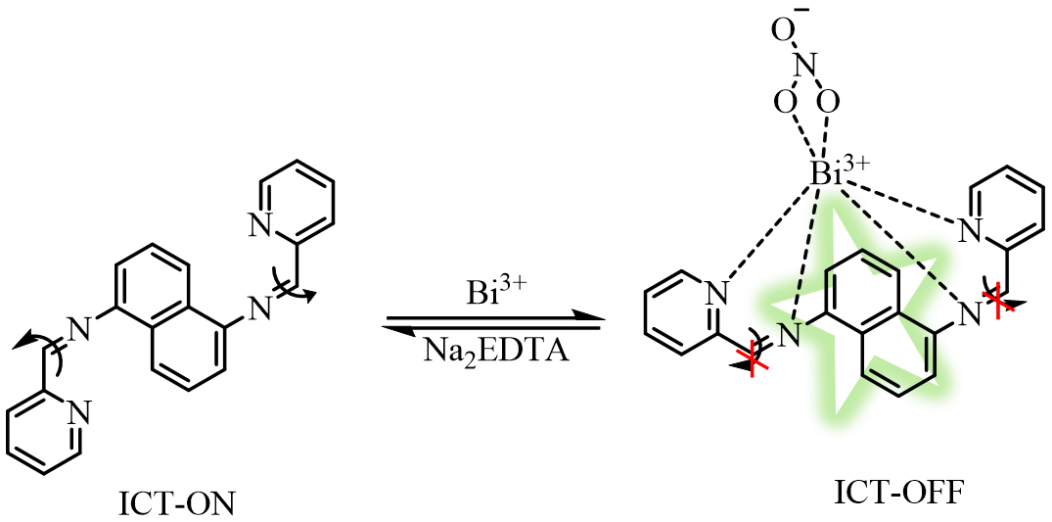

Scheme 1.8: ICT mechanism involved in Bi^{3+} Sensing

1.8.3 Excited-state intramolecular proton transfer

For their distinctive and extraordinary spectral sensitivity to the environmental medium, fluorescent chemosensors have been designed using excited-state intramolecular proton transfer (ESIPT). An intramolecular hydrogen bond, which is a key component of the ESIPT process, facilitates the proton transfer from a proton source (hydroxyl or amino unit) to a recipient unit (carbonyl oxygen or imine nitrogen) atom in the excited state of a fluorophore.[23] **Figure 1.19** represents a graphical explanation of the ESIPT procedure. The ESIPT-based method significantly reduces the photochemical reactivity of excited molecules by switching between the enol and keto forms, which results in enhanced photostability. Furthermore, a significant Stokes change will be seen. Therefore, the ESIPT method is compatible with fluorescent chemosensor designs that require spectrum shift for specific detection.

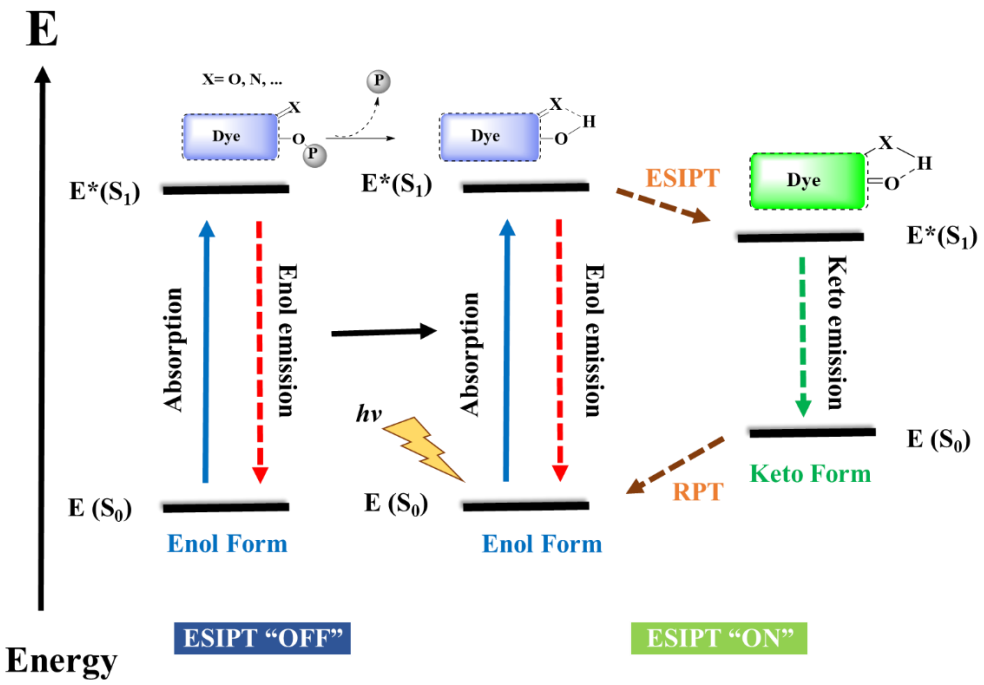

Figure 1.19: Schematic illustration of ESIPT sensing mechanism

The ESIPT mechanism can be used to explain the fluorescence quenching of both sensors by Cu^{2+}. Both ligands displayed intense fluorescence due to the powerful intramolecular hydrogen link, O-H-N. The ESIPT process was blocked upon binding with Cu^{2+}, and as a result, a reduction in fluorescence efficiency had been seen.[86] (**Scheme 1.9**).

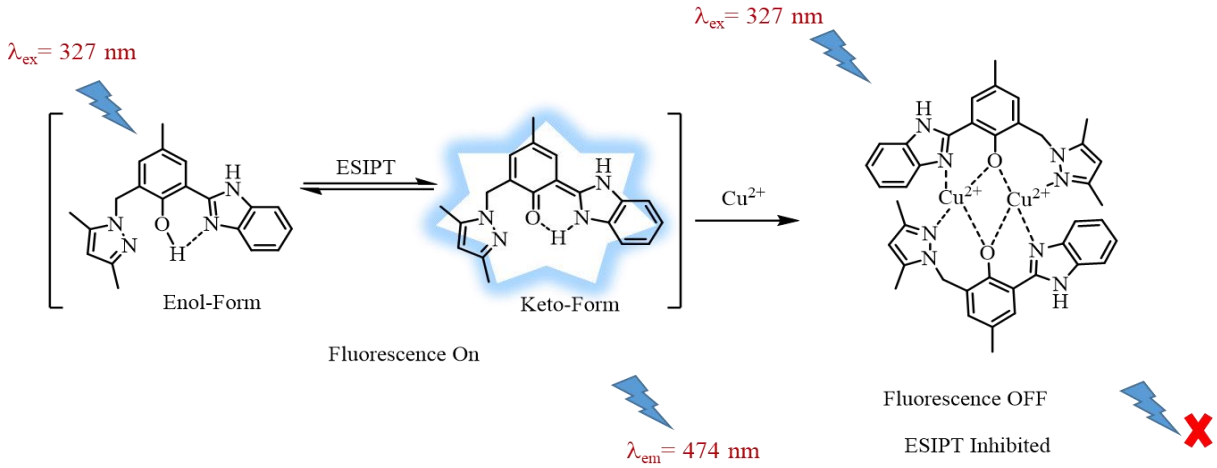

Scheme 1.9: Sensing of Cu^{2+} ion

1.8.4 Fluorescence Resonance Energy Transfer

Another type of fluorescence modification is called fluorescence resonance energy transfer (FRET). A couple of fluorophores that function as energy donors and acceptors, respectively, transfer energy through the FRET mechanism.[24,25] The FRET is dependent on

the distance at which the electrically excited states of two chromophores engage so that non-radiative dipole-dipole coupling transfers the excitation energy from a donor to an acceptor (**Fig. 1.20**). The donor and receiver go through roughly similar vibrational changes. If FRET is active in the molecules, it is usually used to intentionally increase the stokes shift. With a ratio of the fluorescence levels of the donor and acceptor emissions controlled by the target analytes, the emission of the donor at comparatively short wavelengths triggers the acceptor emission at longer wavelengths for sensing uses. When there are significant spectral similarities between the donor emission spectrum and the acceptor absorption spectrum, the FRET effectiveness is increased.[26] When energy is transferred from the donor to the recipient under excitation at 370 nm, the anthracene fluorophore's strong purple fluorescence emission at 434 nm is weaker and the rhodamine fluorophore's strong orange fluorescence emission at 608 nm is increased. In **Scheme 1.10**, the proposed detecting method was described.[87]

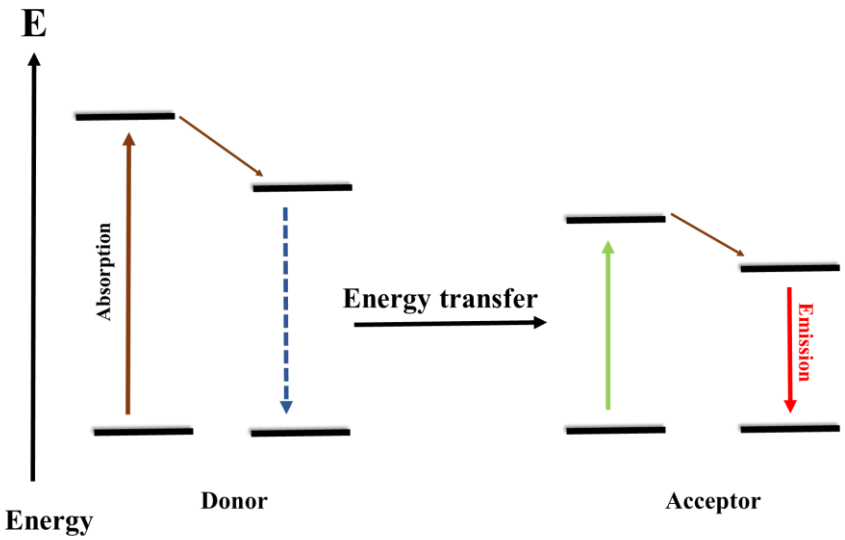

Figure 1.20: Schematic representation of FRET sensing mechanism

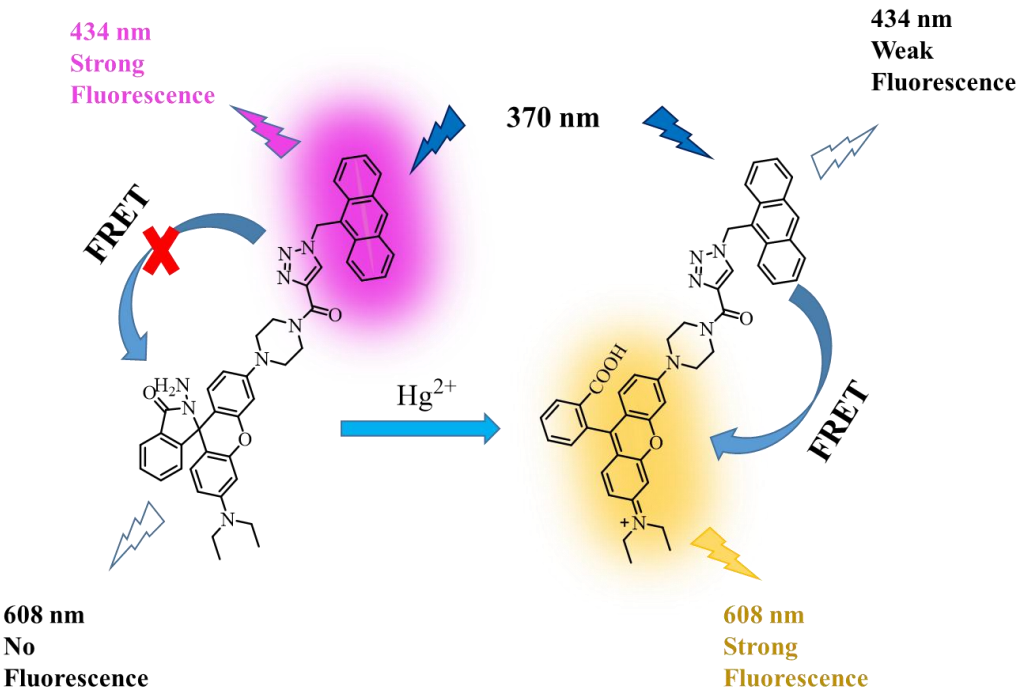

Scheme 1.10: Sensing of Hg^{2+} ion.

1.8.5 Chelation enhanced fluorescence

In this mechanism, the chemosensor initially exists as a non-fluorescent state, but after chelating with metal ion shows highly fluorescence. (**Fig. 1.21**) In bis-tris buffer solution, the fluorescent activity of chemosensors towards different metal ions was investigated (10 mM, pH 7.0). The fluorescence emission from the chemosensor when stimulated at 355 nm was weak (λ_{max} 521 nm), compared to that (37-folds) when Zn^{2+} was detected. Other metal ions, such as Na^{+}, K^{+}, Mg^{2+}, Ca^{2+}, Al^{3+}, Ga^{3+}, Cr^{3+}, Mn^{2+}, Fe^{2+}, Fe^{3+}, Co^{2+}, Ni^{2+}, Cu^{2+}, Zn^{2+}, Ga^{3+}, and Pb^{2+}, on the other hand, did not cause an increase in intensity. As a consequence of these findings, the sensor was shown to be a potential fluorescence chemosensor for Zn^{2+}. The efficient coordination of Zn^{2+} with chemosensor over other metal ions may be responsible for the specific fluorescence enhancement response to Zn^{2+}, which may be explained by the functioning of the CHEF mechanism.[88]

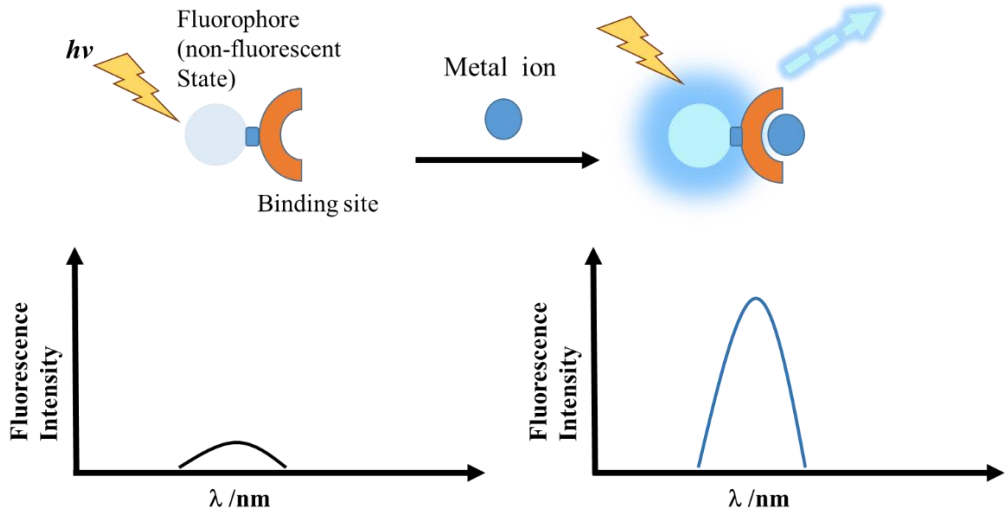

Figure 1.21: Schematic illustration of chelation enhanced fluorescence sensing mechanism

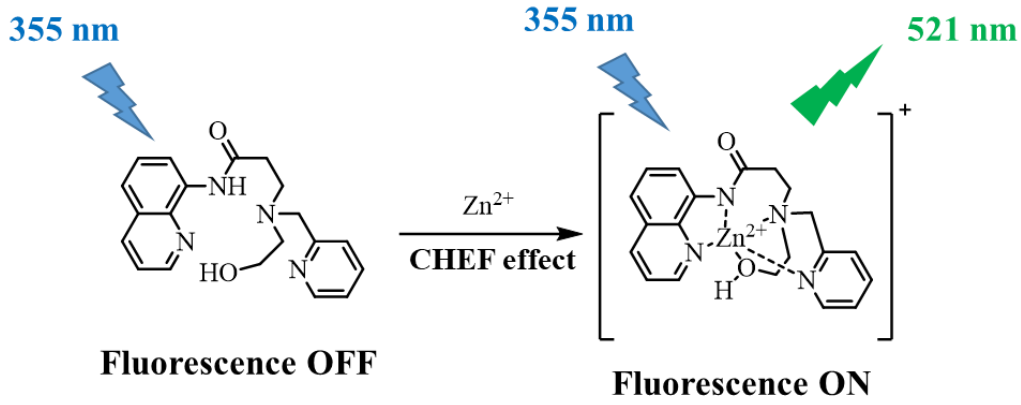

Scheme 1.11: Sensing of Zinc (II) ion.

1.8.6 Aggregation induced emission

Recently, AIE concept playing very important role in supramolecular chemistry, last two decade most of chemosensors were reported by using this mechanism. In 2001, Tang group introduced AIE effect.[89–91] A process for the fluorescence enhancement of probe to Al(III) was suggested (**Scheme 1.12**) on the basis of the following findings: The deprotonated form of probe has excellent water solubility, which accounts for its modest fluorescence strength at 466 nm in aqueous solutions. When probe and Al(III) bond to one another, they can form the complexation polymer (probe-Al(III)), which causes probe to aggregate in the solution. Due to the restriction of TPE moieties intramolecular rotations in probe-Al(III), blue fluorescence was increased.[92]

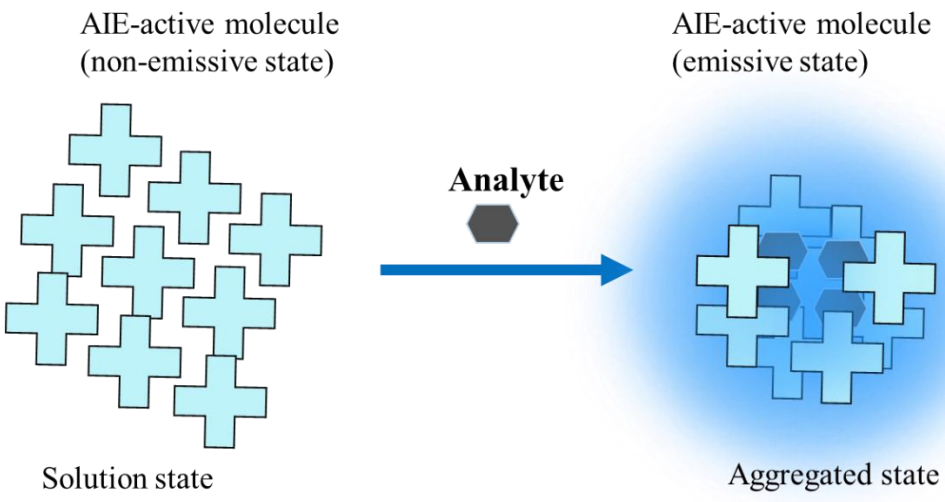

Figure 1.22: Schematic illustration of AIE mechanism for chemosensor

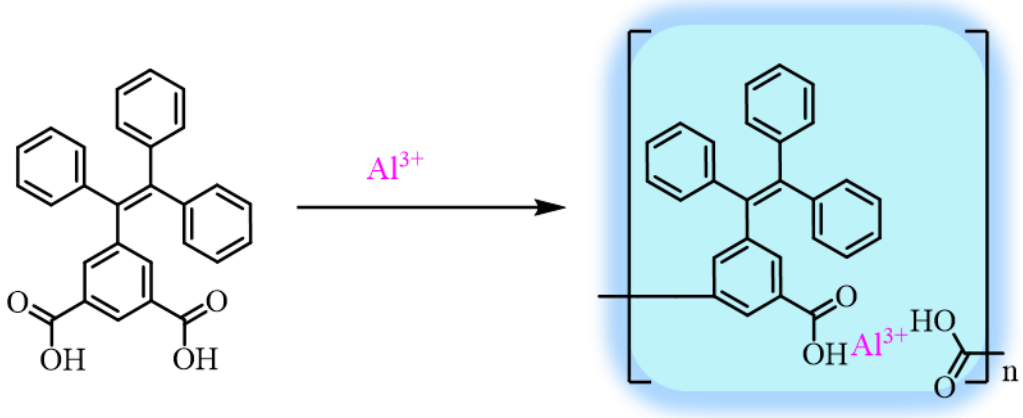

Scheme 1.12: Detection of Al^{3+} ion

1.9 Common luminophores

A number of theoretical and/or practical variables may impact the sensible choice of fluorophores for a given sensing application, including the requirement that fluorophores emit or absorb in a target spectral region in order to function as efficient energy acceptors. To achieve high performance for biological, aqueous-phase uses, there are concerns about the fluorophores solubility in a wide range of circumstances. The fluorophore's resistance to a variety of temperatures, solvents, pH, and other experimental conditions, as needed by the intended use.

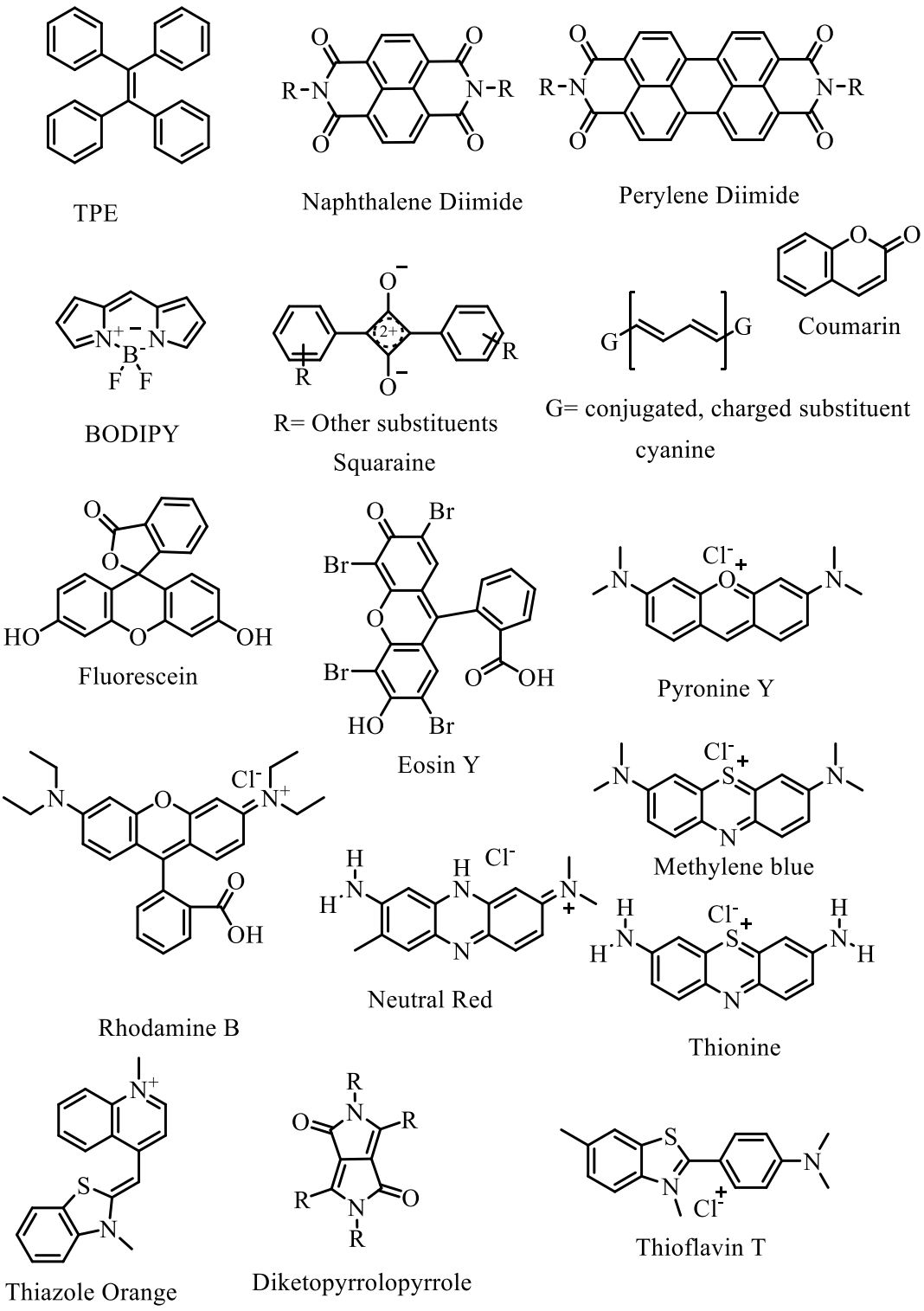

Scheme 1.13: Structures of mostly used luminophores for chemosensor

The convenience with which fluorophores can be obtained through synthesized methods and/or from commercial sources. Most regularly interested luminophores are TPE,[89] Rylene Luminophores,[93] Coumarins,[94] BODIPY,[95,96] Squaraines,[97,98] Cyanine Dyes,[99] Fluorescein,[100] Eosin Y,[101] Pyronine Y,[102] Rhodamines,[87] Methylene Blue,[103] Thionine,[104]

Neutral Red,[105] Thiazole Orange,[106] Thioflavin T,[107] and Diketopyrrolopyrrole Dyes[108] so on. (**Scheme 1.13**)

1.10 Calculating Supramolecular Complexation

1.10.1 Benesi−Hildebrand Binding Constants.

Based on the appearance of a novel absorption peak when both species were mixed, Benesi and Hildebrand understood that association complexes were developing between iodine and aromatic hydrocarbons. The binding strength between iodine and an aromatic hydrocarbon, as described in a later release by the same authors, was quantified using an equation; this binding strength's numerical expression is now known as an association constant. While other binding stoichiometry have also been reported, this method is only useful when the concentration of the host is significantly greater than the concentration of the complex. It is also usually only used for 1:1 host-guest complexes.[109,110]

1.10.2 Stern-Volmer Quenching Constants

The dynamic, or collisional, quenching process of a fluorescence is described by the Stern–Volmer equation, which was first published in 1920. This process results from diffusive interactions between the fluorophore and quencher. Eq. 1 below, where F_0 is the fluorescence intensity in the lack of a quencher, F is the fluorescence intensity in the presence of a quencher, [Q] is the quencher concentration, and K_{SV} is the Stern–Volmer constant, expresses the Stern–Volmer relationship.[111]

$$\frac{F_0}{F} = (1 + K_{SV}[Q]) \qquad (1)$$

1.10.3 Job's Plots

In many instances of supramolecular binding events, other stoichiometries are preferred, including 1:2 complexes, 2:1 complexes, and complex combinations of simultaneous, co-occurring multiple stoichiometry. The aforementioned Benesi–Hildebrand and Stern–Volmer relationships depend on the assumption of a 1:1 host–guest binding stoichiometry. Paul Job first introduced the Job's plot, Job's method, or the technique of continuous variation in 1928, as a way to calculate the stoichiometry of a binding event. This technique involves varying the relative amounts of A and B while maintaining a fixed overall concentration of an A and B solution. The standardized physical measure (P), which is determined using a number of spectroscopic methods (fluorescence, absorbance, NMR, etc.), is then plotted against the mole fraction of A (*x*a). When (*x*a) = 0.5, P_{max} happens when

a 1:1 AB stoichiometry is in play. The A2B binding mode's P_{max} occurs at (xa) = 0.67, while the AB2 binding mode is P_{max} occurs at (xa) = 0.33. This method cannot be used to identify more complex stoichiometric combinations or situations where numerous stoichiometries are present, so caution must be exercised when using it. Because sharper peaks typically correlate to higher constants and wider peaks to lower constants, these graphs are also helpful for estimating host-guest association constants roughly.[112]

1.10.4 Limit of Detection

For the analysis of any sensor that might have a commercial or industrial application, determining a detection limit. The smallest amount of analyte that will give a distinctive signal and a quantification limit the smallest amount of analyte that can be accurately quantified of a given system is invaluable. To determine the concentration of analyte at the point where the signal is three times the standard deviation of the blank for the detection limit or ten times the standard deviation of the blank for the quantitation limit, the most common method is to obtain a calibration line for the system in question and use the equation of that line. However, a review by Belter *et al*. describes a large number of techniques for determining these limits.[113]

1.11 Conclusion

The chemosensors area has advanced significantly since Goppelsroder first described fluorescent chemosensors that were Al^{3+}-selective. Notably, the area of fluorometric chemosensors has undergone tremendous growth over the past 50 years. Consequently, over the past few years, researchers have developed an enormous number of chemosensors. A potential device for identifying poisonous anions and cations in an aqueous medium is chemosensors. This addition provided an overview of the science of chemosensors and their uses. However, various photophysical phenomena, such as PET, CHEF, FRET, ICT, and ESIPT, are required for the identification of these harmful pollutants. The majority of common fluorophores show an ACQ effect, which is thought to be harmful and restricts their use in future applications. It is interesting to note that the AIE occurrence was developed to counteract the ACQ impact. In AIE, molecules originally fluoresce poorly in the solution state but brighten up when they are aggregated. Moreover most common luminophores were discussed such as TPE, Rylene Luminophores, Coumarins BODIPY, Squaraines, Cyanine Dyes, and so. Finally calculation of association constant, stoichiometry and limit of detection was described.

References

(1) Cheng, Y.-L.; Lee, C.-Y.; Huang, Y.-L.; Buckner, C. A.; Lafrenie, R. M.; Dénommée, J. A.; Caswell, J. M.; Want, D. A.; Gan, G. G.; Leong, Y. C.; Bee, P. C.; Chin, E.; Teh, A. K. H.; Picco, S.; Villegas, L.; Tonelli, F.; Merlo, M.; Rigau, J.; Diaz, D.; Masuelli, M.; Korrapati, S.; Kurra, P.; Puttugunta, S.; Picco, S.; Villegas, L.; Tonelli, F.; Merlo, M.; Rigau, J.; Diaz, D.; Masuelli, M.; Tascilar, M.; de Jong, F. A.; Verweij, J.; Mathijssen, R. H. J. We Are IntechOpen , the World ' s Leading Publisher of Open Access Books Built by Scientists , for Scientists TOP 1 %. *Intech* **2016**, *11* (tourism), 13.

(2) Czarnik, A. W. Supramolecular Chemistry, Fluorescence, and Sensing. **1993**, No. 1990, 1–9. https://doi.org/10.1021/bk-1993-0538.ch001.

(3) Liu, S.; Wang, Y. M.; Han, J. Fluorescent Chemosensors for Copper(II) Ion: Structure, Mechanism and Application. *J. Photochem. Photobiol. C Photochem. Rev.* **2017**, *32* (Ii), 78–103. https://doi.org/10.1016/j.jphotochemrev.2017.06.002.

(4) Patil, N. S.; Dhake, R. B.; Ahamed, M. I.; Fegade, U. A Mini Review on Organic Chemosensors for Cation Recognition (2013-19). *J. Fluoresc.* **2020**, *30* (6), 1295–1330. https://doi.org/10.1007/s10895-020-02554-7.

(5) Kowser, Z.; Rayhan, U.; Akther, T.; Redshaw, C.; Yamato, T. A Brief Review on Novel Pyrene Based Fluorometric and Colorimetric Chemosensors for the Detection of Cu2+. *Mater. Chem. Front.* **2021**, *5* (5), 2173–2200. https://doi.org/10.1039/d0qm01008a.

(6) Kollur, S. P.; Shivamallu, C.; Prasad, S. K.; Veerapur, R. Recent Advances on the Development of Chemosensors for the Detection of Mercury Toxicity : A Review. **2021**, 1–16.

(7) Li, M. M.; Huang, S. Y.; Ye, H.; Ge, F.; Miao, J. Y.; Zhao, B. X. A New Pyrazoline-Based Fluorescent Probe for Cu2+ in Live Cells. *J. Fluoresc.* **2013**, *23* (4), 799–806. https://doi.org/10.1007/s10895-013-1203-0.

(8) Ma, S.; Wang, Y.; She, M.; Wang, S.; Yang, Z.; Liu, P.; Zhang, S.; Li, J. Design Strategies and Progress on Xanthene-Based Fluorescent Probe for Metal Ions. *Rev. Anal. Chem.* **2017**, *36* (2). https://doi.org/10.1515/revac-2016-0024.

(9) Kaur, N.; Kaur, G.; Fegade, U. A.; Singh, A.; Sahoo, S. K.; Kuwar, A. S.; Singh, N. Anion Sensing with Chemosensors Having Multiple –NH Recognition Units. *TrAC - Trends Anal. Chem.* **2017**, *95*, 86–109. https://doi.org/10.1016/j.trac.2017.08.003.

(10) Krogstad, D. J.; Sutera, S. P.; Boylan, C. W.; Gluzman, I. Y.; Qian, Z. F.; Rao, P. R. Intraerythrocytic Parasites and Red Cell Deformability: Plasmodium Berghei and Babesia Microti. *Blood Cells* **1991**, *17* (1), 209–221.

(11) WHO. World Health Organisation: Guidelines for Drinking Water Quality, Third Edition, Vol. 1. Recommendations. *Environ. Pollut. Ser. A, Ecol. Biol.* **2004**, *1*, 1–564.

(12) Chaudhuri, S.; DIScenza, D. J.; Smith, B.; Yocum, R.; Levine, M. Array-Based Detection of Isomeric and Analogous Analytes Employing Synthetically Modified Fluorophore Attached β-Cyclodextrin Derivatives. *New J. Chem.* **2017**, *41* (23), 14431–14437. https://doi.org/10.1039/c7nj02968c.

(13) Yin, J.; Huang, L.; Wu, L.; Li, J.; James, T. D.; Lin, W. Small Molecule Based Fluorescent Chemosensors for Imaging the Microenvironment within Specific Cellular Regions. *Chem. Soc. Rev.* **2021**, *50* (21), 12098–12150. https://doi.org/10.1039/d1cs00645b.

(14) Beyeh, N. K.; Jo, H. H.; Kolesnichenko, I.; Pan, F.; Kalenius, E.; Anslyn, E. V.; Ras, R. H. A.; Rissanen, K. Recognition of Viologen Derivatives in Water by N-Alkyl Ammonium Resorcinarene Chlorides. *J. Org. Chem.* **2017**, *82* (10), 5198–5203. https://doi.org/10.1021/acs.joc.7b00449.

(15) Chi, X.; Peters, G. M.; Hammel, F.; Brockman, C.; Sessler, J. L. Molecular Recognition under Interfacial Conditions: Calix[4]Pyrrole-Based Cross-Linkable Micelles for Ion Pair Extraction. *J. Am. Chem. Soc.* **2017**, *139* (27), 9124–9127. https://doi.org/10.1021/jacs.7b04529.

(16) Fatila, E. M.; Twum, E. B.; Sengupta, A.; Pink, M.; Karty, J. A.; Raghavachari, K.; Flood, A. H. Anions Stabilize Each Other inside Macrocyclic Hosts. *Angew. Chemie* **2016**, *128* (45), 14263–14268. https://doi.org/10.1002/ange.201608118.

(17) Lin, T.; Su, X.; Wang, K.; Li, M.; Guo, H.; Liu, L.; Zou, B.; Zhang, Y. M.; Liu, Y.; Zhang, S. X. A. An AIE Fluorescent Switch with Multi-Stimuli Responsive Properties and Applications for Quantitatively Detecting PH Value, Sulfite Anion and Hydrostatic Pressure. *Mater. Chem. Front.* **2019**, *3* (6), 1052–1061. https://doi.org/10.1039/c8qm00544c.

(18) Li, N.; Liu, Y. Y.; Li, Y.; Zhuang, J. B.; Cui, R. R.; Gong, Q.; Zhao, N.; Tang, B. Z. Fine Tuning of Emission Behavior, Self-Assembly, Anion Sensing, and Mitochondria Targeting of Pyridinium-Functionalized Tetraphenylethene by Alkyl Chain Engineering. *ACS Appl. Mater. Interfaces* **2018**, *10* (28), 24249–24257.

https://doi.org/10.1021/acsami.8b04113.

(19) Pan, D.; Don, Y.; Lu, Y.; Xiao, G.; Chi, H.; Hu, Z. AIE Fluorescent Probe Based on Tetraphenylethylene and Morpholine-Thiourea Structures for Detection of HClO. *Anal. Chim. Acta* **2022**, *1235* (July), 340559. https://doi.org/10.1016/j.aca.2022.340559.

(20) Wang, Y.; Liu, H.; Chen, Z.; Pu, S. Aggregation-Induced Emission Enhancement (AIEE)-Active Tetraphenylethene (TPE)-Based Chemosensor for CN−. *Spectrochim. Acta - Part A Mol. Biomol. Spectrosc.* **2021**, *245*, 118928. https://doi.org/10.1016/j.saa.2020.118928.

(21) Wang, C.; Ji, H.; Li, M.; Cai, L.; Wang, Z.; Li, Q.; Li, Z. A Highly Sensitive and Selective Fluorescent Probe for Hypochlorite in Pure Water with Aggregation Induced Emission Characteristics. *Faraday Discuss.* **2017**, *196*, 427–438. https://doi.org/10.1039/c6fd00168h.

(22) Huang, Y.; Zhang, P.; Gao, M.; Zeng, F.; Qin, A.; Wu, S.; Tang, B. Z. Ratiometric Detection and Imaging of Endogenous Hypochlorite in Live Cells and: In Vivo Achieved by Using an Aggregation Induced Emission (AIE)-Based Nanoprobe. *Chem. Commun.* **2016**, *52* (45), 7288–7291. https://doi.org/10.1039/c6cc03415b.

(23) Chua, M. H.; Zhou, H.; Lin, T. T.; Wu, J.; Xu, J. Triphenylethylenyl-Based Donor-Acceptor-Don1. Chua, M. H., Zhou, H., Lin, T. T., Wu, J. & Xu, J. Triphenylethylenyl-Based Donor-Acceptor-Donor Molecules: Studies on Structural and Optical Properties and AIE Properties for Cyanide Detection. J. Mater. Chem. *J. Mater. Chem. C* **2017**, *5* (46), 12194–12203. https://doi.org/10.1039/c7tc04400c.

(24) Zhang, Y.; Li, D.; Li, Y.; Yu, J. Solvatochromic AIE Luminogens as Supersensitive Water Detectors in Organic Solvents and Highly Efficient Cyanide Chemosensors in Water. *Chem. Sci.* **2014**, *5* (7), 2710–2716. https://doi.org/10.1039/c4sc00721b.

(25) Jiang, G.; Liu, X.; Wu, Y.; Wang, J.; Dong, X.; Zhang, G.; Li, Y.; Fan, X. An AIE Based Tetraphenylethylene Derivative for Highly Selective and Light-up Sensing of Fluoride Ions in Aqueous Solution and in Living Cells. *RSC Adv.* **2016**, *6* (64), 59400–59404. https://doi.org/10.1039/c6ra10878d.

(26) Bineci, M.; Ba¸lan, M.; Atilgan, S. AIE Active Pyridinium Fused Tetraphenylethene: Rapid and Selective Fluorescent "Turn-on" Sensor for Fluoride Ion in Aqueous Media. *Sensors Actuators, B Chem.* **2016**, *222*, 315–319. https://doi.org/10.1016/j.snb.2015.08.087.

(27) Li, Y.; Yu, H.; Shao, G.; Gan, F. A Tetraphenylethylene-Based "Turn on"

Fluorescent Sensor for the Rapid Detection of Ag+ Ions with High Selectivity. *J. Photochem. Photobiol. A Chem.* **2015**, *301* (3), 14–19. https://doi.org/10.1016/j.jphotochem.2014.12.013.

(28) Gui, S.; Huang, Y.; Hu, F.; Jin, Y.; Zhang, G.; Yan, L.; Zhang, D.; Zhao, R. Fluorescence Turn-on Chemosensor for Highly Selective and Sensitive Detection and Bioimaging of Al3+ in Living Cells Based on Ion-Induced Aggregation. *Anal. Chem.* **2015**, *87* (3), 1470–1474. https://doi.org/10.1021/ac504153c.

(29) Ruan, Z.; Shan, Y.; Gong, Y.; Wang, C.; Ye, F.; Qiu, Y.; Liang, Z.; Li, Z. Novel AIE-Active Ratiometric Fluorescent Probes for Mercury(II) Based on the Hg2+-Promoted Deprotection of Thioketal, and Good Mechanochromic Properties. *J. Mater. Chem. C* **2018**, *6* (4), 773–780. https://doi.org/10.1039/c7tc04712f.

(30) Neupane, L. N.; Oh, E. T.; Park, H. J.; Lee, K. H. Selective and Sensitive Detection of Heavy Metal Ions in 100% Aqueous Solution and Cells with a Fluorescence Chemosensor Based on Peptide Using Aggregation-Induced Emission. *Anal. Chem.* **2016**, *88* (6), 3333–3340. https://doi.org/10.1021/acs.analchem.5b04892.

(31) Tang, A.; Chen, Z.; Deng, D.; Liu, G.; Tu, Y.; Pu, S. Aggregation-Induced Emission Enhancement (AIEE)-Active Tetraphenylethene (TPE)-Based Chemosensor for Hg2+ with Solvatochromism and Cell Imaging Characteristics. *RSC Adv.* **2019**, *9* (21), 11865–11869. https://doi.org/10.1039/c9ra02119a.

(32) Wang, J.; Tong, J.; Wang, Z. F.; Yuan, Q.; Wang, X. Y.; Yu, S. Y.; Tang, B. Z. Highly Specific and Selective Fluorescent Chemosensor for Sensing of Hg(II) by NH-Pyrazolate-Functionalized AIEgens. *Anal. Chim. Acta* **2022**, *1208*, 339824. https://doi.org/10.1016/j.aca.2022.339824.

(33) Khandare, D. G.; Joshi, H.; Banerjee, M.; Majik, M. S.; Chatterjee, A. An Aggregation-Induced Emission Based Turn-on Fluorescent Chemodosimeter for the Selective Detection of Pb2+ Ions. *RSC Adv.* **2014**, *4* (87), 47076–47080. https://doi.org/10.1039/c4ra09451d.

(34) Huang, Y.; Lin, J.; Wang, L.; Cao, Z.; Wang, Y.; Wu, M. A Specific Fluorescent Probe for Antimony Based on Aggregation Induced Emission. *Zeitschrift fur Anorg. und Allg. Chemie* **2020**, *646* (2), 47–52. https://doi.org/10.1002/zaac.201900268.

(35) Wen, J.; Dong, L.; Hu, S.; Li, W.; Li, S.; Wang, X. Fluorogenic Thorium Sensors Based on 2,6-Pyridinedicarboxylic Acid-Substituted Tetraphenylethenes with Aggregation-Induced Emission Characteristics. *Chem. - An Asian J.* **2016**, *11* (1), 49–53. https://doi.org/10.1002/asia.201500834.

(36) Wen, J.; Huang, Z.; Hu, S.; Li, S.; Li, W.; Wang, X. Aggregation-Induced Emission Active Tetraphenylethene-Based Sensor for Uranyl Ion Detection. *J. Hazard. Mater.* **2016**, *318*, 363–370. https://doi.org/10.1016/j.jhazmat.2016.07.004.

(37) Hong, Y.; Chen, S.; Leung, C. W. T.; Lam, J. W. Y.; Liu, J.; Tseng, N. W.; Kwok, R. T. K.; Yu, Y.; Wang, Z.; Tang, B. Z. Fluorogenic Zn(II) and Chromogenic Fe(II) Sensors Based on Terpyridine-Substituted Tetraphenylethenes with Aggregation-Induced Emission Characteristics. *ACS Appl. Mater. Interfaces* **2011**, *3* (9), 3411–3418. https://doi.org/10.1021/am2009162.

(38) Sun, F.; Zhang, G.; Zhang, D.; Xue, L.; Jiang, H. Aqueous Fluorescence Turn-on Sensor for Zn 2+ with a Tetraphenylethylene Compound. *Org. Lett.* **2011**, *13* (24), 6378–6381. https://doi.org/10.1021/ol2026735.

(39) Zhang, L.; Hu, W.; Yu, L.; Wang, Y. Click Synthesis of a Novel Triazole Bridged AIE Active Cyclodextrin Probe for Specific Detection of Cd2+. *Chem. Commun.* **2015**, *51* (20), 4298–4301. https://doi.org/10.1039/c4cc09769f.

(40) Xu, H.; Wang, H.; Zhou, S.; Xiao, L.; Yan, Y.; Yuan, Q. A Protocol of Self-Assembled Monolayers of Fluorescent Block Molecules for Trace Zn(Ii) Sensing: Structures and Mechanisms. *RSC Adv.* **2015**, *5* (128), 106061–106067. https://doi.org/10.1039/c5ra20198e.

(41) Feng, H. T.; Song, S.; Chen, Y. C.; Shen, C. H.; Zheng, Y. S. Self-Assembled Tetraphenylethylene Macrocycle Nanofibrous Materials for the Visual Detection of Copper(Ii) in Water. *J. Mater. Chem. C* **2014**, *2* (13), 2353–2359. https://doi.org/10.1039/c3tc32373k.

(42) Lu, L.; Ren, X. K.; Liu, R.; Jiang, X. Q.; Geng, L. Y.; Zheng, J. F.; Feng, Y.; Chen, E. Q. Ionic Self-Assembled Derivative of Tetraphenylethylene: Synthesis, Enhanced Solid-State Emission, Liquid-Crystalline Structure, and Cu2+ Detection Ability. *ChemPhysChem* **2017**, *18* (24), 3605–3613. https://doi.org/10.1002/cphc.201700926.

(43) Yang, Y.; Gao, C. Y.; Li, T.; Chen, J. A Tetraphenylethene-Based Rhodamine Hydrazone Chemosensor for Colorimetric and Reversible Detection of Cu2+. *ChemistrySelect* **2016**, *1* (15), 4577–4581. https://doi.org/10.1002/slct.201600883.

(44) Chen, X.; Shen, X. Y.; Guan, E.; Liu, Y.; Qin, A.; Sun, J. Z.; Zhong Tang, B. A Pyridinyl-Functionalized Tetraphenylethylene Fluorogen for Specific Sensing of Trivalent Cations. *Chem. Commun.* **2013**, *49* (15), 1503–1505. https://doi.org/10.1039/c2cc38246f.

(45) Ye, J. H.; Liu, J.; Wang, Z.; Bai, Y.; Zhang, W.; He, W. A New Fe3+ Fluorescent Chemosensor Based on Aggregation-Induced Emission. *Tetrahedron Lett.* **2014**, *55* (27), 3688–3692. https://doi.org/10.1016/j.tetlet.2014.05.008.

(46) Ozturk, S.; Atilgan, S. A Tetraphenylethene Based Polarity Dependent Turn-on Fluorescence Strategy for Selective and Sensitive Detection of Hg2+ in Aqueous Medium and in Living Cells. *Tetrahedron Lett.* **2014**, *55* (1), 70–73. https://doi.org/10.1016/j.tetlet.2013.10.105.

(47) Huang, G.; Zhang, G.; Zhang, D. Turn-on of the Fluorescence of Tetra(4-Pyridylphenyl)Ethylene by the Synergistic Interactions of Mercury(Ii) Cation and Hydrogen Sulfate Anion. *Chem. Commun.* **2012**, *48* (60), 7504–7506. https://doi.org/10.1039/c2cc32504g.

(48) Jiang, G.; Wang, J.; Yang, Y.; Zhang, G.; Liu, Y.; Lin, H.; Zhang, G.; Li, Y.; Fan, X. Fluorescent Turn-on Sensing of Bacterial Lipopolysaccharide in Artificial Urine Sample with Sensitivity down to Nanomolar by Tetraphenylethylene Based Aggregation Induced Emission Molecule. *Biosens. Bioelectron.* **2016**, *85*, 62–67. https://doi.org/10.1016/j.bios.2016.04.071.

(49) Hu, X. M.; Chen, Q.; Wang, J. X.; Cheng, Q. Y.; Yan, C. G.; Cao, J.; He, Y. J.; Han, B. H. Tetraphenylethylene-Based Glycoconjugate as a Fluorescence "Turn-on" Sensor for Cholera Toxin. *Chem. - An Asian J.* **2011**, *6* (9), 2376–2381. https://doi.org/10.1002/asia.201100141.

(50) Zhao, L.; Chen, Y.; Yuan, J.; Chen, M.; Zhang, H.; Li, X. Electrospun Fibrous Mats with Conjugated Tetraphenylethylene and Mannose for Sensitive Turn-on Fluorescent Sensing of Escherichia Coli. *ACS Appl. Mater. Interfaces* **2015**, *7* (9), 5177–5186. https://doi.org/10.1021/am507593p.

(51) Lou, X.; Leung, C. W. T.; Dong, C.; Hong, Y.; Chen, S.; Zhao, E.; Lam, J. W. Y.; Tang, B. Z. Detection of Adenine-Rich SsDNA Based on Thymine-Substituted Tetraphenylethene with Aggregation-Induced Emission Characteristics. *RSC Adv.* **2014**, *4* (63), 33307–33311. https://doi.org/10.1039/c4ra05765a.

(52) Wang, M.; Zhang, G.; Zhang, D.; Zhu, D.; Tang, B. Z. Fluorescent Bio/Chemosensors Based on Silole and Tetraphenylethene Luminogens with Aggregation-Induced Emission Feature. *J. Mater. Chem.* **2010**, *20* (10), 1858–1867. https://doi.org/10.1039/b921610c.

(53) Dong, J.; Liu, M.; Jiang, R.; Huang, H.; Wan, Q.; Wen, Y.; Tian, J.; Dai, Y.; Zhang, X.; Wei, Y. Synthesis and Biological Imaging of Cross-Linked Fluorescent

Polymeric Nanoparticles with Aggregation-Induced Emission Characteristics Based on the Combination of RAFT Polymerization and the Biginelli Reaction. *J. Colloid Interface Sci.* **2018**, *528*, 192–199. https://doi.org/10.1016/j.jcis.2018.05.043.

(54) Jayaram, D. T.; Ramos-Romero, S.; Shankar, B. H.; Garrido, C.; Rubio, N.; Sanchez-Cid, L.; Gómez, S. B.; Blanco, J.; Ramaiah, D. In Vitro and in Vivo Demonstration of Photodynamic Activity and Cytoplasm Imaging through TPE Nanoparticles. *ACS Chem. Biol.* **2016**, *11* (1), 104–112. https://doi.org/10.1021/acschembio.5b00537.

(55) Xu, J.; Xiong, J.; Qin, Y.; Li, Z.; Pan, C.; Huo, Y.; Zhang, H. A Novel Quinolinyl-Tetraphenylethene-Based Fluorescence "Turn-on" Sensor for Zn2+with a Large Stokes Shift and Its Applications for Portable Test Strips and Biological Imaging. *Mater. Chem. Front.* **2020**, *4* (11), 3338–3348. https://doi.org/10.1039/d0qm00446d.

(56) Kalva, N.; Uthaman, S.; Jang, E. H.; Augustine, R.; Jeon, S. H.; Huh, K. M.; Park, I. K.; Kim, I. Aggregation-Induced Emission-Active Hyperbranched Polymer-Based Nanoparticles and Their Biological Imaging Applications. *Dye. Pigment.* **2021**, *186*, 108975. https://doi.org/10.1016/j.dyepig.2020.108975.

(57) Balachandran, Y. L.; Jiang, X. Aggregation-Induced Fluorogens in Bio-Detection, Tumor Imaging, and Therapy: A Review. *CCS Chem.* **2022**, *4* (2), 420–436. https://doi.org/10.31635/ccschem.021.202101307.

(58) Li, Y.; Yu, H.; Qian, Y.; Hu, J.; Liu, S. Amphiphilic Star Copolymer-Based Bimodal Fluorogenic/Magnetic Resonance Probes for Concomitant Bacteria Detection and Inhibition. *Adv. Mater.* **2014**, *26* (39), 6734–6741. https://doi.org/10.1002/adma.201402797.

(59) Woo, H. Y.; Nag, O. K.; Kim, J.; Kang, M.; Bazan, G. C. Water-Soluble Polyelectrolytes for FRET-Based DNA Detection. *Mol. Cryst. Liq. Cryst.* **2008**, *486* (January 2015), 244/[1286]-249/[1291]. https://doi.org/10.1080/15421400801921694.

(60) Gade, A. M.; Meadows, M. K.; Ellington, A. D.; Anslyn, E. V. Differential Array Sensing for Cancer Cell Classification and Novelty Detection. *Org. Biomol. Chem.* **2017**, *15* (46), 9866–9874. https://doi.org/10.1039/c7ob02174g.

(61) Le, N. D. B.; Yesilbag Tonga, G.; Mout, R.; Kim, S. T.; Wille, M. E.; Rana, S.; Dunphy, K. A.; Jerry, D. J.; Yazdani, M.; Ramanathan, R.; Rotello, C. M.; Rotello, V. M. Cancer Cell Discrimination Using Host-Guest "Doubled" Arrays. *J. Am. Chem. Soc.* **2017**, *139* (23), 8008–8012. https://doi.org/10.1021/jacs.7b03657.

(62) Zhang, Q.; Savagatrup, S.; Kaplonek, P.; Seeberger, P. H.; Swager, T. M. Janus

Emulsions for the Detection of Bacteria. *ACS Cent. Sci.* **2017**, *3* (4), 309–313. https://doi.org/10.1021/acscentsci.7b00021.

(63) Pieczywek, P. M.; Cybulska, J.; Szymańska-Chargot, M.; Siedliska, A.; Zdunek, A.; Nosalewicz, A.; Baranowski, P.; Kurenda, A. Early Detection of Fungal Infection of Stored Apple Fruit with Optical Sensors – Comparison of Biospeckle, Hyperspectral Imaging and Chlorophyll Fluorescence. *Food Control* **2018**, *85*, 327–338. https://doi.org/10.1016/j.foodcont.2017.10.013.

(64) Fang, Y.; Ramasamy, R. P. Current and Prospective Methods for Plant Disease Detection. *Biosensors* **2015**, *5* (3), 537–561. https://doi.org/10.3390/bios5030537.

(65) Wu, W.; Ye, S.; Huang, L.; Xiao, L.; Fu, Y.; Huang, Q.; Yu, G.; Liu, Y.; Qin, J.; Li, Q.; Li, Z. A Conjugated Hyperbranched Polymer Constructed from Carbazole and Tetraphenylethylene Moieties: Convenient Synthesis through One-Pot "a 2 + B4" Suzuki Polymerization, Aggregation-Induced Enhanced Emission, and Application as Explosive Chemosensors and PLE. *J. Mater. Chem.* **2012**, *22* (13), 6374–6382. https://doi.org/10.1039/c2jm16514g.

(66) Feng, H. T.; Wang, J. H.; Zheng, Y. S. CH3-π Interaction of Explosives with Cavity of a TPE Macrocycle: The Key Cause for Highly Selective Detection of TNT. *ACS Appl. Mater. Interfaces* **2014**, *6* (22), 20067–20074. https://doi.org/10.1021/am505636f.

(67) Feng, H. T.; Zheng, Y. S. Highly Sensitive and Selective Detection of Nitrophenolic Explosives by Using Nanospheres of a Tetraphenylethylene Macrocycle Displaying Aggregation-Induced Emission. *Chem. - A Eur. J.* **2014**, *20* (1), 195–201. https://doi.org/10.1002/chem.201302638.

(68) Mahendran, V.; Pasumpon, K.; Thimmarayaperumal, S.; Thilagar, P.; Shanmugam, S. Tetraphenylethene-2-Pyrone Conjugate: Aggregation-Induced Emission Study and Explosives Sensor. *J. Org. Chem.* **2016**, *81* (9), 3597–3602. https://doi.org/10.1021/acs.joc.6b00267.

(69) Ghosh, K. R.; Saha, S. K.; Wang, Z. Y. Ultra-Sensitive Detection of Explosives in Solution and Film as Well as the Development of Thicker Film Effectiveness by Tetraphenylethene Moiety in AIE Active Fluorescent Conjugated Polymer. *Polym. Chem.* **2014**, *5* (19), 5638–5643. https://doi.org/10.1039/c4py00673a.

(70) Dong, W.; Pan, Y.; Fritsch, M.; Scherf, U. High Sensitivity Sensing of Nitroaromatic Explosive Vapors Based on Polytriphenylamines with AIE-Active Tetraphenylethylene Side Groups. *J. Polym. Sci. Part A Polym. Chem.* **2015**, *53* (15),

1753–1761. https://doi.org/10.1002/pola.27631.

(71) Dong, X.; Wang, R.; Liu, G.; Liu, P.; Pu, S. A Novel Sensitive Sensor for Cu2+ and Multi-Switch Based on a Diarylethene with a 2-(2′-Hydroxyphenyl)Benzothiazole Unit. *Tetrahedron* **2016**, *72* (22), 2935–2942. https://doi.org/10.1016/j.tet.2016.04.007.

(72) Mohammadi, A.; Jabbari, J. Simple Naked-Eye Colorimetric Chemosensors Based on Schiff-Base for Selective Sensing of Cyanide and Fluoride Ions. *Can. J. Chem.* **2016**, *94* (7), 631–636. https://doi.org/10.1139/cjc-2016-0039.

(73) Kaur, P.; Kaur, S.; Singh, K. Colorimetric Detection of Cyanide in Water Using a Highly Selective Cu2+ Chemosensor. *Inorg. Chem. Commun.* **2009**, *12* (10), 978–981. https://doi.org/10.1016/j.inoche.2009.07.026.

(74) Wang, M.; Leung, K. H.; Lin, S.; Chan, D. S. H.; Kwong, D. W. J.; Leung, C. H.; Ma, D. L. A Colorimetric Chemosensor for CU2+ Ion Detection Based on an Iridium(III) Complex. *Sci. Rep.* **2014**, *4*, 1–7. https://doi.org/10.1038/srep06794.

(75) Park, G. J.; Lee, J. J.; You, G. R.; Nguyen, L.; Noh, I.; Kim, C. A Dual Chemosensor for Zn2+ and Co2+ in Aqueous Media and Living Cells: Experimental and Theoretical Studies. *Sensors Actuators, B Chem.* **2016**, *223*, 509–519. https://doi.org/10.1016/j.snb.2015.09.129.

(76) Wang, J. H.; Liu, Y. M.; Dong, Z. M.; Chao, J. Bin; Wang, H.; Wang, Y.; Shuang, S. M. New Colorimetric and Fluorometric Chemosensor for Selective Hg2+ Sensing in a Near-Perfect Aqueous Solution and Bio-Imaging. *J. Hazard. Mater.* **2020**, *382* (August 2019), 121056. https://doi.org/10.1016/j.jhazmat.2019.121056.

(77) Zeng, S.; Li, S. J.; Liu, T. T.; Sun, X. J.; Xing, Z. Y. A Significant Fluorescent "Turn-on" Chemosensor for Al3+ Detection and Application in Real Sample, Logic Gate and Bioimaging. *Inorganica Chim. Acta* **2019**, *495* (May), 118962. https://doi.org/10.1016/j.ica.2019.118962.

(78) Gupta, A.; Kumar, N. A Review of Mechanisms for Fluorescent "Turn-on" Probes to Detect Al3+ Ions. *RSC Adv.* **2016**, *6* (108), 106413–106434. https://doi.org/10.1039/c6ra23682k.

(79) Riis-Johannessen, T.; Schenk, K.; Severin, K. Turn-off-and-on: Chemosensing Ensembles for Sensing Chloride in Water by Fluorescence Spectroscopy. *Inorg. Chem.* **2010**, *49* (20), 9546–9553. https://doi.org/10.1021/ic1012878.

(80) Wu, D.; Sedgwick, A. C.; Gunnlaugsson, T.; Akkaya, E. U.; Yoon, J.; James, T. D. Fluorescent Chemosensors: The Past, Present and Future. *Chem. Soc. Rev.* **2017**, *46*

(23), 7105–7123. https://doi.org/10.1039/c7cs00240h.

(81) Off, P. N.; Relaxation, V.; Conversion, I.; Crossing, I.; Scale, T.; Links, O. Jablonski Diagram. **2011**, 1–7.

(82) Priestley, E. B.; Haug, A. Phosphorescence Spectrum of Pure Crystalline Naphthalene. *J. Chem. Phys.* **1968**, *49* (2), 622–629. https://doi.org/10.1063/1.1670118.

(83) Jaffé, H. H.; Miller, A. L. The Fates of Electronic Excitation Energy. *J. Chem. Educ.* **1966**, *43* (9), 469–473. https://doi.org/10.1021/ed043p469.

(84) Nagarajan, R.; Vanjare, B. D.; Hwan Lee, K. The First Tryptophan Based Turn-off Chemosensor for Fe2+ Ion Detection. *Spectrochim. Acta - Part A Mol. Biomol. Spectrosc.* **2021**, *262*, 120103. https://doi.org/10.1016/j.saa.2021.120103.

(85) Immanuel David, C.; Movuleeshwaran, P. T.; Jayaraj, H.; Prabakaran, G.; Parimala devi, D.; Kumar, M. S.; Abiram, A.; Satheesh Babu, T. G.; Prabhu, J.; Nandhakumar, R. Highly Selective, Reversible and ICT-Based Fluorescent Chemosensor for Bismuth Ions: Applications in Bacterial Imaging, Logic Gate and Food Sample Analysis. *J. Photochem. Photobiol. A Chem.* **2022**, *422* (September 2021), 113558. https://doi.org/10.1016/j.jphotochem.2021.113558.

(86) Bag, R.; Sikdar, Y.; Sahu, S.; Das Mukhopadhyay, C.; Drew, M. G. B.; Goswami, S. Benzimidazole Based ESIPT Active Chemosensors Enable Nano–Molar Detection of Cu2+ in 90% Aqueous Solution, MCF–7 Cells, and Plants. *J. Photochem. Photobiol. A Chem.* **2022**, *431* (May), 114006. https://doi.org/10.1016/j.jphotochem.2022.114006.

(87) Zhang, Q.; Ding, H.; Xu, X.; Wang, H.; Liu, G.; Pu, S. Rational Design of a FRET-Based Ratiometric Fluorescent Probe with Large Pseudo-Stokes Shift for Detecting Hg2+ in Living Cells Based on Rhodamine and Anthracene Fluorophores. *Spectrochim. Acta - Part A Mol. Biomol. Spectrosc.* **2022**, *276*, 121242. https://doi.org/10.1016/j.saa.2022.121242.

(88) Lee, J. J.; Lee, S. A.; Kim, H.; Nguyen, L.; Noh, I.; Kim, C. A Highly Selective CHEF-Type Chemosensor for Monitoring Zn2+ in Aqueous Solution and Living Cells. *RSC Adv.* **2015**, *5* (52), 41905–41913. https://doi.org/10.1039/c5ra05080d.

(89) La, D. D.; Bhosale, S. V.; Jones, L. A.; Bhosale, S. V. Tetraphenylethylene-Based AIE-Active Probes for Sensing Applications. *ACS Appl. Mater. Interfaces* **2018**, *10* (15), 12189–12216. https://doi.org/10.1021/acsami.7b12320.

(90) Mei, J.; Leung, N. L. C.; Kwok, R. T. K.; Lam, J. W. Y.; Tang, B. Z. Aggregation-

Induced Emission: Together We Shine, United We Soar! *Chem. Rev.* **2015**, *115* (21), 11718–11940. https://doi.org/10.1021/acs.chemrev.5b00263.

(91) Luo, J.; Xie, Z.; Xie, Z.; Lam, J. W. Y.; Cheng, L.; Chen, H.; Qiu, C.; Kwok, H. S.; Zhan, X.; Liu, Y.; Zhu, D.; Tang, B. Z. Aggregation-Induced Emission of 1-Methyl-1,2,3,4,5-Pentaphenylsilole. *Chem. Commun.* **2001**, *18*, 1740–1741. https://doi.org/10.1039/b105159h.

(92) Li, Y.; Xu, K.; Si, Y.; Yang, C.; Peng, Q.; He, J.; Hu, Q.; Li, K. An Aggregation-Induced Emission (AIE) Fluorescent Chemosensor for the Detection of Al(III) in Aqueous Solution. *Dye. Pigment.* **2019**, *171* (May), 107682. https://doi.org/10.1016/j.dyepig.2019.107682.

(93) Bhosale, S. V.; Al Kobaisi, M.; Jadhav, R. W.; Morajkar, P. P.; Jones, L. A.; George, S. Naphthalene Diimides: Perspectives and Promise. *Chem. Soc. Rev.* **2021**, *50* (17), 9845–9998. https://doi.org/10.1039/d0cs00239a.

(94) Wagner, B. D. The Use of Coumarins as Environmentally-Sensitive Fluorescent Probes of Heterogeneous Inclusion Systems. *Molecules* **2009**, *14* (1), 210–237. https://doi.org/10.3390/molecules14010210.

(95) Boens, N.; Leen, V.; Dehaen, W. Fluorescent Indicators Based on BODIPY. *Chem. Soc. Rev.* **2012**, *41* (3), 1130–1172. https://doi.org/10.1039/c1cs15132k.

(96) Zhang, L.; Chen, Y.; Jiang, J. Solid State Fluorescent Functionalized-Triphenylamine Bodipy Detector for HCl Vapor with High Stability and Absolute Fluorescent Quantum Yield. *Dye. Pigment.* **2016**, *124*, 110–119. https://doi.org/10.1016/j.dyepig.2015.09.005.

(97) Liu, T.; Liu, X.; Valencia, M. A.; Sui, B.; Zhang, Y.; Belfield, K. D. Far-Red-Emitting TEG-Substituted Squaraine Dye: Synthesis, Optical Properties, and Selective Detection of Cyanide in Aqueous Solution. *European J. Org. Chem.* **2017**, *2017* (27), 3957–3964. https://doi.org/10.1002/ejoc.201700649.

(98) Sreejith, S.; Carol, P.; Chithra, P.; Ajayaghosh, A. Squaraine Dyes: A Mine of Molecular Materials. *J. Mater. Chem.* **2008**, *18* (3), 264–274. https://doi.org/10.1039/b707734c.

(99) Li, Z.; Zhao, P.; Tofighi, S.; Sharma, R.; Ensley, T. R.; Jang, S. H.; Hagan, D. J.; Van Stryland, E. W.; Jen, A. K. Y. Zwitterionic Cyanine-Cyanine Salt: Structure and Optical Properties. *J. Phys. Chem. C* **2016**, *120* (28), 15378–15384. https://doi.org/10.1021/acs.jpcc.6b03037.

(100) SEYBOLD, P. G.; GOUTERMAN, M.; CALLIS, J. Calorimetric, Photometric and

Lifetime Determinations of Fluorescence Yields of Fluorescein Dyes. *Photochem. Photobiol.* **1969**, *9* (3), 229–242. https://doi.org/10.1111/j.1751-1097.1969.tb07287.x.

(101) Haria, D. P.; König, B. Synthetic Applications of Eosin Y in Photoredox Catalysis. *Chem. Commun.* **2014**, *50* (51), 6688–6699. https://doi.org/10.1039/c4cc00751d.

(102) Zhang, X. F.; Zhang, J.; Lu, X. The Fluorescence Properties of Three Rhodamine Dye Analogues: Acridine Red, Pyronin Y and Pyronin B. *J. Fluoresc.* **2015**, *25* (4), 1151–1158. https://doi.org/10.1007/s10895-015-1610-5.

(103) Zhang, G.; Shuang, S.; Dong, C.; Pan, J. Study on the Interaction of Methylene Blue with Cyclodextrin Derivatives by Absorption and Fluorescence Spectroscopy. *Spectrochim. Acta - Part A Mol. Biomol. Spectrosc.* **2003**, *59* (13), 2935–2941. https://doi.org/10.1016/S1386-1425(03)00123-9.

(104) Krzyszkowska, E.; Walkowiak-Kulikowska, J.; Stienen, S.; Wojcik, A. Thionine-Graphene Oxide Covalent Hybrid and Its Interaction with Light. *Phys. Chem. Chem. Phys.* **2017**, *19* (22), 14412–14423. https://doi.org/10.1039/c7cp01267e.

(105) Singh, M. K.; Pal, H.; Koti, A. S. R.; Sapre, A. V. Photophysical Properties and Rotational Relaxation Dynamics of Neutral Red Bound to β-Cyclodextrin. *J. Phys. Chem. A* **2004**, *108* (9), 1465–1474. https://doi.org/10.1021/jp035075e.

(106) Fei, X.; Gu, Y.; Wang, Y.; Meng, Q.; Zhang, B. Targeted Thiazole Orange Derivative with Folate: Synthesis, Fluorescence and in Vivo Fluorescence Imaging. *Molecules* **2010**, *15* (10), 6983–6992. https://doi.org/10.3390/molecules15106983.

(107) Murudkar, S.; Mora, A. K.; Singh, P. K.; Bandyopadhyay, T.; Nath, S. An Ultrafast Molecular Rotor Based Ternary Complex in a Nanocavity: A Potential "'turn on'" Fluorescence Sensor for the Hydrocarbon Chain. *Phys. Chem. Chem. Phys.* **2015**, *17* (8), 5691–5703. https://doi.org/10.1039/c4cp04636f.

(108) Mako, T. L.; Racicot, J. M.; Levine, M. Supramolecular Luminescent Sensors. *Chem. Rev.* **2019**, *119* (1), 322–477. https://doi.org/10.1021/acs.chemrev.8b00260.

(109) Periasamy, R.; Kothainayaki, S.; Sivakumar, K. Encapsulation of Dicinnamalacetone in β-Cyclodextrin: A Physicochemical Evaluation and Molecular Modeling Approach on 1:2 Inclusion Complex. *J. Macromol. Sci. Part A Pure Appl. Chem.* **2016**, *53* (9), 546–556. https://doi.org/10.1080/10601325.2016.1201750.

(110) Benesi, H. A.; Hildebrand, J. H. Spectrophotometry of Iodine with Aromatic Hydrocarbons. *J. Am. Chem. Soc.* **1949**, *71* (8), 2703–2707.

(111) Blazic, A. 3 0.001. **1950**, No. 1.

(112) Renny, J. S.; Tomasevich, L. L.; Tallmadge, E. H.; Collum, D. B. Method of Continuous Variations: Applications of Job Plots to the Study of Molecular Associations in Organometallic Chemistry. *Angew. Chemie - Int. Ed.* **2013**, *52* (46), 11998–12013. https://doi.org/10.1002/anie.201304157.

(113) Belter, M.; Sajnóg, A.; Barałkiewicz, D. Over a Century of Detection and Quantification Capabilities in Analytical Chemistry - Historical Overview and Trends. *Talanta* **2014**, *129*, 606–616. https://doi.org/10.1016/j.talanta.2014.05.018.

Chapter II

Solvent-induced hierarchical self-assembly of tetraphenylethylene derivative

2.1 Introduction

To develop systems that can strengthen our understanding of some life processes and enable or potential applications in fields like sensors, liquid crystals, and optical activity. The induction and control of supramolecular chiral assembly from achiral functional organic molecules is an important challenge.[1–4] The self-assembly of small organic molecules with chiral groups, such as bola-amphiphile, peptides, lipid bilayers, glucose, and π-conjugated oligomers, has typically been found to produce supramolecular helical or twisted structures.[5–9] In some examples, homochiral molecules or a mixture of chiral and achiral molecules have been used to develop twisted or helical fibers. This can also be accomplished by using chiral molecular templates, in which the handedness of the self-assembled helical structure accepts the molecule chirality.[10–14] It has also been reported that achiral molecules containing azobenzene can assemble supramolecular chiral structures by being exposed to circularly polarized light.[15–17] Only a few reports report the formation of helical nanoparticles from achiral molecules, including asymmetric porphyrins, quinacridone, cationic surfactants, amphiphilic cyanine dyes, and cationic surfactants.[18–24] However, most of these small compounds suffer from aggregation induced quenching (ACQ) effects,[25] which is very essential in the creation of mechanochromic luminescent materials. Investigations into the self-assembly and use of the helices produced by the photo-luminescent achiral molecules are still in their beginnings. The formation of contorted nanoparticles by two achiral luminescent quinacridone (QA) derivatives from THF/ethanol mixtures is described by Zhao et al[19]. The develop of achiral organic functional molecules which can be self-assemble into an architectures with selective handedness and aggregation induced emission (AIE) in the absence of chiral molecule is an crucial step in understanding the role chirality plays within these systems.[26]

Tetraphenylethylene (TPE) and its derivatives unique fluorescence properties have attracted a lot of interest recently. The AIE-effect causes these chromophores, which are weak or non-emissive as unassociated monomers, to become highly fluorescent upon aggregate.[27,28] AIE properties are of interest in various areas including fluorescence chemosensors[29] and electroluminescent organic materials (OLDs).[30] The building of nanofibers made of pyridyl-substituted TPE derivatives and their luminescence properties were recently studied with respect to pH.[31] The self-assembly of TPE-based porphyrin molecules that self-assembled into unique ring nanostructures was also described in a different study; the outcomes are comparable to those of the natural photosynthesis system-II.[32] The assembly of

supramolecular helical structures using achiral AIE-active TPE luminophores as building blocks has never been studied, despite the fact that TPE compounds have been used to examine the interaction of AIE molecules (AIEs) with DNA,[33] proteins,[34,35] or other biostructures.[36]

2.2 Experimental

2.2.1 Material and Methods

All reagents and chemical including solvents were purchased from Sigma-Aldrich, TCI, and AVRA and used without purification. ^{1}H-NMR spectra were recorded on 400 MHz Bruker spectrometer and ^{13}C-NMR using 100 MHz spectrometer as $CDCl_3$-d solutions (trimethylsilane as an internal standard). Mass spectral data were obtained from Bruker ultraflexTOF (MALDI-TOF). IR spectra were recorded on a Perkin Elmer FT-IR spectrometer. UV-Vis absorption spectra were recorded by UV-Vis-1800 Schimadzu and fluorescence emission measured on Agilent Carry Eclipse photoluminescence. Circular dichroism were performed on JASCO.

2.2.2 synthesis of 1,1,2,2-tetraphenylethene 2 :

Compound 2 was synthesized by the reported procedure[37]; a two-neck round bottom flask and reflux condenser were flushed with dry nitrogen gas. To stir a suspension of benzophenone (5 g, 27 mmol) and zinc powder (5.3 g, 82 mmol) in 200 mL dried THF under nitrogen gas at 0 ^{o}C. TiCl4 (5.9 mL, 54 mmol) was injected slowly dropwise by syringe over a period of 30 min. at the same temperature. The resulting black suspension of the reaction mixture was slowly heated up to room temperature under stirring. Afterward, the mixture was reflux at 70 ^{o}C for 12 h. The reaction was quenched by an aqueous solution of K2CO3 and extracted with ethyl acetate (2×150 mL). The organic phase was combined, washed with brine, and dried over anhydrous Na_2SO_4. After filtration, the filtrate was concentrated under a vacuum to afford the crude product, further washed with dry ethanol to get pure as a white solid 2 (90%), M.P = 222-224 °C; ^{1}H NMR (400 MHz, CDCl3): δ (ppm): 7.18-7.7.16 (m, 2H), 7.12–7.02 (m, 18H). ^{13}C NMR (100 MHz, CDCl3): 143.72, 143.46, 140.95, 131.32, 128.52, 128.14, 127.63, 126.40, 126.00, 125.84.

2.2.3 Synthesis of (2-(4-nitrophenyl)ethene-1,1,2-triyl)tribenzene 3: The compound **3** was prepared by using the reported literature procedure[38]: Placed tetraphenylethylene **2** (2 g, 6 mmol) then added glacial acetic acid (1.38 mL, 24 mmol), and dichloromethane (60 mL) and the reaction mixture is cooled to -5 °C using ice-salt bath after cooling added conc. nitric acid (1.13 mL, 18 mmol) while vigorous stirring. Stirred the reaction mixture for a

further 15-20 min maintaining the -5 ^{o}C temperature and the progress of the reaction was monitored by TLC. After completion, the reaction mixture was quenched with ice-cold water, separate the organic phase, and wash with water three times (3×30 mL). The organic phase was dried over anhydrous Na_2SO_4 and filtered. Evaporate the solution to dryness under vacuum. Crude residue obtained was purified by column chromatography (Ethyl acetate: hexane, 5:95) to afford **3** as a yellow solid, 2 gm, 88% yield. (M.P. 76 ^{o}C) Elemental analysis ($C_{26}H_{19}NO_2$): cal. C, 82.74; H, 5.07; N, 3.71., Obs. C, 82.23; H, 5.28; N, 3.59. IR (cm^{-1}):3053, 3022, 1595, 1514, 1344, 752, 698. ^{1}H NMR ($CDCl_3$, 400 MHz) δ ppm: 7.98-796(d, *J*=8 Hz, 2H), 7.20-7.12(m, 11H), 7.05-7.00(m, 6H). ^{13}C NMR ($CDCl_3$, 100 MHz) δ (ppm): 149.56, 146.77, 146.42, 141.73, 141.43, 136.56, 132.05, 131.95, 131.09, 131.03, 128.53, 128.26, 128.02, 127.74, 123.39, and 123.14.

2.2.4 Synthesis of 4-(1,2,2-triphenylvinyl)aniline 4: Compound **4** was synthesized by literatureprocedure[38]: 4-nitro-tetraphenylethene (**3**) (1 g, 2.6 mmol) was added in EtOH (50 mL) then degassed reaction mixture with dry nitrogen, subsequently, added 10% Pd/C (0.50 g), and hydrazine-hydrate (6.00 g, 120 mmol). Kept reaction mixture for 4 hours, after completion of reaction, to remove Pd/C from reaction mixture, filtered the hot reaction mixture through cellite pad. Upon evaporation of reaction, mixture under reduced pressure gives 4-tetraphenylethenylamine (**4**) in 0.85 gm (93% yield). (M.P. 204 ^{o}C) Elemental analysis ($C_{26}H_{21}N$): cal. C, 89.88; H, 6.09; N, 4.03 Obs. 89.68; H, 6.40; N, 3.91. IR (cm^{-1}) 3471, 3379, 3057, 3022, 1620, 1514, 1286, 750, ^{1}H NMR ($CDCl_3$, 400 MHz) δ (ppm): 7.14-7.04 (15H, m), 6.83 (2H, d, *J* = 8 Hz), 6.45 (2H, d, *J* = 12 Hz), 3.59 (2H, s). ^{13}C NMR ($CDCl_3$, 100 MHz) δ ppm: 144.95, 144.52, 144.38, 144.35, 141.12, 139.49, 134.21, 132.66, 131.64, 131.58, 131.53, 127.83, 127.71, 127.69, 126.41, 126.23, 114.50.

2.2.5 Synthesis of N1,N3,N5-tris(4-(1,2,2-triphenylvinyl)phenyl)benzene-1,3,5-tricarboxamide 1: In a clean 25 ml round bottom flask compound **4** (0.563 g, 1.5 mmol) and DMAP (0.2 Equiv.) dissolved in dry DCM (10 ml), Kept the reaction mixture 5 min at the same temp. Then compound **5** (0.1 g, 0.3 mmol) was added to the reaction mixture. Further completion of reaction confirmed by TLC, the reaction mixture extracted with DCM, washed with brine solution, the extracted organic layer dried over anhydrous Na_2SO_4, and filtered. Evaporate the solution to get a solid product through reduced pressure. Crude product purified by column chromatography (Ethyl acetate: hexane, 10:90) to afford **1** as a light yellow solid. (0.40 g, 88%) Elemental analysis ($C_{87}H_{63}N_3O_3$): cal. C, 87.19; H, 5.30; N, 3.51, Obs. C, 86.98; H, 5.45; N, 3.36, IR values in cm^{-1} 3632, 3089, 3067, 3021, 1683,

1523, 1327, ^{1}H NMR ($CDCl_3$, 400 MHz) δ ppm: 8.54 (1H, s),8.24 (1H, s), 7.30 (2H, d, *J* = 8 Hz), 7.08 (9H, m), 7.04 (6H, m), 6.97 (2H, d, *J* = 8 Hz). ^{13}C NMR ($CDCl_3$, 100 MHz) δ ppm: 143.68, 141.16, 132.07, 131.34, 127.85, 127.76, 127.67, 126.57, 119.59., (MALDI-TOF, m/z): $C_{87}H_{63}N_3O_3$ [M^+] cal. for: 1197.486, found: 1198.609(M+H), 1220.582(M+Na)$^+$

2.2.6 UV-Vis spectroscopy: UV-Vis spectra were recorded using a Shimadzu UV-1800 spectrometer. A 3 mL quartz cuvette with a 1 cm length was used for UV-Vis studies. The all readings recorded at room temperature.

2.2.7 Fluorescence spectroscopy: On a Spectrophotometer Carry eclipse (Agilent), fluorescence emission spectra were measured. A 3 ml quartz cell with a 1 cm path length was used for all experiments at room temperature.

2.2.8 Circular Dichroism: At room temperature, CD spectra were recorded using a Jasco spectrometer.

2.2.9 TCSPC: The samples for the TCSPC analysis were prepared in used solvent system evaluated using a 1 cm cuvette at room temperature. Average lifetime measured on (FluoroLog3-Triple Illuminator, IBH Horiba JobinYvon) using a picosecond light emitting diode laser (NanoLED, λ_{ex} = 330 nm). The samples for the TCSPC analysis were prepared in used solvent system evaluated using a 1 cm cuvette at room temperature

2.2.10 Scanning electron microscopy: The SEM analysis performed on a Carl-Ziess Scanning Electron Microscope operating at a high vacuum, providing direct visualization of self-assembled nano-structures. The samples were prepared, first the silicon wafers were washed with acetone followed by distilled water and then Methanol and dried. After samples were placed on silicon wafers by drop cast method, further solvent was evaporated, and then the air-dried sample was sputter-coated with gold for 15 min at a 10 mA (Quorum).

2.2.11 X-ray diffraction: XRD measurements were performed on a Bruker D8 FOCUS diffractometer using a Cu target radiation source (λ = 0.15418 nm).

2.3 Result and discussion

2.3.1 Synthetic route of *N*^{1},*N*^{3},*N*^{5}-tris(4-(1,2,2-triphenylvinyl)phenyl)benzene-1,3,5-tricarboxamide 1

The synthesis of *N*^{1},*N*^{3},*N*^{5}-tris(4-(1,2,2-triphenylvinyl)phenyl)benzene-1,3,5-tricarboxamide **1**, started with McMurry reaction of benzophenone in presence of Titanium

(II) chloride and zinc dust gives TPE **2**. Further, TPE **2** reacts with nitric acid in presence of acetic acid at -15 ^{o}C gives mono nitro TPE **3**. However, mono amino TPE synthesized by reduction of **3** by using palladium carbon 10% and hydrazine hydrate in ethanol. In final step, the synthesized mono amino TPE **3** molecule reacted with **5** in presence of DMAP as catalytic amount in DCM at room temperature gives final product **1.**

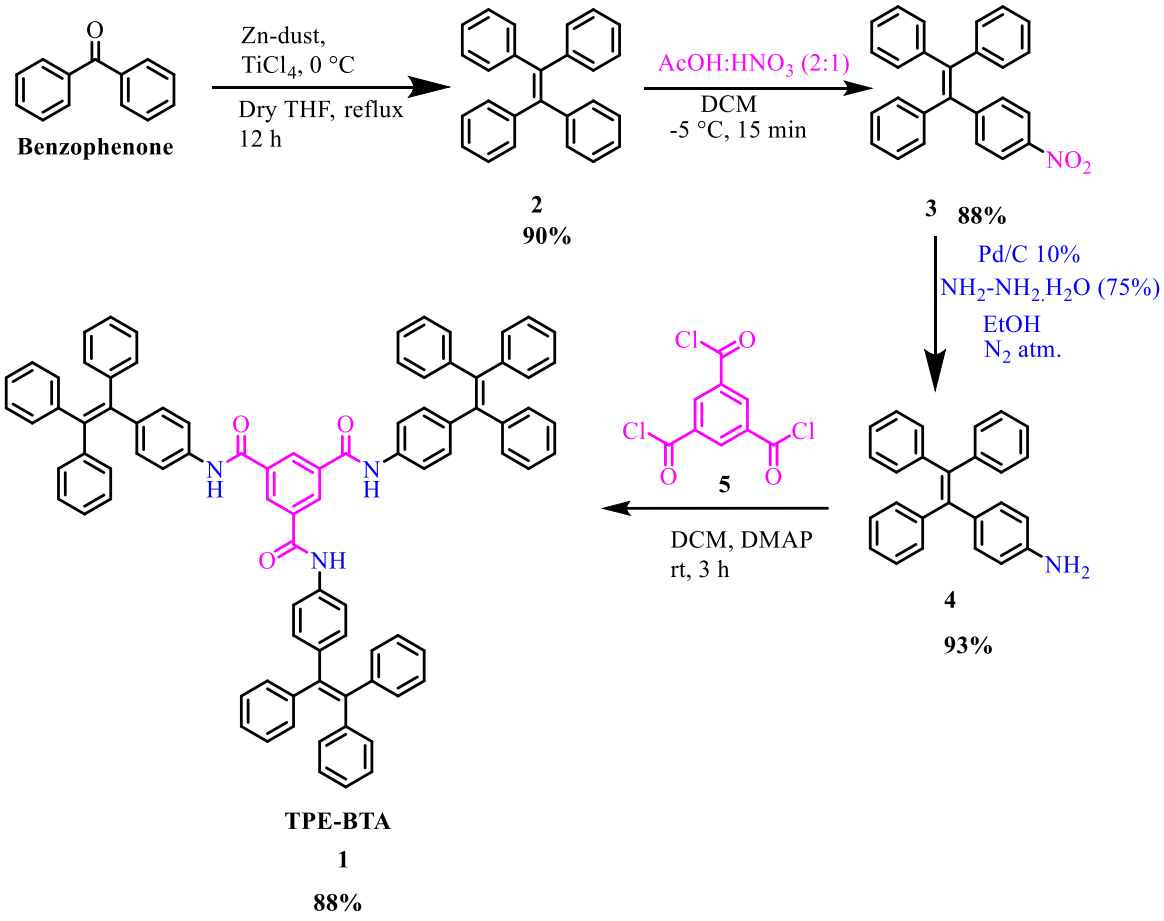

Scheme 2.1: Synthesis of compound **1**

2.3.2 Characterization of synthesized compounds

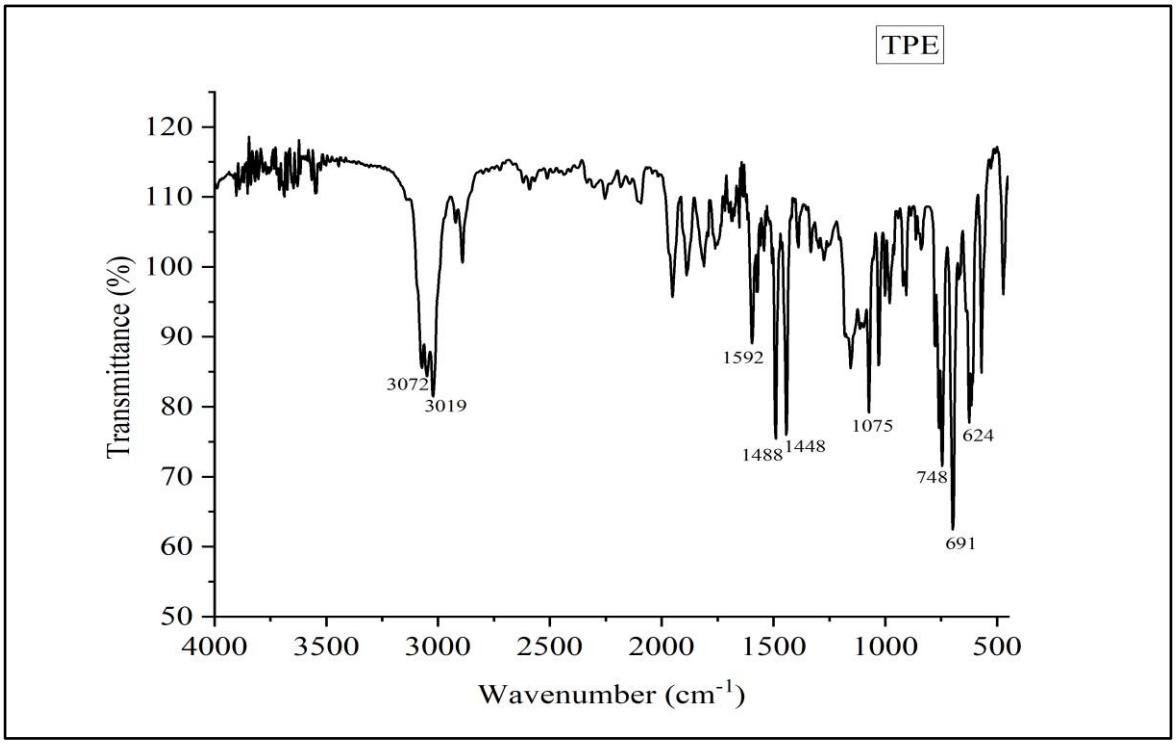

Figure 2.1: FT-IR spectrum of 1,1,2,2-tetraphenylethene **2**

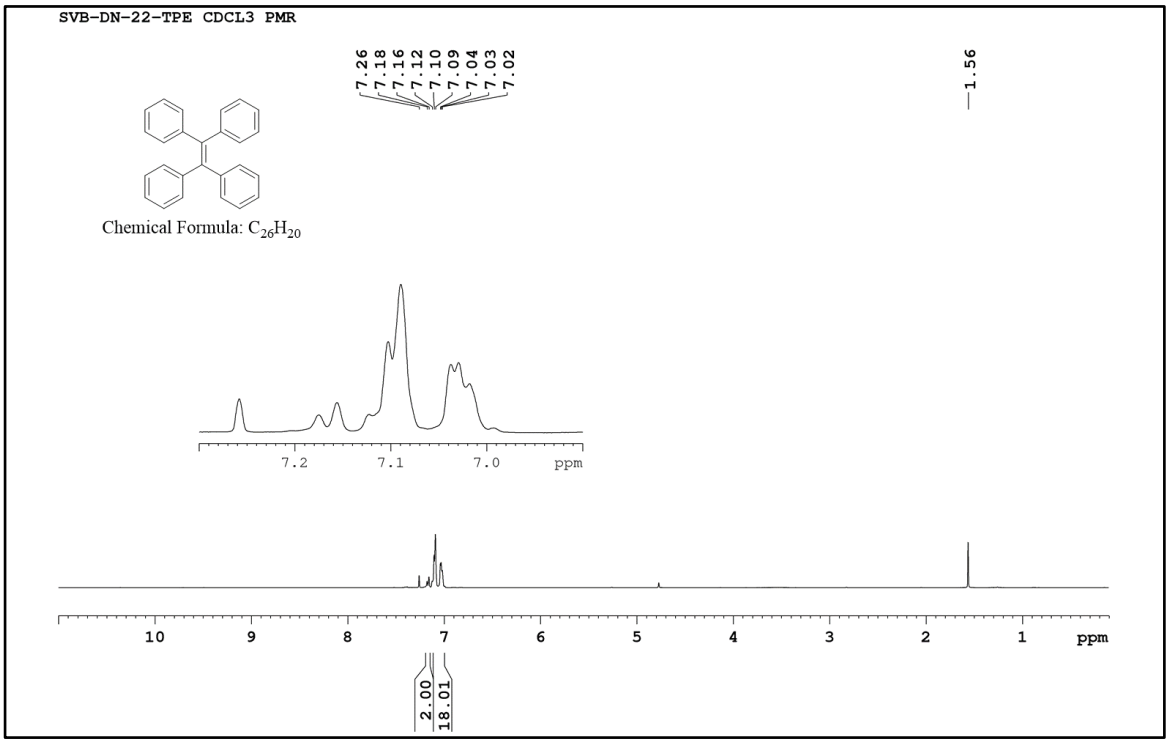

Figure 2.2: ^{1}H NMR spectrum of 1,1,2,2-tetraphenylethene **2**

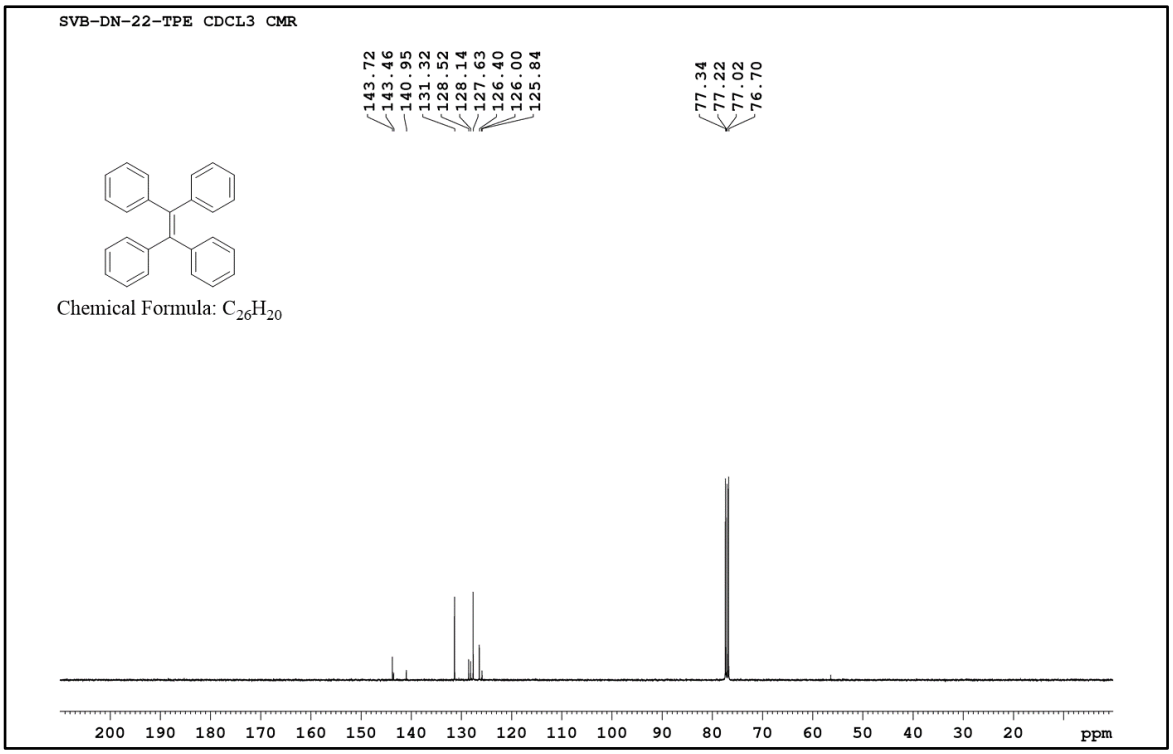

Figure 2.3: ^{13}C NMR spectrum of 1,1,2,2-tetraphenylethene **2**

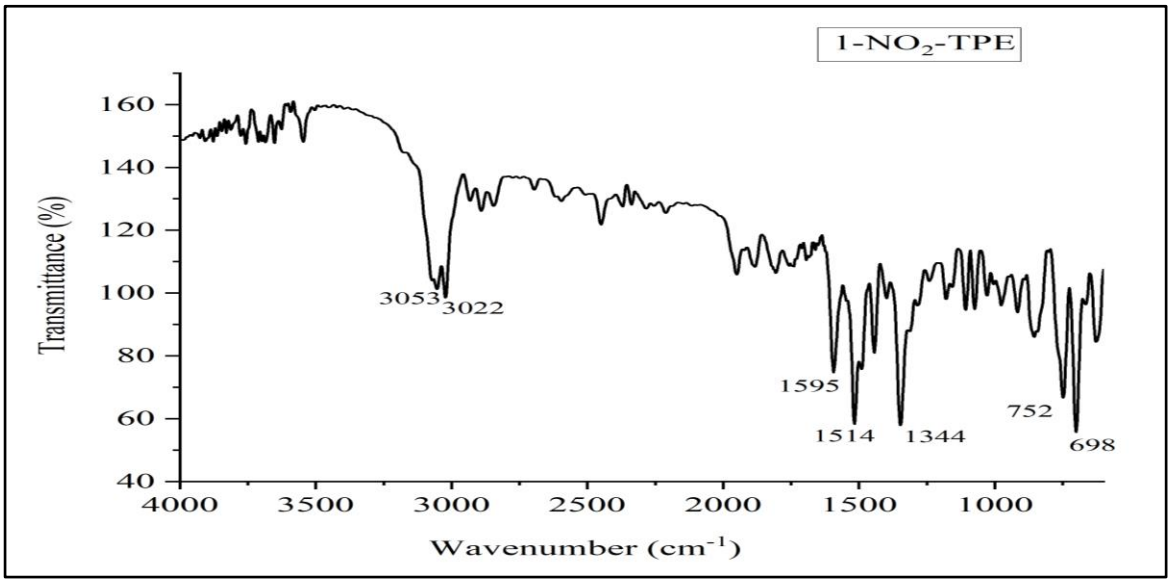

Figure 2.4: FT-IR spectrum of (2-(4-nitrophenyl)ethene-1,1,2-triyl)tribenzene **3**

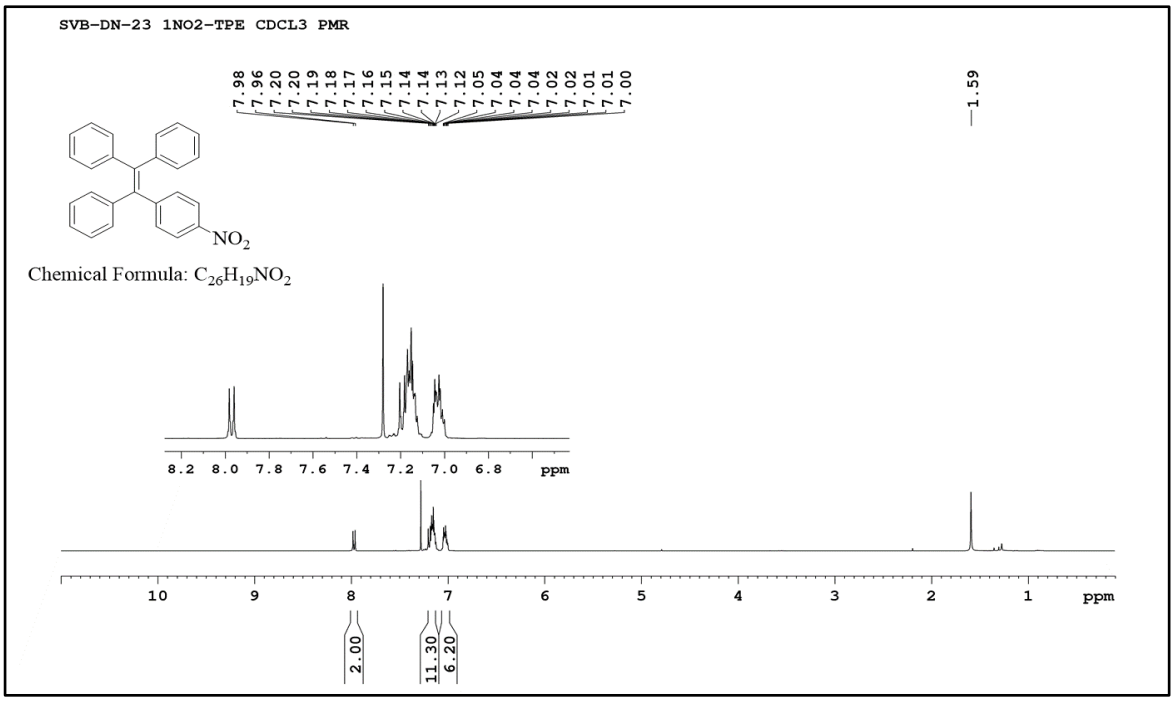

Figure 2.5: ^{1}H NMR spectrum of (2-(4-nitrophenyl)ethene-1,1,2-triyl)tribenzene **3**

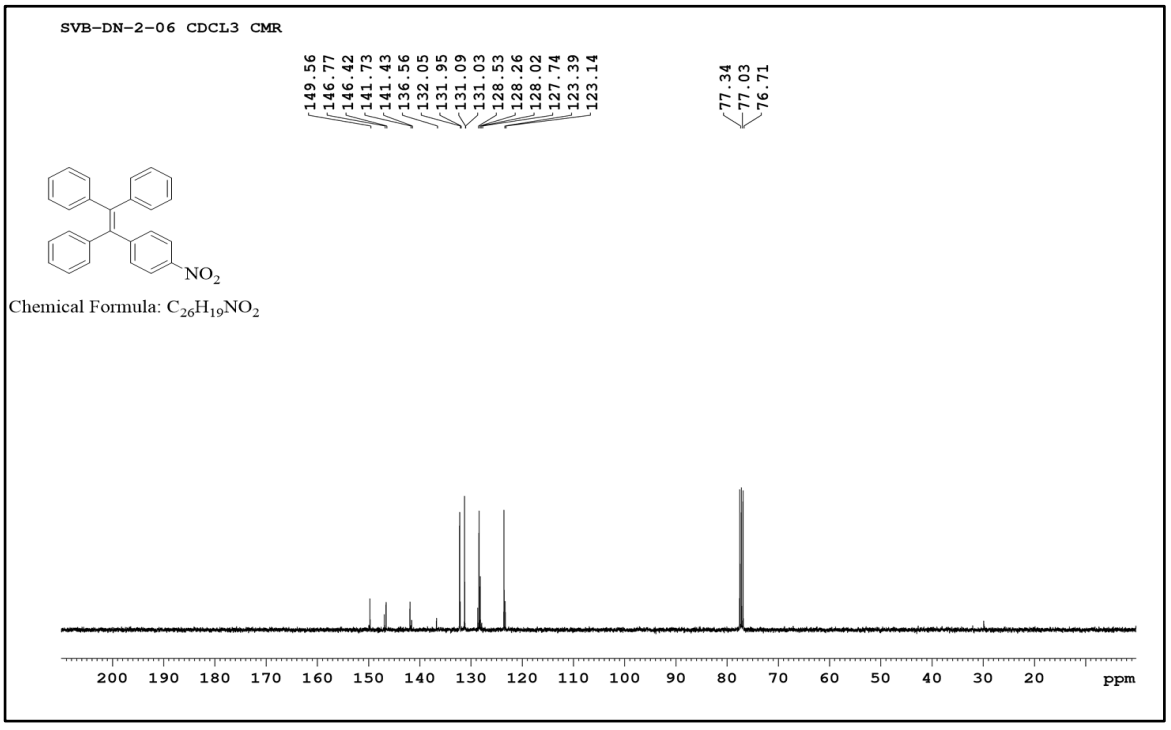

Figure 2.6: ^{13}C NMR spectrum of (2-(4-nitrophenyl)ethene-1,1,2-triyl)tribenzene **3**

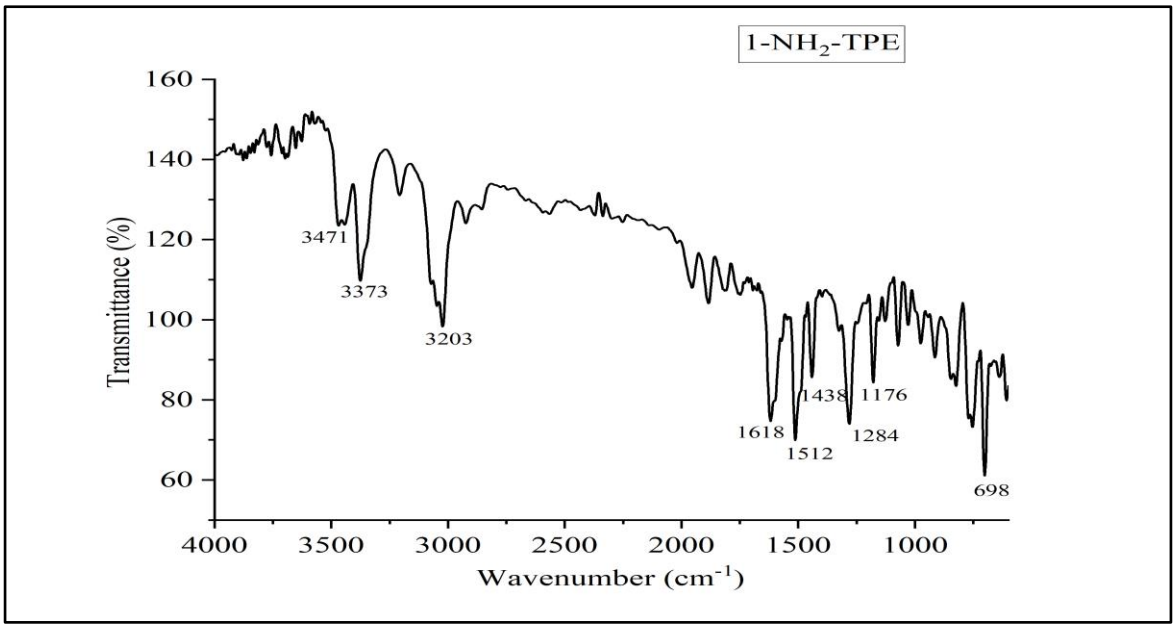

Figure 2.7: FT-IR spectrum of 4-(1,2,2-triphenylvinyl)aniline **4**

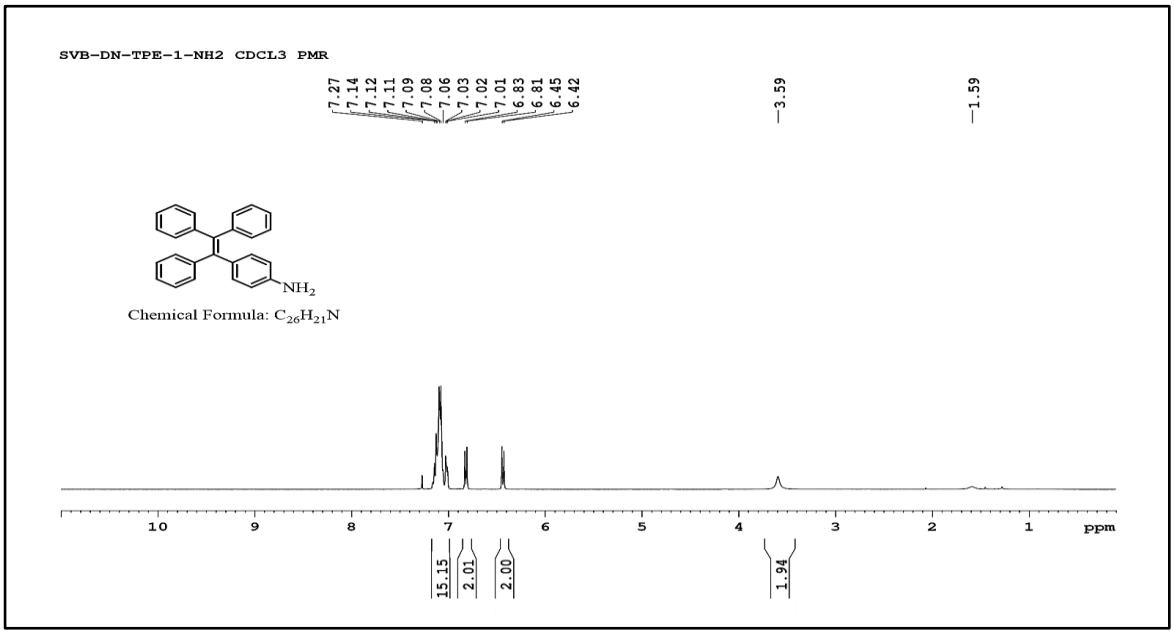

Figure 2.8: ^{1}H NMR spectrum of 4-(1,2,2-triphenylvinyl)aniline **4**

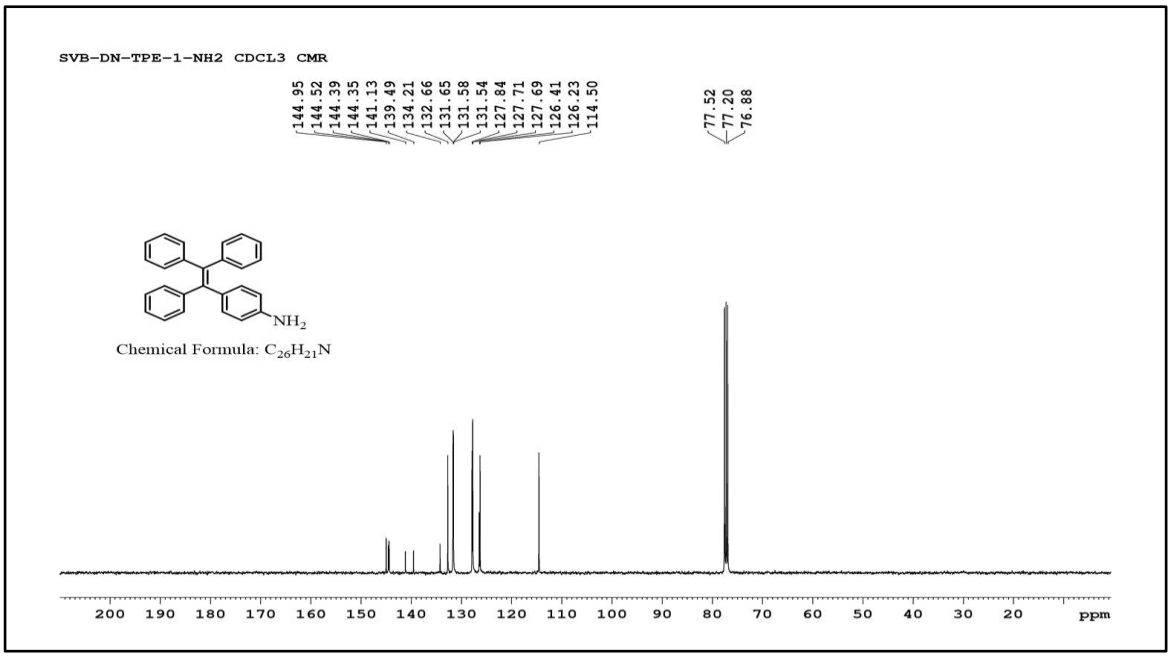

Figure 2.9: ^{13}C NMR spectrum of 4-(1,2,2-triphenylvinyl)aniline **4**

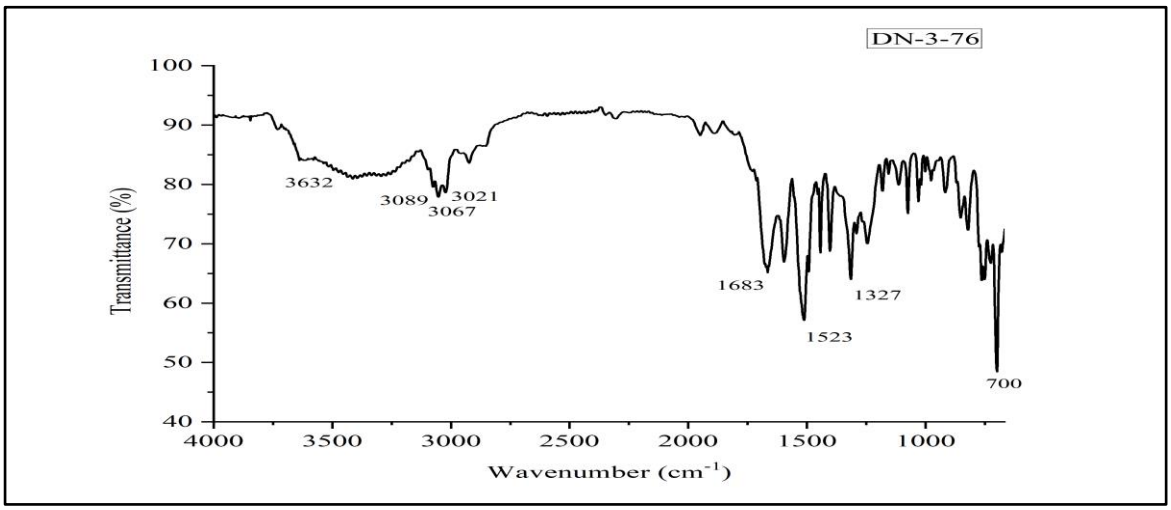

Figure 2.10: FT-IR spectrum of *N*^{1},*N*^{3},*N*^{5}-tris(4-(1,2,2-triphenylvinyl)phenyl)benzene-1,3,5-tricarboxamide **1**

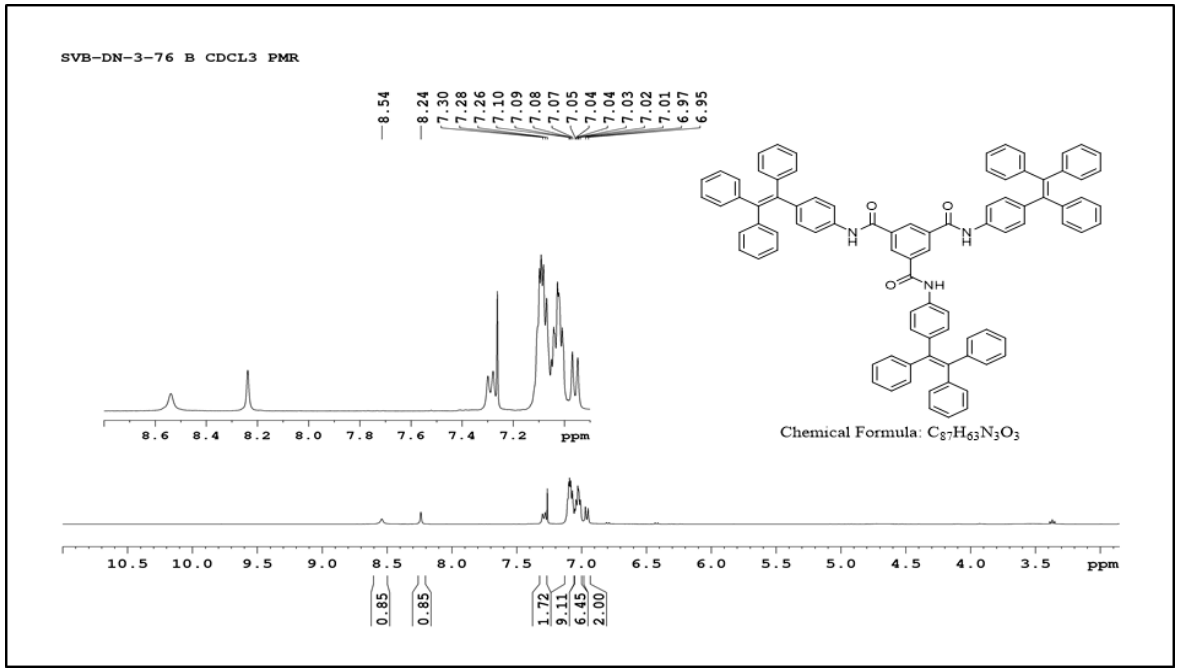

Figure 2.11: ^{1}H NMR spectrum of *N*^{1},*N*^{3},*N*^{5}-tris(4-(1,2,2-triphenylvinyl)phenyl)benzene-1,3,5-tricarboxamide **1**

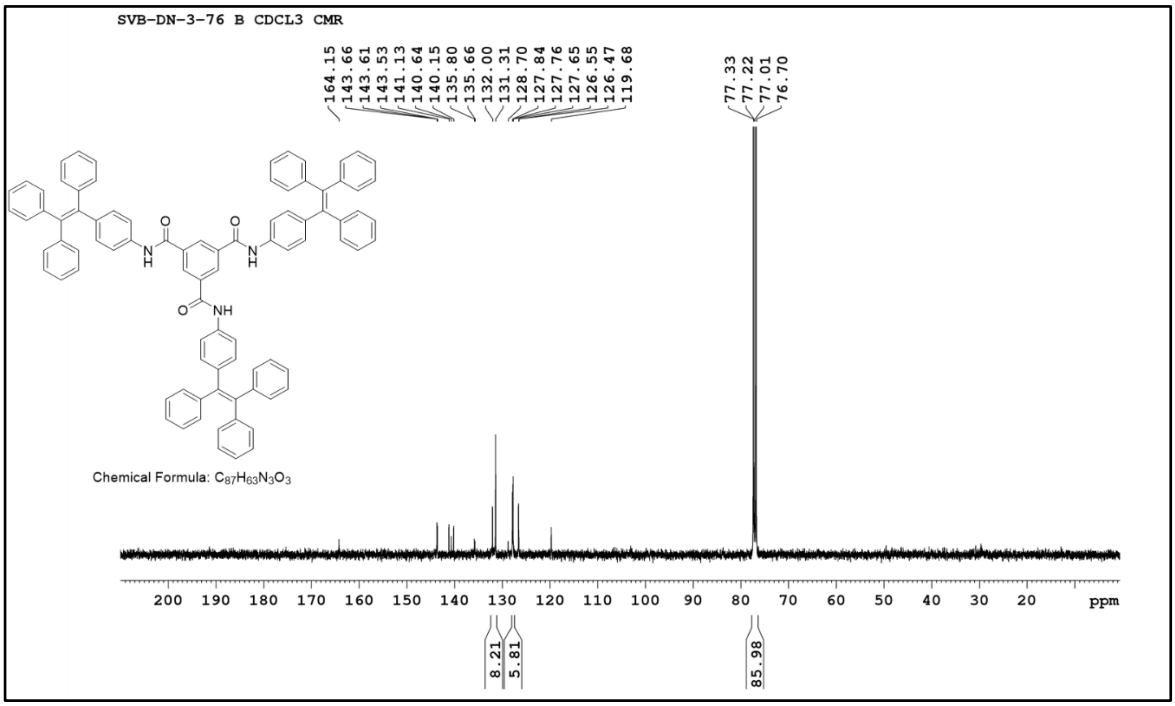

Figure 2.12: ^{13}C NMR spectrum of *N*^{1},*N*^{3},*N*^{5}-tris(4-(1,2,2-triphenylvinyl)phenyl)benzene-1,3,5-tricarboxamide **1**

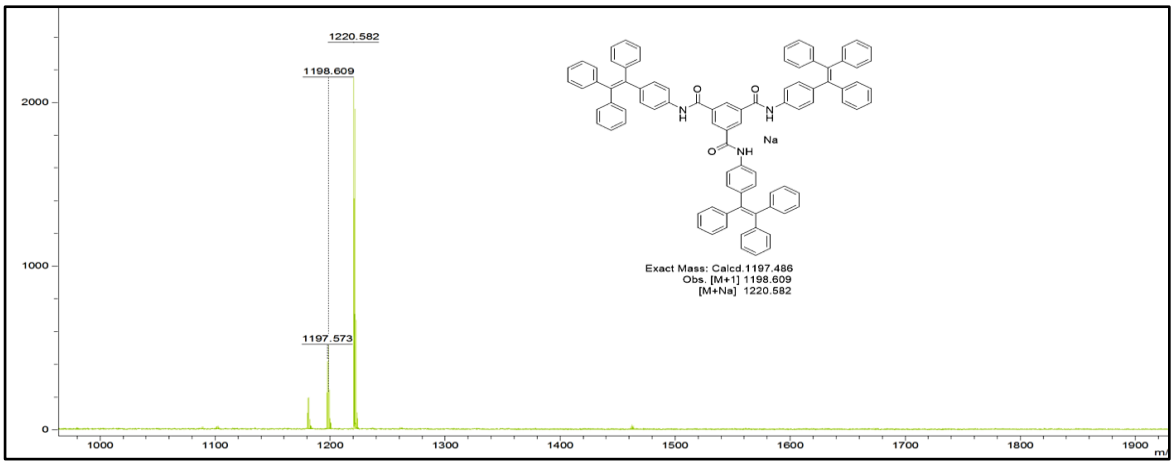

Figure 2.13: MALDI-TOF spectrum of *N*[1],*N*[3],*N*[5]-tris(4-(1,2,2-triphenylvinyl)phenyl)benzene-1,3,5-tricarboxamide **1**

2.3.3 Mechanochromic study

Compound **TPE-BTA** also shows moderate mechanochromic luminescence in a change of fluorescence colors. The **TPE-BTA** exhibited a sky-blue fluorescence in powder form under UV-light (365 nm). After grounded with a pestle, changed to a pale yellowish blue color. Interestingly, when the grounded mixture was fumed with the vapor of an Acetone, as illustrated in **Figure 2.14**, the yellowish-blue colored fluorescence of **TPE-BTA** was observed. The fluorescence spectra of **TPE-BTA** was recorded with excitation of 330 nm in the powder, grinding, and fuming form and its shown slight fluorescence quenching.

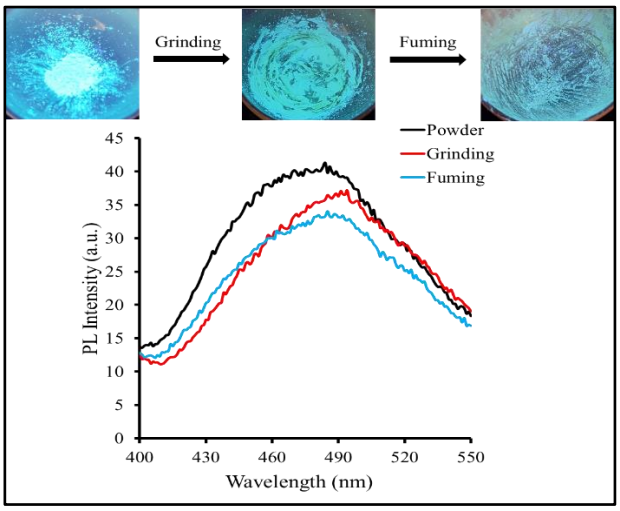

Figure 2.14: Fluorescence color changes of **TPE-BTA** upon grinding and fuming with acetone vapor. Images taken under UV excitation at 365 nm. Fluorescence spectra of **TPE-BTA** in powder, grinding and fuming form was recorded.

2.3.4 Absorbance and emission spectra of TPE-BTA in different solvents

The UV-Vis absorption and fluorescence spectroscopy employed to characterise **TPE-BTA** absorption and fluorescence properties were recorded in different organic solvents, as shown in **Figures 2.15 a & b**, respectively. The absorption spectra in chloroform show a prominent peak with a maximum absorption wavelength of 334 nm and an extinction coefficient of 5.6 $\times 10^4$ $M^{-1}cm^{-1}$. It was determined that the π-transition in the molecular architecture was the cause of the relatively high extinction coefficient (~10^4 $M^{-1}cm^{-1}$) in all of the solvents. Moreover, those extinction coefficient values are mentioned in **table 2.1**. When the solvent's polarity was increased, the form of the absorption peak remained unchanged but in MCH the absorption in decreased (**Fig. 2.15a**). Additionally, the results of a study on the emission characteristics of **TPE-BTA** upon excitation at (λ_{ex} = 330 nm) are shown in **Figure 4.55b**. The **TPE-BTA** was excited (λ_{ex} = 330 nm) in various solvents, and the emission spectra were observed at various wavelengths with a low intensity except in MCH. In various solvents, the **TPE-BTA** band location and shape are almost unchanged by the excitation wavelength. In MCH, **TPE-BTA** shown high intensity at 426 nm, it shown 65% more intensity as compare with chloroform. The **TPE-BTA** shown aggregation in MCH, due to aggregation molecule showed high intensity in fluorescence spectra.

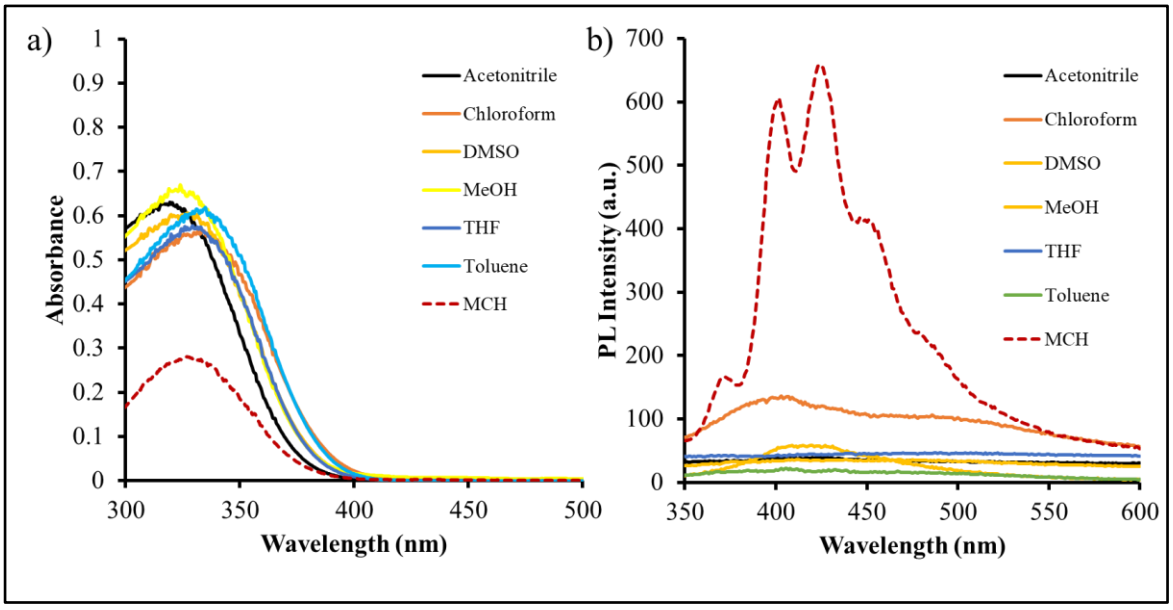

Figure 2.15: a) UV-Vis. and b) PL of **TPE-BTA** (1 $\times 10^{-5}$ M) spectra in various solvent respectively (λ_{ex} = 330 nm).

Table 2.1: UV-Vis absorption data of **TPE-BTA** in different solvents

Solvent	**Maximum wavelength (nm)**	**Extinction coefficient ε ($M^{-1}cm^{-1}$)**
Acetonitrile	316	6.4×10^4
Chloroform	334	5.6×10^4
DMSO	330	6.1×10^4
MeOH	324	6.6×10^4
THF	330	5.7×10^4
Toluene	334	6.2×10^4
MCH	327	2.8×10^4

2.3.5 AIE Study of TPE-BTA

The compound **TPE-BTA** is creamy-white color in solid form and non-emissive in visible light, however in the presence of UV-light molecule shown emissive (**Fig. 2.16 a & b**). Further, the molecule **TPE-BTA** in THF solution shown non-emissive and high emissive 99% water, which can see by naked eye (**Fig. 2.16c**). The absorption spectra recorded increasing water fractions(f_w) in THF; the absorption value was decreased in 99% water (**Fig. 2.16d**). In the emission spectra, water fractions between 0 and 60%, molecule **TPE-BTA** was non-fluorescent, but interestingly, it was shown to be emissive (λ_{max} 490 nm) at f_w = 80% (**Figure 2.16e**) When f_w was raised to 99%, an emission at 495 nm with a 5 nm red-shift ensued, which is an improvement of 70 times over f_w = 0%. When estimated using Rhodamine B as a standard with Φ_F = 70% in ethanol, the quantum yield (Φ_F) of **TPE-BTA** in pure THF solution was 0.03%, which was increased 25-fold to 2.05 and 7.35% with f_w = 80 and 99%, respectively. The molecule **TPE-BTA** shown highly aggregation in 99% water which leaded high fluorescent this phenomenon provide clear evidence that it is AIE active.

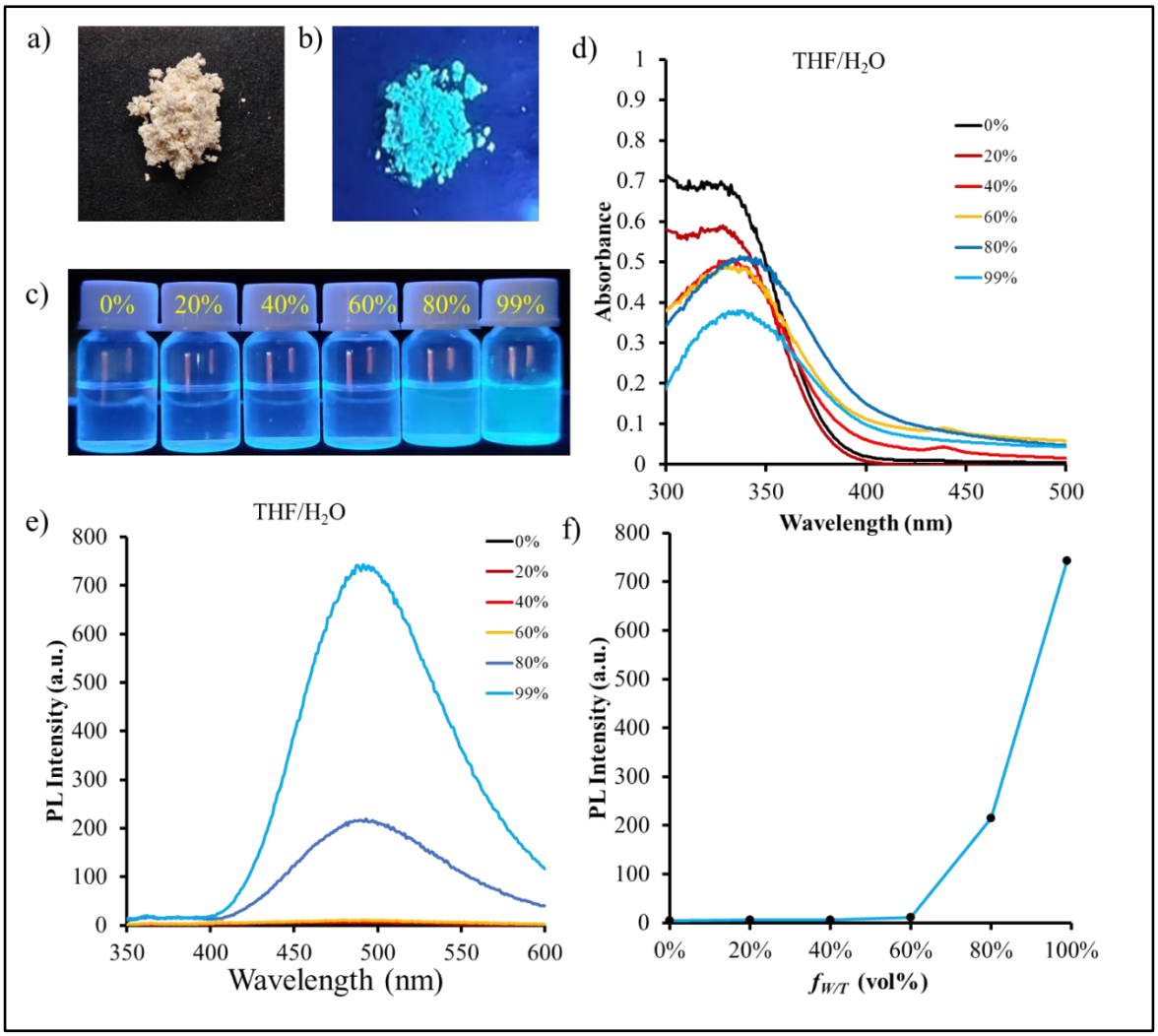

Figure 2.16: TPE-BTA powder under a) visible light b) UV light (365) c) Photograph of TPE-BTA (1 ×10^{-5} M) in various solvent ratios of THF/water, d) UV-Vis., e) and f) PL of spectra TPE-BTA in THF/water respectively(λ_{ex} = 330 nm).

2.3.6 UV-Vis. and Fluorescence study of TPE-BTA in $CHCl_3$/MCH

The absorption and emission study of **TPE-BTA** were studied in a mixture of $CHCl_3$ and MCH with changing ratios of MCH (0-99%) as shown in **Figure 2.17**. **TPE-BTA** in $CHCl_3$ exhibited an absorption maxima peak at 334 nm (ε= 5.6×10^4 M^{-1} cm^{-1}). The absorption bands are nearly same of (0-80%) MCH in $CHCl_3$. Additional increasing concentration of MCH up to 99%, *v/v* ratio, the absorption band of **TPE-BTA** at 327 nm shows blue shift with decrease in intensity and the *H*-type of aggregates.

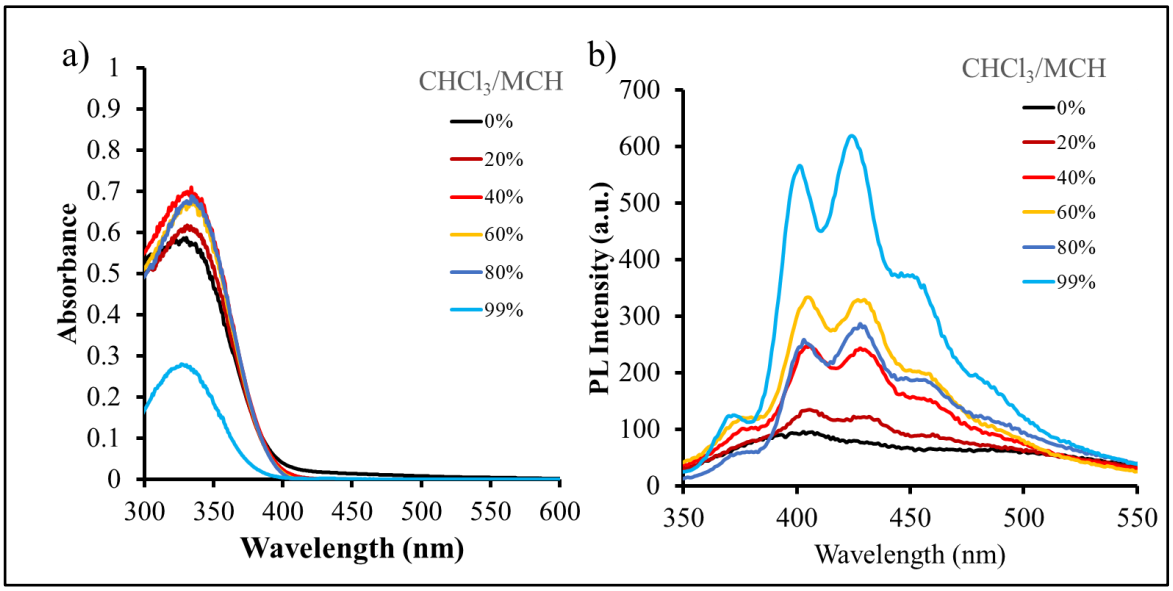

Figure 2.17: a) UV-Vis and b) Fluorescence emission spectra of TPE-BTA in $CHCl_3$:MCH (f_{MCH} = 0 to 99%).

Further, emission study of **TPE-BTA** in chloroform and MCH, where in TPE-BTA shown less emissive in the chloroform (**Fig.2.17b**) solution. While increasing of MCH (f_{MCH}= 20%), emission bands gradually increased in intensity 8% compare to Chloroform. Then MCH (f_{MCH}= 40-80%) which shown nearly same emission intensity up to (20 to 32%). Finally, increased MCH fraction up to 99%, which leads aggregation of **TPE-BTA** molecule, gives 62% emission. This reveals the AIE nature of **TPE-BTA.**

2.3.7 Circular Dichroism study of TPE-BTA

Circular dichroism (CD) spectroscopy was used to elucidate on the chiral aggregation behavior of the **TPE-BTA**. The CD spectra of the self-assembled **TPE-BTA** aggregates at various $CHCl_3$/MCH volume ratios. **TPE-BTA** was CD-inactive in the CD signal when it was in $CHCl_3$, which indicates the molecule is not aggregated. It is normal for achiral compounds to exhibit this behavior in solvated forms. As shown in **Figure 2.18 a**, when MCH (10%) was gradually added to the $CHCl_3$ solution, a significant CD signal was observed. One peak at 302 nm appeared due to a positive Cotton effect indicating solvent-induced chirality in the supramolecular self-assembled materials. Furthermore, when the MCH (20, 40 and 60%), well-resolved CD signals with a strong positive Cotton effect were observed at 305 nm. Moreover, 80% of MCH in CD spectra shown negative cotton effect. However, in 99% of MCH gives positive cotton effect.

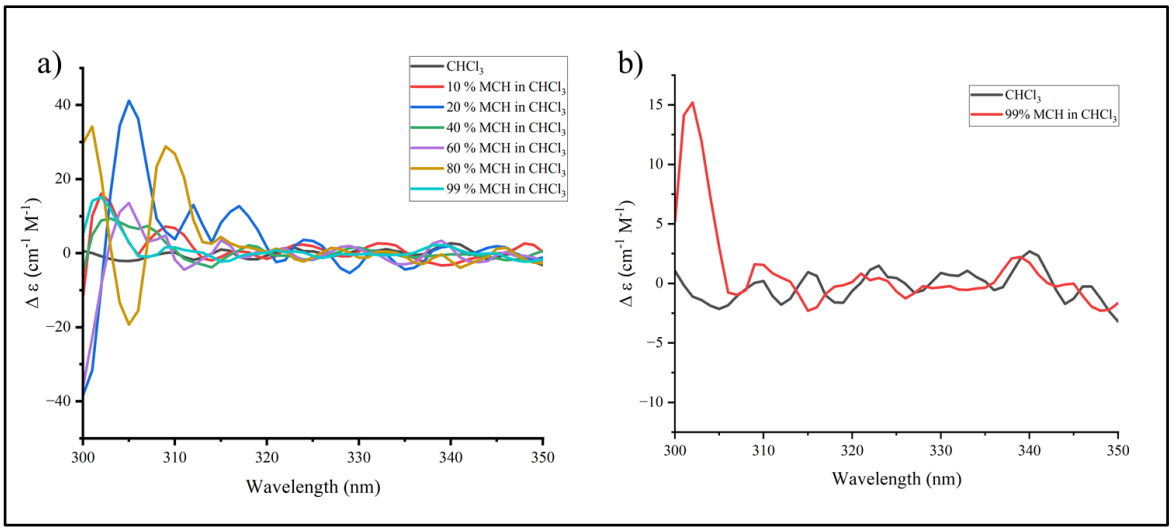

Figure 2.18: Circular dichroism study of TPE-BTA (5×10^{-4} M) in $CHCl_3$/MCH a) Concentration of MCH in 10 to 99%. b) Comparison of CD spectra in $CHCl_3$ and 99% MCH.

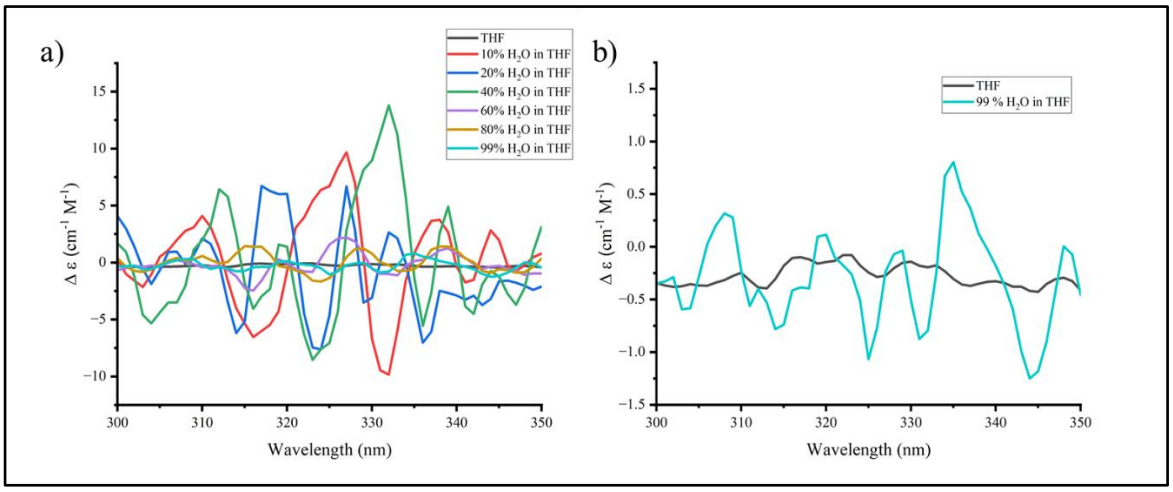

Figure 2.19: Circular dichroism study of TPE-BTA (5×10^{-4} M) in THF/H_2O a) Concentration of H_2O in 10 to 99%. b) Comparison of CD spectra in $CHCl_3$ and 99% H_2O.

CD spectra of **TPE-BTA** also employed in THF/H_2O solvent system. Were in THF CD spectra shown inactive, while increasing percentage of H_2O (20-99%) in THF the **TPE-BTA** shown positive and negative cotton effect in absorption range of it. From this it clearly reveal that achiral **TPE-BTA** molecule can produce chiral assembly by varying solvent systems.

2.3.8 Field-emission scanning electron microscopy study of TPE-BTA

To examine the morphologies of the solid assemblies of **TPE-BTA,** SEM analysis was employed. Samples were deposited by drop cast method then evaporation of solvent on a silicon wafer from a 1×10^{-5} M solution various solvent system.

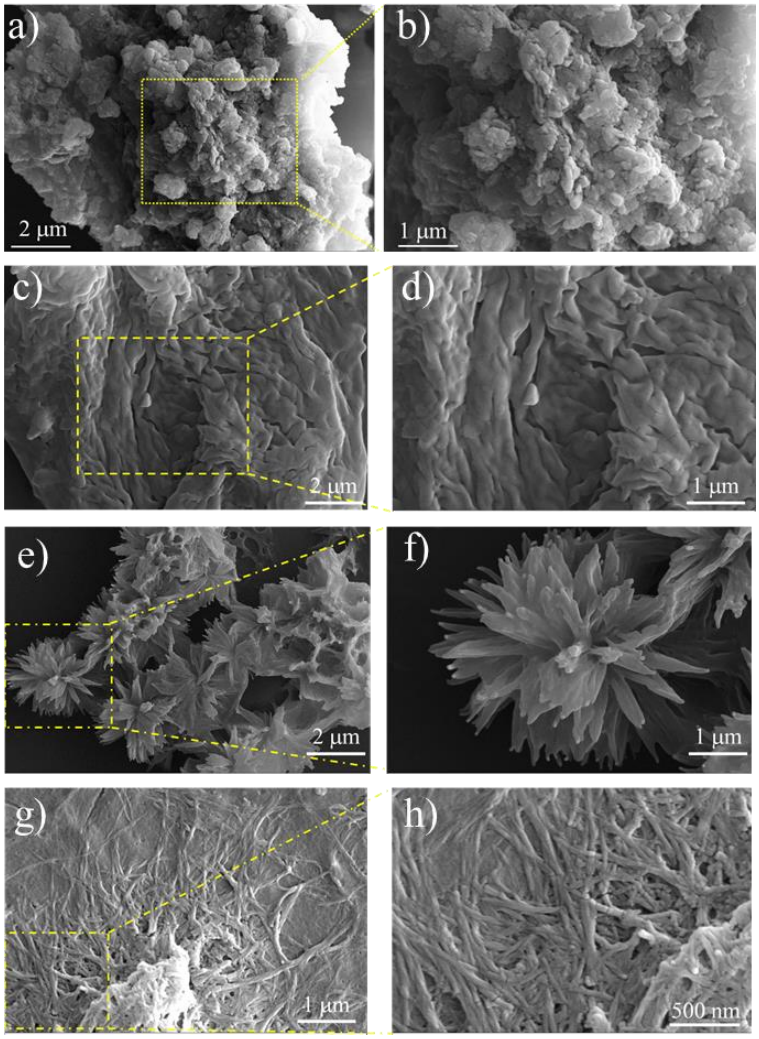

Figure 2.20: SEM images of **TPE-BTA** in a) THF, c) THF/H_2O (1:99 *v/v*), e) $CHCl_3$, g) $CHCl_3$/MCH (1:99 *v/v*), b), d), f), h) zoomed images of a), c), e), and g) respectively.

TPE-BTA shown cotton effect in CD spectra at aggregate state. TPE-BTA was produced particles type morphology (**Fig. 2.20a&b**) in THF and twisted ribbons (**Fig. 2.20c&d**) were observed in THF/H_2O (1:99, *v/v*) solvent system. While in chloroform, it shown flower-like superstructures (**Fig. 2.20e&f**) and in $CHCl_3$/MCH (1:99, *v/v*) helical fibers were obtained (**Fig. 2.20g&h**), due to intermolecular hydrogen bonding of amide group present in TPE-BTA, and aromatic phenyl group were may induce π–π stacking which leads formation of helical fibers.

2.3.9 X-ray diffraction (XRD) analysis

To examine the mode of nano-structural self-assembly of **TPE-BTA** in various solvent system, X-ray diffraction (XRD) measurements were performed. The degree of the twist is reflected in the variation from perfect order in a crystalline structure and is associated with the helical fibers, according to XRD results, which support the microstructure seen by electron microscopy. The 99% MCH in chloroform, which more crystalline nature was observed in XRD plot (**Fig. 2.21)**, which may be aggregation that is more regular, occurred in same solvent system.

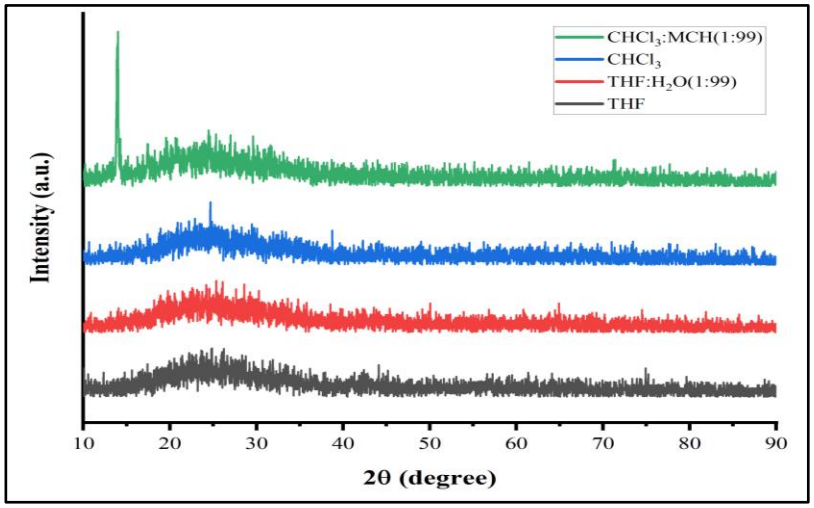

Figure 2.21: X-ray diffraction patterns of **TPE-BTA** in various solvent systems.

2.3.10 Lifetime study of TPE-BTA

The emission behavior of **TPE-BTA** in various solvents was further investigated using time-correlated single-photon counting (TCSPC) with picosecond (ps) using λ_{ex} = 330 nm excitation and results showed in **Figure 2.22** and all the results are summarized in **Table 2.2**. Biexponential fitted decay curve was obtained for **TPE-BTA**. In THF, lifetime τ1 was 0.90 ns (96.70%), τ2 was 5.68 ns (3.30%) and average lifetime τ 1.05 ns. Whereas in THF/H_2O (1:99, *v/v*), the lifetime τ1 was 0.97 ns (73.62%) and τ2 was 7.73 ns (26.38%) and average lifetime τ 2.75 ns. Similarly in $CHCl_3$ TPE-BTA shown lifetime τ1 was 0.92 ns (97.58%), τ2 was 3.71 ns (2.42%) and average lifetime τ 0.99 ns. However, in $CHCl_3$/MCH (1:99, *v/v*) the lifetime τ1 was 1.00 ns (94.57%) and τ2 was 3.91 ns (5.43%) and average lifetime τ 1.16 ns. From results its reveal that molecule **TPE-BTA** shown different average lifetime various solvent system.

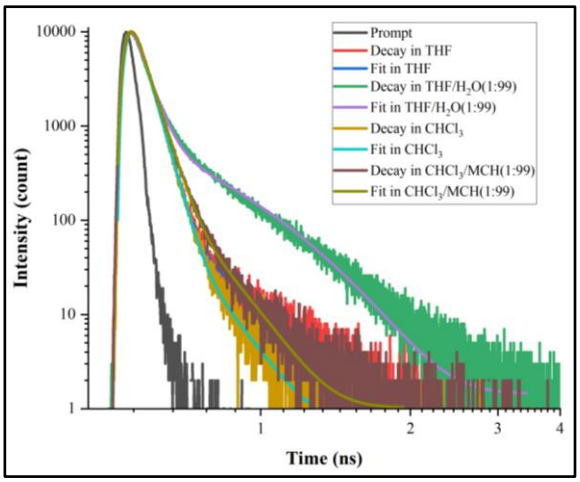

Figure 2.22: TCSPC decay profile of **TPE-BTA** in various solvent system, (λ_{ex} = 330 nm).

Table 2.2: TCSPC Calculation for TPE-BTA (1×10^{-5} M) and average life time in following solvent system.

Solvents	τ_1 **(ns)**	α_1	τ_2 **(ns)**	α_2	**Average Lifetime** τ **(ns)**
THF	0.90	96.70	5.68	3.30	1.05
THF:H_2O (1:99)	0.97	73.62	7.73	26.38	2.75
$CHCl_3$	0.92	97.58	3.71	2.42	0.99
$CHCl_3$:MCH (1:99)	1.00	94.57	3.91	5.43	1.16

2.4 conclusion

Designed and synthesized C_3-symmetrical **TPE-BTA** molecule for chiral assembly, synthesized C_3-symmetrical molecule having an amide functional group. Synthesized **TPE-BTA** confirmed by IR, NMR, and Mass spectroscopy. Additionally, a mechanochromic analysis of TPE-BTA was the outcome of a molecule that displayed comparable fluorescence features in various conditions. In THF/water and $CHCl_3$/MCH, aggregate-induced emission behavior was seen. In 99% H_2O in THF and 99% MCH in $CHCl_3$ solvent systems, TPE-BTA has demonstrated agglomeration. **TPE-BTA** was subjected to a Solvatochromism analysis using different ratios of the solvent systems $CHCl_3$/MCH and THF/water. According to the results of an absorption and emission, studies conducted with various solvents, aggregation and self-assembly were seen in THF/Water and $CHCl_3$/MCH. In SEM, flower-like and helical structures were seen in

$CHCl_3$ and $CHCl_3$/MCH. The cotton effect is apparent across circular dichroism. It's also shown changed average life time in several solvent system. Conclusion drawn from these results is that using different solvents to manipulate an achiral molecule could indeed trigger chirality.

References

(1) Engelkamp, A. H.; Middelbeek, S.; Nolte, R. J. M.; Engelkamp, H.; Middelbeek, S.; Nolte, R. J. M. Self-Assembly of Disk-Shaped Molecules to Coiled-Coil Aggregates with Tunable Helicity Published by : American Association for the Advancement of Science Stable URL : Http://Www.Jstor.Org/Stable/2898312 Linked References Are Available on JSTOR for This Article : Self-AssembLy of Disk-Shaped Molecules to CoiLed-Coil Aggregates with TunabLe Helicity. **2016**, *284* (5415), 785–788.

(2) Mateos-Timoneda, M. A.; Crego-Calama, M.; Reinhoudt, D. N. Supramolecular Chirality of Self-Assembled Systems in Solution. *Chem. Soc. Rev.* **2004**, *33* (6), 363–372. https://doi.org/10.1039/b305550g.

(3) Jonkheijm, P.; Van Der Schoot, P.; Schenning, A. P. H. J.; Meijer, E. W. Probing the Solvent-Assisted Nucleation Pathway in Chemical Self-Assembly. *Science (80-.).* **2006**, *313* (5783), 80–83. https://doi.org/10.1126/science.1127884.

(4) Dressel, C.; Reppe, T.; Prehm, M.; Brautzsch, M.; Tschierske, C. Chiral Self-Sorting and Amplification in Isotropic Liquids of Achiral Molecules. *Nat. Chem.* **2014**, *6* (11), 971–977. https://doi.org/10.1038/nchem.2039.

(5) Fuhrhop, J. H.; Helfrich, W. Fluid and Solid Fibers Made of Lipid Molecular Bilayers. *Chem. Rev.* **1993**, *93* (4), 1565–1582. https://doi.org/10.1021/cr00020a008.

(6) Thalacker, C.; Würthner, F. Chiral Perylene Bisimide-Melamine Assemblies: Hydrogen Bond-Directed Growth of Helically Stacked Dyes with Chiroptical Properties. *Adv. Funct. Mater.* **2002**, *12* (3), 209–218. https://doi.org/10.1002/1616-3028(200203)12:3<209::AID-ADFM209>3.0.CO;2-Y.

(7) Bae, J.; Choi, J. H.; Yoo, Y. S.; Oh, N. K.; Kim, B. S.; Lee, M. Helical Nanofibers from Aqueous Self-Assembly of an Oligo(p-Phenylene)- Based Molecular Dumbbell. *J. Am. Chem. Soc.* **2005**, *127* (27), 9668–9669. https://doi.org/10.1021/ja051961m.

(8) Ajayaghosh, A.; Praveen, V. K. π-Organogels of Self-Assembled p-Phenylenevinylenes: Soft Materials with Distinct Size, Shape, and Functions. *Acc.*

Chem. Res. **2007**, *40* (8), 644–656. https://doi.org/10.1021/ar7000364.

(9) Goh, M.; Kyotani, M.; Akagi, K. Highly Twisted Helical Polyacetylene with Morphology Free from the Bundle of Fibrils Synthesized in Chiral Nematic Liquid Crystal Reaction Field. *J. Am. Chem. Soc.* **2007**, *129* (27), 8519–8527. https://doi.org/10.1021/ja070701x.

(10) Green, M. M.; Peterson, N. C.; Sato, T.; Teramoto, A.; Cook, R.; Lifson, S. A Helical Polymer with a Cooperative Response to Chiral Information. *Science (80).* **1995**, *268* (5219), 1860–1866. https://doi.org/10.1126/science.268.5219.1860.

(11) Green, M. M.; Park, J. W.; Sato, T.; Teramoto, A.; Lifson, S.; Selinger, R. L. B.; Selinger, J. V. The Macromolecular Route to Chiral Amplification. *Angew. Chemie - Int. Ed.* **1999**, *38* (21), 3138–3154. https://doi.org/10.1002/(sici)1521-3773(19991102)38:21<3138::aid-anie3138>3.0.co;2-c.

(12) Palmans, A. R. A.; Meijer, E. W. Amplification of Chirality in Dynamic Supramolecular Aggregates. *Angew. Chemie - Int. Ed.* **2007**, *46* (47), 8948–8968. https://doi.org/10.1002/anie.200701285.

(13) Palmans, a. R. a.; Vekemans, J. a. J. M.; Havinga, E. E.; Meijer, E. W. Keywords: Amorphous Materials Glasses Structure Elucidation - - Atomic Force Microscopy. *Mater. Sci. Technol.* **1997**, *36* (23), 2648–2651.

(14) Maeda, K.; Yashima, E. Dynamic Helical Structures: Detection and Amplification of Chirality. *Top. Curr. Chem.* **2006**, *265* (March), 47–88. https://doi.org/10.1007/128_035.

(15) Nikolova, L.; Todorov, T.; Ivanov, M.; Andruzzi, F.; Hvilsted, S.; Ramanujam, P. S. Photoinduced Circular Anisotropy in Side-Chain Azobenzene Polyesters. *Opt. Mater. (Amst).* **1997**, *8* (4), 255–258. https://doi.org/10.1016/S0925-3467(97)00046-3.

(16) Choi, S.-W.; Izumi, T.; Hoshino, Y.; Takanishi, Y.; Ishikawa, K.; Watanabe, J.; Takezoe, H. Circular-Polarization-Induced Enantiomeric Excess in Liquid Crystals of an Achiral, Bent-Shaped Mesogen. *Angew. Chemie* **2006**, *118* (9), 1410–1413. https://doi.org/10.1002/ange.200503767.

(17) Iftime, G.; Labarthet, F. L.; Natansohn, A.; Rochon, P. Control of Chirality of an Azobenzene Liquid Crystalline Polymer with Circularly Polarized Light. *J. Am. Chem. Soc.* **2000**, *122* (51), 12646–12650. https://doi.org/10.1021/ja001244m.

(18) Gibaud, T.; Barry, E.; Zakhary, M. J.; Henglin, M.; Ward, A.; Yang, Y.; Berciu, C.; Oldenbourg, R.; Hagan, M. F.; Nicastro, D.; Meyer, R. B.; Dogic, Z. Reconfigurable

Self-Assembly through Chiral Control of Interfacial Tension. *Nature* **2012**, *481* (7381), 348–351. https://doi.org/10.1038/nature10769.

(19) Zhao, Y.; Fan, Y.; Mu, X.; Gao, H.; Wang, J.; Zhang, J.; Yang, W.; Chi, L.; Wang, Y. Self-Assembly of Luminescent Twisted Fibers Based on Achiral Quinacridone Derivatives. *Nano Res.* **2009**, *2* (6), 493–499. https://doi.org/10.1007/s12274-009-9045-4.

(20) Simon, F. X.; Khelfallah, N. S.; Schmutz, M.; Díaz, N.; Mésini, P. J. Formation of Helical Mesopores in Organic Polymer Matrices. *J. Am. Chem. Soc.* **2007**, *129* (13), 3788–3789. https://doi.org/10.1021/ja067261e.

(21) Huang, X.; Li, C.; Jiang, S.; Wang, X.; Zhang, B.; Liu, M. Self-Assembled Spiral Nanoarchitecture and Supramolecular Chirality in Langmuir-Blodgett Films of an Achiral Amphiphilic Barbituric Acid. *J. Am. Chem. Soc.* **2004**, *126* (5), 1322–1323. https://doi.org/10.1021/ja036878i.

(22) Labuta, J.; Futera, Z.; Ishihara, S.; Kouřilová, H.; Tateyama, Y.; Ariga, K.; Hill, J. P. Chiral Guest Binding as a Probe of Macrocycle Dynamics and Tautomerism in a Conjugated Tetrapyrrole. *J. Am. Chem. Soc.* **2014**, *136* (5), 2112–2118. https://doi.org/10.1021/ja4124175.

(23) Takeuchi, M.; Tanaka, S.; Shinkai, S. On the Influence of Porphyrin π-π Stacking on Supramolecular Chirality Created in the Porphyrin-Based Twisted Tape Structure. *Chem. Commun.* **2005**, No. 44, 5539–5541. https://doi.org/10.1039/b512128k.

(24) Sakakibara, K.; Chithra, P.; Das, B.; Mori, T.; Akada, M.; Labuta, J.; Tsuruoka, T.; Maji, S.; Furumi, S.; Shrestha, L. K.; Hill, J. P.; Acharya, S.; Ariga, K.; Ajayaghosh, A. Aligned 1-D Nanorods of a Π-Gelator Exhibit Molecular Orientation.Pdf. **2014**, 8–11.

(25) Hong, Y.; Lam, J. W. Y.; Tang, B. Z. Aggregation-Induced Emission: Phenomenon, Mechanism and Applications. *Chem. Commun.* **2009**, No. 29, 4332–4353. https://doi.org/10.1039/b904665h.

(26) Sly, J.; Kasák, P.; Gomar-Nadal, E.; Rovira, C.; Górriz, L.; Thordarson, P.; Amabilino, D. B.; Rowan, A. E.; Nolte, R. J. M. Chiral Molecular Tapes from Novel Tetra(Thiafulvalene-Crown-Ether)- Substituted Phthalocyanine Building Blocks. *Chem. Commun.* **2005**, No. 10, 1255–1257. https://doi.org/10.1039/b416034g.

(27) Zhao, Z.; Lam, J. W. Y.; Tang, B. Z. Tetraphenylethene: A Versatile AIE Building Block for the Construction of Efficient Luminescent Materials for Organic Light-Emitting Diodes. *J. Mater. Chem.* **2012**, *22* (45), 23726–23740.

https://doi.org/10.1039/c2jm31949g.

(28) Shustova, N. B.; Ong, T. C.; Cozzolino, A. F.; Michaelis, V. K.; Griffin, R. G.; Dincă, M. Phenyl Ring Dynamics in a Tetraphenylethylene-Bridged Metal-Organic Framework: Implications for the Mechanism of Aggregation-Induced Emission. *J. Am. Chem. Soc.* **2012**, *134* (36), 15061–15070. https://doi.org/10.1021/ja306042w.

(29) Hong, Y.; Lam, J. W. Y.; Tang, B. Z. Aggregation-Induced Emission. *Chem. Soc. Rev.* **2011**, *40* (11), 5361–5388. https://doi.org/10.1039/c1cs15113d.

(30) Hong, Y.; Xiong, H.; Lam, J. W. Y.; Häußler, M.; Liu, J.; Yu, Y.; Zhong, Y.; Sung, H. H. Y.; Williams, I. D.; Wong, K. S.; Tang, B. Z. Fluorescent Bioprobes: Structural Matching in the Docking Processes of Aggregation-Induced Emission Fluorogens on DNA Surfaces. *Chem. - A Eur. J.* **2010**, *16* (4), 1232–1245. https://doi.org/10.1002/chem.200900778.

(31) Rananaware, A.; Bhosale, R. S.; Patil, H.; Al Kobaisi, M.; Abraham, A.; Shukla, R.; Bhosale, S. V.; Bhosale, S. V. Precise Aggregation-Induced Emission Enhancement via H+ Sensing and Its Use in Ratiometric Detection of Intracellular PH Values. *RSC Adv.* **2014**, *4* (103), 59078–59082. https://doi.org/10.1039/c4ra10511g.

(32) Rananaware, A.; Bhosale, R. S.; Ohkubo, K.; Patil, H.; Jones, L. A.; Jackson, S. L.; Fukuzumi, S.; Bhosale, S. V.; Bhosale, S. V. Tetraphenylethene-Based Star Shaped Porphyrins: Synthesis, Self-Assembly, and Optical and Photophysical Study. *J. Org. Chem.* **2015**, *80* (8), 3832–3840. https://doi.org/10.1021/jo502760e.

(33) Li, S.; Langenegger, S. M.; Häner, R. Control of Aggregation-Induced Emission by DNA Hybridization. *Chem. Commun.* **2013**, *49* (52), 5835–5837. https://doi.org/10.1039/c3cc42706d.

(34) Tong, H.; Hong, Y.; Dong, Y.; Häussler, M.; Li, Z.; Lam, J. W. Y.; Dong, Y.; Sung, H. H. Y.; Williams, I. D.; Tang, B. Z. Protein Detection and Quantitation by Tetraphenylethene-Based Fluorescent Probes with Aggregation-Induced Emission Characteristics. *J. Phys. Chem. B* **2007**, *111* (40), 11817–11823. https://doi.org/10.1021/jp073147m.

(35) Wang, M.; Zhang, D.; Zhang, G.; Zhu, D. The Convenient Fluorescence Turn-on Detection of Heparin with a Silole Derivative Featuring an Ammonium Group. *Chem. Commun.* **2008**, No. 37, 4469–4471. https://doi.org/10.1039/b808877b.

(36) Leung, C. W. T.; Hong, Y.; Chen, S.; Zhao, E.; Lam, J. W. Y.; Tang, B. Z. A Photostable AIE Luminogen for Specific Mitochondrial Imaging and Tracking. *J. Am. Chem. Soc.* **2013**, *135* (1), 62–65. https://doi.org/10.1021/ja310324q.

(37) Jiao, J.; Li, Z.; Qiao, Z.; Li, X.; Liu, Y.; Dong, J.; Jiang, J.; Cui, Y. Design and Self-Assembly of Hexahedral Coordination Cages for Cascade Reactions. *Nat. Commun.* **2018**, *9* (1). https://doi.org/10.1038/s41467-018-06872-0.

(38) Parthiban, C.; M., P.; L., V. K. R.; Sen, D.; S., M. S.; Singh, N. D. P. Visible-Light - Triggered Fluorescent Organic Nanoparticles for Chemo-Photodynamic Therapy with Real-Time Cellular Imaging. *ACS Appl. Nano Mater.* **2018**, *1* (11), 6281–6288. https://doi.org/10.1021/acsanm.8b01495.

Chapter III

Synthesis and characterization of naphthalene diimide derivative bearing BINOL moiety for chiral assembly

3.1 Introduction

Naphthalene diimide (NDI) and perylenediimide (PDI) are homologue of the rylenediimides (RDI).[1–3] Both NDIs and RDIs are ideal options for organic electronics applications, photovoltaic devices, and flexible displays due to their high electron affinity, strong charge carrier mobility, and outstanding thermal and oxidative durability.[2,4–6] On the alternative side, 1,4,5,8-naphthalenetetracarboxylic acid dianhydride (NDA), which serves as the primary starting material for the synthesis of a number of NDI compounds, has also been used as a starting material for the synthesis of perinone pigments that are useful for the industrial sector.[7] and it is easily functionalized with arylamino or alkylamino groups in the anhydride position. Due to their excellent fluorescent properties, PDI[2,3,8] and its higher analogues, the rylene diimides,[9–11] have been used for a long time.[12] Most research on these molecules has focused on their practical application, such as in fluorescence spectroscopy,[13] organic electrical and photovoltaic devices,[5–14] metallo- and supramolecular structures,[15,16] and their interactions with DNA and RNA.[17]

Supramolecular chemistry, as well defined as "chemistry beyond the molecule," generally studies molecular recognition and high-order assemblies produced by noncovalent interactions.[18] In the building of thermodynamically stable structures at the cellular and subcellular levels, within nanometer to millimetre dimensions, self-assembly and self-organization of molecules play significant roles and implement a "bottom-up" or "bioinspired" strategy. Structural systems that are linked together by noncovalent interactions to form supramolecular systems are capable of responding to stimuli.[19]

The study of design principles has benefited from the use of naphthelene diimides (NDIs), which are simple to prepare, have n-type electron-accepting properties, are neutral, planar, and chemically adaptable. They share some common features with the naturally occurring acceptors of bacterial photosynthesis reaction centers because they are also redox-active and have high melting temperatures.[1,20–22] NDIs are one of the most favored groups of molecules from this perspective. These molecules having optical and electrical properties are highly dependent on their structural characteristics, so it is possible to modify them by substituting at either of the diimide locations or directly on the NDI core. The self-assembly of NDIs and their application in the formation of various self-assembled architectures, such as cages, catenanes and rotaxanes, nanotubes, nanowires, sensors, ion channels, and their applications, have both been extensively exploited. Another method for changing the electronic properties is by inducing intermolecular interaction using noncovalent forces such

as H-bonding, coordination, and π–π stacking.

In many applications, including self-assembly, aggregation, production of chirality, molecular recognition, molecular machines, molecular sensors, gas absorption, nanoreactors, chemical catalysis, drug delivery, optoelectronics, and chemosensors, core-unsubstituted NDI derivatives have been used.[23–26] Because of this, supramolecular study frequently involves multiple disciplines, including materials science, biological science, engineering, organic, physical, coordination, and polymer chemistry.[27] For the formation of supramolecular nanostructures, aromatic (π–π stacking) interactions and solvophobicity are important.[28] In this respect, large macrocyclic polyaromatics like hexabenzocoronene and PDI have been used to produce well-defined nanostructures like nanowires, vesicles, nanobelts, and gels.[29–37] However, NDIs have attracted significant interest among aromatic compounds that have been useful, particularly in the design of conducting materials, because of their fascinating electro-optical properties and potential to make n-type semiconductor materials.[38]

Importantly, NDIs have four polar carboxyl groups and an aromatic core that exhibit stacking in the solid state through π-π stabilization. As a result, depending on the imide's substituent, they are typically soluble in low polarity solvents like DCM, $CHCl_3$, and toluene as well as polar aprotic solvents like acetonitrile and DMF. This behavior can help develop continuous stacks in supramolecular uses, but if the solubility is big a problem, it can also create an enormous challenge. The solubility of NDIs accordingly majorly depends on the substituents in the imide position, and normally, NDIs with long and bulky aliphatic substituents have enhanced solubility.[39] The aggregation of NDI in both the solution and solid phases can advantage from this feature as well.[40]

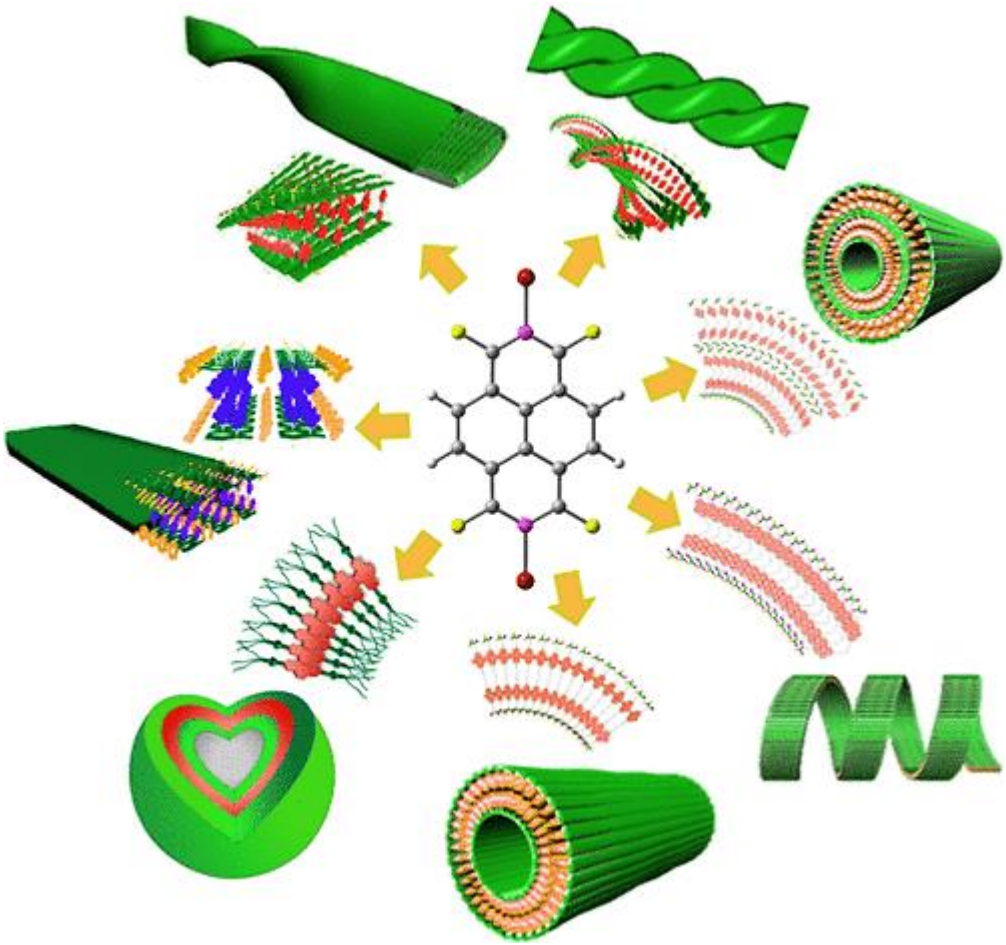

Figure 3.1: NDI molecules previously reported various nanostructures.[41]

The development of chiral nanostructures is a crucial step in better understanding some aspects of biological function, and it may also open up opportunities for sensing, liquid crystal, and optical activity applications. Particularly for molecules like planar NDIs, the induction and regulation of supramolecular chiral assembly from achiral/homochiral functional organic molecules is a significant task.[42] Recent research from the George group describes chirality-derived self-sorting to regulate supramolecular structure of donor-acceptor molecules in multilayer self-assembly in solution.[43] These results are therefore especially interesting because the present system is built on an optically active NDI component and may have uses in the design and production of novel materials for optoelectronic devices. In order to accomplish precise regulation of molecular structure in solution, alternate aromatic donor and acceptor interactions, which are directed by π-π interactions, are frequently used. Because the donor and acceptor in π-π stacked components are excited, these systems usually show charge-transfer (CT) absorption properties.

3.2 Experimental

3.2.1 Materials and Methods

All reagents and chemical including solvents were are purchased from Sigma-Aldrich, TCI, and AVRA and used without purification. ^{1}H-NMR spectra were recorded on 400 MHz Bruker spectrometer and ^{13}C-NMR using 100 MHz spectrometer as $CDCl_3$-d solutions (trimethylsilane as an internal standard). Mass spectral data were obtained from Bruker ultraflex TOF (MALDI-TOF). IR spectra were recorded on a Perkin Elmer FT-IR spectrometer. UV-Vis absorption spectra were recorded by Jasco V-750 UV-Visible spectrophotometer and emission spectra were recorded on FLS1000 spectrometer, Circular dichroism were performed on Jasco

3.2.2 Synthesis of 2,3,6,7-tetrabromo-NDA

In round-bottom flask, NDA (1 g, 3.72 mmol) was dispersed in concentrated sulfuric acid (20 mL) at room temperature. DBH (3.19 g, 11.1 mmol) was added in portions.[44] The subsequent brown solution was stirred at room temperature for 4 h and then the reaction mixture was heated at 80 ^{o}C for 12 h. The reaction mixture was poured into ice water to precipitate the solid. The precipitated solid was filtered, washed with water and methanol, then lastly dried under vacuum to obtain 4-Br-NDA as yellow solid (2.06 g, 95 %); IR (cm^{-1}) 3086, 1788, 1730, 1404, 1369, 1190, 1141, 1079, 775, 700.

3.2.3 Synthesis of *N,N'*-bis(*n*-octyl)-tetrabromo-NDI 2

As per literature[45] **4-Br-NDA** (1 g, 1.71 mmol) was treated with of n-octylamine (0.66 g, 5.14 mmol) in glacial acetic acid (15 ml) at 120 ^{o}C for 30 min, its gives ring-opened 2,3,6,7-tetrabromo-4,8-bis(n-octylcarbamoyl)naphthalene-1,5-dicarboxylic acid. After which was further treated with PBr_3 in toluene at reflux for 6 h to gives ring-closed product *N,N'*-bis(*n*-octyl)-tetrabromo-NDI **2** (0.82 g, 60%). IR (cm^{-1}) : 2956, 2920, 2849, 1712, 1667, 1435, 1409, 1373, 1286, 1172, 1145, 789. ^{1}H NMR (400 MHz, $CDCl_3$), δ (ppm): 4.22-4.19 (t, 4H), 1.77-1.74(m, 4H), 1.42-1.34(m, 8H), 1.30-1.27 (m, 12H), 0.89-0.86 (t, 6H). ^{13}C NMR (100 MHz, $CDCl_3$), δ: 159.82, 135.58, 126.66, 125.67, 42.92, 31.77, 29.24, 29.21, 27.98, 27.10, 22.64, 14.10. in DEPT135 -CH_2 groups shown negative peaks at δ : 42.92, 31.77, 29.24, 29.21, 27.98, 27.10, 22.64.

3.2.4 Synthesis of NDI-R-BINOL

The R-BINOL(44 mg, 0.15mmol) was dissolved in dry DCM and NaH(10 mg, 0.37mmol) was added to form sodium salt of BINOL. After 30 min of stirring the **4-Br-NDI**(50 mg, 0.06 mmol) was added in reaction mixture and kept it room temperature for 24 h. it gives yellow color product which was further purified by column chromatography(1:9, ethyl acetate: hexane) yielded (29 mg, 45%) IR (cm^{-1}): 3055, 2952, 2925, 2854, 1712, 1672, 1413, 1252, 1056, 944, 820, 753. ^{1}H NMR (400 MHz, $CDCl_3$), δ (ppm): 7.93-7.87 (m, 8H), 7.66-7.61(m, 8H), 7.47-7.43(m, 4H), 7.38-7.33(m, 4H), 4.14-3.98 (m, 4H), 1.69-1.59(m, 4H), 1.31-1.21(m, 12H), 1.14(m, 8H), 0.77-0.74(t, 6H). ^{13}C NMR (100 MHz, $CDCl_3$), δ: 159.39, 152.57, 149.48, 131.13, 130.80, 129.98, 127.42, 125.91, 124.81, 124.30, 120.62, 119.72, 116.69, 40.30, 30.71, 28.68, 28.19, 26.92, 26.19, 21.57, 13.03. DEPT135 -CH_2 groups shown negative peaks at δ: 40.30, 30.71, 28.68, 28.19, 26.92, 26.19, and 21.57. MALDI-TOF for $C_{70}H_{58}N_2O_8$ mass cal. 1054.419[M^+], Obs. 1055.507 [M+1]

3.2.5 Synthesis of NDI-S-BINOL

Previous synthesis protocol followed for NDI-S-BINOL it give yield (31 mg, 48%) IR(cm^{-1}): 3055, 2948, 2930, 2849, 1717, 1672, 1467, 1404, 1257, 1070, 941, 820, 758. ^{1}H NMR (400 MHz, $CDCl_3$), δ (ppm): 7.92-7.87 (m, 8H), 7.66-7.60(m, 8H), 7.45(m, 4H), 7.37-7.35(m, 4H), 4.14-3.99 (m, 4H), 1.65-1.60(m, 4H), 1.31-1.15(m, 20H), 0.77(t, 6H). ^{13}C NMR (100 MHz, $CDCl_3$), δ:159.38, 152.56, 149.47, 131.12, 130.79, 129.98, 127.41, 125.90, 124.81, 124.29, 120.61, 119.72, 116.69, 40.29, 30.89, 30.71, 30.40, 29.16, 28.67, 28.19, 26.92, 26.18, 21.56, 13.02. DEPT 135 -CH_2 groups shown negative peaks at δ: 40.27, 30.68, 28.66, 28.16, 26.89, 26.16, and 21.54. MALDI-TOF for $C_{70}H_{58}N_2O_8$ mass cal. 1054.419[M^+], Obs. 1055.482 [M+1]

3.2.6 UV-Vis spectroscopy: At room temperature, UV-Vis spectra were recorded using a Jasco V-750 UV-Visible spectrophotometer. A 10×2 mm cuvette was used for UV-vis investigations.

3.2.7 Fluorescence spectroscopy: On a spectrofluorometer Jasco FLS1000 spectrometer, fluorescence emission spectra were measured. A 10×2 mm cuvette for all experiments.

3.2.8 Circular dichroism: Circular Dichroism (CD) spectra were recorded on a Jasco J-815 spectrometer where the sensitivity, time constant and scan rate were chosen appropriately.

3.2.9 TCSPC: Fluorescence lifetimes were performed on a Horiba Delta Flex time-correlated single-photon-counting (TCSPC) instrument.

3.2.10 Dynamic Light Scattering: The measurements were carried out in Malvern

Zetasizer ULTRA instrument. The size measurements were carried out in a 10 mm glass cuvette at 25 ºC.

3.3 Result and Discussion

3.3.1 Synthesis of NDI-R/S-BINOL

The synthesis of started with **4-Br-NDA** from NDA via bromination by using DBH at 80 ºC for 4 hour. Then 4-Br-NDA was treated with octyl amine to convert it into product crude product which continued for next step, in presence of acetic acid and further reflux with PBr_3 in toluene for 6 hour gives product **2**. Finally, the compound **2** reacted with R-BINOL and S-BINOL to produce NDI-R-BINOL and NDI-S-BINOL respectively, in presence of NaH in DCM at room temperature.

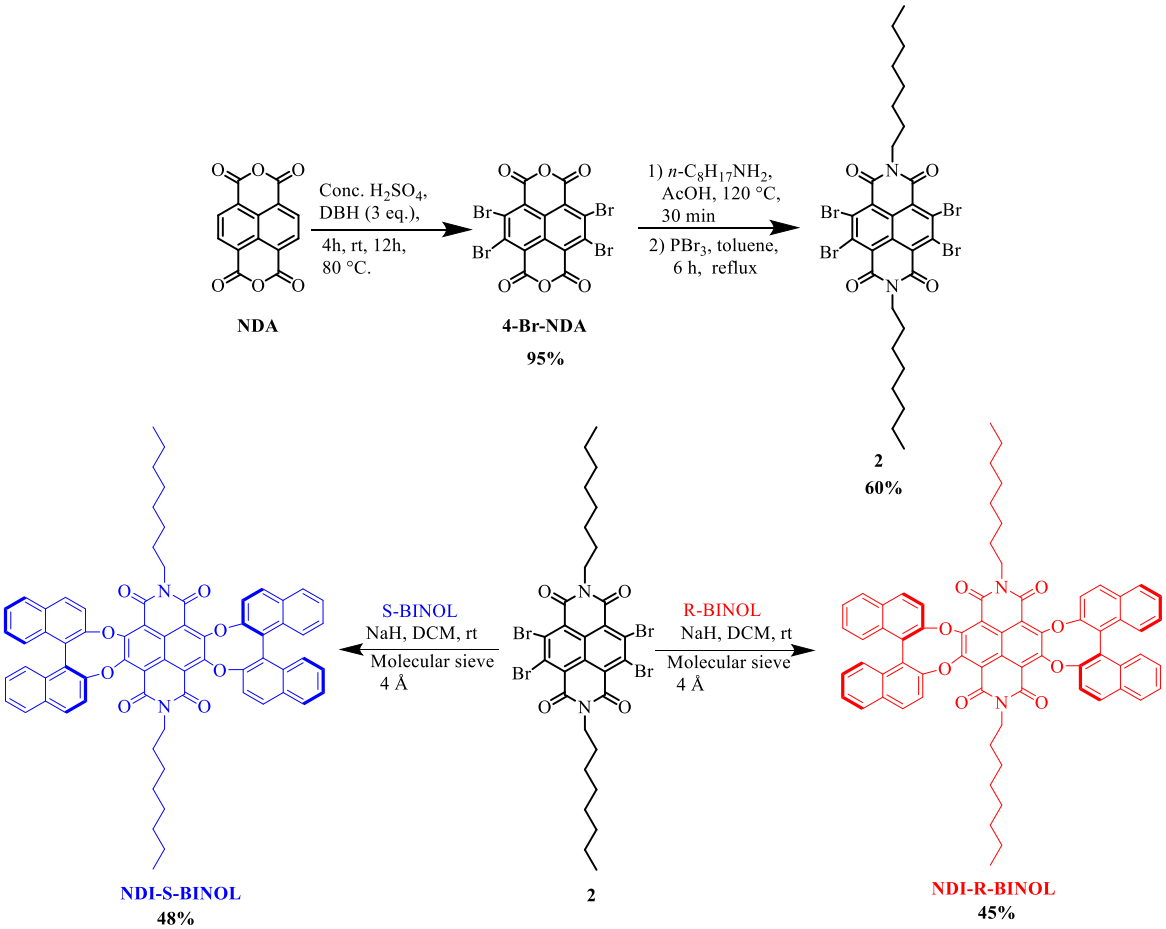

Scheme 3.1: Synthesis of NDI-R/S-BINOL.

3.3.2 Characterization of synthesized compound by IR, NMR, and Mass spectroscopy

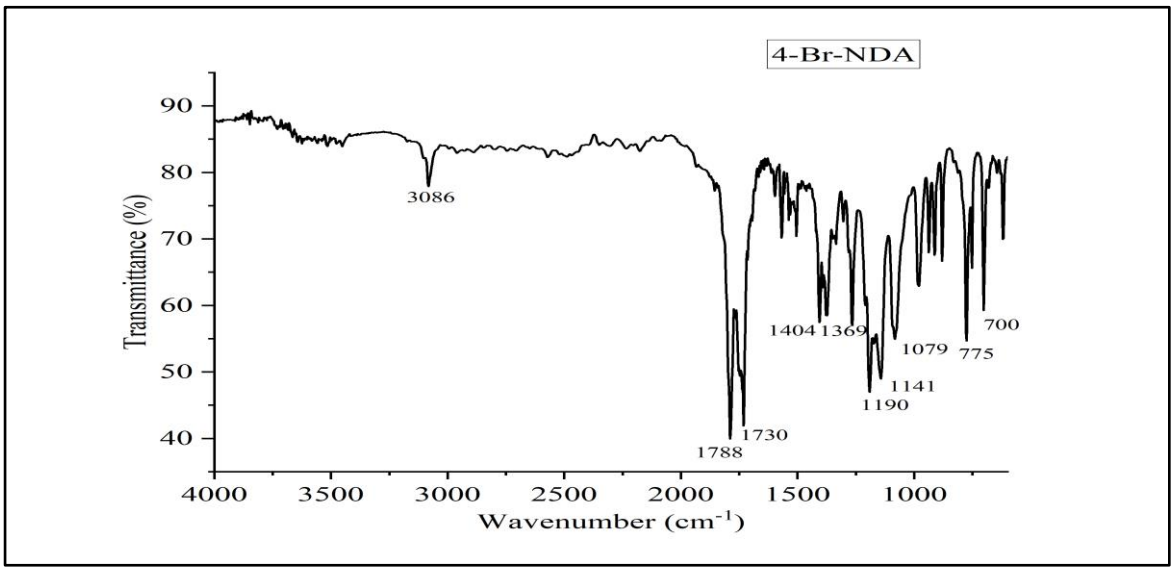

Figure 3.2: FT-IR spectrum of 2,3,6,7-tetrabromo-NDA **4-Br-NDA**

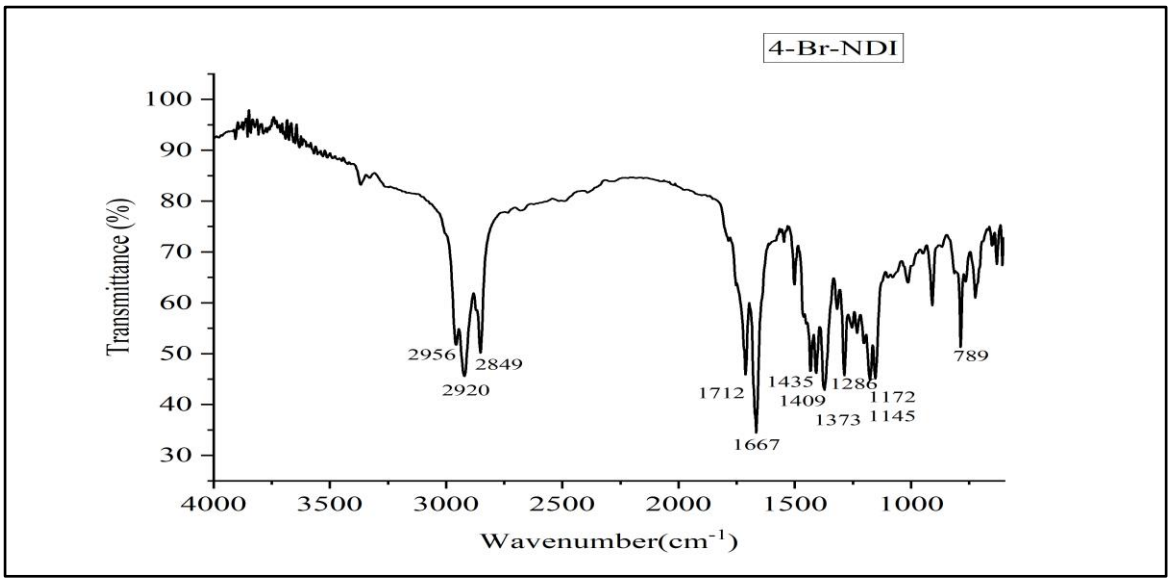

Figure 3.3: FT-IR spectrum of *N,N'*-bis(*n*-octyl)-tetrabromo-NDI **2**

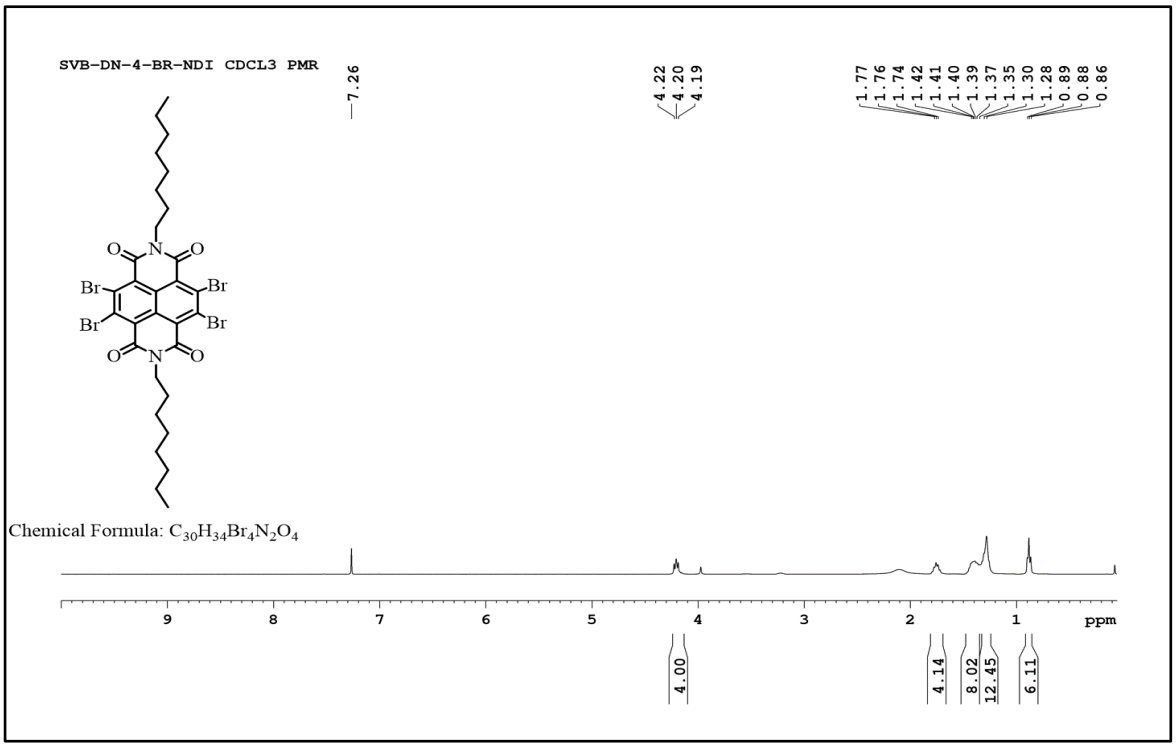

Figure 3.4: ^{1}H NMR spectrum of *N,N'*-bis(*n*-octyl)-tetrabromo-NDI **2**

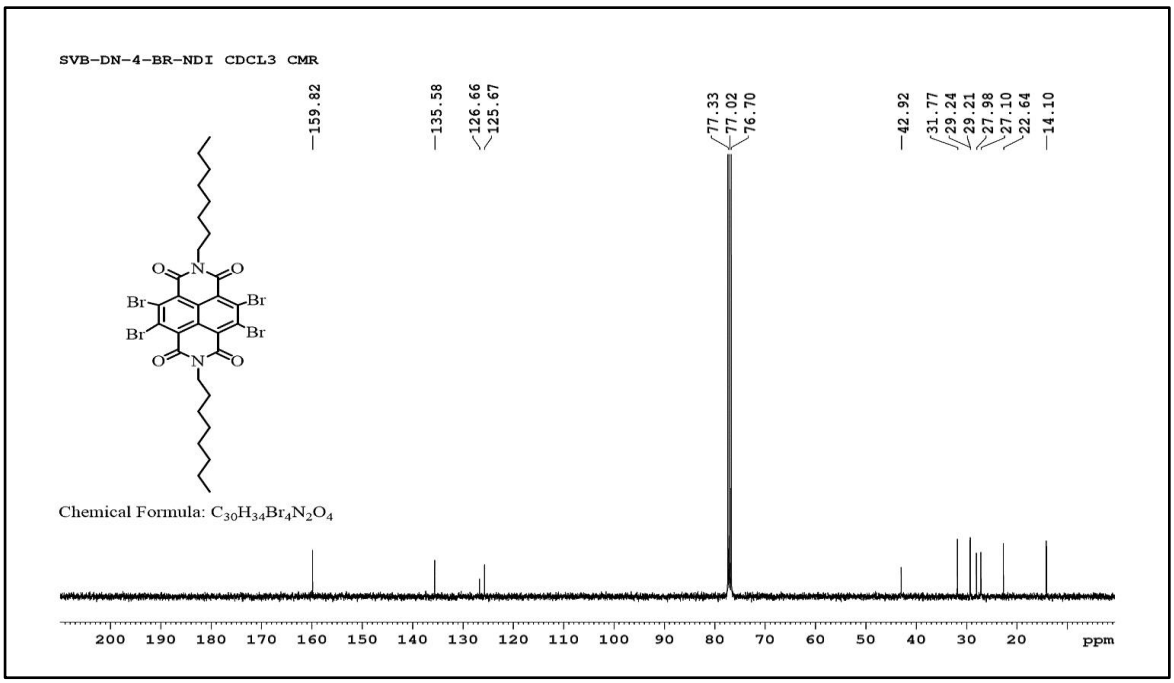

Figure 3.5: ^{13}C NMR spectrum of *N,N'*-bis(*n*-octyl)-tetrabromo-NDI **2**

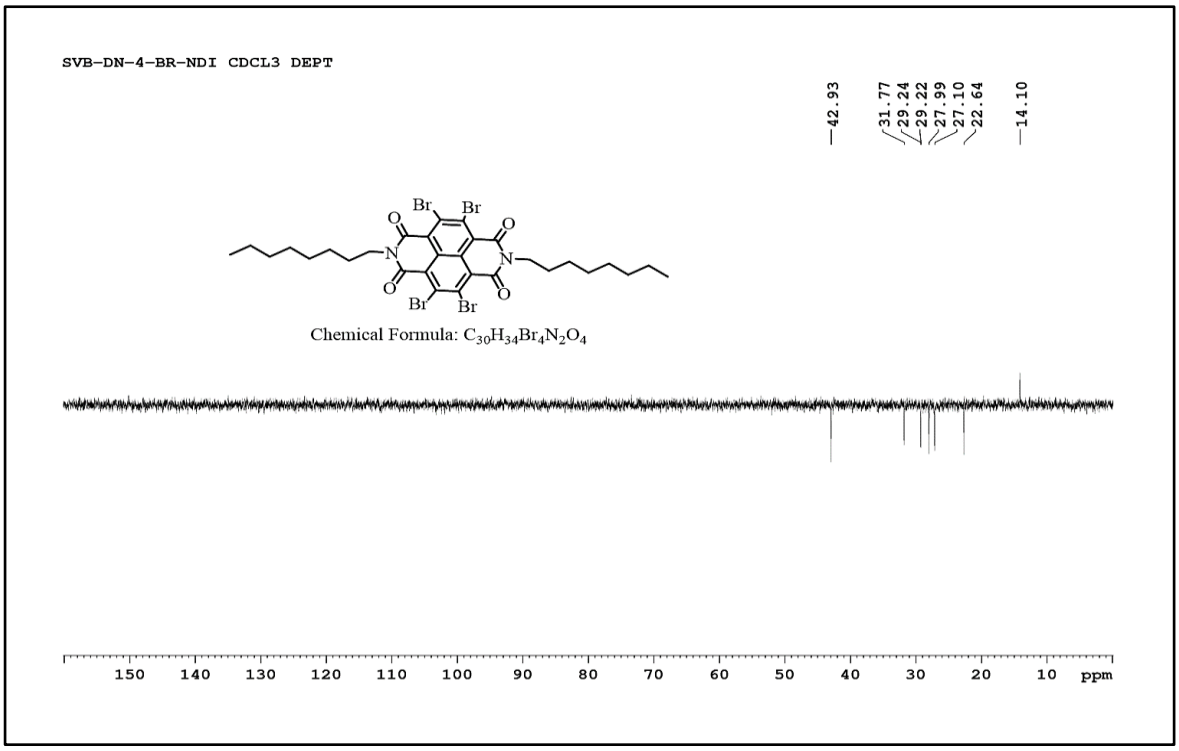

Figure 3.6: DEPT135 NMR spectrum of *N,N'*-bis(*n*-octyl)-tetrabromo-NDI **2**

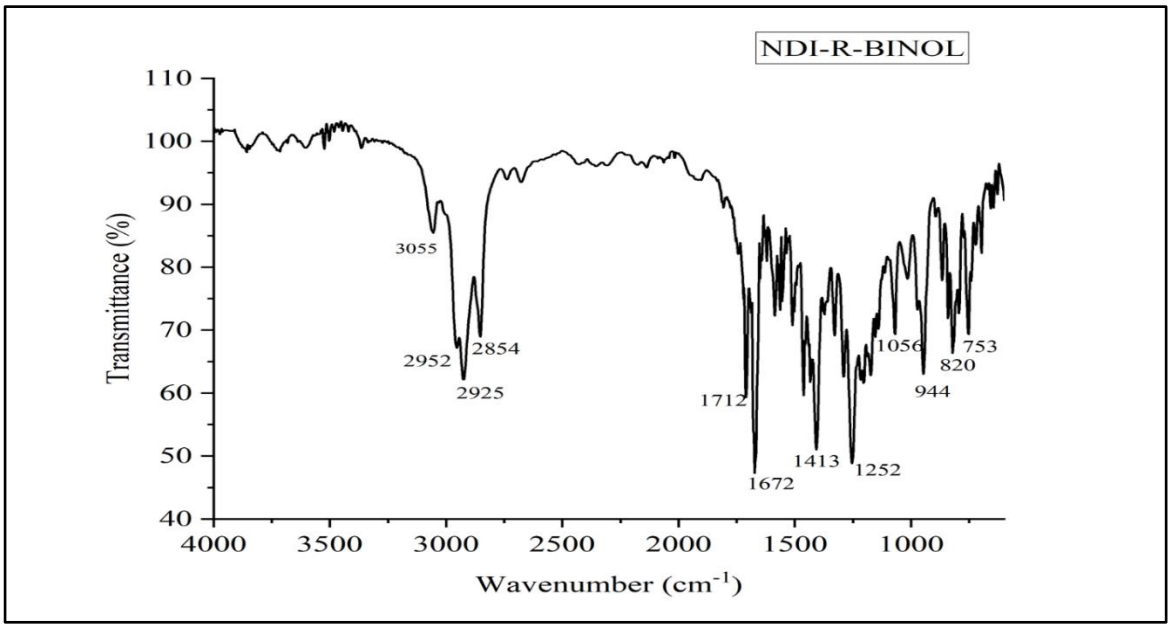

Figure 3.7: FT-IR spectrum of NDI-R-BINOL

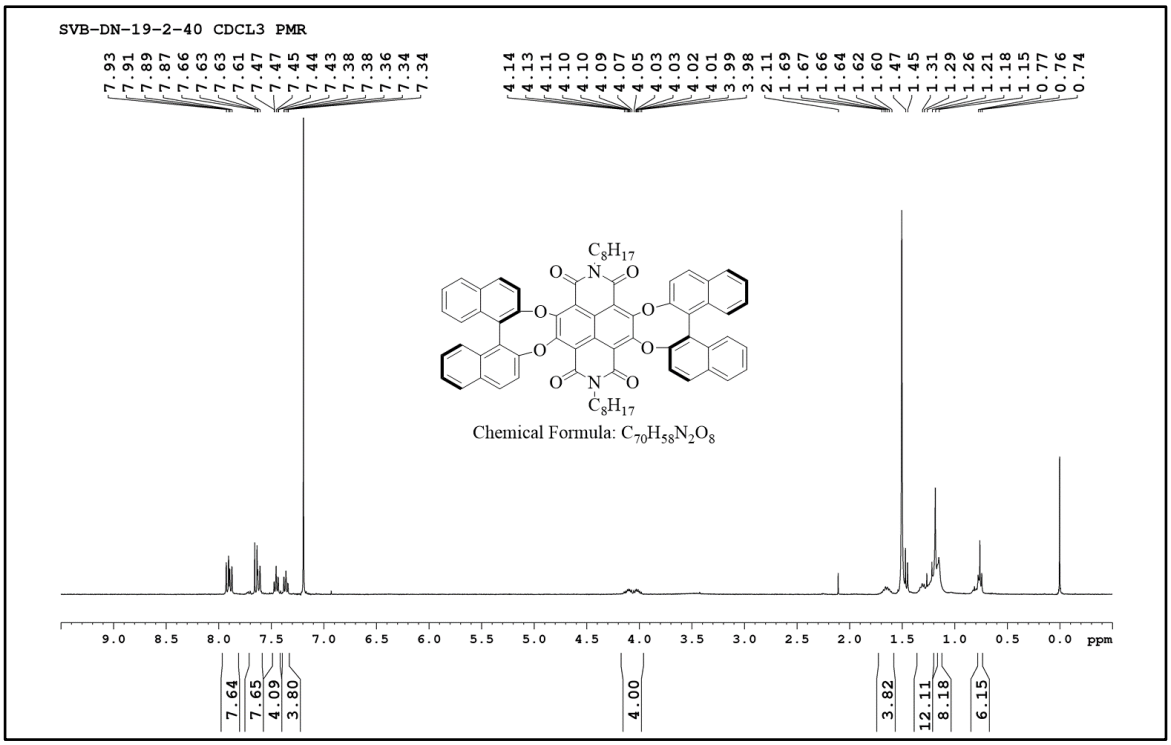

Figure 3.8: ^{1}H NMR spectrum of NDI-R-BINOL

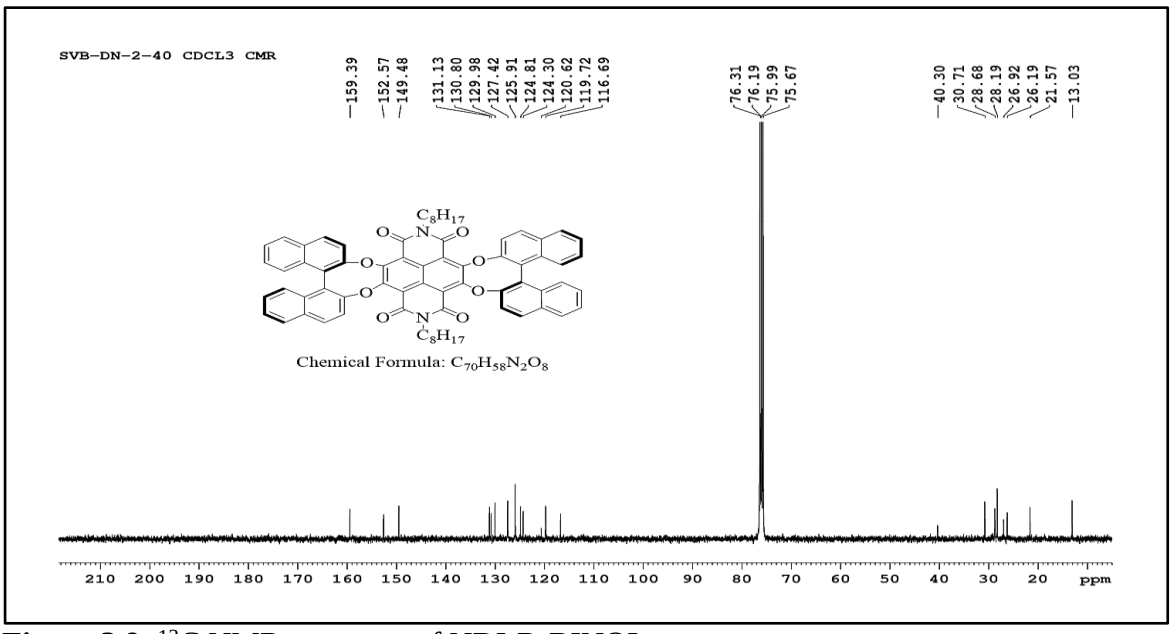

Figure 3.9: ^{13}C NMR spectrum of NDI-R-BINOL

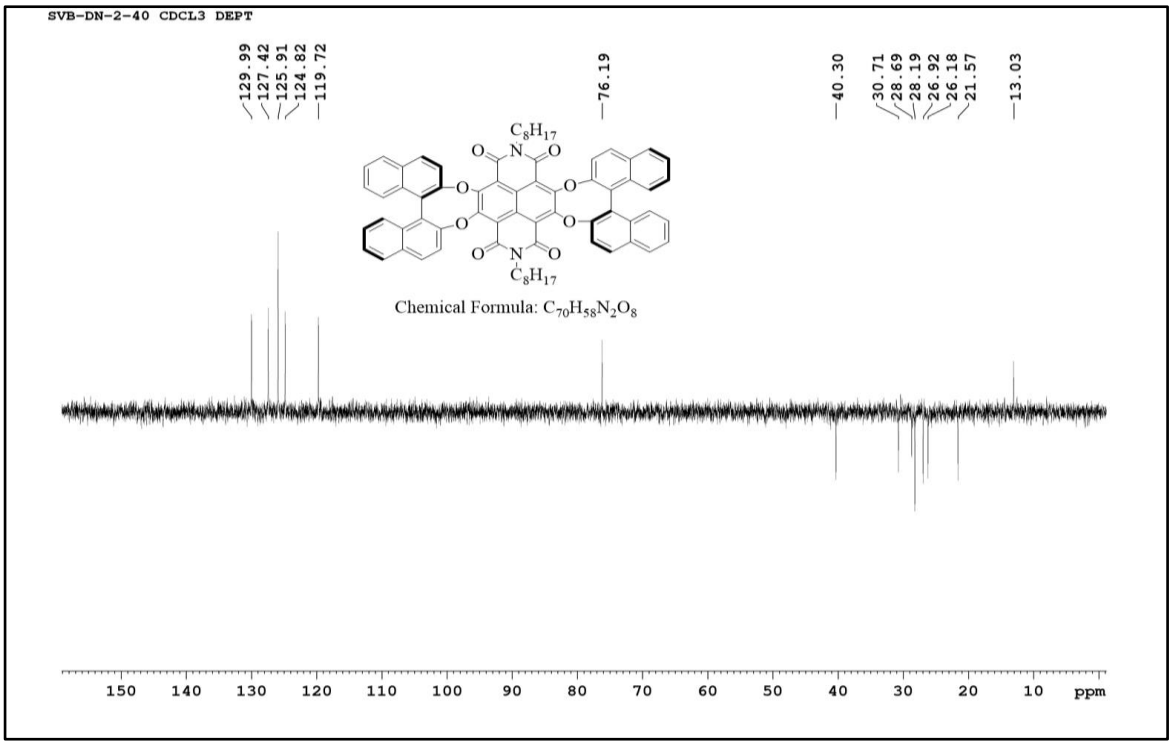

Figure 3.10: DEPT135 NMR spectrum of NDI-R-BINOL

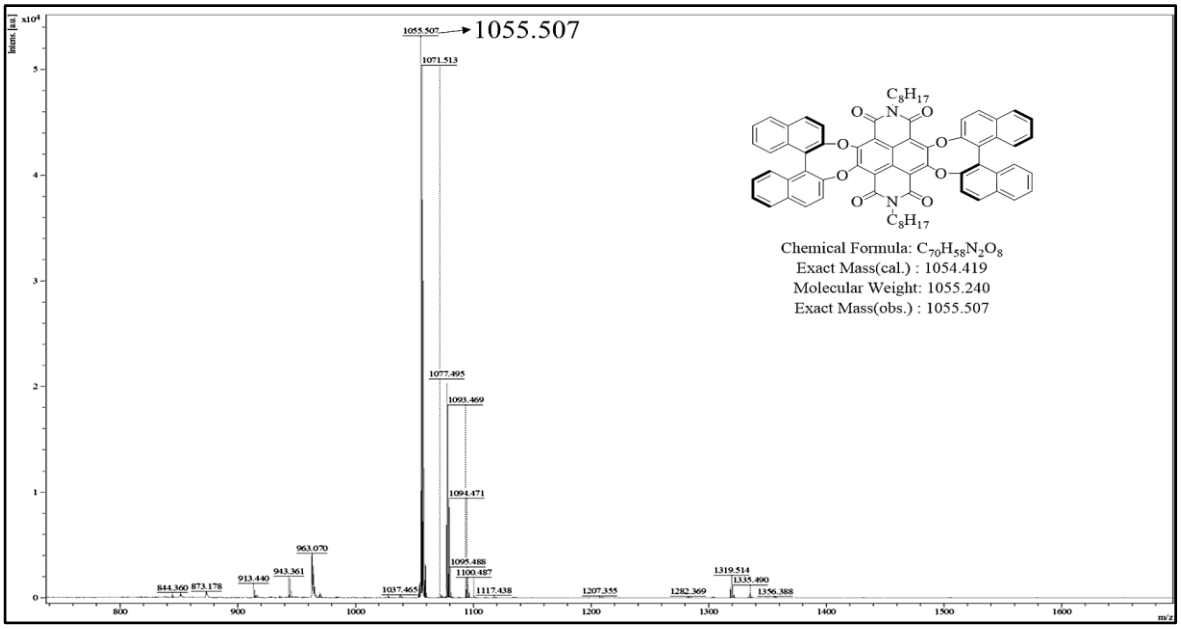

Figure 3.11: MALDI-TOF mass spectrum of NDI-R-BINOL

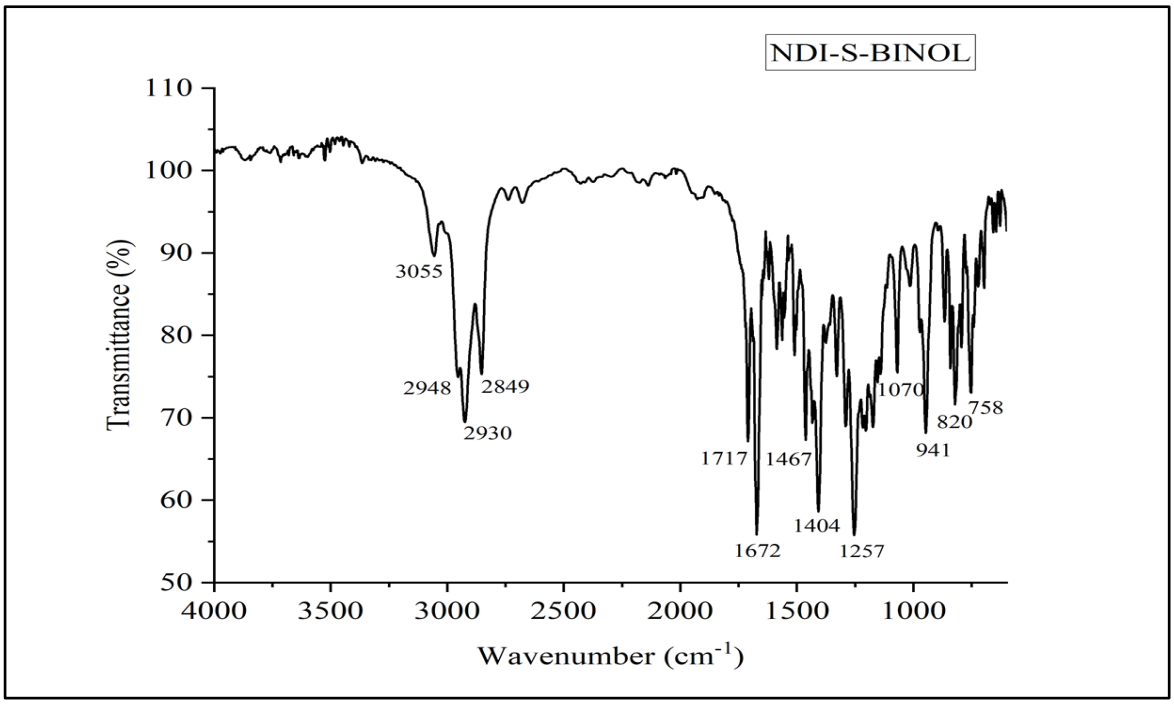

Figure 3.12: FT-IR spectrum of NDI-S-BINOL

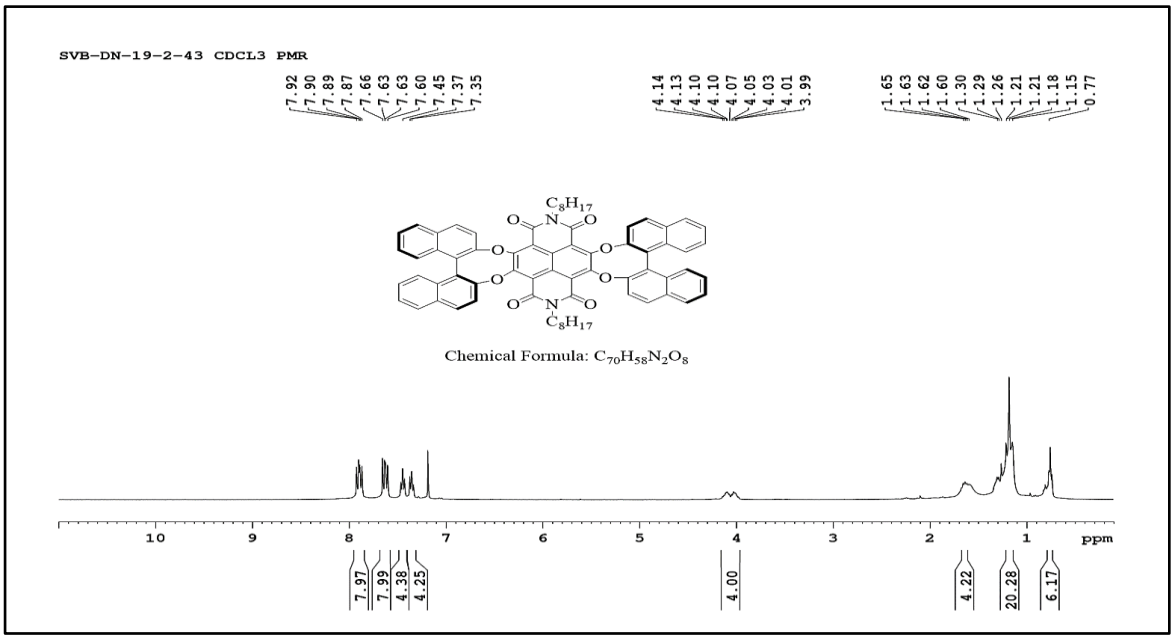

Figure 3.13: ^{1}H NMR spectrum of NDI-S-BINOL

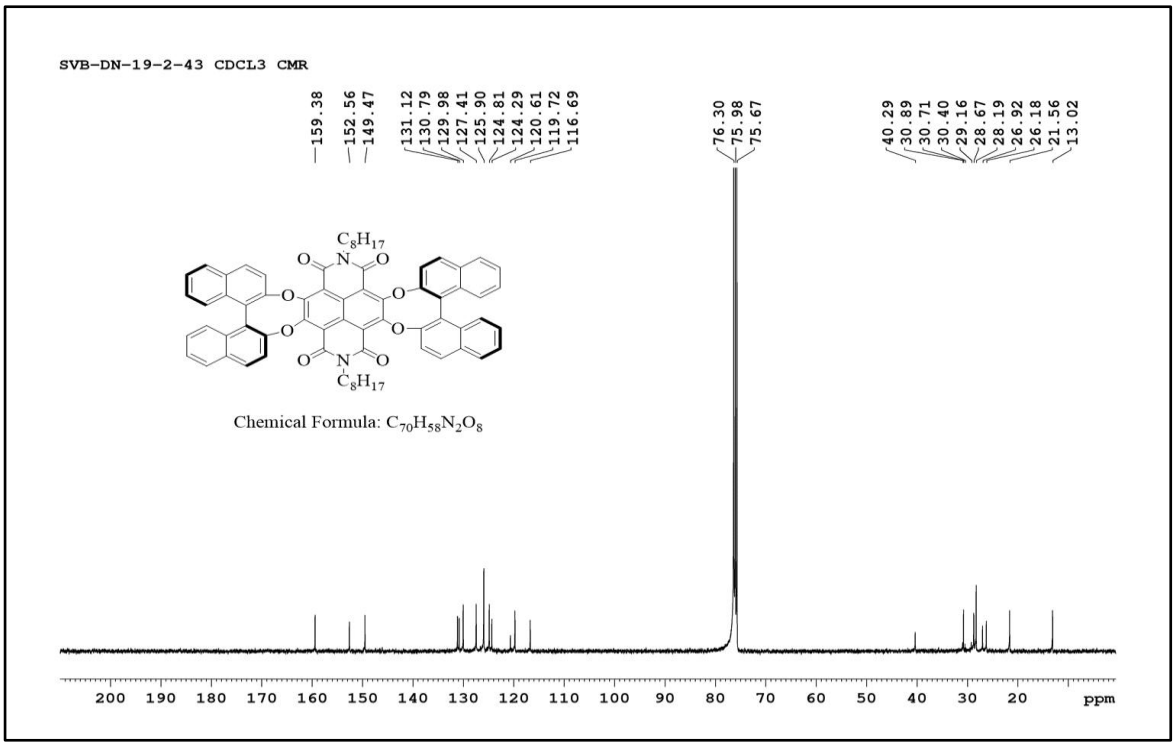

Figure 3.14: ^{13}C NMR spectrum of NDI-S-BINOL

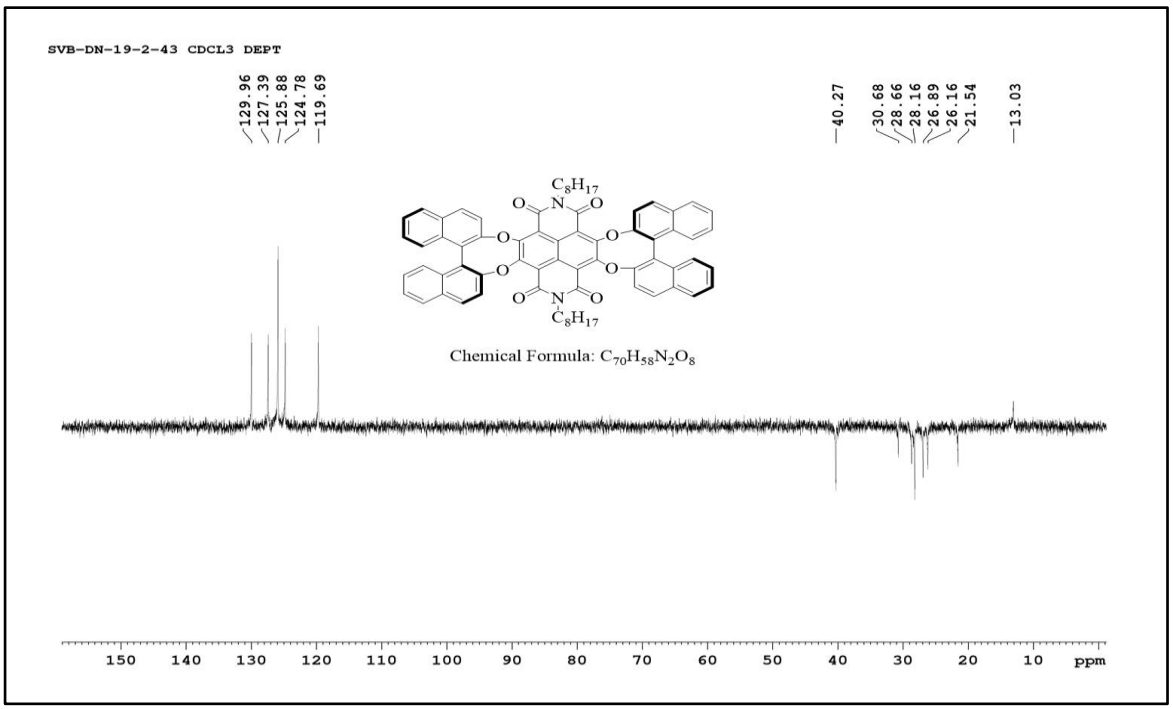

Figure 3.15: DEPT135 NMR spectrum of NDI-S-BINOL

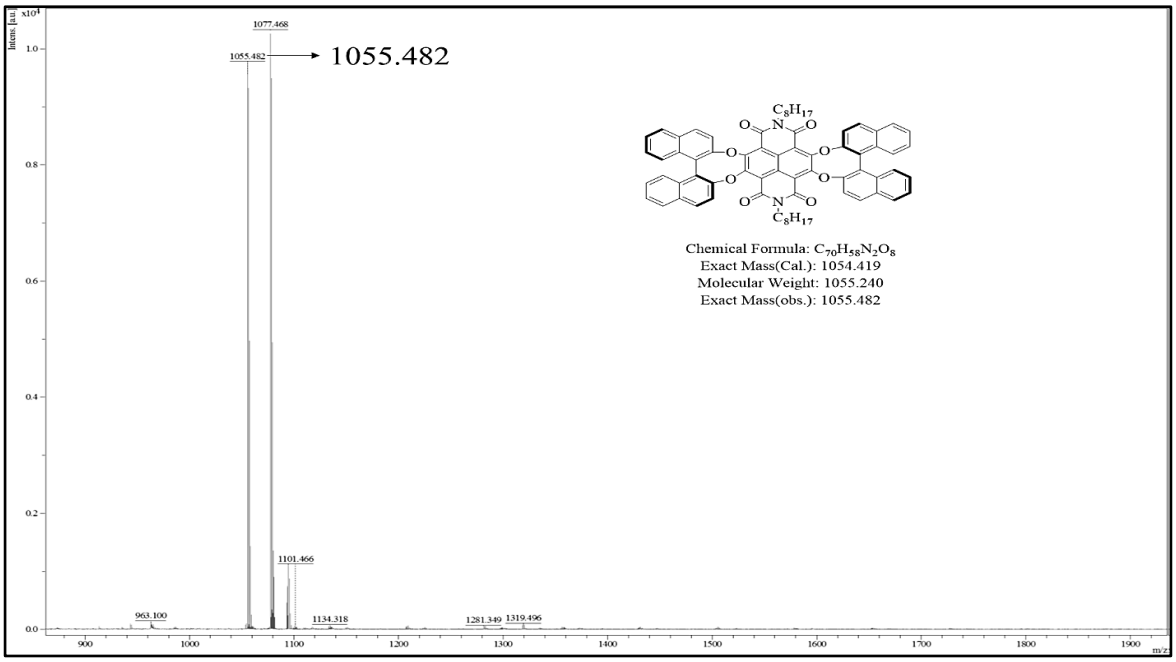

Figure 3.16: MALDI-TOF mass spectrum of NDI-S-BINOL

3.3.3 Solvatochromism

The photophysical properties of **NDI-R-BINOL** was studied by means of the electronic absorption and emission techniques in both polar aprotic and polar protic solvents including methanol (MeOH), acetonitrile (ACN), tetrachloroethane (TCE), tetrahydrofuran (THF), toluene (Tol), and methyl cyclohexane (MCH), at room temperature. **NDI-R-BINOL** shows the absorption peak ~425 nm in all used solvents, (**Fig. 3.17a**) it is due to aromatic core of NDI. The emission spectra of **NDI-R-BINOL** was recorded in above mention solvents and its shown broad range of emission 540 to 610 nm (λ_{ex} = 425nm). Were in TCE, the molecules shown emission at 610 nm. (**Fig. 3.17b**) However, in methanol and acetonitrile the emission spectra was shown 680 nm peak due to ICT effect. ICT effect may be due to charge transfer from BINOL moiety to NDI core.

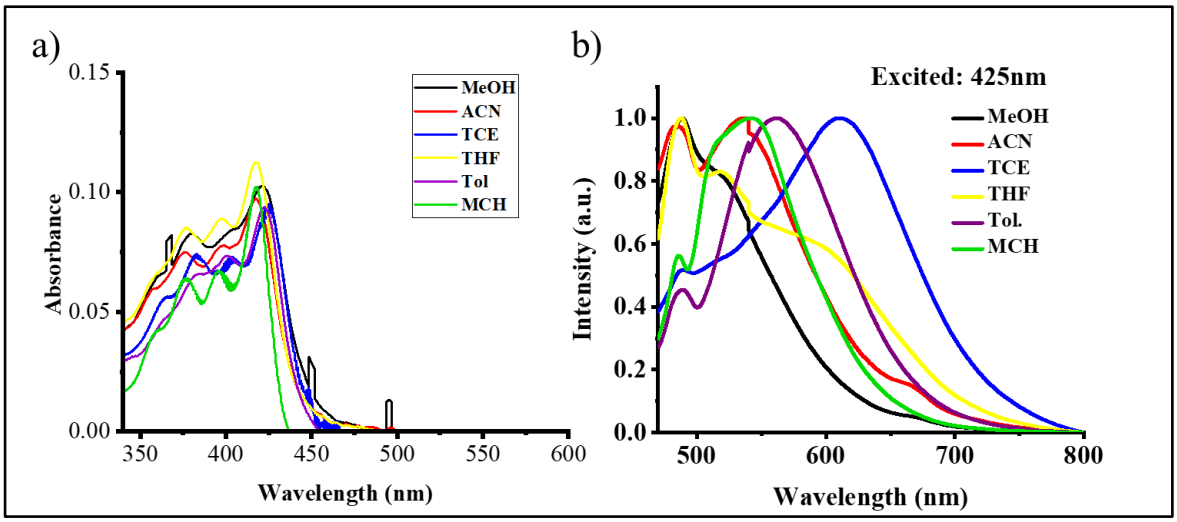

Figure 3.17: a) Absorption and b) normalized emission spectra of NDI-R-BINOL (1.5×10^{-5} M) recorded in various solvents (λ_{ex} = 425nm).

3.3.4Absorption and circular dichroism study

The absorption spectra of both derivatives recorded in TCE and its shown similar peak pattern and λ_{max} at 425 nm with two-shoulder peaks at 400 nm and 380 nm (**Fig. 3.18a**). To understand the chiral nature of both derivative, CD spectra was employed and it reveals that both the isomer was opposite (**Fig. 3.18b**). The **NDI-R-BINOL** shown positive cotton effect and while **NDI-S-BINOL** was Negative. gCD value at CD maxima 380nm was same for both just opposite in sign. There was no change spectral features of CD on different solvent composition of TCE/MCH. CD spectra was retained cotton effect of both derivative while changing solvent composition of TCE/MCH (**Fig. 3.18c**). From CD data, it concluded that the BINOL moieties were induced and controlled the chirality in planar and achiral NDI molecule.

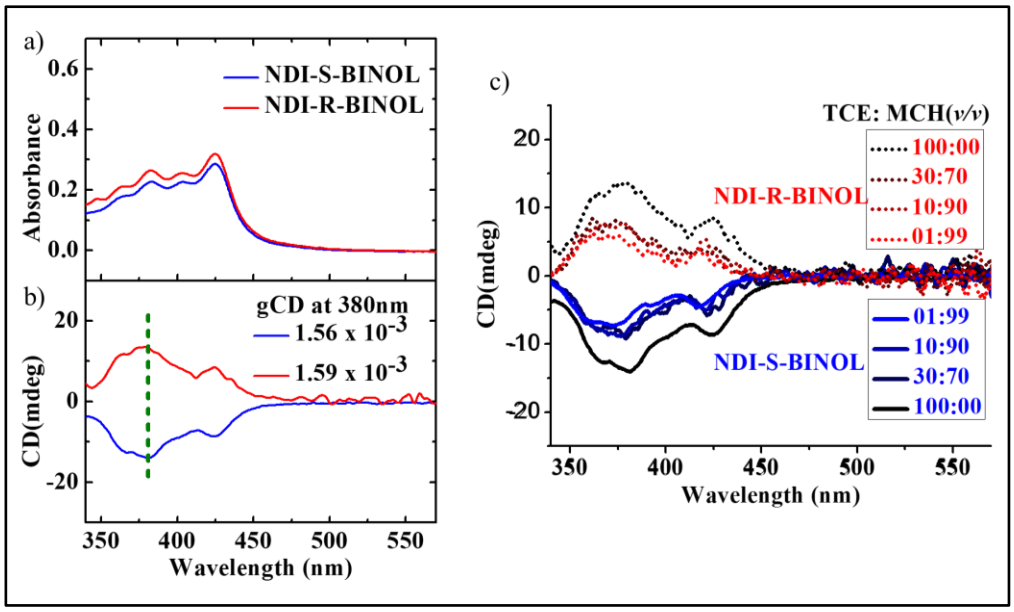

Figure 3.18: a) UV-Vis and b), c) CD spectra of NDI-R/S-BINOL (5×10^{-5} M) in TCE: MCH solvent system

3.3.5 Absorption and Emission study

The absorption and emission study of both derivatives **NDI-R/S-BINOL** were performed in TCE/MCH solvent system. Where TCE was good solvent for both derivatives and MCH was bad. The absorption spectra of **NDI-R/S-BINOL** were recorded in various composition of TCE/MCH, and its shown λ_{max} at 425 nm. (**Fig. 3.19a & 3.20a**) While increasing of MCH percentage in TCE the hypochromic shift was observed, it may be due to aggregation of molecule in non-polar solvent. And excitation spectra also were recorded in same solvent system, collected at 670 nm (**Fig. 3.19b & 3.20b**). Excitation spectra reveals decreasing intensity while increasing percentage of MCH. Further, emission spectra were studied in various solvent composition of TCE/ MCH. Emission peak observed at 560 nm (**Fig. 3.19c & 3.20c).** Where the normalized emission spectra at 560 nm, reveals that ICT effect was obsessed in both derivatives (**Fig. 3.19d & 3.20d)**

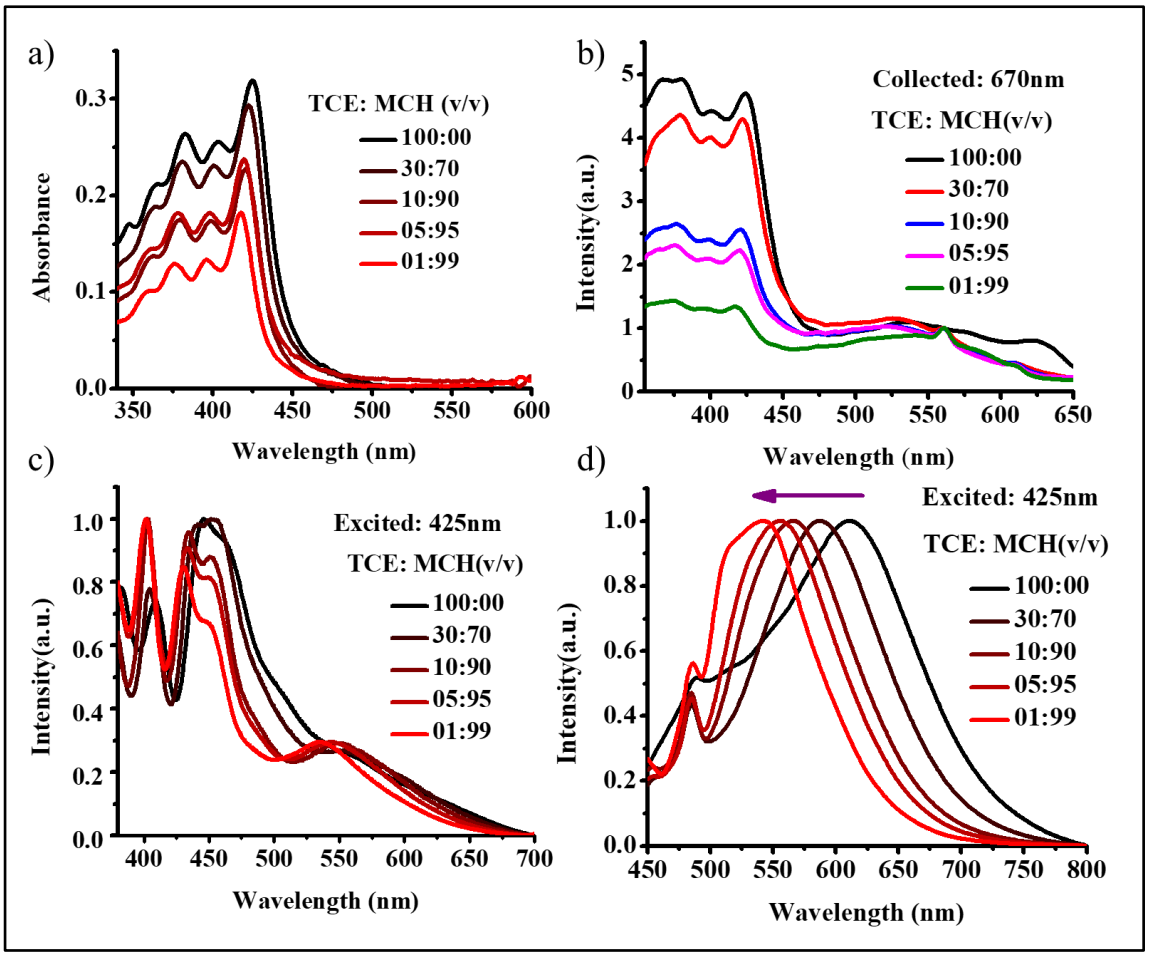

Figure 3.19: a) UV-Vis, b) excitation, c) Emission (λ_{ex} = 425nm), d) Normalized emission spectra at 560 nm of NDI-R-BINOL (5×10^{-5} M) in TCE:MCH solvent system.

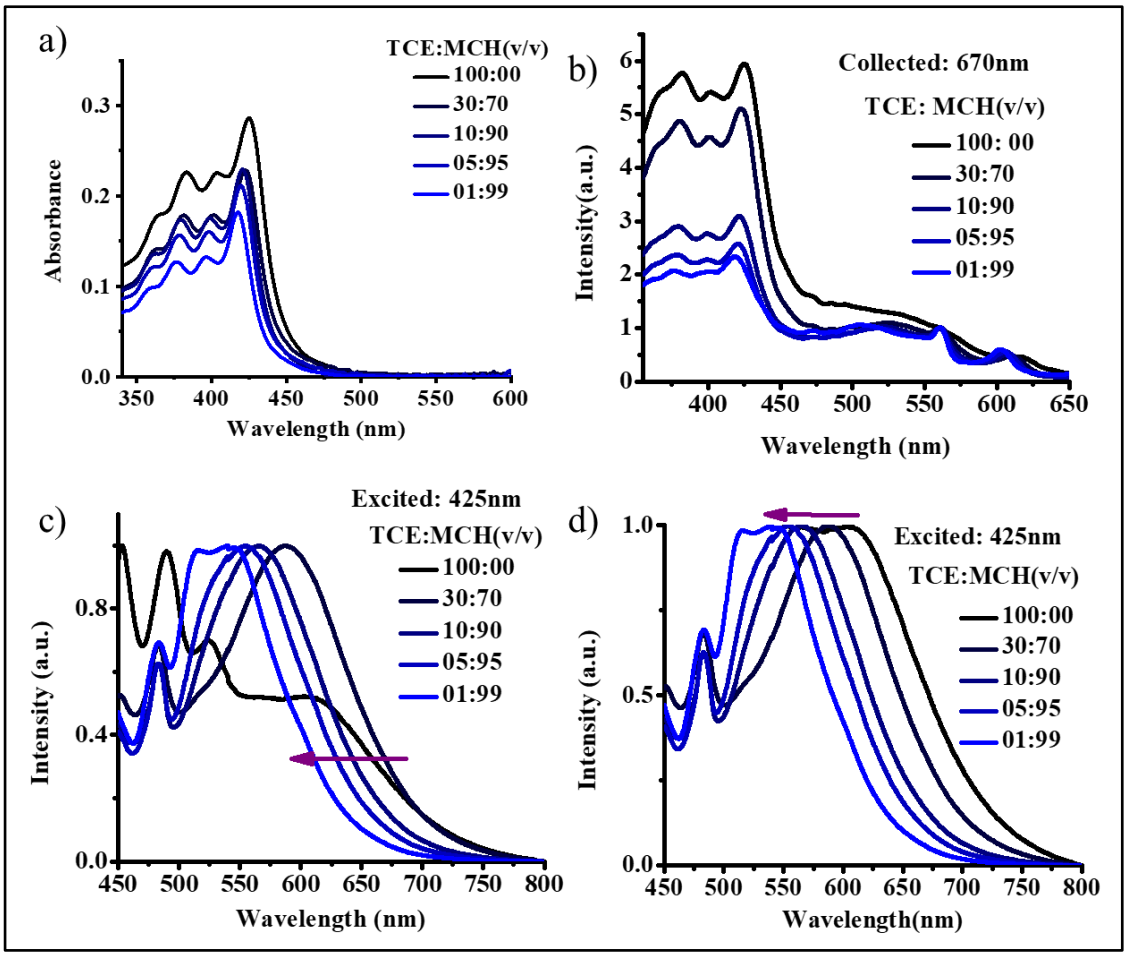

Figure 3.20: a) UV-Vis, b) excitation, c) Emission (λ_{ex} = 425nm), d) normalized emission spectra at 560 nm of NDI-S-BINOL (5×10^{-5} M) in TCE/MCH solvent system.

3.3.6 Dynamic light scattering

To determine the size of aggregates in different solvents, such as 100% TCE, 01% TCE in MCH. Dynamic Light Scattering (DLS) was utilized at room temperature. **NDI-R-BINOL** in 100% TCE and 01% TCE in MCH displayed the hydrodynamic radius (R_h) of 100 nm and 600 nm, respectively (**Fig.3.21**). The increasing R_h value suggesting noticeable aggregation of **NDI-R-BINOL** in 01% TCE in MCH

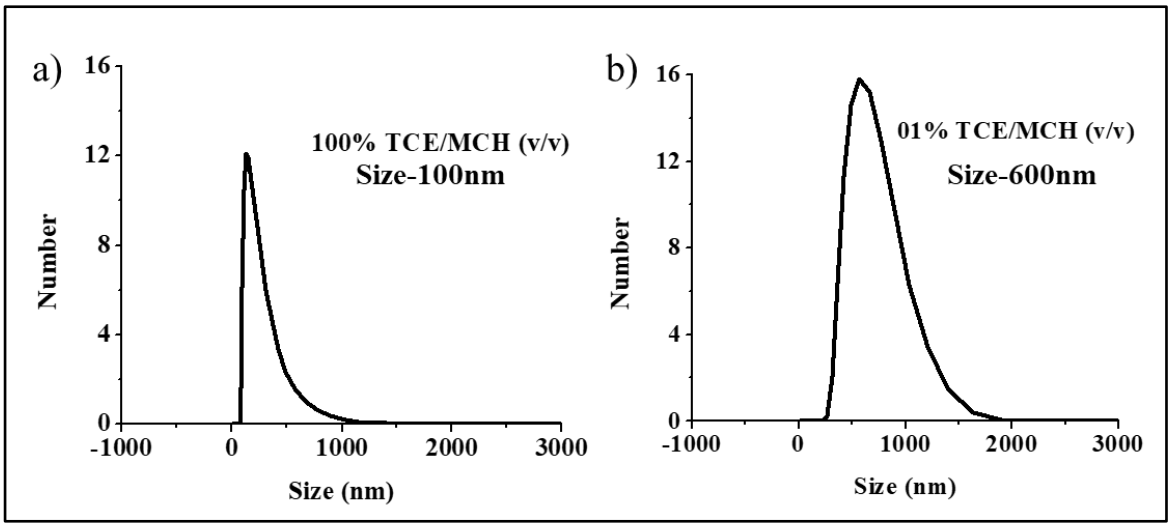

Figure 3.21: DLS spectra of **NDI-R-BINOL** (5×10^{-5} M) a) 100% TCE/MCH and b) 01% TCE/MCH.

3.3.7 Lifetime

The emission behavior of **NDI-R-BINOL** in various solvent composition of TCE/MCH was further investigated using time-correlated single-photon counting (TCSPC) with picosecond (ps) using λ_{ex} = 405 nm excitation and collected at 600 nm, results showed in **Figure 3.22** and all the results are summarized in **Table 3.1**. triexponential fitted decay curve was obtained for **NDI-R-BINOL**. In 100% TCE, lifetime τ1 was 0.8 ns (40.67%), τ2 was 3.4 ns (47.90%), τ3 was 14.98 ns (11.43) and average lifetime τ was 3.7 ns. Whereas in 01% TCE in MCH the lifetime τ1 was 0.48 ns (45.54%) and τ2 was 2.72 ns (32.60%), τ3 was 9.16 ns (21.87) and average lifetime τ 2.75 ns. From data, clearly suggest these results due to ICT effect.

Table 3.1: TCSPC Calculation for **NDI-R-BINOL** (5×10^{-5} M) and average life time in following solvent system

Solvent	**Wavelength (nm)**	**τ1 (ns)**	**Rel %**	**τ2 (ns)**	**Rel %**	**τ3 (ns)**	**Rel %**	**τ(avg.)**
100% TCE	600	0.8	40.67	3.4	47.90	14.98	11.43	3.7 ns
01% TCE	600	0.48	45.54	2.72	32.60	9.16	21.87	3.1 ns

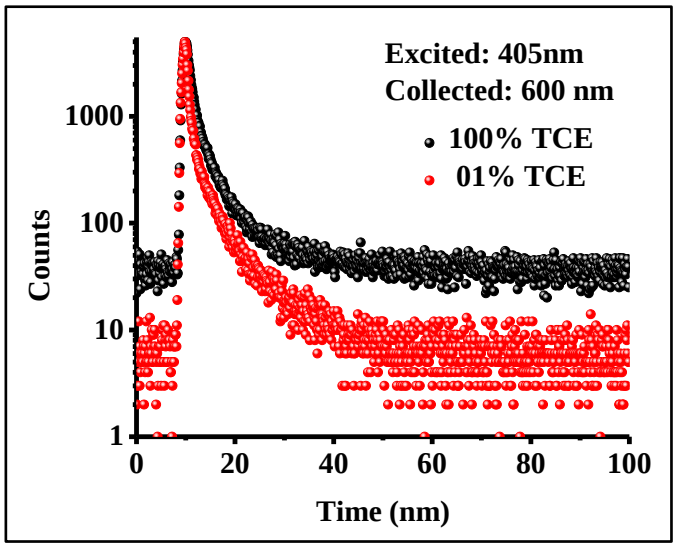

Figure 3.22: Average lifetime of NDI-R-BINOL in TCE/MCH.

3.4 Conclusion

Designed and successfully synthesized **NDI-R-BINOL** and **NDI-S-BINOL** molecules. Confirmed by IR, ^{1}H and ^{13}C NMR, and Mass spectroscopy. Both molecules shown same absorption and emission properties. Further, CD spectra reveals that both derivatives have opposite CD spectra. However, the absorption and emission study of both derivatives, where recorded in TCE/MCH it shown very similar results. Finally, the DLS study reveals that the **NDI-R-BINOL** was aggregating at 01% TCE in MCH. From all data, it concluded that the planar NDI molecule converted into chiral via inducing BINOL molecule, and controlled by using R and S isomers of BINOL. This type of molecule may be useful to study of circular polarized luminescence and various optoelectronic application.

References

(1) Bhosale, S. V.; Jani, C. H.; Langford, S. J. Chemistry of Naphthalene Diimides. *Chem. Soc. Rev.* **2008**, *37* (2), 331–342. https://doi.org/10.1039/b615857a.

(2) Würthner, F. Perylene Bisimide Dyes as Versatile Building Blocks for Functional Supramolecular Architectures. *Chem. Commun.* **2004**, *4* (14), 1564–1579. https://doi.org/10.1039/b401630k.

(3) Huang, C.; Barlow, S.; Marder, S. R. Perylene-3,4,9,10-Tetracarboxylic Acid Diimides: Synthesis, Physical Properties, and Use in Organic Electronics. *J. Org. Chem.* **2011**, *76* (8), 2386–2407. https://doi.org/10.1021/jo2001963.

(4) Würthner, F.; Stolte, M. Naphthalene and Perylene Diimides for Organic Transistors. *Chem. Commun.* **2011**, *47* (18), 5109–5115. https://doi.org/10.1039/c1cc10321k.

(5) Zhan, X.; Facchetti, A.; Barlow, S.; Marks, T. J.; Ratner, M. A.; Wasielewski, M. R.; Marder, S. R. Rylene and Related Diimides for Organic Electronics. *Adv. Mater.* **2011**, *23* (2), 268–284. https://doi.org/10.1002/adma.201001402.

(6) Jones, B. A.; Facchetti, A.; Wasielewski, M. R.; Marks, T. J. Tuning Orbital Energetics in Arylene Diimide Semiconductors. Materials Design for Ambient Stability of n-Type Charge Transport. *J. Am. Chem. Soc.* **2007**, *129* (49), 15259–15278. https://doi.org/10.1021/ja075242e.

(7) Ed, K. H. Industrial Organic Pigments Further Titles of Interest : **2004**, 3–527.

(8) Langhals, H. Cyclic Carboxylic Imide Structures as Structure Elements of High Stability. Novel Developments in Perylene Dye Chemistry. *Heterocycles* **1995**, *40* (1), 477–500. https://doi.org/10.3987/REV-94-SR2.

(9) Holtrup, F. O.; Müller, G. R. J.; Quante, H.; De Feyter, S.; De Schryver, F. C.; Müllen, K. Terrylenimides: New NIR Fluorescent Dyes. *Chem. - A Eur. J.* **1997**, *3* (2), 219–225. https://doi.org/10.1002/chem.19970030209.

(10) Geerts, Y.; Quante, H.; Platz, H.; Mahrt, R.; Hopmeier, M.; Böhm, A.; Müllen, K. Quaterrylenebis(Dicarboximide)s: Near Infrared Absorbing and Emitting Dyes. *J. Mater. Chem.* **1998**, *8* (11), 2357–2369. https://doi.org/10.1039/a804337j.

(11) Avlasevich, Y.; Li, C.; Müllen, K. Synthesis and Applications of Core-Enlarged Perylene Dyes. *J. Mater. Chem.* **2010**, *20* (19), 3814–3826. https://doi.org/10.1039/c000137f.

(12) De Schryver, F. C.; Vosch, T.; Cotlet, M.; Van Der Auweraer, M.; Müllen, K.; Hofkens, J. Energy Dissipation in Multichromophoric Single Dendrimers. *Acc. Chem. Res.* **2005**, *38* (7), 514–522. https://doi.org/10.1021/ar040126r.

(13) Weil, T.; Vosch, T.; Hofkens, J.; Peneva, K.; Müllen, K. The Rylene Colorant Family-Tailored Nanoemitters for Photonics Research and Applications. *Angew. Chemie - Int. Ed.* **2010**, *49* (48), 9068–9093. https://doi.org/10.1002/anie.200902532.

(14) Liu, Z.; Zhang, G.; Cai, Z.; Chen, X.; Luo, H.; Li, Y.; Wang, J.; Zhang, D. New Organic Semiconductors with Imide/Amide-Containing Molecular Systems. *Adv. Mater.* **2014**, *26* (40), 6965–6977. https://doi.org/10.1002/adma.201305718.

(15) Castellano, F. N. Transition Metal Complexes Meet the Rylenes. *Dalt. Trans.* **2012**, *41* (28), 8493–8501. https://doi.org/10.1039/c2dt30765k.

(16) Würthner, F. Bay-Substituted Perylene Bisimides: Twisted Fluorophores for Supramolecular Chemistry. *Pure Appl. Chem.* **2006**, *78* (12), 2341–2349. https://doi.org/10.1351/pac200678122341.

(17) Görl, D.; Zhang, X.; Würthner, F. Molecular Assemblies of Perylene Bisimide Dyes in Water. *Angew. Chemie - Int. Ed.* **2012**, *51* (26), 6328–6348. https://doi.org/10.1002/anie.201108690.

(18) Lehn, J. M. From Supramolecular Chemistry towards Constitutional Dynamic Chemistry and Adaptive Chemistry. *Chem. Soc. Rev.* **2007**, *36* (2), 151–160. https://doi.org/10.1039/b616752g.

(19) Whitesides, M.; Simanek, E. E.; Gordon, M. Noncovalent Synthesis: Using Physical-Organic Chemistry. **2001**, No. 4, 1–8.

(20) Suraru, S. L.; Würthner, F. Strategies for the Synthesis of Functional Naphthalene Diimides. *Angew. Chemie - Int. Ed.* **2014**, *53* (29), 7428–7448. https://doi.org/10.1002/anie.201309746.

(21) Paquin, F.; Rivnay, J.; Salleo, A.; Stingelin, N.; Silva, C. Multi-Phase Semicrystalline Microstructures Drive Exciton Dissociation in Neat Plastic Semiconductors. *J. Mater. Chem. C* **2015**, *3* (207890), 10715–10722. https://doi.org/10.1039/b000000x.

(22) Sakai, N.; Mareda, J.; Vauthey, E.; Matile, S. Core-Substituted Naphthalenediimides. *Chem. Commun.* **2010**, *46* (24), 4225–4237. https://doi.org/10.1039/c0cc00078g.

(23) Chen, Z.; Lohr, A.; Saha-Möller, C. R.; Würthner, F. Self-Assembled π-Stacks of Functional Dyes in Solution: Structural and Thermodynamic Features. *Chem. Soc. Rev.* **2009**, *38* (2), 564–584. https://doi.org/10.1039/b809359h.

(24) Mirkin, C. A.; Letsinger, R. L.; Mucic, R. C.; Storhoff, J. J. A DNA-Based Method for Rationally Assembling Nanoparticles into Macroscopic Materials. *Nature*. 1996, pp 607–609. https://doi.org/10.1038/382607a0.

(25) Zhang, X.; Rehm, S.; Safont-Sempere, M. M.; Würthner, F. Vesicular Perylene Dye Nanocapsules as Supramolecular Fluorescent PH Sensor Systems. *Nat. Chem.* **2009**, *1* (8), 623–629. https://doi.org/10.1038/nchem.368.

(26) Aida, T.; Meijer, E. W.; Stupp, S. I. Functional Supramolecular Polymers. *Science (80-.).* **2012**, *335* (6070), 813–817. https://doi.org/10.1126/science.1205962.

(27) Sisson, A. L.; Shah, M. R.; Bhosale, S.; Matile, S. Synthetic Ion Channels and Pores (2004–2005). *Chem. Soc. Rev.* **2006**, *35* (12), 1269–1286. https://doi.org/10.1039/b512423a.

(28) Shao, L.; Zhou, J.; Hua, B.; Yu, G. A Dual-Responsive Supra-Amphiphile Based on a Water-Soluble Pillar[7]Arene and a Naphthalene Diimide-Containing Guest. *Chem. Commun.* **2015**, *51* (33), 7215–7218. https://doi.org/10.1039/c5cc00937e.

(29) Che, Y.; Datar, A.; Balakrishnan, K.; Zang, L. Ultralong Nanobelts Self-Assembled

from an Asymmetric Perylene Tetracarboxylic Diimide. *J. Am. Chem. Soc.* **2007**, *129* (23), 7234–7235. https://doi.org/10.1021/ja071903w.

(30) Zhang, X.; Chen, Z.; Würthner, F. Morphology Control of Fluorescent Nanoaggregates by Co-Self-Assembly of Wedge- and Dumbbell-Shaped Amphophilic Perylene Bisimides. *J. Am. Chem. Soc.* **2007**, *129* (16), 4886–4887. https://doi.org/10.1021/ja070994u.

(31) Yan, P.; Chowdhury, A.; Holman, M. W.; Adams, D. M. Self-Organized Perylene Diimide Nanofibers. *J. Phys. Chem. B* **2005**, *109* (2), 724–730. https://doi.org/10.1021/jp046133e.

(32) Balakrishnan, K.; Datar, A.; Oitker, R.; Chen, H.; Zuo, J.; Zang, L. Nanobelt Self-Assembly from an Organic n-Type Semiconductor: Propoxyethyl-PTCDI. *J. Am. Chem. Soc.* **2005**, *127* (30), 10496–10497. https://doi.org/10.1021/ja052940v.

(33) Piot, L.; Marie, C.; Dou, X.; Feng, X.; Mullen, K.; Fichou, D. Growth of Long, Highly Stable, and Densely Packed Worm-like Nanocolumns of Hexa-Peri-Hexabenzocoronenes via Chemisorption on Au(111). *J. Am. Chem. Soc.* **2009**, *131* (4), 1378–1379. https://doi.org/10.1021/ja808752b.

(34) Jin, W.; Yamamoto, Y.; Fukushima, T.; Ishii, N.; Kim, J.; Kato, K.; Takata, M.; Aida, T. Systematic Studies on Structural Parameters for Nanotubular Assembly of Hexa-Peri-Hexabenzocoronenes. *J. Am. Chem. Soc.* **2008**, *130* (29), 9434–9440. https://doi.org/10.1021/ja801179e.

(35) Nolde, F.; Pisula, W.; Müller, S.; Kohl, C.; Müllen, K. Synthesis and Self-Organization of Core-Extended Perylene Tetracarboxdiimides with Branched Alkyl Substituents. *Chem. Mater.* **2006**, *18* (16), 3715–3725. https://doi.org/10.1021/cm060742c.

(36) Hill, J. P.; Jin, W.; Kosaka, A.; Fukushima, T.; Ichihara, H.; Shimomura, T.; Ito, K.; Hashizume, T.; Ishii, N.; Aida, T. Self-Assembled Hexa-Peri-Hexabenzocoronene Graphitic Nanotube. *Science (80-.).* **2004**, *304* (5676), 1481–1483. https://doi.org/10.1126/science.1097789.

(37) Hoeben, F. J. M.; Zhang, J.; Lee, C. C.; Pouderoijen, M. J.; Wolffs, M.; Würthner, F.; Schenning, A. P. H. J.; Meijer, E. W.; De Feyter, S. Visualization of Various Supramolecular Assemblies of Oligo(Para- Phenylenevinylene)-Melamine and Perylene Bisimide. *Chem. - A Eur. J.* **2008**, *14* (28), 8579–8589. https://doi.org/10.1002/chem.200800760.

(38) Miller, L. L.; Mann, K. R. π-Dimers and π-Stacks in Solution and in Conducting

Polymers. *Acc. Chem. Res.* **1996**, *29* (9), 417–423. https://doi.org/10.1021/ar9600446.

(39) Erten, S.; Posokhov, Y.; Alp, S.; Içli, S. The Study of the Solubility of Naphthalene Diimides with Various Bulky Flanking Substituents in Different Solvents by UV-Vis Spectroscopy. *Dye. Pigment.* **2005**, *64* (2), 171–178. https://doi.org/10.1016/j.dyepig.2004.04.011.

(40) Zhong, C. J.; Kwan, W. S. V.; Miller, L. L. Self-Assembly of Delocalized π-Stacks in Solution. Assessment of Structural Effects. *Chem. Mater.* **1992**, *4* (6), 1423–1428. https://doi.org/10.1021/cm00024a052.

(41) Kobaisi, M. Al; Bhosale, S. V.; Latham, K.; Raynor, A. M.; Bhosale, S. V. Functional Naphthalene Diimides: Synthesis, Properties, and Applications. *Chem. Rev.* **2016**, *116* (19), 11685–11796. https://doi.org/10.1021/acs.chemrev.6b00160.

(42) Aleshinloye, A. O.; Bodapati, J. B.; Icil, H. Synthesis, Characterization, Optical and Electrochemical Properties of a New Chiral Multichromophoric System Based on Perylene and Naphthalene Diimides. *J. Photochem. Photobiol. A Chem.* **2015**, *300*, 27–37. https://doi.org/10.1016/j.jphotochem.2014.12.007.

(43) Narayan, B.; Bejagam, K. K.; Balasubramanian, S.; George, S. J. Autoresolution of Segregated and Mixed P-n Stacks by Stereoselective Supramolecular Polymerization in Solution. *Angew. Chemie - Int. Ed.* **2015**, *54* (44), 13053–13057. https://doi.org/10.1002/anie.201506435.

(44) Bhosale, S. V.; Jani, C.; Lalander, C. H.; Langford, S. J. Solvophobic Control of Core-Substituted Naphthalene Diimide Nanostructures. *Chem. Commun.* **2010**, *46* (6), 973–975. https://doi.org/10.1039/b920015k.

(45) Sasikumar, M.; Suseela, Y. V.; Govindaraju, T. Dibromohydantoin: A Convenient Brominating Reagent for 1,4,5,8-Naphthalenetetracarboxylic Dianhydride. *Asian J. Org. Chem.* **2013**, *2* (9), 779–785. https://doi.org/10.1002/ajoc.201300088.

Chapter IV

Synthesis and characterization of tetraphenylethylene derivatives for sensing applications

4.1 Introduction

New photo-luminescent materials are required to eliminate the aggregation-caused quenching (ACQ) effect in the aggregated state. Naphthalene, porphyrins, perylene diimide, pyrene, anthracene, phenanthrene, fluoranthene, perylene, carbazole, triphenylamine, phenothiazine, cyanine, diketopyrrolopyrrole, and fluorescein are all examples of aromatic molecules that have been used for a comprehensive range of potential application. Nevertheless, all these molecules shows ACQ effect.[1] Aggregation-induced emission (AIE), a novel phenomenon, was first described by Tang group in 2001. It describes how normally tiny organic molecules, which are low emitters when fully dissolved in solvents like toluene, THF, and chloroform, become extremely luminous in the supramolecular aggregated state as well as in solid films.[2] Understanding the underlying processes for the AIE phenomenon is vital to the search for fundamental photophysical knowledge, and it will also direct our efforts to create innovative luminogens, consider useful applications, and improve technological breakthroughs. Restriction of Intramolecular Rotations (RIR), Restriction of Intramolecular Vibrations (RIV) and Restriction of Intramolecular Motions (RIM) are the three primary theories for the mechanistic reasons of the AIE effects.[3] Tetraphenylethylene (TPE) derivatives have garnered a lot of interest among the AIE-active luminophores created because of their weak intermolecular contacts and great solubility in organic solvents. They also feature a structure that is accessible to functionalization on the planar phenyl groups, which may result in AIE activity.[4] The TPE shows weakly emissive in 100 % THF while adding water in increasing order TPE got aggregate in 99% water were its exhibited highly emissive as shown in **Figure 4.1**

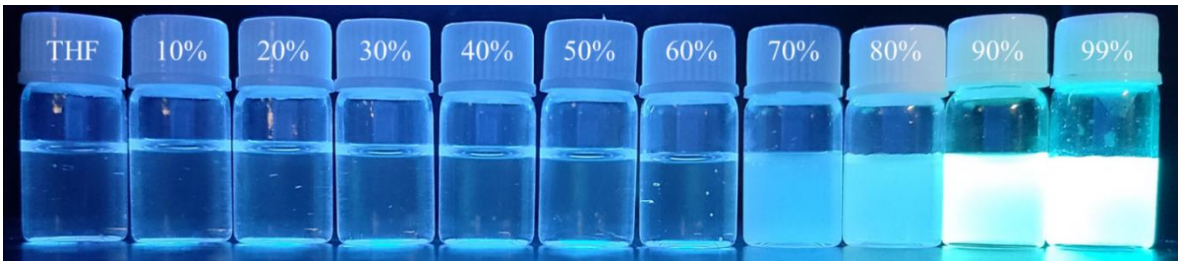

Figure 4.1: Emission properties of TPE molecule in solution phase and aggregated phase under UV light of 365 nm.

The oldest synthetic process for synthesizing TPE was published by Boissieu in 1888. It entailed brominating diphenylmethane to produce dibromodiphenylmethane, which was then heated, distilled, and recrystallized from benzene to produce TPE with a satisfactory yield.[5] The copper-catalysed self-coupling of dichloro diphenylmethane **6** in DMSO occurs

at room temperature to produce TPE in a decent yield, according to a technique Tezuka and colleagues published in 1990. [6] Afterword, in 2004, Okuma proposed a synthetic procedure for the synthesis of TPE molecules, in which seleno-benzophenones **4** interacted with diphenyl diazomethane **5** in DCM at 78 °C to produce TPE in good yields.[7] Laschat[8] reported utilizing a McMurry coupling method to produce TPE. $TiCl_4$ and Zn powder were used in this process, which involves the reductive coupling of benzophenone **3** in dry THF at -5 °C. The synthesis of symmetrical and asymmetrical TPE derivatives has made considerable use of this synthetic technique. A method for producing TPE with a 100% yield was described by Woollins et al. in 2007 by heating two equivalents of ketone **3** in toluene with the Woollins reagents.[9] Using a phosphapalladacycle catalyst, Rafiee et al.[10] developed another efficient high yield synthetic approach for the synthesis of TPE in 2009. Another synthetic method was reported by Kumara Swamy et al. [11] for TPE preparation in 2010. The following strategy the utilizing phenylboronic acid, the double arylation process of diphenyl acetylene **7** was carried out. Palladium (II) acetate is present in the reactions of boranic acid **8** and iodobenzene **9** in DMSO produces TPE. An intermediate tertiary alcohol was produced by treating the diphenylmethane **1** with n-BuLi in dry THF at 0 °C and then adding benzophenone **3**. In order to produce a white solid of TPE with a good yield, the produced tertiary alcohol was subjected to a dehydration process using para-toluene sulphonic acid (pTSA) in toluene. [12] Lin et al.[13] published a reductive synthesis approach for synthesis of TPE in 2014 that involved treating a range of ketones and aldehydes with ytterbium (Yb) in conjunction with $TiCl_4$ (cat.) in dry THF.

In a diluted solution, the isolated TPE molecules produce no light. The exciting energy is non-radioactively dissipated by the dynamic rotations of the aromatic rotors against the olefinic stator around the single-bond axis. The central olefinic double bond may open in the excited state, producing two units of diphenylmethylene (DPM). The exictions relax without emitting radiation because of the friction that their rotating or twisting movements against one another and the solvent media generate. The restricted intramolecular rotation (RIR) and the highly twisted molecular shape that restrict the intermolecular stacking interaction have a synergistic impact on the emission of TPE after aggregation formation.[3]

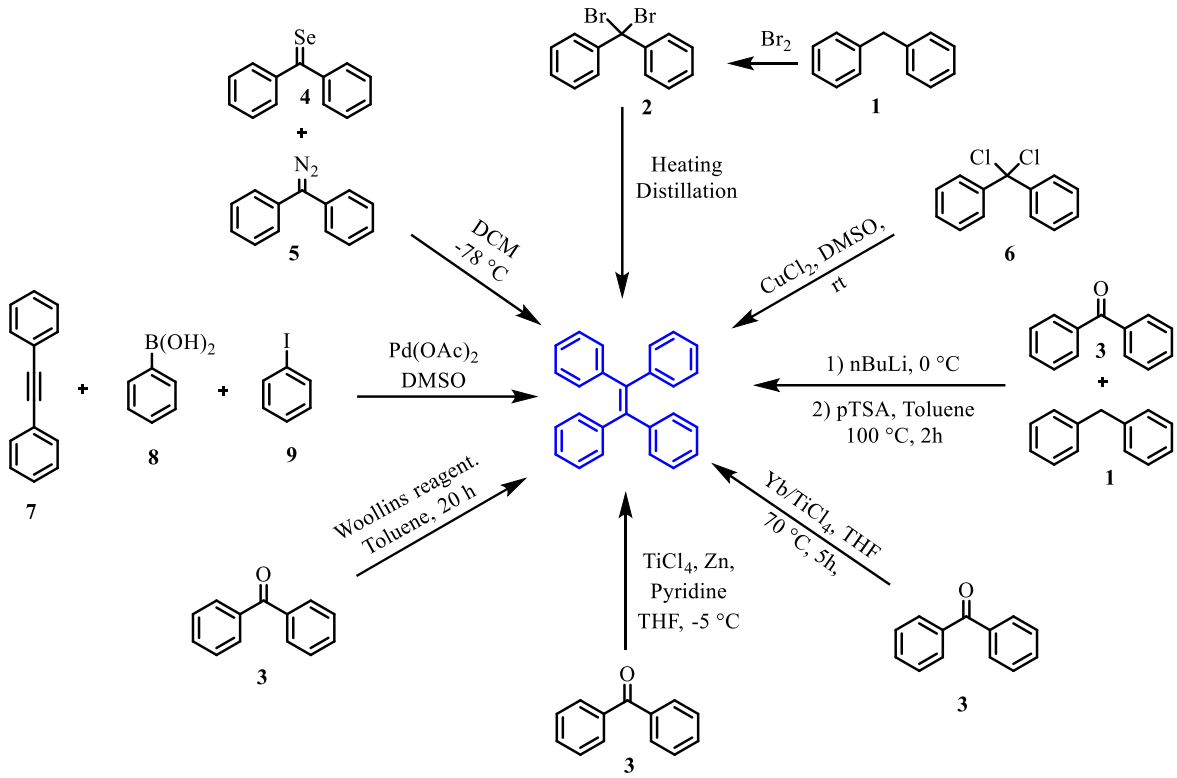

Scheme 4.1: Synthetic methods for the preparation of the **TPE**

Why Tetraphenylethylene derivatives are important, because they are largely applicable (**Fig. 4.2**) in various application such as biomolecule sensing,[14–18] bio molecular imaging,[19–23] pH responsive,[24–28] detection of explosives compounds,[29–34] sensing of organic volatile and gaseous compounds.[35–38]Further they are also used in Sensing of peroxide[39] and hazardous species[40–42] and real-world application for fingerprints,[43] induction of chirality[44–47], stimuli response towards viscosity[48] and temperature,[49] self-assembly, organic light-emitting diodes (OLEDs),[50,51] organic field-effect transistors (OFETs), circularly polarized luminescence (CPL),[52–54] and chemo-sensing of cations[40,55–64], anions[65–70] and neutral molecules.[14–18]. This part mainly focus on tetraphenylethylene derivatives, which were utilized for chemo sensing of cations and anions.

Because the TPE core is a typical AIE fluorophore, TPE derivatives require an ion chelating or binding moiety in order to establish a stable complex with the target ions in the detecting medium. A change in the electronic and molecular properties of the TPE-based fluorophore core is often required for a variation in observable fluorescence to be induced by the binding site of an ion to a TPE derivative. These modifications can be made by electron transfer or photo excited TPE luminogens, which can switch on due to the TPE derivatives strong AIE fluorescence.

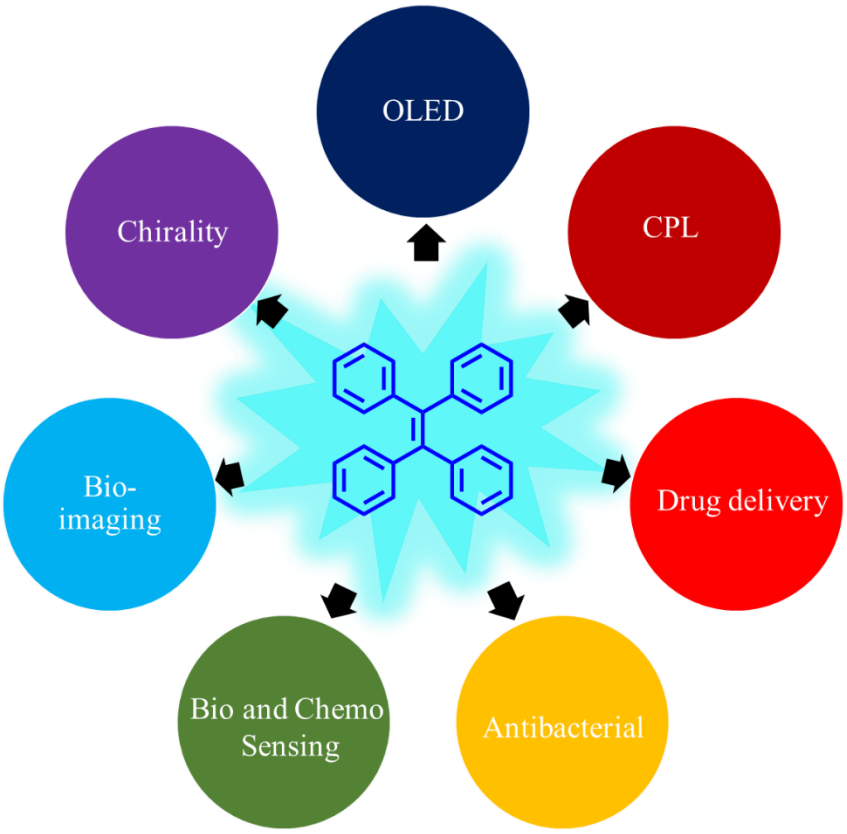

Figure 4.2: Various applications of TPE derivatives

Based on this process, a number of AIE-active TPE derivatives have been designed and employed as chemosensor substitutes for the detection of cations such Hg^{2+}, Zn^{2+}, Fe^{3+}, Cr^{3+}, Al^{3+}, Cu^{2+}, Ag^{+}, Cd^{2+}, Sb^{3+}, Pb^{2+}, Th^{2+}, and UO_2^{2+}.

In 2013, Ozturk et al.[71] reported selective and sensitive detection of Hg^{2+} by using tetraphenylethene based **10** popularity-dependent "turn-on" fluorescence strategy in an aqueous medium and in living cells. Zhang and his group[72] described the "Turn-on" of the fluorescence of tetra(4-pyridylphenyl)ethylene **11** by the synergistic interactions of Hg^{2+} and hydrogen sulfate anion. Ruan et al.[73] in 2012 has synthesized a novel thioketal containing AIE-active probes **12 &13** for Mercury (II), based on the Hg^{2+}-promoted deprotection of thioketal. In 2016, Neupane et al.[74] synthesized AIE-active TPE derivative **14** probe for selectively and sensitively detecting Hg^{2+} ion in 100% aqueous solution and cells. Tang et al.[59] in 2019, reported chemosensor for Hg^{2+} tetraphenylethylene (TPE)-based fluorescent sensor **15** with aggregation-induced emission enhancement (AIEE) activity. It's interesting that the synthesized luminogen were detect Hg^{2+} in an acetonitrile solution with good selectivity and the detection low limit without interference from other competing metal ions. Additionally, the luminogen displayed intriguing solvatochromis activity and

improved cell-imaging capabilities. In 2022, Wang et al.[61] reported a NH-pyrazolate-functionalized AIEgens **16** which were utilized to highly specific and selective fluorescent chemosensor for sensing of Hg^{2+}. Yuan and his group[75] conjugated TPE-C4-L2 molecules **17** were constructed as a graphite-based self-assembled monolayers (SAM) that was utilised for detecting tiny quantities of Zn (II). That SAM's quenched FL response to Zn^{2+} was the reverse of whatever occurred to TPE-C4-L2 molecules in aqueous solution when Zn (II) was added, which was a FL enhancement. Hong et al.[57] synthesized AIE-based terpyridine-substituted tetraphenylethenes **18 & 19** for fluoregenic Zn^{2+} and chromogenic Fe^{2+} sensors. Sun et al.[76] reported tetraphenylethylene derivative **20** which was "turn-on" sensor for Zn^{2+} in aqueous condition and also intracellular Zn^{2+} imaging. Afterword, Weijiang He and his group[58] synthesized AIE-active molecules **21** for Fe^{3+}**.** AIE-active molecule tetraphenylethylene (TPE)-based chemosensor bearing triazole, pyridine, and thiophene moieties. That molecule **21** exhibited AIE quenching mechanism with highly sensitive and selective sensing toward Fe^{3+} in THF/water solution. And A pyridinyl-functionalized tetraphenylethylene fluorogen **22** was synthesized by Chen et al.[77] for trivalent metal cations sensing (M^{3+}, M = Cr, Fe, Al). Fluorogen **22** was shown highly sensitive toward only these three trivalent metal cation over a other of divalent and monovalent metal cations. Shilang Gui, et al.[62] synthesized a new AIE-active molecule TPE having carboxyl group **23**, the molecule shown "turn-on" fluorescence against Al^{3+} cation in aqueous environment and also in living Hela cells. There are many reports on chemosensor based on TPE as a core molecule, after trivalent metal cation in this section focused on some other divalent metal cations such as follow. Yang et al.[64] synthesized a TPE-based rhodamine hydrazone **24** for colorimetric and reversible detection of Cu^{2+}, A distinct color change from colourless to purple was produced when Cu^{2+} were detected because the metal causes spirolactam to open its ring. The detection limit was reported very low 10^{-6} mol/L in normal water, and it was shown that there was a non-linear connection between the intensity of the absorbance and the concentration of Cu^{2+}. It could operate in a wide pH range (5.0 to 9.0), with pH 6.0 to 8.0 providing the optimum Cu^{2+} detection. The Job's plot demonstrated that the interaction of **24** with Cu^{2+} through the O-N-O binding site was a 1:1 mode. By adding EDTA, the ring-opened **24** may be recovered and used as a reversible "naked eye" indicator for Cu^{2+} ions.

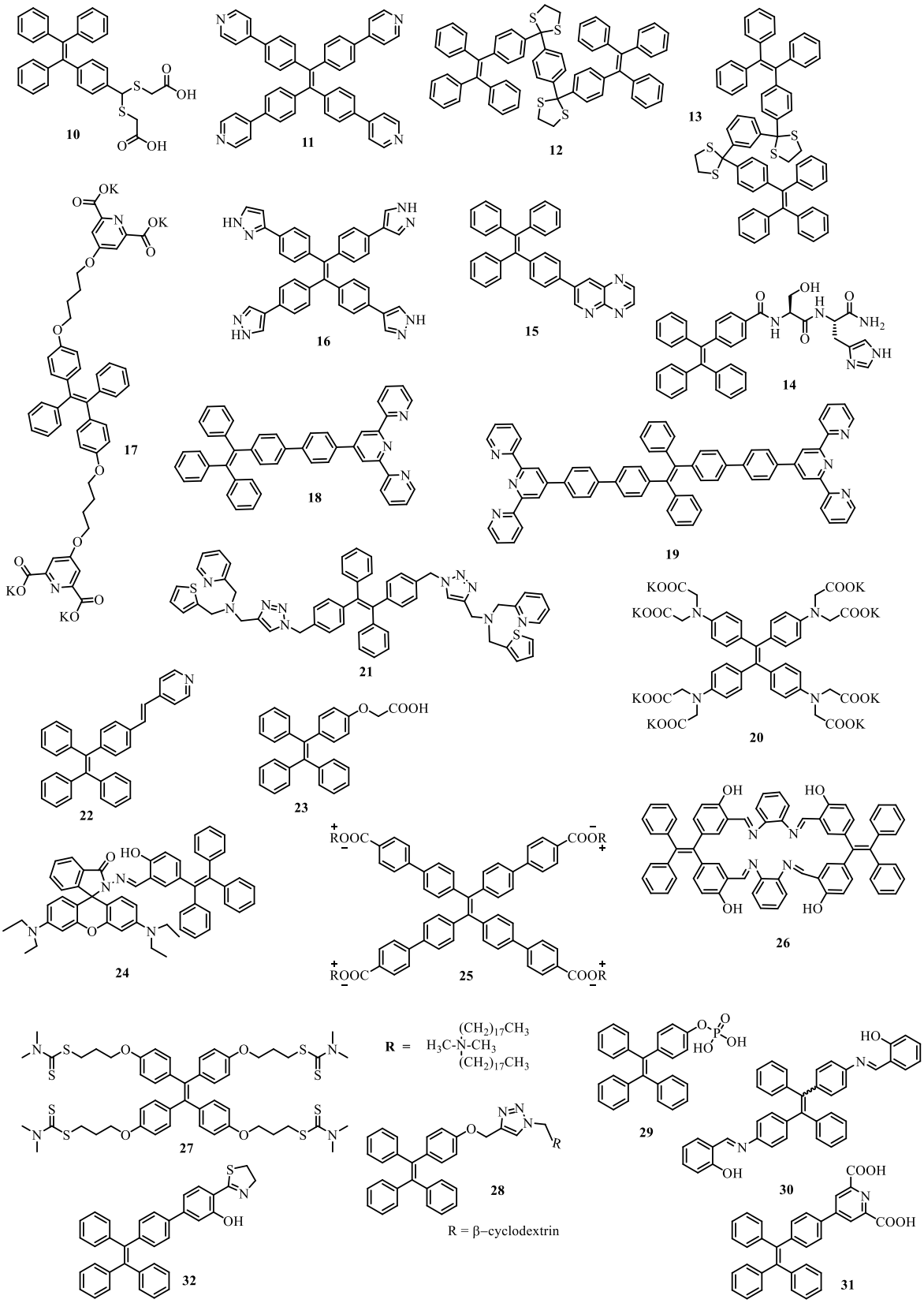

Scheme 4.2: Previously reported TPE-based chemosensor for cations such as Hg^{2+} (**10-16**), Zn^{2+}(**17-20**), Fe^{3+}(**21-22**), Al^{3+}& Cr^{3+}(**23**), Cu^{2+}(**24-26**), Ag^{+}(**27**), Cd^{2+}(**28**), Pb^{2+}(**29**), Sb^{3+}(**30**), Th^{4+}(**31**), and UO_2^{2+}(**32**)

Chen and his group[78] synthesized tetraphenylethylene derivative **25**. Ionic self-assembly of **25** was developed by using quaternary ammonium salt which enhanced fluorescence efficiency. However ionic self-assembly shown highly selective sensing of Cu^{2+} with very low LOD. Feng et al.[79] synthesized TPE Schiff base macrocycle **26**, further it aggregated and formed fluorescent nanofibers and it shown high potential for the selective and sensitive detection of Cu^{2+} in pure and real water. Yong et al.[80] reported a "turn on" fluorescent sensor for the rapid detection of Ag^{+} ions. TPE-based **27** shown large stokes shift while sensing with Ag^{+} cation. Binding aggregation of **27** with Ag^{+} which proven by NMR and DLS spectra. Zhang et al.[81] reported detection of Cd^{2+} by using triazole bridged TPE-cyclodextrin molecule **28**. By utilizing click chemistry **28** was synthesized combining with cyclodextrin with TPE molecule. Further synthesis they have been performed sensing studies, and they found that **28** shown "turn-on" fluorescence response towards Cd^{2+} in neutral condition and 0.01 μM LOD. Khandare et al.[82] designed and synthesized phosphate functionalized TPE molecule **29**, which further used for lead ions detection. In this report the phosphate functionalized tetraphenylethylene derivative and lead forms lead–TPE complex has very low solubility in working solvent and causes aggregation induced emission. It shown highly efficient, cost-effective and 10 ppb a low detection limit. Yuansong et al.[83] **30** in this report designed and synthesized a new fluorescent probe TPE-2IPH **30** for the specific detection of antimony (Sb^{3+}). Sensing mechanism shown fluorescent response of TPE-2IPH to Sb^{3+} was due to coordinate of Sb^{3+} and the IPH functional groups in TPE-2IPH under aggregate state. Wen et al.[40] synthesized 2,6-pyridinedicarboxylic acid-Substituted tetraphenylethene **31** for turn-on fluorescence sensor for the recognition of Th^{4+} in aqueous solution. Due to AIE phenomenon Th^{4+} was detected by the naked eye at ppb levels. And they complex formation of Thorium ion and probe studied by DFT calculations. Same group[84] reported another chemosensor for uranyl ion**,** were they synthesized a 2-(4, 5-dihydrothiazol-2-yl) phenol-containingTPE **32**. The probe shown turn-off fluorescence for uranyl ion (UO_2^{2+}) in aqueous solution. Because its AIE is quenched upon binding, uranyl detected with the naked eye using the designed sensor. And also author described that the sensor demonstrated a broad effective pH range, superior selectivity for uranyl ions as compared to all other tested metals, and no interference from other metals when trying to detect uranyl ions.

Recent year the scientist in the field of sensing are highly interested towards anions sensing because of wide range of applications in biological and environment. A significant class of anions is made up of halides and other anions because of their prevalence in nature,

usefulness in industry, and critical involvement in biological processes. In this section, AIE-based fluorescent sensors for the selective detection of fluoride ion (F^-), cyanide (CN^-), hypocholorous acid (HClO), hypochlorite (ClO^-), Nitrate (NO_3^-) and pyrophosphate are also summarized in this section.

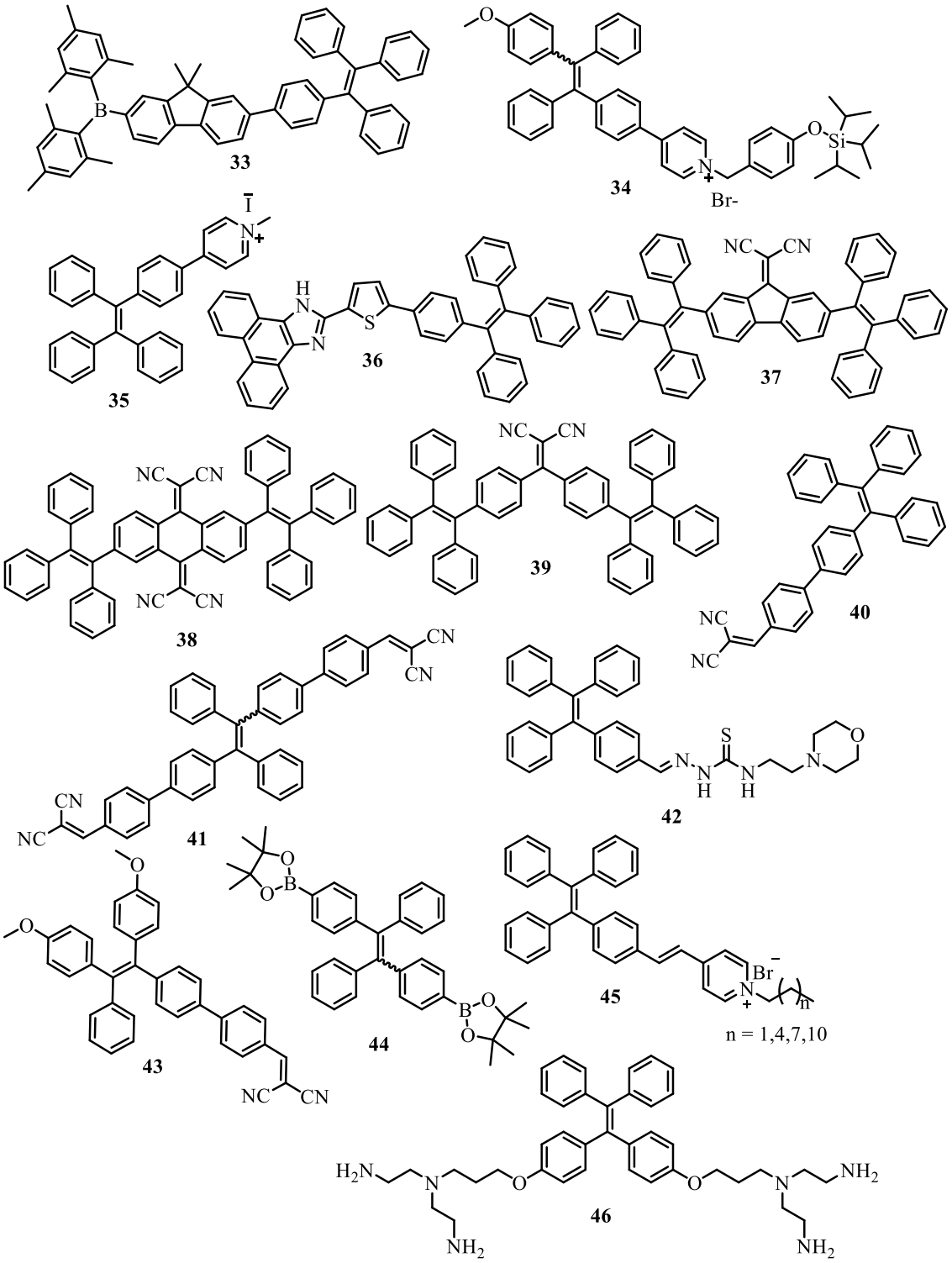

Scheme 4.3: Previously reported TPE-based chemosensor for anions such as F^-, CN^-, $HClO^-$, ClO^-, NO_3^- and $P_2O_7^{4-}$.

Ben Zhong Tang and his group[85] synthesized blue AIEgen basesd on TPE **33**, which is further utilized for fluorine ion sensing and organic light-emitting diode. A blue emissive TPE derivative **33**, which is containing dimesitylboryl and fluorene groups which also posses a good thermal stability with high *T*g and *T*d of 121 and 354 ^{o}C, respectively, and exhibits worthy AIE characteristic, with a high ϕ_F of 64% in solid film. Jiang et al.[86] synthesized TPE derivative **34**, a tetraphenylethylene derivative with a pyridinium pendant and the pyridinium moiety rendered

MOTIPS-TPE. some solubility in water, and as a result, the solution of **34** exhibited weak emission in PBS. The fluoride ion promoted cleavage of the triisopropylsily group in **34** accompanied by the subsequent elimination of *p*-quinone- methide generated deported TPE derivative with poor water solubility. Resulting the turn-on fluorescence toward fluoride ion.

Atılgan and his group[87] reported fluoride ion sensor in aqueous media, based on TPE derivative **35.** Pyridinium group was fused with tetraphenylethene gives **35.** This reported a new methology for sensing of fluoride ion by using TPE-salt **35.**

Wang et al.[66] reported a tetraphenylethylene-based chemosensor phenanthro[9,10-d]imidazole-TPE **36** for Cyanide ion. According to changing fluorescence and visible colour, the probes demonstrated very sensitive real-time naked-eye detection. In the meanwhile, the sensor used to detect CN^- qualitatively and quantitatively on test paper strips.

Chua et al.[88] synthesized the middle acceptor of six new compounds with donor-acceptor-donor (D-A-D) configurations was bordered by two electron-rich triphenylthylenyl moieties. It was discovered that compounds **37, 38 & 39** were sensitive to the cyanide ion's nucleophilic attack, hence their potential as optical cyanide sensors were studied. The primary cyanated byproducts of **37** and **39** were discovered to be aggregation-induced emission (AIE) active and were effectively separated and thoroughly described. Tetraphenylethene (TPE) derivatives **40** and **41** with dicyanovinyl groups were synthesized, according to Zhang et al.[89] and they exhibit exceptional dual characteristics of Solvatochromism and aggregation-induced emission (AIE). Both compounds have a significant Solvatochromism effect due to the interaction between the electron-donating TPE and the electron-accepting dicyanovinyl group. Emissions changed from blue to red by switching the solvent from apolar to polar. Both compounds can function as colorimetric and fluorescence sensors for the very sensitive and selective detection of CN- in aqueous environments with the help of cetyltrimethylammonium bromide because of the AIE

property of TPE and the nucleophilic addition of cyanide (CTAB). Low detection limit of 0.2 μM.

Hypochlorous acid (HClO), a crucial signal molecule in the living organism, takes part in a number of physiological procedures. Too much hypochlorous acid will result in some oxidative harm. Tetraphenylethylene (TPE)-based organic aggregation-induced emission luminogens (AIEgens) **42**, which are fluorescent probe materials, have lately attracted a lot of study attention. Pan et al.[67] reported a water-soluble fluorescent probe **42** for the detection of HClO based on TPE and morpholine-thiourea compounds. The addition of morpholine structures improved the TPE-water solubility. The polarity of the solvent has a significant impact on the fluorescence characteristics of the **42**. The fluorescent probe **42** also showed a single identification characteristic for HClO due to the presence of thiourea structures, according to the cation-anion and reactive oxygen species recognition assays. the limit of detection found for HClO is 0.25 μM. Huang et al.[90] have successfully constructed a highly fluorescent and ratiometric nano-probe **43** for ClO^- detection and imaging by utilizing the AIE technique. This sensor has a quick fluorescence response and detect ClO^- preferentially over other similar species. Importantly, live cell and in vivo imaging investigations demonstrate that this nano-probe successfully detect endogenous ClO^-. Hypochlorite (OCl^-), a reactive oxygen species (ROS), is a critical component of oxidative stress and signal transmission, which regulates a variety of physiological activities. Furthermore, if the residual quantity of OCl^- was too high, it may be dangerous to human health to use it widely in the treatment of food and water. Sensitive technologies used to selectively monitor OCl^- in aqueous samples in situ are still currently rare and desperately required. Because of its consistent reactive activity, boric ester or acid is regarded as a good functional group for the detection of hydrogen peroxide. Wang et al.[91]synthesized **44** a very sensitive and specific OCl^- probe TPE-based on the mechanism of aggregation-induced emission has been created in this study (AIE). Tang and his group[92] synthesized series of pyridinium-functionalized tetraphenylethylene salts **45** with various alkyl chains, and the impact of chain length on their optical properties were examined. Because of their distinctive hydrophobic properties, the fluorogens display opposing emission behavior in aqueous conditions, and their solid-state emission changed from green to red due to their distinctive molecular arrangement. Further the microstructure of the self-assembled fluorogens changes from microplates to microrods with a variety of emission colors when the chain length is increased. Also, **45** (n=1) shows dual-mode fluorescence "turn-on" sensitivities to NO_3^- and ClO_4^- in aqueous

conditions because the anions drive fluorogens to self-assemble. The fluorogens also exhibit cellular uptake selectivity, and the exact alkyl chain drives them to pass through the cell membrane and accumulate with great specificity in the mitochondria. Liu et al.[93] TPE derivative **46** which has been synthesized using diethylenetriamine functionalization, interacts efficiently and specifically with pyrophosphate, leading to an intermolecular self-assembly and FL shown turn-on emission. The cross-linking phenomena were fully resolved, and a direct pyrophosphate analysis LOD of 66.7 nM was observed. The system's rapid reaction to pyrophosphate enabled it to detect ALP with great sensitivity (LOD = 0.09 mU mL^{-1}). Finally, the biosensor system was effectively used in an immunoassay to replace the traditional chromatic substrate with one that was more sensitive and stable. This finding suggests that the novel approach may be more widely used in immunoassays for biomedical diagnostics.

Section I: Study of the azo-tetraphenylethylene molecule for encapsulation and release of C60

4.2 Introduction

In the history of organic nanomaterials, the discovery of fullerene is considered as a turning point.[94–96] C60 is a spherical framework devoid of any functional groups, making it difficult for chemists to build its receptor. Several host molecules for C60 serve as examples of the inventiveness of molecular architecture.[97] By addressing the difficult synthesis of molecular bowls, hoops, peapods, and various other flexible structures that undergo induced-fit around the molecule, complementarity of the buckyball's spherical form has been accomplished. Cycloparaphenylene acetylenes enable supramolecular complexation with fullerene derivatives.[98] It has also been claimed that platinum-based molecular cages can enclose the C60.[99] C60 and other analogues of fullerene are encapsulated by aromatic compounds such as cycloparaphenylene rings.[100,101] It has been shown that an aza-buckybowl-based system works as effective receptors for C60 and C70 with a high association constant.[102] Molecular "peapods" are formed by larger aromatics, such cyclochrysenylenes. Concave bowl-shaped molecules like corannulenes, sumanenes, and even an extended rosarin derivative have proved successful in complementing the convex surface of the buckyball.[103–106] Recently, even a buckybowl with nitrogen and its construction with C60 have been reported.[107] Due to the geometric complementarity of their concave forms to the spherical surface of the C60, non-planar hydrocarbons like triptycene also form complexes with fullerenes.[108] The fullerene guest was more attractive to fusion of several receptor units in a single host molecule. For instance, it has been noted that a receptor with two corannulene units is a "bucky-catcher" with a high binding constant.[109]

The possibility of managing bucky balls and other carbon-based frameworks with greater controls utilizing stimuli like pH, electrical or magnetic fields, electrochemical signals, and photonic signals is made possible by stimulus-responsive supramolecular hosts for fullerenes.[110–114] One of the most often employed stimuli is light because of its non-invasiveness and ease of modulation through careful exposure area of focus, wavelength adjustment, and intensity adjustment.[115,116] Recent reports have described several light- and redox-triggered releases of guest compounds.[117–120] In the presence of an Ag(I) ion, a bispyridine ligand with embedded anthracene panels selectively recognized C60, and its light-mediated release was investigated.[121] By including photochromic units in the

supramolecular systems, it is possible to create reversible host-guest complexation and decomplexation that is activated by light.[122] Azobenzene is a strong photo responsive compound that may undergo considerable chemical and structural changes when exposed to UV and visible light. Numerous biological processes have been rapidly and precisely modulated using these photoswitches.[123–138]

Further experimental synthesis of photo responsive hosts is anticipated as a result of a theoretical investigation into the host-guest interactions between C60 and a photo responsive group host that contains nanorings.[139] Reversible binding and release of C60 are still difficult to achieve. It is known that C60 may create stable supramolecular complexes with a number of substances that have adaptable phenyl rings.[140] Tetraphenylethene (C60-TPE)-containing crystal structures provide evidence of non-covalent van der Waals interactions between the two species.[141] TPE have been quite popular in recent years because of their unusual characteristics, such as being non-luminescent in a solution state and becoming extremely emissive upon solidification (also known as aggregation induced emission, or AIE).[3,47]

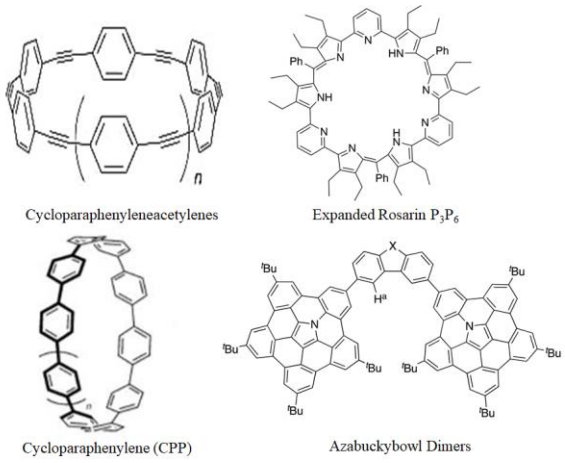

Scheme 4.4: Previously reported some receptors for C60 and C70.

4.3 Experimental

4.3.1 Materials and Methods

All reactants and reagents were commercially available and used without further purification. tetraphenylethelene (TPE), chloroform ($CHCl_3$), chloroform-d ($CDCl_3$), methanol (MeOH), dichloromethane (DCM), tetrahydrofuran (THF), *N,N'*-dimethylformamide (DMF) were purchased from Aldrich and used without purification unless otherwise specified. Solvents used were purified and dried by standard methods. The structures of the compounds were confirmed by nuclear magnetic resonance spectroscopy

and other spectroscopic techniques. ^{1}H-NMR spectra were recorded on 300 and 400 MHz Bruker spectrometer and ^{13}C-NMR using 78 and 100 MHz spectrometer as $CDCl_3$ solutions (trimethylsilane as an internal standard). Chemical shifts were reported in δ values relative to the solvent peak. The solvents used for the spectroscopy experiments were of the spectroscopic grades and free from any fluorescent impurities. Double distilled water was used for the spectroscopy experiments. UV spectra were recorded with a Hitachi U-4100 UV-Vis spectrophotometer. Fluorescence measurements were carried out using a Fluoromax-3 (Horiba Jobin Yvon). Mass data were obtained from an Acquity TM ultra-performance LC. Mass spectra (MS) were obtained by using Bruker AutoFlex Matrix Assisted Laser Desorption Ionization (MALDI) Time of Flight (TOF)-Mass Spectrometer (MALDI-TOF-MS). Mostly, all reactions were carried out under an inert and dry atmosphere of nitrogen or argon.

4.3.2 Synthesis of (2-(4-bromophenyl) ethene-1, 1, 2-triyl) tribenzene 4: This compound was prepared by following a known literature procedure.[57] A solution of n-butyl-lithium in hexane (2.5 M; 9.5 mL, 23.79 mmol) was added drop wise to a solution of **2** (4.0 g, 23.79 mmol) in dry THF (175 mL) at 0 °C under nitrogen atmosphere and stirred at same temp for 2 h. Then to it was added a solution of **3** (4.88 g, 18.79 mmol) in THF (30 mL), and resultant was stirred at RT for 10 h. Reaction completion was checked by TLC analysis. Reaction mixture was quenched with aq. NH_4Cl solution and extracted with DCM (3 × 50 mL). The organic layer was dried over anhydrous $MgSO_4$, evaporated on rotary evaporator to give a crude alcohol intermediate. This crude intermediate was further dissolved in toluene (50 mL), and to it was added pTSA (2 g). Resultant was then further refluxed for 16 h. Reaction mixture was cooled to RT, evaporated on rotavapour and crude residue obtained was purified by silica gel chromatography (40−60 nm) to give compound **4** as white solid in 81.6% yield (7.96 g). IR (cm^{-1}): 3072, 3019, 1605, 1485, 1444, 1391, 1065, 1012, 811, 753, 704. ^{1}H NMR (400 MHz, $CDCl_3$) δ: 7.22-7.20 (d, *J* = 8 Hz, 2H), 7.14-7.09 (m, 9H), 7.02-7.00 (m, 6H), 6.90-6.88 (d, *J* = 8 Hz, 2H); ^{13}C NMR (100 MHz, $CDCl_3$) δ : 143.37, 143.28, 143.18, 142.66, 141.54, 139.59, 132.95, 131.26, 131.21, 131.19, 130.81, 127.84, 127.74, 127.65, 126.66, 126.61, 126.56, 120.40.

4.3.3 Synthesis of (4-(1, 2, 2-triphenylvinyl) phenyl) boronic acid 5:This compound was prepared by following a known literature procedure.[142] To a stirred solution of **4** (4.11 g, 9.997 mmol) in anhydrous THF (80 mL) was added 2.5 M solution of nBuLi in hexane (4.8 mL, 11.99 mmol) at -78 ^{o}C and stirred at same temp for 3 h. Then, trimethyl borate (2.28

mL, 19.99 mmol) was added at -78 ^{o}C and resultant was allowed to warm at room temperature for 16 h. Reaction completion was checked by TLC analysis. After completion, reaction was quenched by adding conc. HCl and water and then extracted with DCM (3 X 30 mL). Organic layer was separated, dried over $MgSO_4$ and evaporated to get crude residue which was then purified by flash column chromatography to afford **5** as white solid in 75.6% yield (2.85 g). IR (cm^{-1}): 3055, 3019, 1600, 1489, 1445, 1244, 1070, 1030, 758, 691, 624. ^{1}H NMR (400 MHz, $CDCl_3$) δ: 7.32-7.30(d, *J*=8 Hz, 2H), 7.10-7.03(m, 17H), 1.25(s, 2H). ^{13}C NMR (100 MHz, $CDCl_3$) 143.74, 142.73, 141.04, 140.53, 138.23, 131.75, 131.40, 131.34, 127.76, 127.66, 127.63, 126.46, 126.41, 125.89.

4.3.4 Synthesis of 1, 2-bis (4-bromophenyl) diazene 7: This compound was prepared by following a known literature procedure.[143] A finely grinded mixture of $KMnO_4$ (2.9 g, 18.38 mmol) and $CuSO_4.5H_2O$ (2.93 g, 18.38 mmol) was added to a stirred solution of **6** (1 g, 13.7 mmol) in degassed DCM (80 mL) and stirred at room temperature for 3-days. After completion, reaction mixture was filtered through celite bed and the residue washed with excess of DCM. Filtrate was evaporated to complete dryness to obtain the crude product. which was further purified by column chromatography to afford **7** as an orange solid in 91.9 % yield (1.81 g). IR (cm^{-1}): 3090, 2920, 1569, 1467, 1396, 1056, 999, 829. ^{1}H NMR (400 MHz, $CDCl_3$) δ: 7.79 (d, *J*= 8Hz, 4H), 7.60(4H), ^{13}C NMR (100 MHz, $CDCl_3$) δ : 151.15, 132.42, 127.25, 125.78, 123.92.

4.3.5 Synthesis of 1, 2-bis (4'-(1, 2, 2-triphenylvinyl)-[1, 1'-biphenyl]-4-yl) diazene 1: To a stirred solution of **7** (0.15 g, 0.441 mmol) in degassed 1,2-dimethoxyethane (10 mL) was added **5** (0.497 g, 1.323 mmol), 2M Na_2CO_3 solution (3 mL) and resultant was degassed for 15 min using nitrogen atmosphere. Then to it was added $Pd(PPh_3)_4$ (0.025 g, 0.022 mmol) and again degassed for 10 min. Resultant suspension was allowed to heat at 100 ^{o}C for 24 h. Reaction completion was confirmed by TLC analysis. After completion, solvent was evaporated to complete dryness and obtained crude product, which was purified by flash column chromatography (40-60 nm) to afford **1** as an orange colour solid in 69.5% yield (0.26 g). ^{1}H NMR (300 MHz, $CDCl_3$) δ (ppm): 7.87 (d, *J* = 8.6 Hz, 4H), 7.58 (d, *J* = 8.6 Hz, 4H), 7.32 (t, *J* = 7.4 Hz, 4H), 7.12 – 6.92 (m, 34H); ^{13}C NMR (78 MHz, $CDCl_3$) δ (ppm): 151.78, 143.60 143.14, 141.41, 140.38, 137.79, 131.93, 131.38, 127.67, 126.58, 126.28, 123.34, 77.68, 76.83, 76.59; MALDI-TOF: for $C_{64}H_{46}N_2$ calculated [M^+]: 842.3661; found: 843.3721 $[M+1]^+$.

4.3.6 Photoisomerization studies

Photoisomerization experiments of azobenzene-TPE **1** were carried out in CS_2. By exposing the sample to 254 nm UV light (8W, sample put 12 cm from the source) under ice-cold conditions, the E to Z photoisomerization of compound **1** was observed (0 ^oC). Exposure to visible light (more than 400 nm, 200W, and 14 cm) caused the reverse isomerization (Z to E). The isomerization of the targeted molecule was examined by UV-Vis. absorption spectroscopy, fluorescence spectroscopy, and ^1H NMR spectroscopy.

4.3.7 Binding studies with C60

For absorption and emission study, stock solutions of compound **1** (1.0 mM) and C60 (1.0 mM) were prepared in $CHCl_3$ and CS_2, respectively, Increasing quantities of C60 in CS_2 were added to 6 μM solutions of **1** in both E and Z forms for all tests. By examining the alteration in the UV-Vis. absorption spectra, fluorescence spectra, and NMR spectra, the binding of C60 with both the E and Z forms was investigated.

4.3.8 Molecular modeling

The Gaussian 09 software package was used to perform density functional theory (DFT) calculations without taking dispersion interactions in the gas phase into account.

4.4 Result and Discussion

4.4.1 Synthesis of azobenzene-TPE 1

Azobenzene-TPE **1** **(Scheme 4.5)** was synthesized by reacting 1,2-bis(4-bromophenyl)diazene with 3 equivalents of (4-(1,2,2-triphenylvinyl)phenyl)boronic acid in degassed mixture of 1,2 dimethoxyethane (DME) and2 M Na_2CO_3 using tetrakis(triphenylphosphine)palladium(0) ($Pd(PPh_3)_4$) as a catalyst. The mixture was refluxed at 100 °C for 24 h to yield **1** in 69.5%.

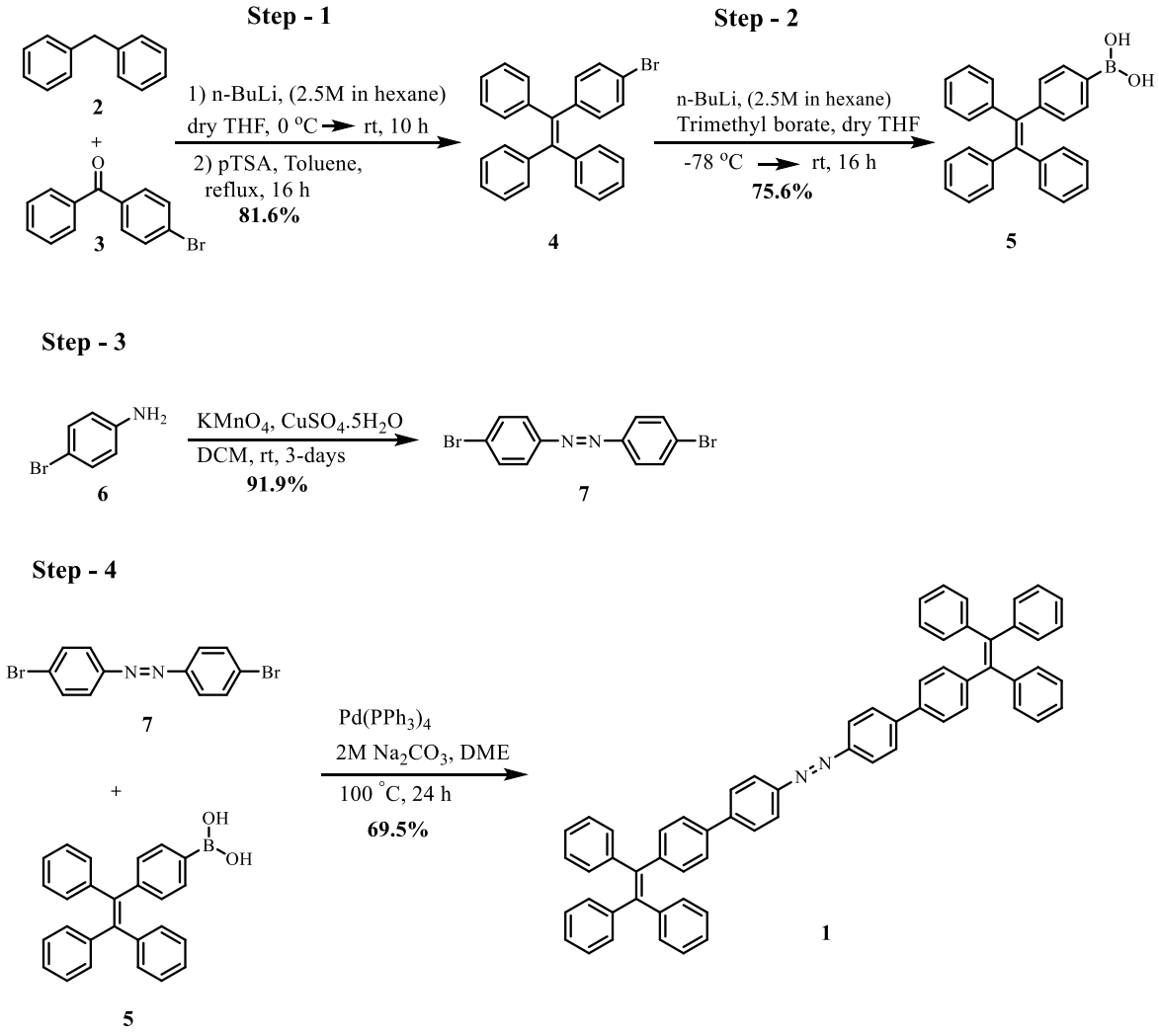

Scheme 4.5: Synthetic route of azobenzene-TPE **1.**

4.4.2 Characterization of compound 1 by IR, NMR and Mass spectroscopy

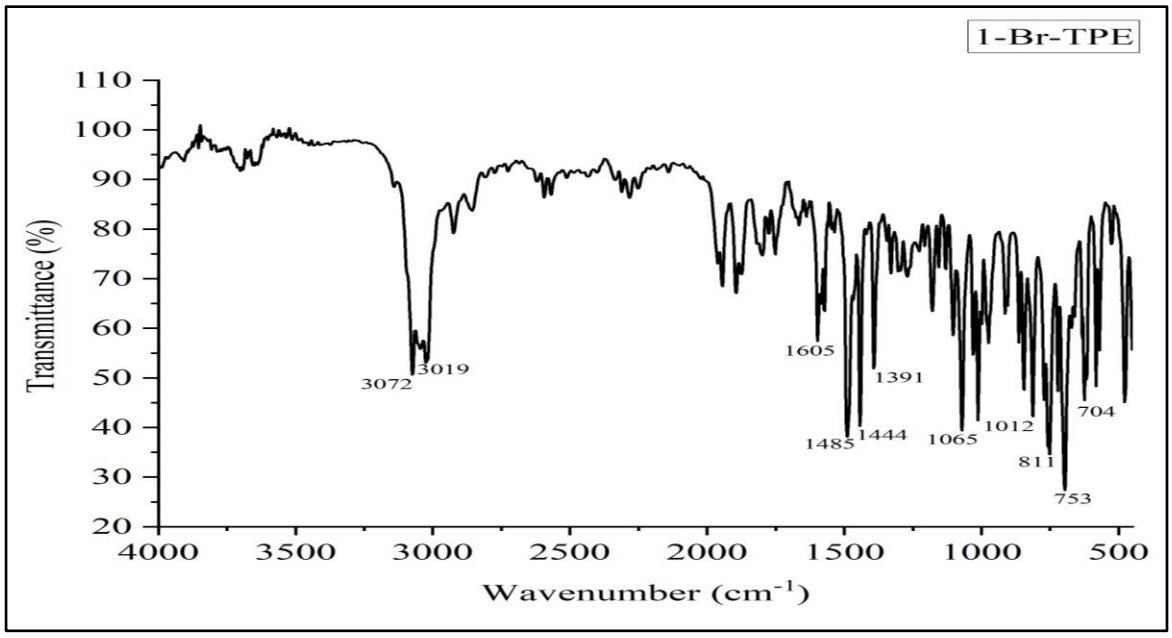

Figure 4.3: FT-IR spectrum of (2-(4-bromophenyl) ethene-1, 1, 2-triyl) tribenzene **4**

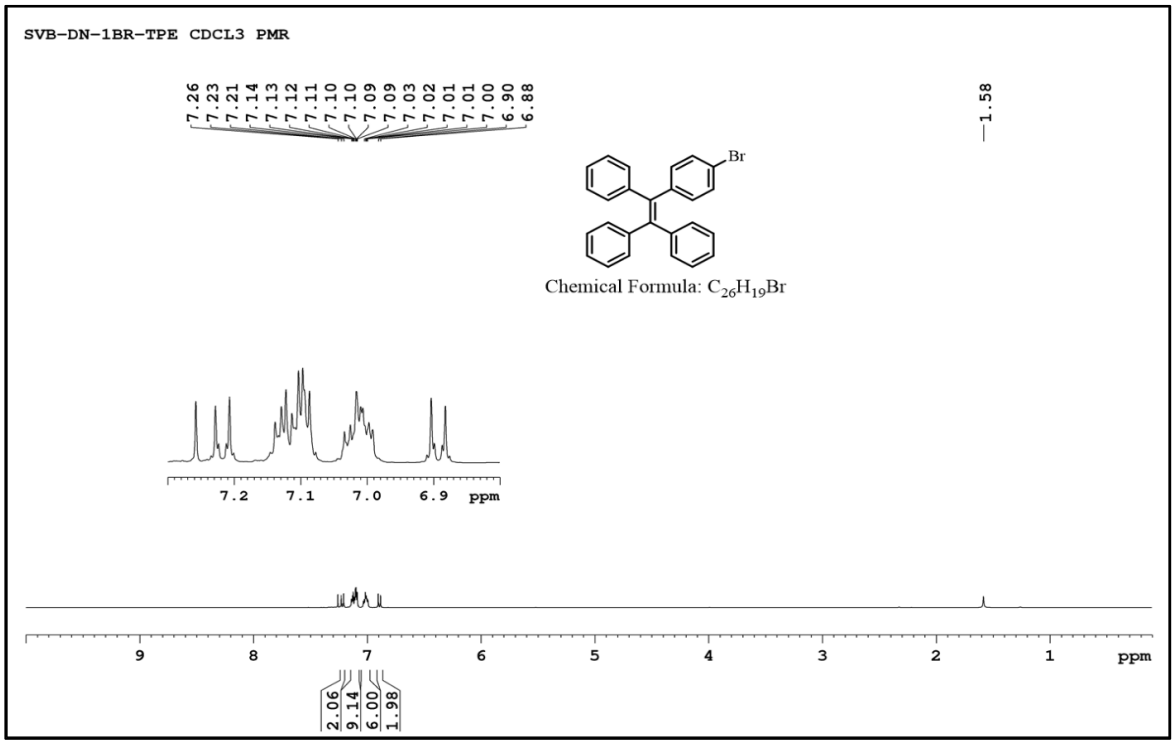

Figure 4.4: ^{1}H NMR spectrum of (2-(4-bromophenyl) ethene-1, 1, 2-triyl) tribenzene **4**

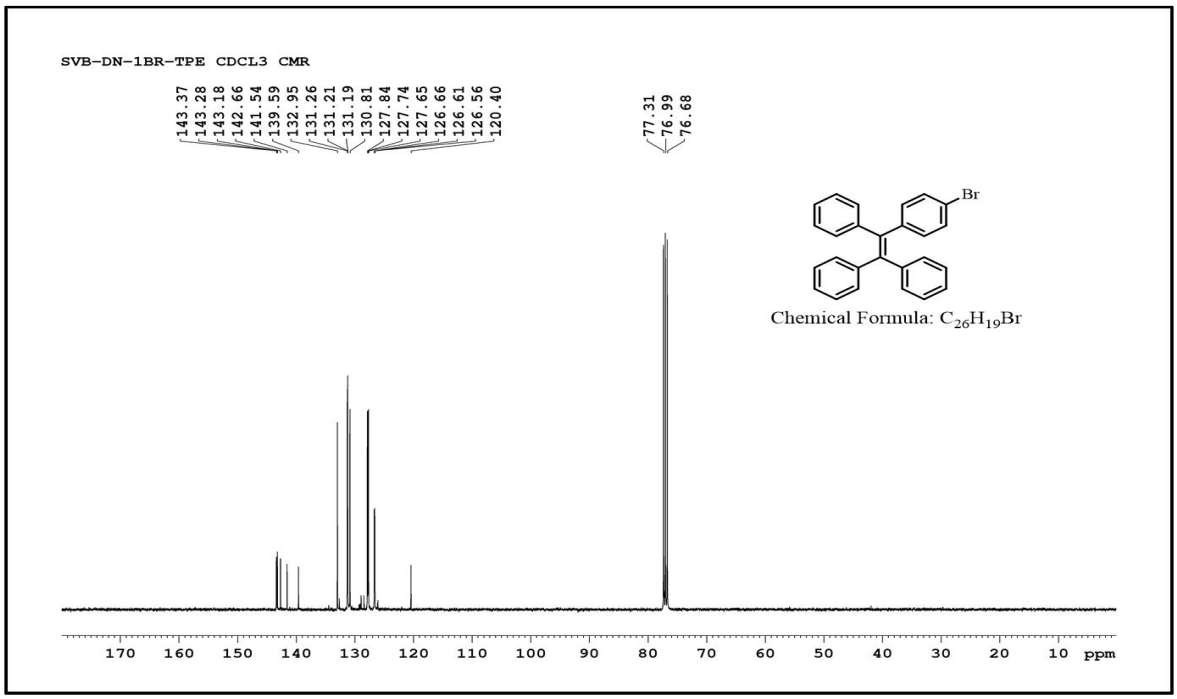

Figure 4.5: ^{13}C NMR spectrum of (2-(4-bromophenyl) ethene-1, 1, 2-triyl) tribenzene **4**

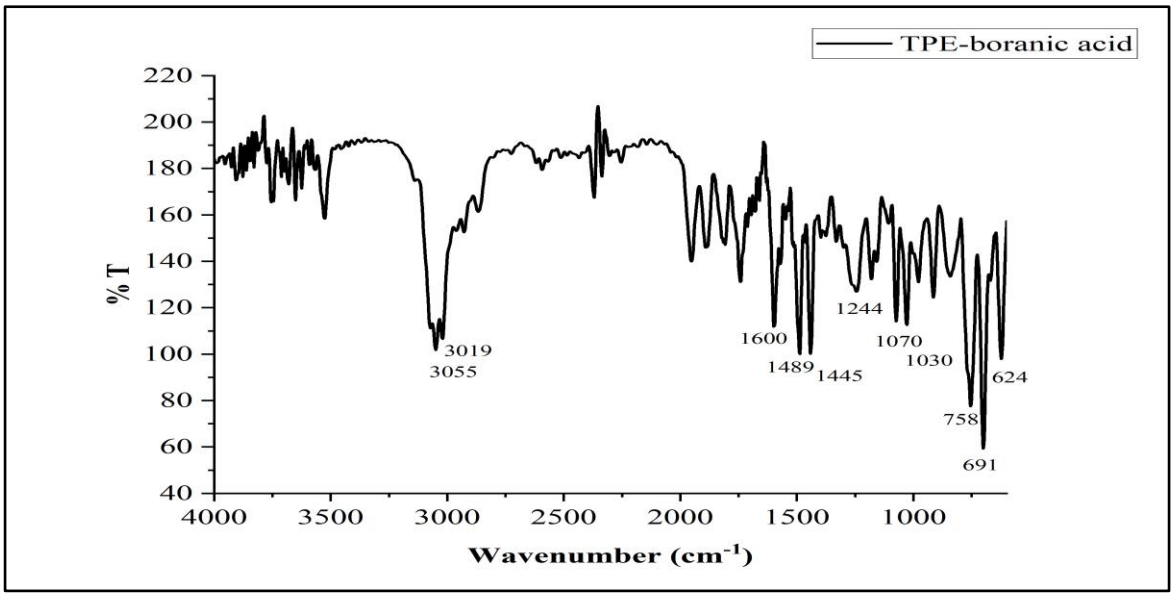

Figure 4.6: FT-IR spectrum of (4-(1, 2, 2-triphenylvinyl) phenyl) boronic acid **5**

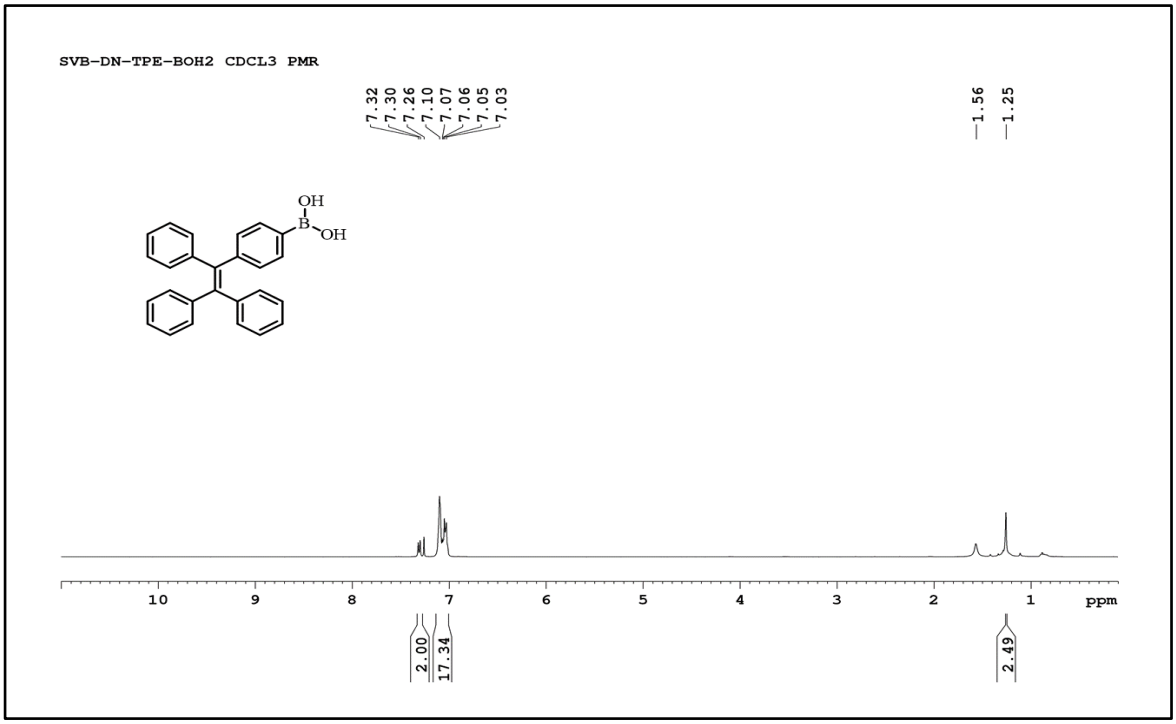

Figure 4.7: ^{1}H NMR spectrum of (4-(1, 2, 2-triphenylvinyl) phenyl) boronic acid **5**

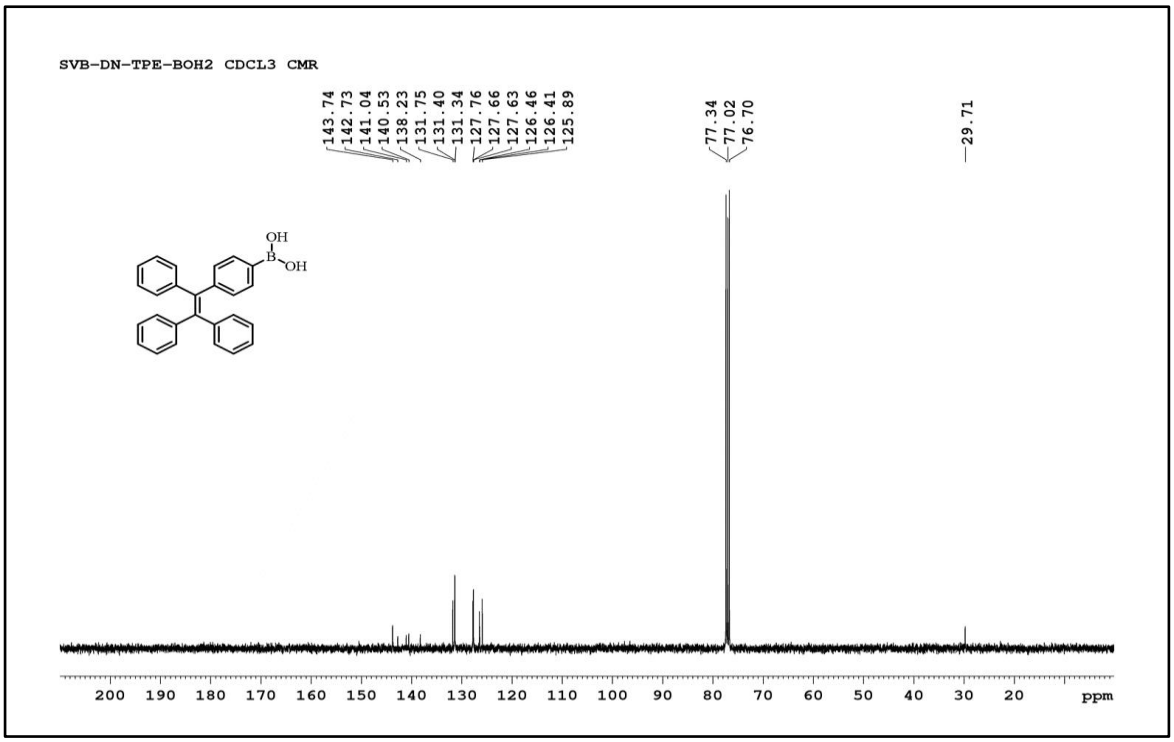

Figure 4.8: ^{13}C NMR spectrum of (4-(1, 2, 2-triphenylvinyl) phenyl) boronic acid **5**

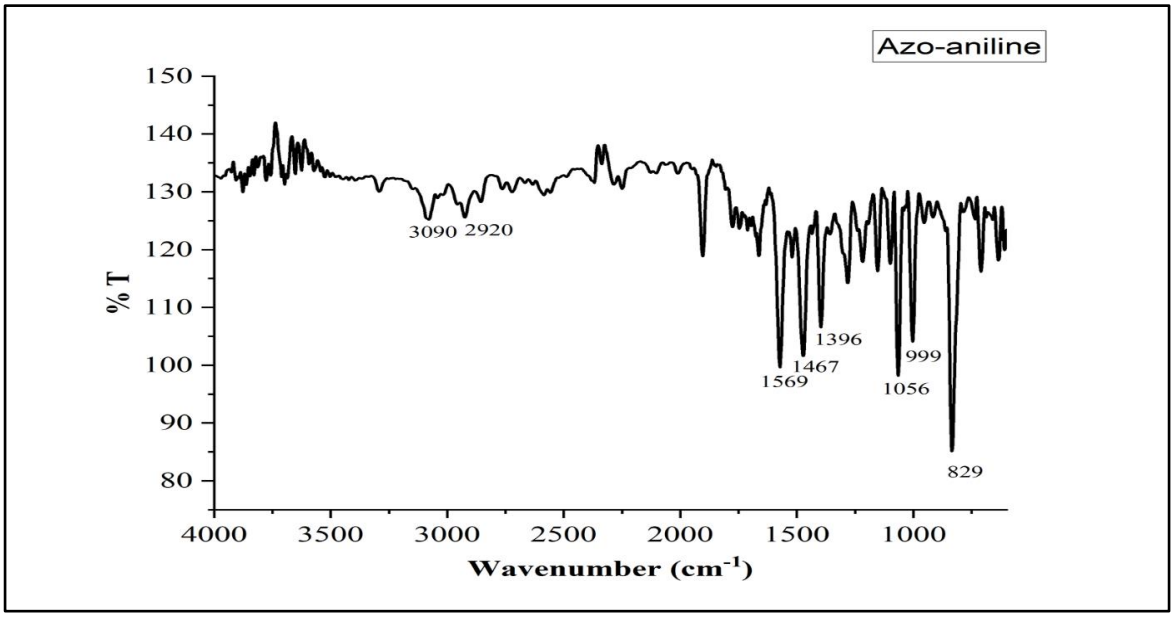

Figure 4.9: FT-IR spectrum of 1, 2-bis (4-bromophenyl) diazene **7**

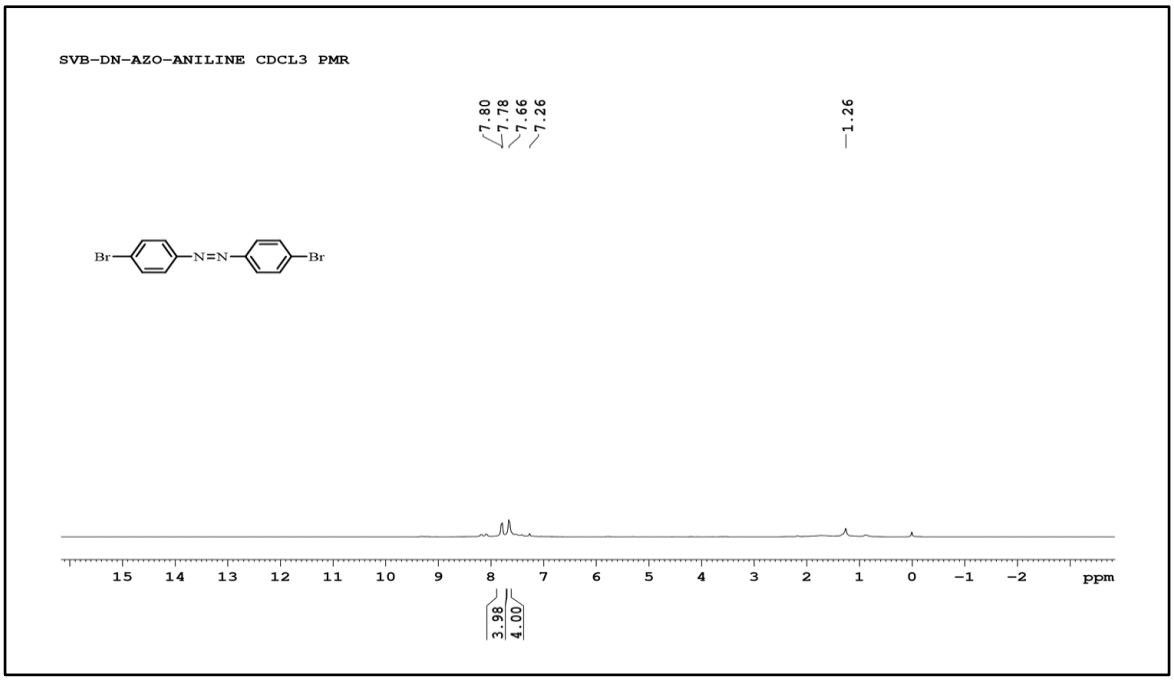

Figure 4.10: ^{1}H NMR spectrum of 1, 2-bis (4-bromophenyl) diazene **7**

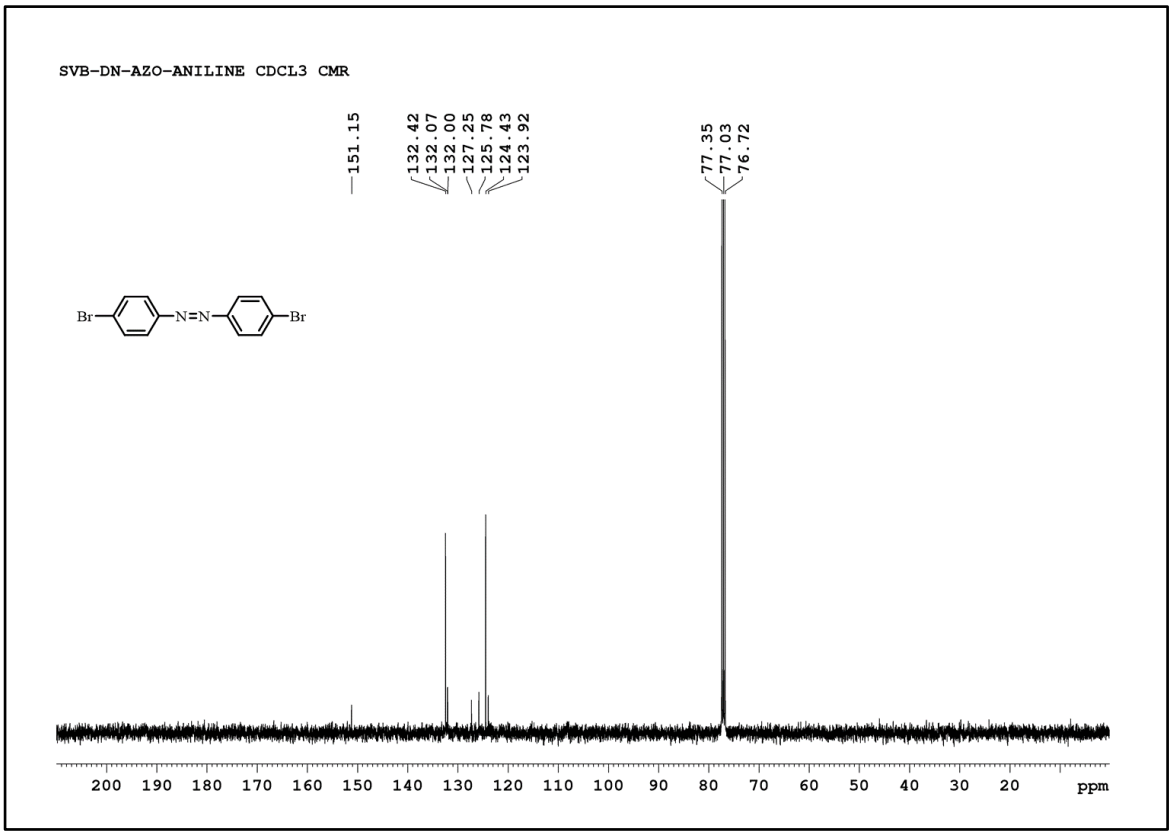

Figure 4.11: ^{13}C NMR spectrum of 1, 2-bis (4-bromophenyl) diazene **7**

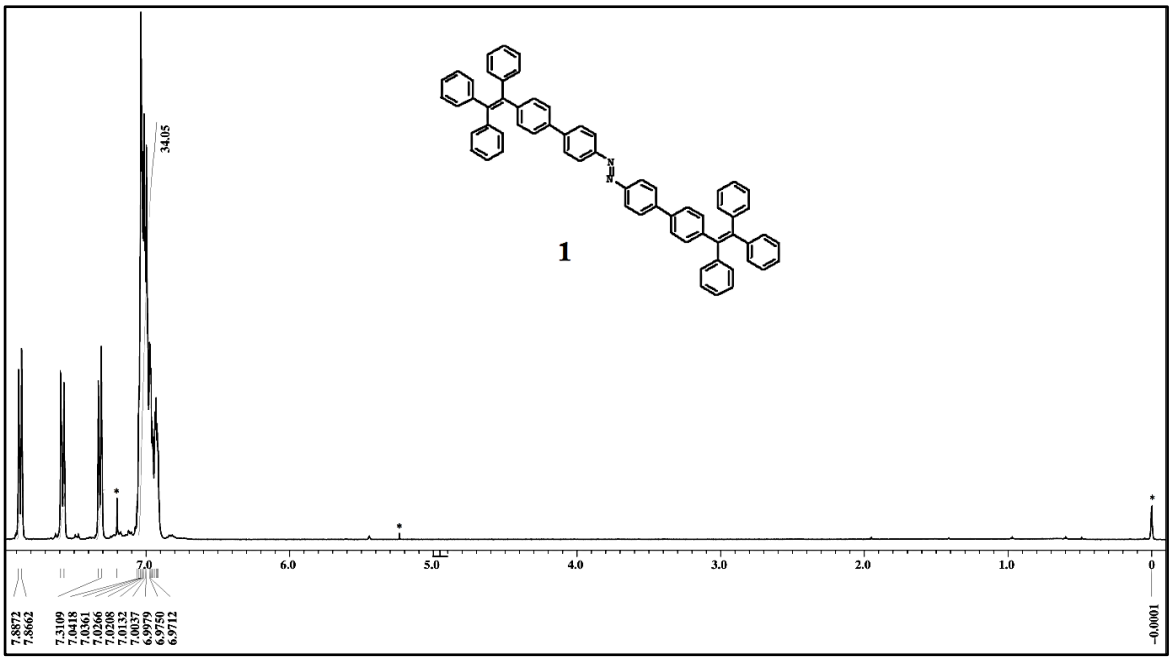

Figure 4.12: ^{1}H NMR spectrum of azobenzene-TPE **1**

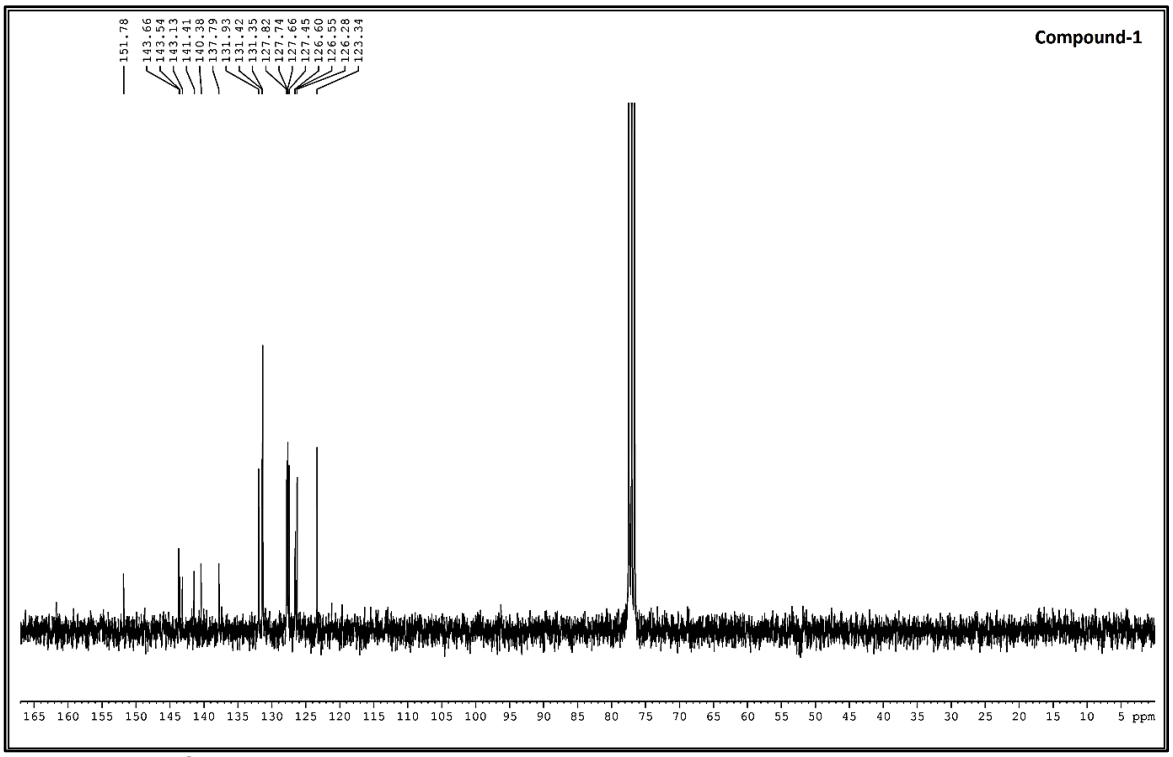

Figure 4.13: ^{13}C NMR spectrum of azobenzene-TPE **1**

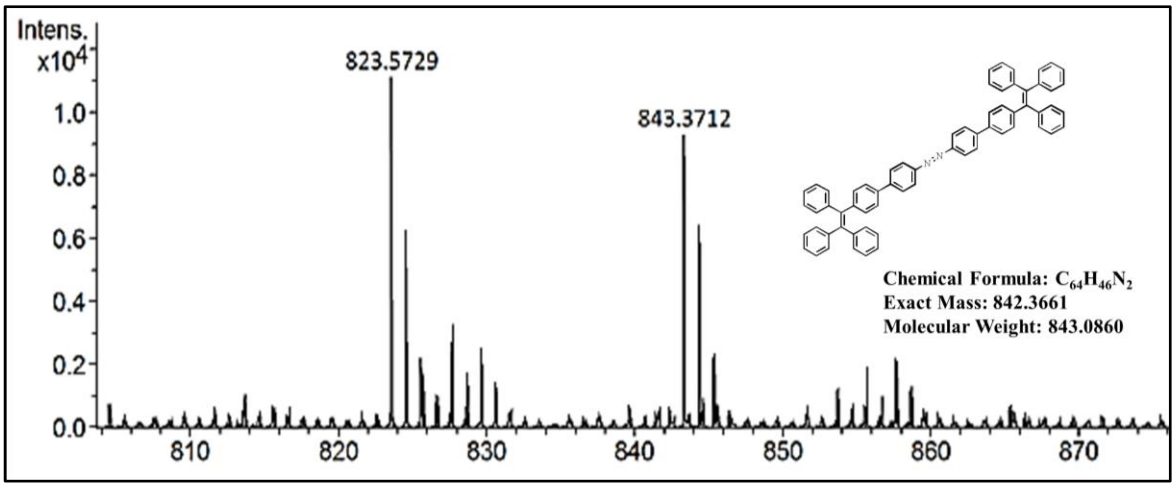

Figure 4.14: MALDI-TOF HRMS spectrum of azobenzene-TPE **1**

4.4.3 Crystal structure of azobenzene-TPE 1

A gradual diffusion of CH_2Cl_2 solution was used to produce single crystals of azobenzene-TPE **1**. A SuperNova, Dual, Cu at zero, Eos diffractometer was used to obtain crystal data using graphite monochromated Mo K_α radiation (λ= 0.71073 Å). The crystal was kept at 100.00 K during data collection. Using Olex2,[144]the structure was solved with the ShelXs[145] structure solution program using direct methods and refined with the ShelXL[146] refinement package using the least square minimization. All hydrogen atoms were added according to the riding model. Crystallographic parameters for azobenzene-TPE **1** were included in **Table 4.1** The selected bond lengths and bond angles of azobenzene-TPE **1** comprised in **Table 4.2** and **Table 4.3** respectively.

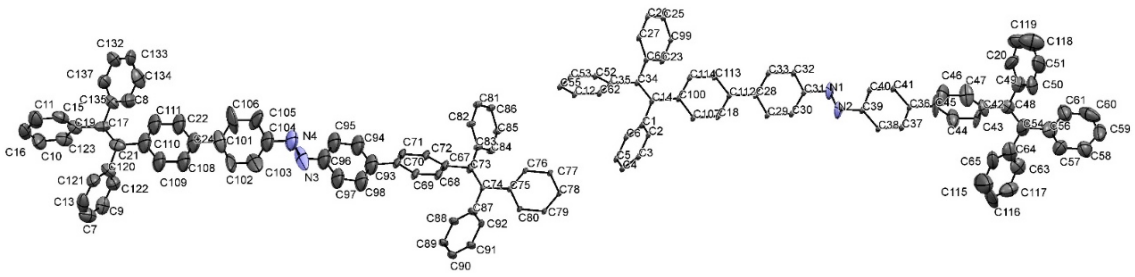

Figure 4.15: ORTEP diagram of **1** (thermal ellipsoid plot with 50% probability).

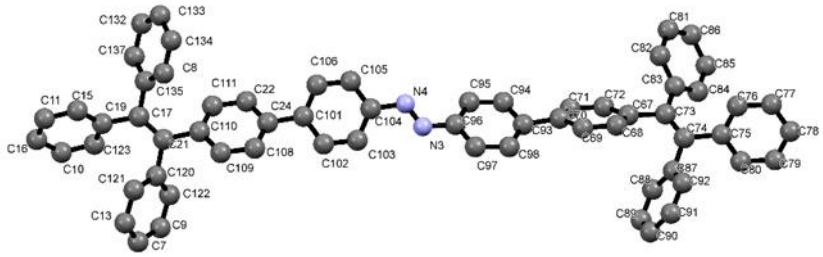

Figure 4.16: Crystal structure of **1**.

Table 4.1: Crystallographic parameters for **1.**

Empirical formula	$C_{128}\ H_{96}\ N_4$
F.W.	1690.09
Crystal system	Monoclinic
Space group	$P2_1$
a(Å)	9.7559(7)
b(Å)	9.2557(3)
c(Å)	59.868(2)
α(°)	90
β(°)	93.802(5)
γ(°)	90
V, Å^3	5394.1(5)
Z	2
λ, Å	0.71073
$\rho_{calc,}$ mg/mm^3	1.040
Crystal size, mm^3	0.39 × 0.26 × 0.13
T, K	100
μ, mm^{-1}	0.06
F(000)	2006
2Θ range for data collection	4.0–54.4°
Index ranges	$-12 \le h \le 12, -12 \le k \le 5, -28 \le l \le 79$
Reflections collected	15644
Independent reflections	15644[R(int) = 0.047]
Data/restraints/parameters	15644/5/566
Final R indexes [I>=2σ (I)]	$R_1 = 0.091$, $wR_2 = 0.212$
GOF	1.355
Largest diff. peak/hole / e Å^{-3}	0.70, −0.70
w	$1/[\sigma^2(F_o^2) + (0.2P)^2]$ where $P = (F_o^2 + 2F_c^2)/3$

Table 4.2: Selected bond lengths (Å) of **1**

C14	C34	1.366 (7)	C31	N1	1.478 (8)
C28	C112	1.496 (7)	N1	N2	1.187 (11)

Table 4.3: Selected bond angles (deg) of **1**

C3	C2	C1	120.0	C30	C31	N1	119.9 (6)
C2	C1	C14	119.5 (3)	N1	N2	C39	115.8 (7)
C100	C14	C1	115.6 (4)	C34	C14	C1	121.8 (5)

4.4.4 Photoisomerization study of 1 by UV-Vis. and PL spectroscopy

The forward and backward reactions of the molecule **1** display *E*-*Z* photochromism, which is entirely reversible upon exposure to UV and visible light, respectively. The *E* isomer can be converted to the *Z* isomer as demonstrated in **Figure 4.17a** by selectively excitation of the n-π* band under 254 nm light. This phenomenon may be seen with the naked eye when exposed to 254 nm light (**Fig. 4.17b**). The band at 400 nm, which has a molar extinction (ε) of ~1.04×10^5 $M^{-1}cm^{-1}$) grows wide by the exposure of 254 nm UV radiation, and its intensity increases with exposure timeframe. The n-π* transition of the *Z* isomer, which intensifies with the 254 nm radiation, results in a new broad peak at 550 nm (ε = ~9.8×10^3 M^{-1} cm^{-1}). During the Photoisomerization reaction, a visible change in color was observed where, the yellow color of E isomer has changed to intense orange color of Z isomer.(**Fig. 4.17c**). A first order kinetics with a rate constant of 6.6×10^{-2} m^{-1} was used to analyse the *E* to *Z* conversion using ^{1}H NMR spectroscopy. Using visible light and a 400 nm cutoff filter, the reverse *Z*-*E* conversion process was accomplished. The conversion obtained using the NMR techniques has a rate constant of 8.3×10^{-4} m^{-1}. In addition, the *E*-1 fluorescence spectra at λ_{ex} = 405 nm showed a wide band with two peaks at 440 and 470 nm (Φ_F = 0.01) and a shoulder at ~550 nm. However, the fluorescence intensity of the Z isomer was less intense (Φ_F = 0.004) with a single band at 480 nm **(Figure 4.17d)**.

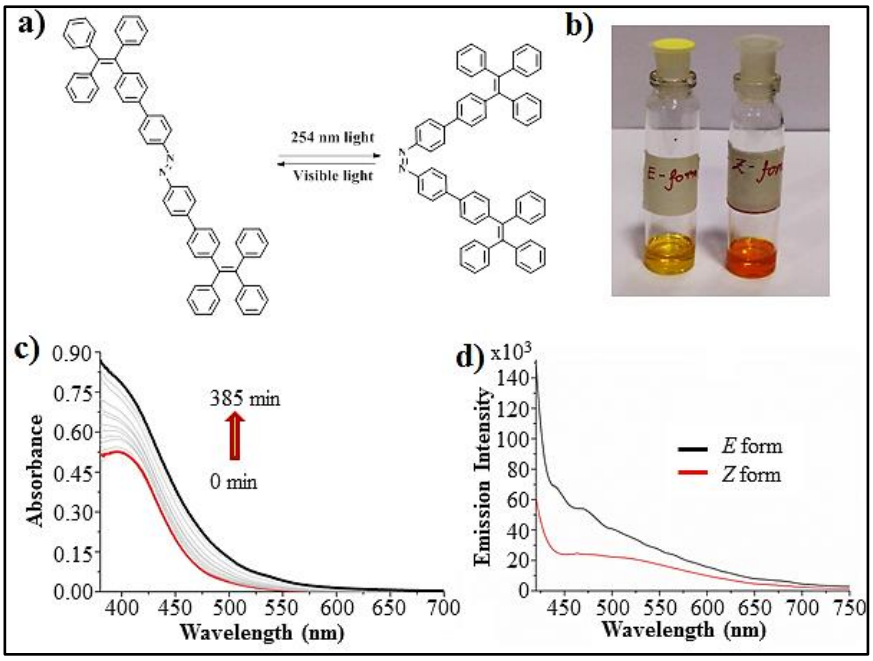

Figure 4.17: Photoisomerization studies of **1**, **a)** chemical illustration of *E*-*Z* isomerization of the molecule **1**. **b)** Naked eye visualisation of *E*-*Z* isomers. **c)** The changes in absorption spectra of the *E* to *Z* isomerization of the molecule **1** (6 µM) in CS_2. **d)** Fluorescence spectra of the azobenzene-TPE **1** in both *E* and *Z* forms.

4.4.5 Photoisomerization study of 1 by ^{1}H NMR

^{1}H spectroscopy was used to monitor the *E*-*Z* isomerization of **1** when it was exposed to 254 nm light using CS_2 as the solvent and a little quantity of $CDCl_3$ to lock the instrument. The azobenzene moiety of the *E*-isomer of molecule **1** has shown the characteristic signals at 7.87 (H_a), 7.58 (H_b), and 7.32. (H_c). When exposed to 254 nm UV radiation, the ^{1}H resonances underwent conversion to the *Z*-isomer, which resulted in protons appearing at 7.34 (H_c'), 7.19 (H_b'), and 6.83 (H_a') Hz, respectively (**Fig. 4.18**). Due to the existence of overlapping multiplets, the TPE protons appeared as multiplets and the change in the ^{1}H NMR spectra could not be used to identify them. The composition exposed to radiation in the NMR tube equaled the ratio of the *Z* to *E* isomer by around 3:1.

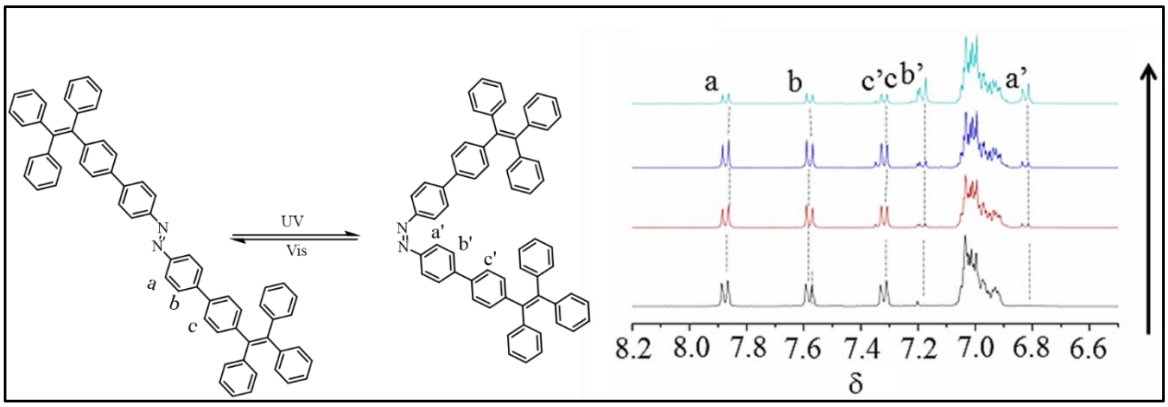

Figure 4.18: ^{1}H NMR spectra of *E* to *Z* isomerization of the molecule **1**.

4.4.6 Light triggered encapsulation of C60

The immediate shift in the absorption spectra upon the addition of C60 to *Z*-1 revealed the formation of *Z*-1.C60. The spectra reveal an increase in the peak at 540 nm in the presence of C60, in addition to the clear visual change in the solution *Z*-1 with C60 following mixing (**Figure. 4.19b**). The interaction between the molecule **1** Z form and C60 is shown by an increase in the absorbance band in the range >470 nm. The chemical representation shown in **Figure 4.19a.** However, with *E*-1, similar alterations were not noticed (**Fig. 4.19c**). In the presence of C60, a new band at 725 nm was seen in fluorescence spectra (**Fig. 4.19d & e**). In addition, it was discovered that the intensity of *Z*-1 initial fluorescence band and its shoulder at 520 nm had decreased. An association with 1:1 stoichiometry of the host **1** and guest C60 was clearly shown in a plot of continuous variation (Job's plot, **Figure. 4.20**) measured at 460 nm. From the emission data, the binding constant of C60 with *Z*-1 and *E*-1 have both been calculated. As expected, 4.02×10^{4} M^{-1} was determined to be the association constant(**Figure. 4.21**) between C60 and *Z*-1, whereas 1.76×10^{3} M^{-1} was found to be the binding constant between *E*-1 and C60. Employing ^{13}C NMR spectroscopy, the interaction between *Z*-1 and C60 was also clearly visible (**Figure. 4.19g**). The peak of the C60 at 143.0 ppm underwent an upfield shift to 142.9 ppm upon addition of C60 to *Z*-1 in $CDCl_3$ and CS_2 (1:10, *v/v*) due to the encapsulation inside the aromatic rings of *Z*-1. The shift of the host's ^{13}C resonance also revealed the binding site associated with the formation of the Z-1 and C60 host-guest complexes, respectively. Importantly, a sample containing *Z*-1.C60 shown by MALDI-TOF MS revealed the existence of a species that closely fits the predicted isotopic pattern (**Figure. 4.19h**).

The interactions between the receptor and fullerene were clearly visible in a three-dimensional model of the system created by computer modelling utilising DFT calculations

at the B3LYP level. In the aromatic cavity of the *Z*-1 form, the C60 molecule fits exactly. The supramolecular structure was formed in such a way that phenyl rings few of the molecule's puckered around to perfectly compliment the C60's shape (**Fig. 4.22**).

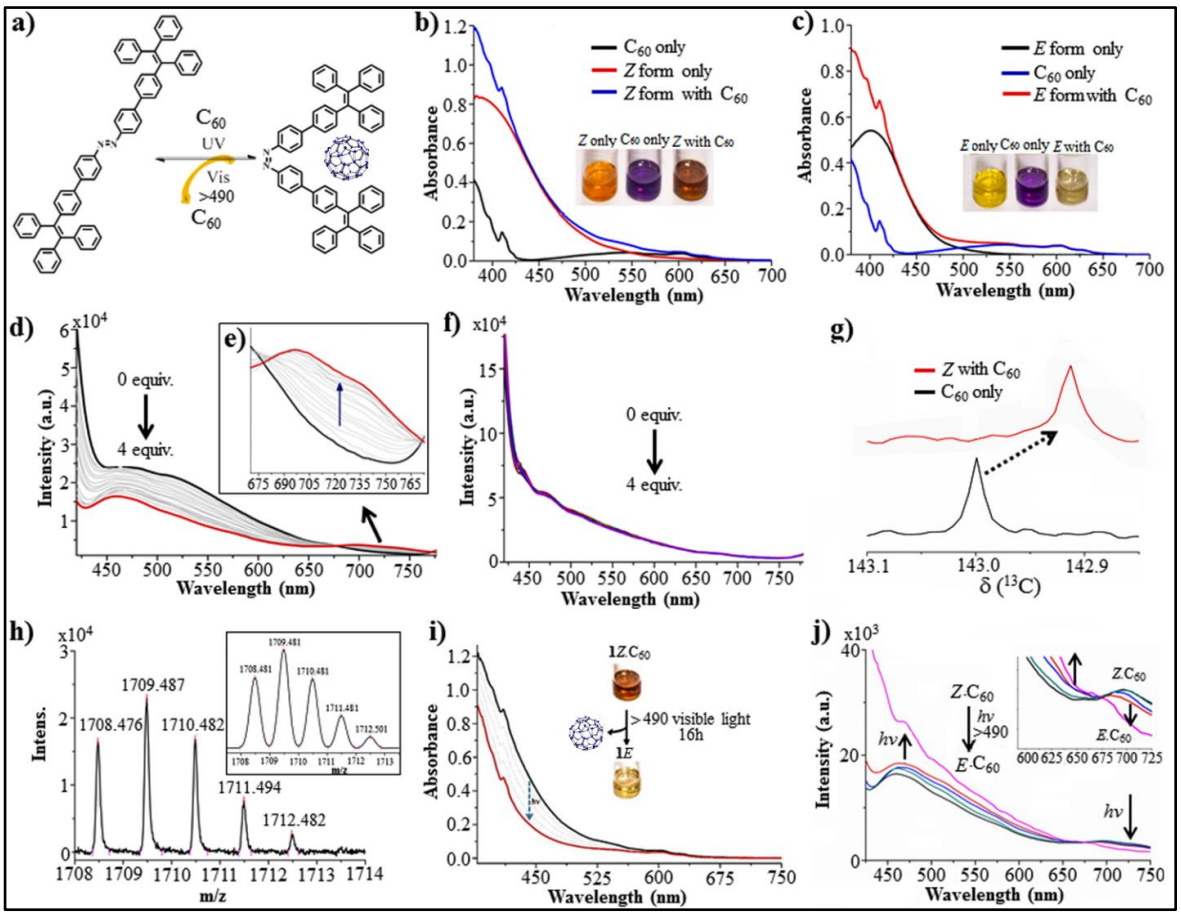

Figure 4.19: Encapsulation and release of C60 by the *Z* form of the molecule**. a** structural illustration of host-guest complex and release of guest. **b, c** Absorbance spectra of the molecule **1** (6 µM) in *Z* forms with C_{60} and *E* form with C60 (6 µM) in CS_2, respectively. **d**, **e** Fluorescence spectra of the molecule **1** (6 µM) in *Z* forms with C60. **f** *E* form with C60 (0 to 24 µM) in CS_2, respectively. **g** Changes in ^{13}C NMR spectra of C_{60} in presence and in absence of *Z*-isomer of the molecule **1**. **h** The MALDI-TOF MS of a sample containing ***Z*-1.C**$_{60}$ indicated the presence of the species perfecly matches well with the calculated isotopic pattern. Changes in (i) UV-Vis spectra and (j) fluorescence spectra of *Z* form of the molecule **1** with C_{60} under the exposure of visible light in CS_2, which clearly shows release of C_{60} from *Z* form i.e. converting *Z* to *E* isomer with excitation at λ_{max} >490 nm.

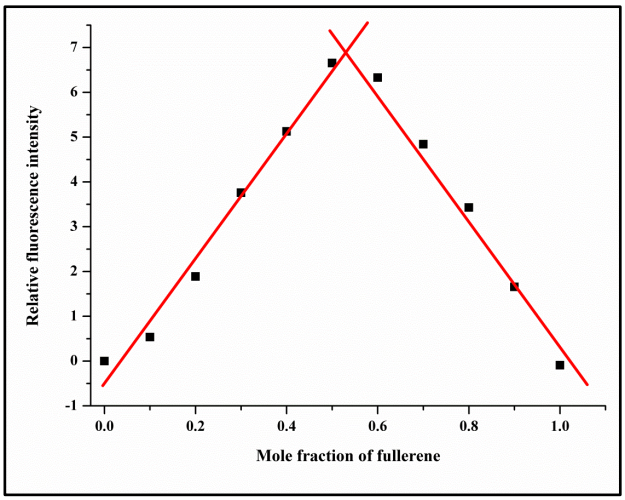

Figure 4.20: The Job's plot of the molecule **1** in *Z* form in CS_2.

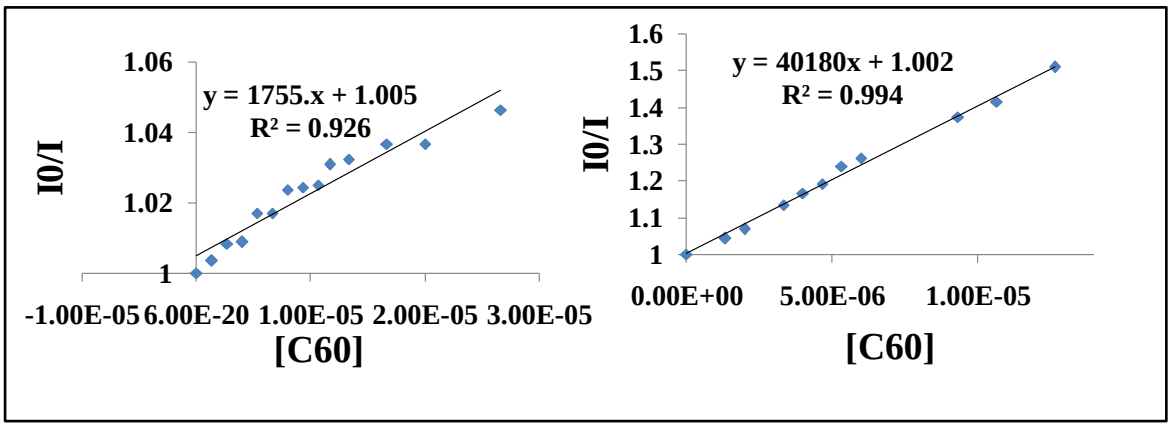

Figure 4.21: Stern-Volmer plots of the compound in ***E*-1** and **Z-1** form and C60 association.

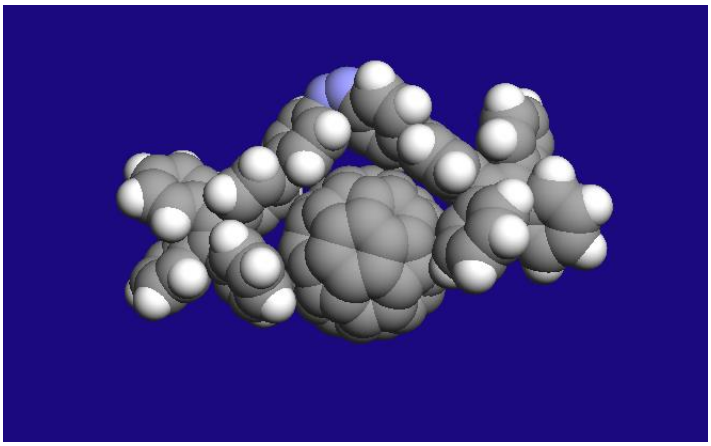

Figure 4.22: Molecular modeling studies of the encapsulation of C60 with the *Z* form of the molecule **1**.

4.4.7 Light-triggered release of C60 from the Z form of the molecule 1

Once the *Z* form of molecule **1** was exposed to visible light at a wavelength more than 490 nm while being in the presence of C60, the broad characteristic charge transfer band in the area above 470 nm gradually decreased (**Fig. 4.19i**). The band at >700 nm also eventually disappeared in fluorescence spectra (**Fig. 4.19j**). The UV-Vis spectra showed that the azobenzene unit was nearly quantitatively converted to the *E* form. This was verified by comparing the spectra (**Fig. 4.19c**) to the one produced by adding C60 to the pure E form of **1**, and by *Z*-**1** and C60 spectroscopic investigations, which also suggested the formation of a host-guest complex between the two. In the presence of visible light, the encapsulated guest molecule (C60) is released. The encapsulation and release of C60 by the *Z* form of the molecule is further demonstrated by the sharp changes in the NMR spectra. The *Z* form of molecule **1** was used in the ^{1}H NMR investigation along with one equivalent of C60 in CS_2. The modifications in the ^{13}C NMR were obvious, even though they were less pronounced in the ^{1}H NMR (**Fig. 4.23**) except from the somewhat lessened peaks at 7.34, 7.19, and 6.83. There, the C60 peak at 143.0 ppm moved upfield to 142.9 ppm (**Fig. 4.19g**). Under the impact of visible light, this transformation was reversible. This is expected because the C60 undergoes a shielding effect after being encapsulated by the host TPE groups in **Z** form, which causes an upfield shift to the C60 nuclei. The earlier absorption spectroscopy observation of this shift was reversible under the influence of visible light.

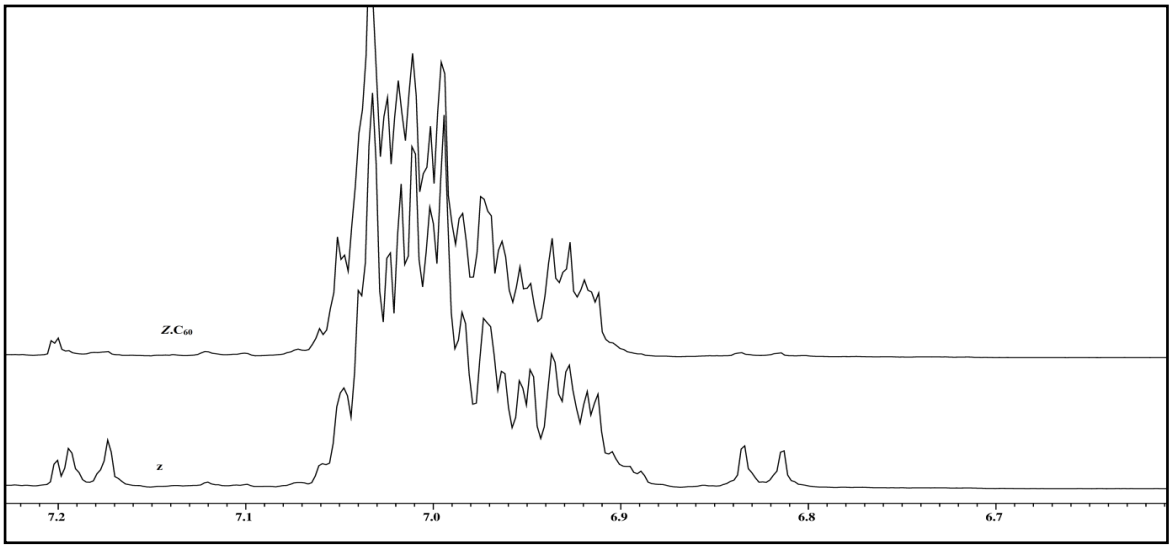

Figure 4.23: ^{1}H NMR spectra of **Z** form of the molecule **1** with C60 in $CDCl_3/CS_2$ (1: 10).

4.5 Conclusion

A TPE-based azobenzene-TPE **1** is photoswitchable molecule has been synthesized and characterized with the help of different spectroscopic methods. The E-Z isomerization of compound **1** results in a structural alteration that may allow a complementary pocket to develop, which might house a C60 visitor molecule. With both the *E* and *Z* isomers of **1** and the C60 molecule, host-guest interactions have been studied using various spectroscopic techniques. It was found that the *Z*-1.C60 association was stronger than the interaction between the E-1.C60 isomer. When the system is exposed to light of higher wavelength (more than 490 nm), the Z-1 form converted into the E-1 form and weakened the host-guest binding. As a result, the Z-1.C60 association can be destroyed. The construction of the host system is highly stimuli responsive and can be exploited for light-induced association and dissociation of a C60 molecule and can be demonstrated by this study.[147]

References

(1) Bhosale, R. S.; Aljabri, M.; La, D. D.; Bhosale, S. V.; Jones, L. A.; Bhosale, S. V. *Tetraphenylethene Derivatives: A Promising Class of Aie Luminogens-Synthesis, Properties, and Applications*; 2018. https://doi.org/10.1007/978-3-319-99037-8_9.

(2) Luo, J.; Xie, Z.; Xie, Z.; Lam, J. W. Y.; Cheng, L.; Chen, H.; Qiu, C.; Kwok, H. S.; Zhan, X.; Liu, Y.; Zhu, D.; Tang, B. Z. Aggregation-Induced Emission of 1-Methyl-1,2,3,4,5-Pentaphenylsilole. *Chem. Commun.* **2001**, *18*, 1740–1741. https://doi.org/10.1039/b105159h.

(3) Mei, J.; Leung, N. L. C.; Kwok, R. T. K.; Lam, J. W. Y.; Tang, B. Z. Aggregation-Induced Emission: Together We Shine, United We Soar! *Chem. Rev.* **2015**, *115* (21), 11718–11940. https://doi.org/10.1021/acs.chemrev.5b00263.

(4) Han, T.; Yan, D.; Wu, Q.; Song, N.; Zhang, H.; Wang, D. Aggregation-Induced Emission: A Rising Star in Chemistry and Materials Science. *Chinese J. Chem.* **2021**, *39* (3), 677–689. https://doi.org/10.1002/cjoc.202000520.

(5) La, D. D.; Bhosale, S. V.; Jones, L. A.; Bhosale, S. V. Tetraphenylethylene-Based AIE-Active Probes for Sensing Applications. *ACS Appl. Mater. Interfaces* **2018**, *10*

(15), 12189–12216. https://doi.org/10.1021/acsami.7b12320.

(6) Tezuka, Y.; Hashimoto, A.; Ushizaka, K.; Imai, K. Generation and Reactions of Novel Copper Carbenoids through a Stoichiometric Reaction of Copper Metal with Gem-Dichlorides in Dimethyl Sulfoxide. *J. Org. Chem.* **1990**, *55* (1), 329–333. https://doi.org/10.1021/jo00288a056.

(7) Okuma, K.; Kojima, K.; Oyama, K.; Kubo, K.; Shioji, K. Selenobenzophenones and Diazoalkanes: Isolation of Tetraarylethylenes by the Reaction of Benzophenone Hydrazones with Diselenium Dibromide. *European J. Org. Chem.* **2004**, No. 4, 820–825. https://doi.org/10.1002/ejoc.200300510.

(8) Schreivogel, A.; Maurer, J.; Winter, R.; Baro, A.; Laschat, S. Synthesis and Electrochemical Properties of Tetrasubstituted Tetraphenylethenes. *European J. Org. Chem.* **2006**, No. 15, 3395–3404. https://doi.org/10.1002/ejoc.200600123.

(9) Hua, G.; Li, Y.; Slawin, A. M. Z.; Woollins, J. D. Stereoselective Synthesis of Olefins by a Reductive Coupling Reaction. *J. Chem. Soc. Dalt. Trans.* **2007**, No. 15, 1477–1480. https://doi.org/10.1039/b702818k.

(10) Nadri, S.; Joshaghani, M.; Ranee, E. Catalytic Performance of a Phosphapalladacycle Bearing a Biphenyl Moiety, Possessing an Sp3 C - Pd Bond, toward the Heck Coupling Reaction. *Organometallics* **2009**, *28* (21), 6281–6287. https://doi.org/10.1021/om9006483.

(11) Sajna, K. V.; Srinivas, V.; Kumara Swamy, K. C. Efficient Palladium-Catalyzed Double Arylation of Phosphonoalkynes and Diarylalkynes in Water: Use of a Dinuclear Palladium(I) Catalyst. *Adv. Synth. Catal.* **2010**, *352* (17), 3069–3081. https://doi.org/10.1002/adsc.201000579.

(12) Wang, W.; Lin, T.; Wang, M.; Liu, T. X.; Ren, L.; Chen, D.; Huang, S. Aggregation Emission Properties of Oligomers Based on Tetraphenylethylene. *J. Phys. Chem. B* **2010**, *114* (18), 5983–5988. https://doi.org/10.1021/jp911311j.

(13) Zhang, L.; Yu, X.; Zhang, L.; Zhou, X.; Lin, Y. A Simple and Practical Catalytic Electron Transfer System Composed of TiCl4 and Metallic Yb: Application in Carbonyl Olefination and Insight into the Mechanism. *Org. Chem. Front.* **2014**, *1* (8), 929–935. https://doi.org/10.1039/c4qo00140k.

(14) Hu, X. M.; Chen, Q.; Wang, J. X.; Cheng, Q. Y.; Yan, C. G.; Cao, J.; He, Y. J.; Han, B. H. Tetraphenylethylene-Based Glycoconjugate as a Fluorescence "Turn-on" Sensor for Cholera Toxin. *Chem. - An Asian J.* **2011**, *6* (9), 2376–2381. https://doi.org/10.1002/asia.201100141.

(15) Zhao, L.; Chen, Y.; Yuan, J.; Chen, M.; Zhang, H.; Li, X. Electrospun Fibrous Mats with Conjugated Tetraphenylethylene and Mannose for Sensitive Turn-on Fluorescent Sensing of Escherichia Coli. *ACS Appl. Mater. Interfaces* **2015**, *7* (9), 5177–5186. https://doi.org/10.1021/am507593p.

(16) Lou, X.; Leung, C. W. T.; Dong, C.; Hong, Y.; Chen, S.; Zhao, E.; Lam, J. W. Y.; Tang, B. Z. Detection of Adenine-Rich SsDNA Based on Thymine-Substituted Tetraphenylethene with Aggregation-Induced Emission Characteristics. *RSC Adv.* **2014**, *4* (63), 33307–33311. https://doi.org/10.1039/c4ra05765a.

(17) Jiang, G.; Wang, J.; Yang, Y.; Zhang, G.; Liu, Y.; Lin, H.; Zhang, G.; Li, Y.; Fan, X. Fluorescent Turn-on Sensing of Bacterial Lipopolysaccharide in Artificial Urine Sample with Sensitivity down to Nanomolar by Tetraphenylethylene Based Aggregation Induced Emission Molecule. *Biosens. Bioelectron.* **2016**, *85*, 62–67. https://doi.org/10.1016/j.bios.2016.04.071.

(18) Li, Y.; Yu, H.; Qian, Y.; Hu, J.; Liu, S. Amphiphilic Star Copolymer-Based Bimodal Fluorogenic/Magnetic Resonance Probes for Concomitant Bacteria Detection and Inhibition. *Adv. Mater.* **2014**, *26* (39), 6734–6741. https://doi.org/10.1002/adma.201402797.

(19) Balachandran, Y. L.; Jiang, X. Aggregation-Induced Fluorogens in Bio-Detection, Tumor Imaging, and Therapy: A Review. *CCS Chem.* **2022**, *4* (2), 420–436. https://doi.org/10.31635/ccschem.021.202101307.

(20) Xu, J.; Xiong, J.; Qin, Y.; Li, Z.; Pan, C.; Huo, Y.; Zhang, H. A Novel Quinolinyl-Tetraphenylethene-Based Fluorescence “Turn-on” Sensor for Zn2+with a Large Stokes Shift and Its Applications for Portable Test Strips and Biological Imaging. *Mater. Chem. Front.* **2020**, *4* (11), 3338–3348. https://doi.org/10.1039/d0qm00446d.

(21) Dong, J.; Liu, M.; Jiang, R.; Huang, H.; Wan, Q.; Wen, Y.; Tian, J.; Dai, Y.; Zhang, X.; Wei, Y. Synthesis and Biological Imaging of Cross-Linked Fluorescent Polymeric Nanoparticles with Aggregation-Induced Emission Characteristics Based on the Combination of RAFT Polymerization and the Biginelli Reaction. *J. Colloid Interface Sci.* **2018**, *528*, 192–199. https://doi.org/10.1016/j.jcis.2018.05.043.

(22) Kalva, N.; Uthaman, S.; Jang, E. H.; Augustine, R.; Jeon, S. H.; Huh, K. M.; Park, I. K.; Kim, I. Aggregation-Induced Emission-Active Hyperbranched Polymer-Based Nanoparticles and Their Biological Imaging Applications. *Dye. Pigment.* **2021**, *186*, 108975. https://doi.org/10.1016/j.dyepig.2020.108975.

(23) Jayaram, D. T.; Ramos-Romero, S.; Shankar, B. H.; Garrido, C.; Rubio, N.; Sanchez-

Cid, L.; Gómez, S. B.; Blanco, J.; Ramaiah, D. In Vitro and in Vivo Demonstration of Photodynamic Activity and Cytoplasm Imaging through TPE Nanoparticles. *ACS Chem. Biol.* **2016**, *11* (1), 104–112. https://doi.org/10.1021/acschembio.5b00537.

(24) Huang, W.; Bender, M.; Seehafer, K.; Wacker, I.; Schröder, R. R.; Bunz, U. H. F. Novel Functional TPE Polymers: Aggregation-Induced Emission, PH Response, and Solvatochromic Behavior. *Macromol. Rapid Commun.* **2019**, *40* (6), 1–6. https://doi.org/10.1002/marc.201800774.

(25) Chen, Y.; Han, H.; Tong, H.; Chen, T.; Wang, H.; Ji, J.; Jin, Q. Zwitterionic Phosphorylcholine-TPE Conjugate for PH-Responsive Drug Delivery and AIE Active Imaging. *ACS Appl. Mater. Interfaces* **2016**, *8* (33), 21185–21192. https://doi.org/10.1021/acsami.6b06071.

(26) Rodrigues, A. C. B.; Pina, J.; Dong, W.; Forster, M.; Scherf, U.; Seixas De Melo, J. S. Aggregation-Induced Emission in Phenothiazine-TPE and -TPAN Polymers. *Macromolecules* **2018**, *51* (21), 8501–8512. https://doi.org/10.1021/acs.macromol.8b01758.

(27) Cai, Y.; Gui, C.; Samedov, K.; Su, H.; Gu, X.; Li, S.; Luo, W.; Sung, H. H. Y.; Lam, J. W. Y.; Kwok, R. T. K.; Williams, I. D.; Qin, A.; Tang, B. Z. An Acidic PH Independent Piperazine-TPE AIEgen as a Unique Bioprobe for Lysosome Tracing. *Chem. Sci.* **2017**, *8* (11), 7593–7603. https://doi.org/10.1039/c7sc03515b.

(28) Chen, S.; Hong, Y.; Liu, Y.; Liu, J.; Leung, C. W. T.; Li, M.; Kwok, R. T. K.; Zhao, E.; Lam, J. W. Y.; Yu, Y.; Tang, B. Z. Erratum: Correction to "Full-Range Intracellular PH Sensing by an Aggregation-Induced Emission-Active Two-Channel Ratiometric Fluorogen." *J. Am. Chem. Soc.* **2014**, *136* (31), 11196. https://doi.org/10.1021/ja506638j.

(29) Ghosh, K. R.; Saha, S. K.; Wang, Z. Y. Ultra-Sensitive Detection of Explosives in Solution and Film as Well as the Development of Thicker Film Effectiveness by Tetraphenylethene Moiety in AIE Active Fluorescent Conjugated Polymer. *Polym. Chem.* **2014**, *5* (19), 5638–5643. https://doi.org/10.1039/c4py00673a.

(30) Feng, H. T.; Zheng, Y. S. Highly Sensitive and Selective Detection of Nitrophenolic Explosives by Using Nanospheres of a Tetraphenylethylene Macrocycle Displaying Aggregation-Induced Emission. *Chem. - A Eur. J.* **2014**, *20* (1), 195–201. https://doi.org/10.1002/chem.201302638.

(31) Wu, W.; Ye, S.; Huang, L.; Xiao, L.; Fu, Y.; Huang, Q.; Yu, G.; Liu, Y.; Qin, J.; Li, Q.; Li, Z. A Conjugated Hyperbranched Polymer Constructed from Carbazole and

Tetraphenylethylene Moieties: Convenient Synthesis through One-Pot "a 2 + B4" Suzuki Polymerization, Aggregation-Induced Enhanced Emission, and Application as Explosive Chemosensors and PLE. *J. Mater. Chem.* **2012**, *22* (13), 6374–6382. https://doi.org/10.1039/c2jm16514g.

(32) Dong, W.; Pan, Y.; Fritsch, M.; Scherf, U. High Sensitivity Sensing of Nitroaromatic Explosive Vapors Based on Polytriphenylamines with AIE-Active Tetraphenylethylene Side Groups. *J. Polym. Sci. Part A Polym. Chem.* **2015**, *53* (15), 1753–1761. https://doi.org/10.1002/pola.27631.

(33) Mahendran, V.; Pasumpon, K.; Thimmarayaperumal, S.; Thilagar, P.; Shanmugam, S. Tetraphenylethene-2-Pyrone Conjugate: Aggregation-Induced Emission Study and Explosives Sensor. *J. Org. Chem.* **2016**, *81* (9), 3597–3602. https://doi.org/10.1021/acs.joc.6b00267.

(34) Feng, H. T.; Wang, J. H.; Zheng, Y. S. CH3-π Interaction of Explosives with Cavity of a TPE Macrocycle: The Key Cause for Highly Selective Detection of TNT. *ACS Appl. Mater. Interfaces* **2014**, *6* (22), 20067–20074. https://doi.org/10.1021/am505636f.

(35) Dong, Y.; Lam, J. W. Y.; Qin, A.; Liu, J.; Li, Z.; Tang, B. Z.; Sun, J.; Kwok, H. S. Aggregation-Induced Emissions of Tetraphenylethene Derivatives and Their Utilities as Chemical Vapor Sensors and in Organic Light-Emitting Diodes. *Appl. Phys. Lett.* **2007**, *91* (1), 88–91. https://doi.org/10.1063/1.2753723.

(36) Dong, J.; Tummanapelli, A. K.; Li, X.; Ying, S.; Hirao, H.; Zhao, D. Fluorescent Porous Organic Frameworks Containing Molecular Rotors for Size-Selective Recognition. *Chem. Mater.* **2016**, *28* (21), 7889–7897. https://doi.org/10.1021/acs.chemmater.6b03376.

(37) Zhang, M.; Feng, G.; Song, Z.; Zhou, Y. P.; Chao, H. Y.; Yuan, D.; Tan, T. T. Y.; Guo, Z.; Hu, Z.; Tang, B. Z.; Liu, B.; Zhao, D. Two-Dimensional Metal-Organic Framework with Wide Channels and Responsive Turn-on Fluorescence for the Chemical Sensing of Volatile Organic Compounds. *J. Am. Chem. Soc.* **2014**, *136* (20), 7241–7244. https://doi.org/10.1021/ja502643p.

(38) Zhang, W.; Kang, J.; Li, P.; Wang, H.; Tang, B. Dual Signaling Molecule Sensor for Rapid Detection of Hydrogen Sulfide Based on Modified Tetraphenylethylene. *Anal. Chem.* **2015**, *87* (17), 8964–8969. https://doi.org/10.1021/acs.analchem.5b02169.

(39) Hu, F.; Huang, Y.; Zhang, G.; Zhao, R.; Zhang, D. A Highly Selective Fluorescence Turn-on Detection of Hydrogen Peroxide and d-Glucose Based on the

Aggregation/Deaggregation of a Modified Tetraphenylethylene. *Tetrahedron Lett.* **2014**, *55* (8), 1471–1474. https://doi.org/10.1016/j.tetlet.2014.01.056.

(40) Wen, J.; Dong, L.; Hu, S.; Li, W.; Li, S.; Wang, X. Fluorogenic Thorium Sensors Based on 2,6-Pyridinedicarboxylic Acid-Substituted Tetraphenylethenes with Aggregation-Induced Emission Characteristics. *Chem. - An Asian J.* **2016**, *11* (1), 49–53. https://doi.org/10.1002/asia.201500834.

(41) Jakku, R. K.; Mirzadeh, N.; Privér, S. H.; Reddy, G.; Vardhaman, A. K.; Lingamallu, G.; Trivedi, R.; Bhargava, S. K. Tetraphenylethylene-Substituted Bis(Thienyl)Imidazole (Dtitpe), an Efficient Molecular Sensor for the Detection and Quantification of Fluoride Ions. *Chemosensors* **2021**, *9* (10). https://doi.org/10.3390/chemosensors9100285.

(42) Naik, V. G.; Hiremath, S. D.; Thakuri, A.; Hemmadi, V.; Biswas, M.; Banerjee, M.; Chatterjee, A. A Coumarin Coupled Tetraphenylethylene Based Multi-Targeted AIEgen for Cyanide Ion and Nitro Explosive Detection, and Cellular Imaging. *Analyst* **2022**, *147* (13), 2997–3006. https://doi.org/10.1039/d2an00040g.

(43) Li, Y.; Xu, L.; Su, B. Aggregation Induced Emission for the Recognition of Latent Fingerprints. *Chem. Commun.* **2012**, *48* (34), 4109–4111. https://doi.org/10.1039/c2cc30553d.

(44) Qiao, W. G.; Xiong, J. Bin; Yuan, Y. X.; Zhang, H. C.; Yang, D.; Liu, M.; Zheng, Y. S. Chiroptical Property of TPE Triangular Macrocycle Crown Ethers from Propeller-like Chirality Induced by Chiral Acids. *J. Mater. Chem. C* **2018**, *6* (13), 3427–3434. https://doi.org/10.1039/c7tc05759h.

(45) Luo, H.; Ren, X. K.; Zhang, B. H.; Huang, Y. Q.; Lu, L.; Song, J. Synthesis and Properties of Tetraphenylethylene Derivatives with Different Chiral Substituents: From Helical Supermolecular Structure to Circularly Polarized Luminescence. *Dye. Pigment.* **2021**, *188* (November 2020), 109148. https://doi.org/10.1016/j.dyepig.2021.109148.

(46) Anuradha; La, D. D.; Al Kobaisi, M.; Gupta, A.; Bhosale, S. V. Chiral Assembly of AIE-Active Achiral Molecules: An Odd Effect in Self-Assembly. *Chem. - A Eur. J.* **2017**, *23* (16), 3950–3956. https://doi.org/10.1002/chem.201605458.

(47) Anuradha; La, D. D.; Al Kobaisi, M.; Bhosale, S. V. Right Handed Chiral Superstructures from Achiral Molecules: Self-Assembly with a Twist. *Sci. Rep.* **2015**, *5* (August), 1–11. https://doi.org/10.1038/srep15652.

(48) Li, J.; Zhang, Y.; Mei, J.; Lam, J. W. Y.; Hao, J.; Tang, B. Z. Aggregation-Induced

Emission Rotors: Rational Design and Tunable Stimuli Response. *Chem. - A Eur. J.* **2015**, *21* (2), 907–914. https://doi.org/10.1002/chem.201405118.

(49) Paquin, F.; Rivnay, J.; Salleo, A.; Stingelin, N.; Silva, C. Multi-Phase Semicrystalline Microstructures Drive Exciton Dissociation in Neat Plastic Semiconductors. *J. Mater. Chem. C* **2015**, *3* (207890), 10715–10722. https://doi.org/10.1039/b000000x.

(50) Shi, J.; Xu, L.; Lv, X.; Ding, Q.; Li, W.; Sun, Q.; Xue, S.; Yang, W. Tetraphenylethylene-Substituted Phenothiazine-Based AIEgens for Non-Doped Deep-Blue Organic Light-Emitting Diodes with Negligible Efficiency Roll-Off. *Dye. Pigment.* **2019**, *161*, 97–103. https://doi.org/10.1016/j.dyepig.2018.09.033.

(51) Xu, L.; Yu, Y.; Shi, J.; Cui, W.; Lv, X.; Cang, M.; Sun, Q.; Xue, S.; Yang, W. Highly Efficient Nondoped Blue Organic Light-Emitting Diodes Based on a Star-Group Tetraphenylethylene-Substituted Aggregation-Induced-Emission-Active Organic Fluorescent Small Molecules. *Dye. Pigment.* **2020**, *175*, 108082. https://doi.org/10.1016/j.dyepig.2019.108082.

(52) Jiang, S.; Qiu, J.; Lin, L.; Guo, H.; Yang, F. Circularly Polarized Luminescence Based on Columnar Self-Assembly of Tetraphenylethylene with Multiple Cholesterol Units. *Dye. Pigment.* **2019**, *163* (December 2018), 363–370. https://doi.org/10.1016/j.dyepig.2018.12.021.

(53) Yuan, Y. X.; Hu, M.; Zhang, K. R.; Zhou, T. T.; Wang, S.; Liu, M.; Zheng, Y. S. The Largest CPL Enhancement by Further Assembly of Self-Assembled Superhelices Based on the Helical TPE Macrocycle. *Mater. Horizons* **2020**, *7* (12), 3209–3216. https://doi.org/10.1039/d0mh01303j.

(54) Li, H.; Cheng, J.; Zhao, Y.; Lam, J. W. Y.; Wong, K. S.; Wu, H.; Li, B. S.; Tang, B. Z. L-Valine Methyl Ester-Containing Tetraphenylethene: Aggregation-Induced Emission, Aggregation-Induced Circular Dichroism, Circularly Polarized Luminescence, and Helical Self-Assembly. *Mater. Horizons* **2014**, *1* (5), 518–521. https://doi.org/10.1039/c4mh00078a.

(55) Alam, P.; Leung, N. L. C.; Zhang, J.; Kwok, R. T. K.; Lam, J. W. Y.; Tang, B. Z. AIE-Based Luminescence Probes for Metal Ion Detection. *Coord. Chem. Rev.* **2021**, *429*, 213693. https://doi.org/10.1016/j.ccr.2020.213693.

(56) Tang, A.; Yin, Y.; Chen, Z.; Fan, C.; Liu, G.; Pu, S. A Multifunctional Aggregation-Induced Emission (AIE)-Active Fluorescent Chemosensor for Detection of Zn2+ and Hg2+. *Tetrahedron* **2019**, *75* (36), 130489. https://doi.org/10.1016/j.tet.2019.130489.

(57) Hong, Y.; Chen, S.; Leung, C. W. T.; Lam, J. W. Y.; Liu, J.; Tseng, N. W.; Kwok, R. T. K.; Yu, Y.; Wang, Z.; Tang, B. Z. Fluorogenic Zn(II) and Chromogenic Fe(II) Sensors Based on Terpyridine-Substituted Tetraphenylethenes with Aggregation-Induced Emission Characteristics. *ACS Appl. Mater. Interfaces* **2011**, *3* (9), 3411–3418. https://doi.org/10.1021/am2009162.

(58) Ye, J. H.; Liu, J.; Wang, Z.; Bai, Y.; Zhang, W.; He, W. A New Fe3+ Fluorescent Chemosensor Based on Aggregation-Induced Emission. *Tetrahedron Lett.* **2014**, *55* (27), 3688–3692. https://doi.org/10.1016/j.tetlet.2014.05.008.

(59) Tang, A.; Chen, Z.; Deng, D.; Liu, G.; Tu, Y.; Pu, S. Aggregation-Induced Emission Enhancement (AIEE)-Active Tetraphenylethene (TPE)-Based Chemosensor for Hg2+ with Solvatochromism and Cell Imaging Characteristics. *RSC Adv.* **2019**, *9* (21), 11865–11869. https://doi.org/10.1039/c9ra02119a.

(60) Jagadhane, K. S.; Bhosale, S. R.; Gunjal, D. B.; Nille, O. S.; Kolekar, G. B.; Kolekar, S. S.; Dongale, T. D.; Anbhule, P. V. Tetraphenylethene-Based Fluorescent Chemosensor with Mechanochromic and Aggregation-Induced Emission (AIE) Properties for the Selective and Sensitive Detection of Hg2+and Ag+Ions in Aqueous Media: Application to Environmental Analysis. *ACS Omega* **2022**, *7* (39), 34888–34900. https://doi.org/10.1021/acsomega.2c03437.

(61) Wang, J.; Tong, J.; Wang, Z. F.; Yuan, Q.; Wang, X. Y.; Yu, S. Y.; Tang, B. Z. Highly Specific and Selective Fluorescent Chemosensor for Sensing of Hg(II) by NH-Pyrazolate-Functionalized AIEgens. *Anal. Chim. Acta* **2022**, *1208*, 339824. https://doi.org/10.1016/j.aca.2022.339824.

(62) Gui, S.; Huang, Y.; Hu, F.; Jin, Y.; Zhang, G.; Yan, L.; Zhang, D.; Zhao, R. Fluorescence Turn-on Chemosensor for Highly Selective and Sensitive Detection and Bioimaging of Al3+ in Living Cells Based on Ion-Induced Aggregation. *Anal. Chem.* **2015**, *87* (3), 1470–1474. https://doi.org/10.1021/ac504153c.

(63) Yan, Y.; Che, Z.; Yu, X.; Zhi, X.; Wang, J.; Xu, H. Fluorescence "on-off-on" Chemosensor for Sequential Recognition of Fe 3+ and Hg2+ in Water Based on Tetraphenylethylene Motif. *Bioorganic Med. Chem.* **2013**, *21* (2), 508–513. https://doi.org/10.1016/j.bmc.2012.11.005.

(64) Yang, Y.; Gao, C. Y.; Li, T.; Chen, J. A Tetraphenylethene-Based Rhodamine Hydrazone Chemosensor for Colorimetric and Reversible Detection of Cu2+. *ChemistrySelect* **2016**, *1* (15), 4577–4581. https://doi.org/10.1002/slct.201600883.

(65) Chua, M. H.; Shah, K. W.; Zhou, H.; Xu, J. Recent Advances in Aggregation-Induced

Emission Chemosensors for Anion Sensing. *Molecules* **2019**, *24* (15). https://doi.org/10.3390/molecules24152711.

(66) Wang, Y.; Liu, H.; Chen, Z.; Pu, S. Aggregation-Induced Emission Enhancement (AIEE)-Active Tetraphenylethene (TPE)-Based Chemosensor for CN−. *Spectrochim. Acta - Part A Mol. Biomol. Spectrosc.* **2021**, *245*, 118928. https://doi.org/10.1016/j.saa.2020.118928.

(67) Pan, D.; Don, Y.; Lu, Y.; Xiao, G.; Chi, H.; Hu, Z. AIE Fluorescent Probe Based on Tetraphenylethylene and Morpholine-Thiourea Structures for Detection of HClO. *Anal. Chim. Acta* **2022**, *1235* (July), 340559. https://doi.org/10.1016/j.aca.2022.340559.

(68) Gu, B.; Liu, M.; Long, J.; Ye, X.; Xu, Z.; Shen, Y. An AIE Based Fluorescent Chemosensor for Ratiometric Detection of Hypochlorous Acid and Its Application. *Spectrochim. Acta - Part A Mol. Biomol. Spectrosc.* **2022**, *278*, 121290. https://doi.org/10.1016/j.saa.2022.121290.

(69) Ortiz-Gómez, I.; González-Alfaro, S.; Sánchez-Ruiz, A.; de Orbe-Payá, I.; Capitán-Vallvey, L. F.; Navarro, A.; Salinas-Castillo, A.; García-Martínez, J. C. Reversal of a Fluorescent Fluoride Chemosensor from Turn-Off to Turn-On Based on Aggregation Induced Emission Properties. *ACS Sensors* **2022**, *7* (1), 37–43. https://doi.org/10.1021/acssensors.1c02196.

(70) Liu, H. X.; Fu, X. M.; Hu, J. H. AIE Based Colorimetric and Fluorescent Sensor for the Selective Detection of CN− in Aqueous Media. *Inorg. Chem. Commun.* **2022**, *142* (April), 109662. https://doi.org/10.1016/j.inoche.2022.109662.

(71) Ozturk, S.; Atilgan, S. A Tetraphenylethene Based Polarity Dependent Turn-on Fluorescence Strategy for Selective and Sensitive Detection of Hg2+ in Aqueous Medium and in Living Cells. *Tetrahedron Lett.* **2014**, *55* (1), 70–73. https://doi.org/10.1016/j.tetlet.2013.10.105.

(72) Huang, G.; Zhang, G.; Zhang, D. Turn-on of the Fluorescence of Tetra(4-Pyridylphenyl)Ethylene by the Synergistic Interactions of Mercury(Ii) Cation and Hydrogen Sulfate Anion. *Chem. Commun.* **2012**, *48* (60), 7504–7506. https://doi.org/10.1039/c2cc32504g.

(73) Ruan, Z.; Shan, Y.; Gong, Y.; Wang, C.; Ye, F.; Qiu, Y.; Liang, Z.; Li, Z. Novel AIE-Active Ratiometric Fluorescent Probes for Mercury(II) Based on the Hg2+-Promoted Deprotection of Thioketal, and Good Mechanochromic Properties. *J. Mater. Chem. C* **2018**, *6* (4), 773–780. https://doi.org/10.1039/c7tc04712f.

(74) Neupane, L. N.; Oh, E. T.; Park, H. J.; Lee, K. H. Selective and Sensitive Detection of Heavy Metal Ions in 100% Aqueous Solution and Cells with a Fluorescence Chemosensor Based on Peptide Using Aggregation-Induced Emission. *Anal. Chem.* **2016**, *88* (6), 3333–3340. https://doi.org/10.1021/acs.analchem.5b04892.

(75) Xu, H.; Wang, H.; Zhou, S.; Xiao, L.; Yan, Y.; Yuan, Q. A Protocol of Self-Assembled Monolayers of Fluorescent Block Molecules for Trace Zn(Ii) Sensing: Structures and Mechanisms. *RSC Adv.* **2015**, *5* (128), 106061–106067. https://doi.org/10.1039/c5ra20198e.

(76) Sun, F.; Zhang, G.; Zhang, D.; Xue, L.; Jiang, H. Aqueous Fluorescence Turn-on Sensor for Zn 2+ with a Tetraphenylethylene Compound. *Org. Lett.* **2011**, *13* (24), 6378–6381. https://doi.org/10.1021/ol2026735.

(77) Chen, X.; Shen, X. Y.; Guan, E.; Liu, Y.; Qin, A.; Sun, J. Z.; Zhong Tang, B. A Pyridinyl-Functionalized Tetraphenylethylene Fluorogen for Specific Sensing of Trivalent Cations. *Chem. Commun.* **2013**, *49* (15), 1503–1505. https://doi.org/10.1039/c2cc38246f.

(78) Lu, L.; Ren, X. K.; Liu, R.; Jiang, X. Q.; Geng, L. Y.; Zheng, J. F.; Feng, Y.; Chen, E. Q. Ionic Self-Assembled Derivative of Tetraphenylethylene: Synthesis, Enhanced Solid-State Emission, Liquid-Crystalline Structure, and Cu2+ Detection Ability. *ChemPhysChem* **2017**, *18* (24), 3605–3613. https://doi.org/10.1002/cphc.201700926.

(79) Feng, H. T.; Song, S.; Chen, Y. C.; Shen, C. H.; Zheng, Y. S. Self-Assembled Tetraphenylethylene Macrocycle Nanofibrous Materials for the Visual Detection of Copper(Ii) in Water. *J. Mater. Chem. C* **2014**, *2* (13), 2353–2359. https://doi.org/10.1039/c3tc32373k.

(80) Li, Y.; Yu, H.; Shao, G.; Gan, F. A Tetraphenylethylene-Based "Turn on" Fluorescent Sensor for the Rapid Detection of Ag+ Ions with High Selectivity. *J. Photochem. Photobiol. A Chem.* **2015**, *301* (3), 14–19. https://doi.org/10.1016/j.jphotochem.2014.12.013.

(81) Zhang, L.; Hu, W.; Yu, L.; Wang, Y. Click Synthesis of a Novel Triazole Bridged AIE Active Cyclodextrin Probe for Specific Detection of Cd2+. *Chem. Commun.* **2015**, *51* (20), 4298–4301. https://doi.org/10.1039/c4cc09769f.

(82) Khandare, D. G.; Joshi, H.; Banerjee, M.; Majik, M. S.; Chatterjee, A. An Aggregation-Induced Emission Based Turn-on Fluorescent Chemodosimeter for the Selective Detection of Pb2+ Ions. *RSC Adv.* **2014**, *4* (87), 47076–47080.

https://doi.org/10.1039/c4ra09451d.

(83) Huang, Y.; Lin, J.; Wang, L.; Cao, Z.; Wang, Y.; Wu, M. A Specific Fluorescent Probe for Antimony Based on Aggregation Induced Emission. *Zeitschrift fur Anorg. und Allg. Chemie* **2020**, *646* (2), 47–52. https://doi.org/10.1002/zaac.201900268.

(84) Wen, J.; Huang, Z.; Hu, S.; Li, S.; Li, W.; Wang, X. Aggregation-Induced Emission Active Tetraphenylethene-Based Sensor for Uranyl Ion Detection. *J. Hazard. Mater.* **2016**, *318*, 363–370. https://doi.org/10.1016/j.jhazmat.2016.07.004.

(85) Li, Y.; Zhuang, Z.; Lin, G.; Wang, Z.; Shen, P.; Xiong, Y.; Wang, B.; Chen, S.; Zhao, Z.; Tang, B. Z. A New Blue AIEgen Based on Tetraphenylethene with Multiple Potential Applications in Fluorine Ion Sensors, Mechanochromism, and Organic Light-Emitting Diodes. *New J. Chem.* **2018**, *42* (6), 4089–4094. https://doi.org/10.1039/c7nj04742h.

(86) Jiang, G.; Liu, X.; Wu, Y.; Wang, J.; Dong, X.; Zhang, G.; Li, Y.; Fan, X. An AIE Based Tetraphenylethylene Derivative for Highly Selective and Light-up Sensing of Fluoride Ions in Aqueous Solution and in Living Cells. *RSC Adv.* **2016**, *6* (64), 59400–59404. https://doi.org/10.1039/c6ra10878d.

(87) Bineci, M.; Baɨlan, M.; Atilgan, S. AIE Active Pyridinium Fused Tetraphenylethene: Rapid and Selective Fluorescent "Turn-on" Sensor for Fluoride Ion in Aqueous Media. *Sensors Actuators, B Chem.* **2016**, *222*, 315–319. https://doi.org/10.1016/j.snb.2015.08.087.

(88) Chua, M. H.; Zhou, H.; Lin, T. T.; Wu, J.; Xu, J. Triphenylethylenyl-Based Donor-Acceptor-Don1. Chua, M. H., Zhou, H., Lin, T. T., Wu, J. & Xu, J. Triphenylethylenyl-Based Donor-Acceptor-Donor Molecules: Studies on Structural and Optical Properties and AIE Properties for Cyanide Detection. J. Mater. Chem. *J. Mater. Chem. C* **2017**, *5* (46), 12194–12203. https://doi.org/10.1039/c7tc04400c.

(89) Zhang, Y.; Li, D.; Li, Y.; Yu, J. Solvatochromic AIE Luminogens as Supersensitive Water Detectors in Organic Solvents and Highly Efficient Cyanide Chemosensors in Water. *Chem. Sci.* **2014**, *5* (7), 2710–2716. https://doi.org/10.1039/c4sc00721b.

(90) Huang, Y.; Zhang, P.; Gao, M.; Zeng, F.; Qin, A.; Wu, S.; Tang, B. Z. Ratiometric Detection and Imaging of Endogenous Hypochlorite in Live Cells and: In Vivo Achieved by Using an Aggregation Induced Emission (AIE)-Based Nanoprobe. *Chem. Commun.* **2016**, *52* (45), 7288–7291. https://doi.org/10.1039/c6cc03415b.

(91) Wang, C.; Ji, H.; Li, M.; Cai, L.; Wang, Z.; Li, Q.; Li, Z. A Highly Sensitive and Selective Fluorescent Probe for Hypochlorite in Pure Water with Aggregation

Induced Emission Characteristics. *Faraday Discuss.* **2017**, *196*, 427–438. https://doi.org/10.1039/c6fd00168h.

(92) Li, N.; Liu, Y. Y.; Li, Y.; Zhuang, J. B.; Cui, R. R.; Gong, Q.; Zhao, N.; Tang, B. Z. Fine Tuning of Emission Behavior, Self-Assembly, Anion Sensing, and Mitochondria Targeting of Pyridinium-Functionalized Tetraphenylethene by Alkyl Chain Engineering. *ACS Appl. Mater. Interfaces* **2018**, *10* (28), 24249–24257. https://doi.org/10.1021/acsami.8b04113.

(93) Liu, W.; Yu, W.; Li, X.; Zhao, X.; Zhang, Y.; Song, P.; Yin, Y.; Xi, R.; Meng, M. Pyrophosphate-Triggered Intermolecular Cross-Linking of Tetraphenylethylene Molecules for Multianalyte Detection. *Sensors Actuators, B Chem.* **2018**, *266*, 170–177. https://doi.org/10.1016/j.snb.2018.03.126.

(94) Schön, J. H.; Kloc, C.; Batlogg, B. Superconductivity at 52 K in Hole-Doped C60. *Nature* **2000**, *408* (6812), 549–552. https://doi.org/10.1038/35046008.

(95) Schön, J. H.; Kloc, C.; Batlogg, B. High-Temperature Superconductivity in Lattice-Expanded C 60. *Science (80).* **2001**, *293* (5539), 2432–2434. https://doi.org/10.1126/science.1064773.

(96) Dresselhaus, M. S.; Dresselhaus, G.; Eklund, P. C. Historical Introduction. In *Science of Fullerenes and Carbon Nanotubes*; Dresselhaus, M. S., Dresselhaus, G., Eklund, P. C., Eds.; Elsevier: San Diego, 1996; pp 1–14. https://doi.org/10.1016/B978-012221820-0/50001-0.

(97) Haley, M. M. and Tykwinski, R. R. *Carbon-Rich Compounds*; Haley, M. M., Tykwinski, R. R., Eds.; Wiley: Weinheim, FRG, 2006. https://doi.org/10.1002/3527607994.

(98) Kawase, T.; Tanaka, K.; Fujiwara, N.; Darabi, H. R.; Oda, M. Complexation of a Carbon Nanoring with Fullerenes. *Angew. Chemie - Int. Ed.* **2003**, *42* (14), 1624–1628. https://doi.org/10.1002/anie.200250728.

(99) Zhang, M.; Xu, H.; Wang, M.; Saha, M. L.; Zhou, Z.; Yan, X.; Wang, H.; Li, X.; Huang, F.; She, N.; Stang, P. J. Platinum(II)-Based Convex Trigonal-Prismatic Cages via Coordination-Driven Self-Assembly and C60 Encapsulation. *Inorg. Chem.* **2017**, *56* (20), 12498–12504. https://doi.org/10.1021/acs.inorgchem.7b01967.

(100) Xia, J.; Bacon, J. W.; Jasti, R. Gram-Scale Synthesis and Crystal Structures of [8]- and [10]CPP{,} and the Solid-State Structure of C60@[10]CPP. *Chem. Sci.* **2012**, *3* (10), 3018–3021. https://doi.org/10.1039/C2SC20719B.

(101) Iwamoto, T.; Watanabe, Y.; Sadahiro, T.; Haino, T.; Yamago, S. Size-Selective

Encapsulation of C60 by [10]Cycloparaphenylene: Formation of the Shortest Fullerene-Peapod. *Angew. Chemie - Int. Ed.* **2011**, *50* (36), 8342–8344. https://doi.org/10.1002/anie.201102302.

(102) Takeda, M.; Hiroto, S.; Yokoi, H.; Lee, S.; Kim, D.; Shinokubo, H. Azabuckybowl-Based Molecular Tweezers as C60 and C70 Receptors. *J. Am. Chem. Soc.* **2018**, *140* (20), 6336–6342. https://doi.org/10.1021/jacs.8b02327.

(103) Sakurai, H.; Daiko, T.; Hirao, T. A Synthesis of Sumanene, a Fullerene Fragment. *Science (80-.).* **2003**, *301* (5641), 1878. https://doi.org/10.1126/science.1088290.

(104) Mehta, G.; Shahk, S. R.; Ravikumarc, K. Towards the Design of Tricyclopenta [Def{,} Jkl{,} Pqr] Triphenylene ('Sumanene'): A 'Bowl-Shaped' Hydrocarbon Featuring a Structural Motif Present in C60(Buckminsterfullerene). *J. Chem. Soc.{,} Chem. Commun.* **1993**, No. 12, 1006–1008. https://doi.org/10.1039/C39930001006.

(105) Dawe, L. N.; AlHujran, T. A.; Tran, H.-A.; Mercer, J. I.; Jackson, E. A.; Scott, L. T.; Georghiou, P. E. Corannulene and Its Penta-Tert-Butyl Derivative Co-Crystallize 1 : 1 with Pristine C60-Fullerene. *Chem. Commun.* **2012**, *48* (45), 5563–5565. https://doi.org/10.1039/C2CC30652B.

(106) Ke, X. S.; Kim, T.; Brewster, J. T.; Lynch, V. M.; Kim, D.; Sessler, J. L. Expanded Rosarin: A Versatile Fullerene (C60) Receptor. *J. Am. Chem. Soc.* **2017**, *139* (13), 4627–4630. https://doi.org/10.1021/jacs.7b00735.

(107) Yokoi, H.; Hiraoka, Y.; Hiroto, S.; Sakamaki, D.; Seki, S.; Shinokubo, H. Nitrogen-Embedded Buckybowl and Its Assembly with C60. *Nat. Commun.* **2015**, *6*, 1–9. https://doi.org/10.1038/ncomms9215.

(108) Veen, E. M.; Postma, M.; Jonkman, H. T.; Spek, A. L.; Feringa, B. L. Solid State Organisation of C 60 by Inclusion Crystallisation with Triptycenes † Triptycene and Azatriptycene Act as Concave Receptor Molecules for C 60 , Resulting in the Solid State Organisation of C 60 in a Layered and a Hexagonal Pattern , Respectivel. *Convergence* **1999**, 1709–1710.

(109) Sygula, A.; Fronczek, F. R.; Sygula, R.; Rabideau, P. W.; Olmstead, M. M. A Double Concave Hydrocarbon Buckycatcher. *J. Am. Chem. Soc.* **2007**, *129* (13), 3842–3843. https://doi.org/10.1021/ja070616p.

(110) Dsouza, R. N.; Pischel, U.; Nau, W. M. Fluorescent Dyes and Their Supramolecular Host/Guest Complexes with Macrocycles in Aqueous Solution. *Chem. Rev.* **2011**, *111* (12), 7941–7980. https://doi.org/10.1021/cr200213s.

(111) Adriaenssens, L.; Ballester, P. Hydrogen Bonded Supramolecular Capsules with

Functionalized Interiors: The Controlled Orientation of Included Guests. *Chem. Soc. Rev.* **2013**, *42* (8), 3261–3277. https://doi.org/10.1039/c2cs35461f.

(112) Hapiot, F.; Tilloy, S.; Monflier, E. Cyclodextrins as Supramolecular Hosts for Organometallic Complexes. *Chem. Rev.* **2006**, *106* (3), 767–781. https://doi.org/10.1021/cr050576c.

(113) Ballester, P. Anion Binding in Covalent and Self-Assembled Molecular Capsules. *Chem. Soc. Rev.* **2010**, *39* (10), 3810–3830. https://doi.org/10.1039/b926229f.

(114) Biros, S. M.; Rebek, J. Structure and Binding Properties of Water-Soluble Cavitands and Capsules. *Chem. Soc. Rev.* **2007**, *36* (1), 93–104. https://doi.org/10.1039/b508530f.

(115) Rananaware, A.; Samanta, M.; Bhosale, R. S.; Kobaisi, M. Al; Roy, B.; Bheemireddy, V.; Bhosale, S. V.; Bandyopadhyay, S.; Bhosale, S. V. Photomodulation of Fluoride Ion Binding through Anion-φ Interactions Using a Photoswitchable Azobenzene System. *Sci. Rep.* **2016**, *6* (March), 1–10. https://doi.org/10.1038/srep22928.

(116) Yagai, S.; Kitamura, A. Recent Advances in Photoresponsive Supramolecular Self-Assemblies. *Chem. Soc. Rev.* **2008**, *37* (8), 1520–1529. https://doi.org/10.1039/b703092b.

(117) Han, M.; Michel, R.; He, B.; Chen, Y. S.; Stalke, D.; John, M.; Clever, G. H. Light-Triggered Guest Uptake and Release by a Photochromic Coordination Cage. *Angew. Chemie - Int. Ed.* **2013**, *52* (4), 1319–1323. https://doi.org/10.1002/anie.201207373.

(118) Clever, G. H.; Tashiro, S.; Shionoya, M. Light-Triggered Crystallization of a Molecular Host-Guest Complex. *J. Am. Chem. Soc.* **2010**, *132* (29), 9973–9975. https://doi.org/10.1021/ja103620z.

(119) Dube, H.; Ajami, D.; Rebek, J. Photochemical Control of Reversible Encapsulation. *Angew. Chemie - Int. Ed.* **2010**, *49* (18), 3192–3195. https://doi.org/10.1002/anie.201000876.

(120) Natali, M.; Giordani, S. Molecular Switches as Photocontrollable "Smart" Receptors. *Chem. Soc. Rev.* **2012**, *41* (10), 4010–4029. https://doi.org/10.1039/c2cs35015g.

(121) Kishi, N.; Akita, M.; Kamiya, M.; Hayashi, S.; Hsu, H. F.; Yoshizawa, M. Facile Catch and Release of Fullerenes Using a Photoresponsive Molecular Tube. *J. Am. Chem. Soc.* **2013**, *135* (35), 12976–12979. https://doi.org/10.1021/ja406893y.

(122) Yuan, K.; Guo, Y. J.; Zhao, X. A Novel Photo-Responsive Azobenzene-Containing Nanoring Host for Fullerene-Guest Facile Encapsulation and Release. *Phys. Chem.*

Chem. Phys. **2014**, *16* (48), 27053–27064. https://doi.org/10.1039/c4cp03687e.

(123) Frank, J. A.; Moroni, M.; Moshourab, R.; Sumser, M.; Lewin, G. R.; Trauner, D. Photoswitchable Fatty Acids Enable Optical Control of TRPV1. *Nat. Commun.* **2015**, *6* (May). https://doi.org/10.1038/ncomms8118.

(124) Reiter, A.; Skerra, A.; Trauner, D.; Schiefner, A. A Photoswitchable Neurotransmitter Analogue Bound to Its Receptor. *Biochemistry* **2013**, *52* (50), 8972–8974. https://doi.org/10.1021/bi4014402.

(125) Yuan, K.; Guo, Y. J.; Zhao, X. A Novel Photo-Responsive Azobenzene-Containing Nanoring Host for Fullerene-Guest Facile Encapsulation and Release. *Phys. Chem. Chem. Phys.* **2014**, *16* (48), 27053–27064. https://doi.org/10.1039/c4cp03687e.

(126) Yan, Y.; Wang, X.; Chen, J. I. L.; Ginger, D. S. Depends on Local Sequence. **2013**.

(127) Liu, M.; Asanuma, H.; Komiyama, M. Azobenzene-Tethered T7 Promoter for Efficient Photoregulation of Transcription. *J. Am. Chem. Soc.* **2006**, *128* (3), 1009–1015. https://doi.org/10.1021/ja055983k.

(128) Liang, X.; Asanuma, H.; Kashida, H.; Takasu, A.; Sakamoto, T.; Kawai, G.; Komiyama, M. NMR Study on the Photoresponsive DNA Tethering an Azobenzene. Assignment of the Absolute Configuration of Two Diastereomers and Structure Determination of Their Duplexes in the Trans-Form. *J. Am. Chem. Soc.* **2003**, *125* (52), 16408–16415. https://doi.org/10.1021/ja037248j.

(129) Liang, X.; Asanuma, H.; Komiyama, M. Photoregulation of DNA Triplex Formation by Azobenzene. *J. Am. Chem. Soc.* **2002**, *124* (9), 1877–1883. https://doi.org/10.1021/ja011988f.

(130) Li, Z.; Liang, J.; Xue, W.; Liu, G.; Liu, S. H.; Yin, J. Switchable Azo-Macrocycles: From Molecules to Functionalisation. *Supramolecular Chemistry*. Taylor & Francis 2014, pp 54–65. https://doi.org/10.1080/10610278.2013.822970.

(131) Kienzler, M. A.; Reiner, A.; Trautman, E.; Yoo, S.; Trauner, D.; Isacoff, E. Y. A Red-Shifted, Fast-Relaxing Azobenzene Photoswitch for Visible Light Control of an Ionotropic Glutamate Receptor. *J. Am. Chem. Soc.* **2013**, *135* (47), 17683–17686. https://doi.org/10.1021/ja408104w.

(132) Zhang, X.; Zhao, H.; Tian, D.; Deng, H.; Li, H. A Photoresponsive Wettability Switch Based on a Dimethylamino Calix[4]Arene. *Chem. - A Eur. J.* **2014**, *20* (30), 9367–9371. https://doi.org/10.1002/chem.201402476.

(133) Commins, P.; Garcia-Garibay, M. A. Photochromic Molecular Gyroscope with Solid State Rotational States Determined by an Azobenzene Bridge. *J. Org. Chem.* **2014**,

79 (4), 1611–1619. https://doi.org/10.1021/jo402516n.

(134) Zhang, Y.; Wang, M.; Collins, S. D.; Zhou, H.; Phan, H.; Proctor, C.; Mikhailovsky, A.; Wudl, F.; Nguyen, T. Q. Enhancement of the Photoresponse in Organic Field-Effect Transistors by Incorporating Thin DNA Layers. *Angew. Chemie - Int. Ed.* **2014**, *53* (1), 244–249. https://doi.org/10.1002/anie.201306763.

(135) Chen, S. L.; Chu, C. C.; Hsiao, V. K. S. Reversible Light-Modulated Photoluminescence from Azobenzene-Impregnated Porous Silicon. *J. Mater. Chem. C* **2013**, *1* (22), 3529–3531. https://doi.org/10.1039/c3tc30329b.

(136) Zhao, Y. L.; Fraser Stoddart, J. Azobenzene-Based Light-Responsive Hydrogel System. *Langmuir* **2009**, *25* (15), 8442–8446. https://doi.org/10.1021/la804316u.

(137) Shirai, Y.; Sasaki, T.; Guerrero, J. M.; Yu, B. C.; Hodge, P.; Tour, J. M. Synthesis and Photoisomerization of Fullerene- and Oligo(Phenylene Ethynylene) - Azobenzene Derivatives. *ACS Nano* **2008**, *2* (1), 97–106. https://doi.org/10.1021/nn700294m.

(138) Banerjee, I. A.; Yu, L.; Matsui, H. Application of Host-Guest Chemistry in Nanotube-Based Device Fabrication: Photochemically Controlled Immobilization of Azobenzene Nanotubes on Patterned α-CD Monolayer/Au Substrates via Molecular Recognition. *J. Am. Chem. Soc.* **2003**, *125* (32), 9542–9543. https://doi.org/10.1021/ja0344011.

(139) Yuan, K.; Dang, J. S.; Guo, Y. J.; Zhao, X. Theoretical Prediction of the Host-Guest Interactions between Novel Photoresponsive Nanorings and C60: A Strategy for Facile Encapsulation and Release of Fullerene. *J. Comput. Chem.* **2015**, *36* (8), 518–528. https://doi.org/10.1002/jcc.23824.

(140) Yamamura, M.; Saito, T.; Nabeshima, T. Phosphorus-Containing Chiral Molecule for Fullerene Recognition Based on Concave/Convex Interaction. *J. Am. Chem. Soc.* **2014**, *136* (40), 14299–14306. https://doi.org/10.1021/ja507913u.

(141) Litvinov, A. L.; Konarev, D. V.; Kovalevsky, A. Y.; Neretin, I. S.; Slovokhotov, Y. L.; Coppens, P.; Lyubovskaya, R. N. Molecular Complexes of Fullerene C60 with Aromatic Hydrocarbons Containing Flexible Phenyl Substituents. *CrystEngComm* **2002**, *4* (104), 618–622. https://doi.org/10.1039/b209875j.

(142) Rananaware, A.; Bhosale, R. S.; Ohkubo, K.; Patil, H.; Jones, L. A.; Jackson, S. L.; Fukuzumi, S.; Bhosale, S. V.; Bhosale, S. V. Tetraphenylethene-Based Star Shaped Porphyrins: Synthesis, Self-Assembly, and Optical and Photophysical Study. *J. Org. Chem.* **2015**, *80* (8), 3832–3840. https://doi.org/10.1021/jo502760e.

(143) Grebel-Koehler, D.; Liu, D.; De Feyter, S.; Enkelmann, V.; Weil, T.; Engels, C.; Samyn, C.; Müllen, K.; De Schryver, F. C. Synthesis and Photomodulation of Rigid Polyphenylene Dendrimers with an Azobenzene Core. *Macromolecules* **2003**, *36* (3), 578–590. https://doi.org/10.1021/ma021135n.

(144) Dolomanov, O. V; Bourhis, L. J.; Gildea, R. J.; Howard, J. A. K.; Puschmann, H. {\it OLEX2}: A Complete Structure Solution, Refinement and Analysis Program. *J. Appl. Crystallogr.* **2009**, *42* (2), 339–341. https://doi.org/10.1107/S0021889808042726.

(145) Sheldrick, G. M. A Short History of {\it SHELX}. *Acta Crystallogr. Sect. A* **2008**, *64* (1), 112–122. https://doi.org/10.1107/S0108767307043930.

(146) Sheldrick, G. M. Crystal Structure Refinement with {\it SHELXL}. *Acta Crystallogr. Sect. C* **2015**, *71* (1), 3–8. https://doi.org/10.1107/S2053229614024218.

(147) Catti, L.; Kishida, N.; Kai, T.; Akita, M.; Yoshizawa, M. Polyaromatic Nanocapsules as Photoresponsive Hosts in Water. *Nat. Commun.* **2019**, *10* (1), 1–8. https://doi.org/10.1038/s41467-019-09928-x.

Section II: Study of tetraphenylethylene cyclic urea molecule for fluoride ion sensing

4.6 Introduction

Anion sensing has become a highly difficult and significant problem in a range of recent decades, including biological, medicinal, and environmental sciences.[1,2] The optical signaling unit of many chemosensors, such as those made of urea, [3–5] thiourea, [6,7] amides,[8] phenols,[9,10] pyrroles,[11] dipyrrolyl-bis-sulphonamide,[12] imidazolium salt, triazole, azide,[13] and quinoxaline[14] subunits, is covalently associated (or bonded) to a neutral receptor. These groups offer one or more donor sites for H-bonding, which are commonly used to sense anions like F^-, AcO^-, $H_2PO_4^-$, etc. However, the basicity of the anion and the H-bonding moieties have a characteristics significant impact on the sensor's selectivity. Fluoride anions (F^-) are particularly significant since they are essential in preventing tooth decay and treating osteoporosis.[15,16] Therefore, it is important to develop a perfect novel strategies for the selective detection of F^- ions. Depending on the intrinsic acidity of the H-bond donor group of the artificial receptor, fluoride ions make strong H-bonds with the NH or OH fragments of the receptor, which may result in proton transfer processes.[17–19] This is applicable for amide-, phenol-, and urea-based receptors with electron-withdrawing substituents, respectively. However, a significant difference in the optical characteristics of the chemosensor in the presence and absence of ions should be visible, either with the naked eye or under UV irradiation.

Ben Zhong Tang and his group designed and synthesized blue AIEgen using TPE **8**, which is also used to build organic light-emitting diodes and fluorine ion sensors. A blue emissive TPE derivative **8** with a high quantum yield of 64% in solid film with dimesitylboryl and fluorine groups that also demonstrate notable AIE characteristics and strong thermal stability.[20] Jiang et al.[21] developed the TPE derivative **9** (a tetraphenylethylene derivative with a pyridinium pendant and pyridinium moiety rendered MOTIPS-TPE), which had a modest emission in PBS due to its solubility in water. The triisopropylsilyl group in **9** was encouraged to cleave by the fluoride ion, and this was followed by the removal of the p-quinone-methide-generated deported TPE derivative with weak water solubility. Triggering the fluorescence to turn on toward the fluoride ion. Based on a TPE derivative **10**, Atlgan and his group[22] proposed a fluoride ion sensor in aqueous environment. Tetraphenylethylene and the pyridinium group fused together produce **10**. This article described a new method

for detecting fluoride ions using TPE-salt **10**.

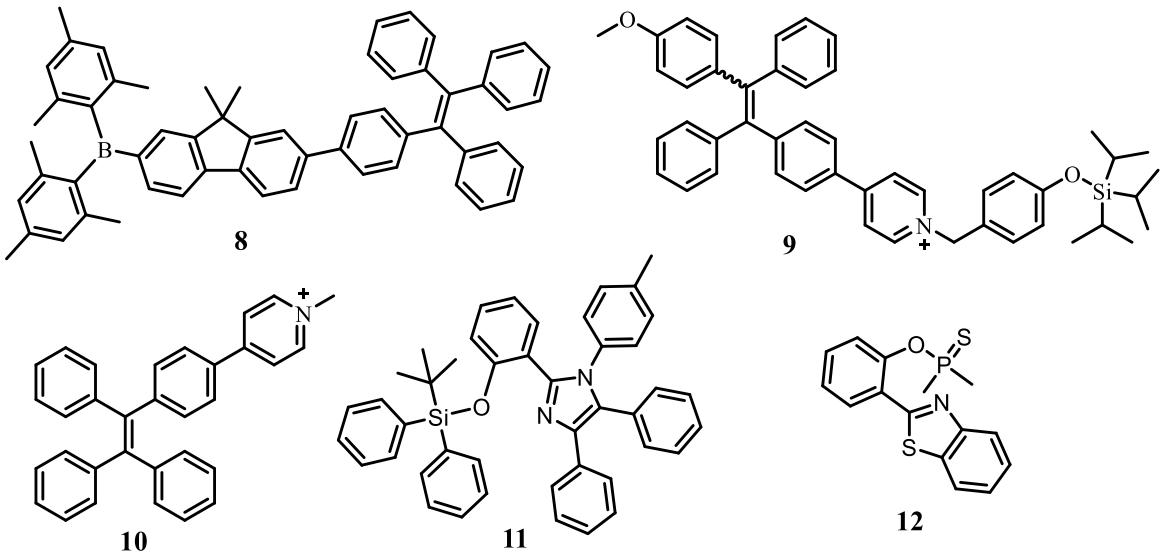

Scheme 4.6: Previously reported molecules for fluoride ion detection.

From straightforward synthetic starting materials, Kunchala[23] et al. and his coworkers rationally developed and produced a new ESIPT-based ratiometric fluorescence sensor. When the fluoride ions were added, the non-ESIPT chromophore probe **11**, which had previously produced normal Stokes shifted emission (386 nm), was transformed into the ESIPT chromophore deprotected -OH group, which produces significant Stoke's shifted emission (473 nm). Due to the great affinity of silicon towards fluoride ions, the probe **11** demonstrates high fluoride ion selectivity over a number of other anions, which were significant. In order to produce the AIE-active 2-(2'-hydroxyphenyl)benzothiazole (HBT) product, Man et al.[24] devised a fluorescence sensor **12** that takes use of the desired properties of the dimethylphosphinothionyl group as a fluoride triggering-based cleavable group. The HBT moiety's excited state intramolecular proton transfer (ESIPT) is prevented by the probe's design. The recovery of the ESIPT is achieved by removing a free HBT moiety by hydrolysis as a result of fluoride ion chemodosimetric approach to the probe.

Due to its aggregation induced emissive (AIE) behaviour[25] and absence of alternative chromophores, such as naphthalene diimide, porphyrin, etc., are frequently employed for sensing applications,[21,22,26] tetraphenylethylene (TPE) has lately been exploited as a versatile luminophores. The study's AIE-active receptors may be employed to detect fluoride ions with the naked eye. Since other receptors often only exhibit one of the two signaling qualities, the impact of selective fluoride binding may also be seen with the naked eye and optical devices. [12,18,19]

4.7 Experimental

4.7.1 Materials and Methods

^{1}H-NMR spectra were recorded on 400 MHz Bruker spectrometer and ^{13}C-NMR using 100 MHz spectrometer as DMSO-d_6 or $CDCl_3$ solutions (trimethylsilane as an internal standard). Mass spectral data were obtained using the positive ion electrospray ionization (ESI-MS) technique on an Agilent Technologies 1100 Series (Agilent Chemistation Software) mass spectrometer. High-resolution mass spectra (HRMS) were obtained by electrospray ionization quadrupole time-of-flight mass spectrometry (ESI-QTOF-MS). IR spectra were recorded on a Perkin Elmer FT-IR 400 spectrometer. UV-Vis absorption spectra were recorded by UV-Vis-1800 Shimadzu spectrophotometer and fluorescence emission measured on RF-6000 (Shimadzu, Japan) spectrofluorophotometer.

4.7.2 Synthesis of *N, N'*-di-(*tert*-butoxycarbonyl)-3,4-diaminobenzo phenone 3

This compound was prepared following a literature procedure.[16] Typically, to a stirred solution of guanidine hydrochloride (Gu.HCl, 0.27 g, 15 mmol %) in 20 mL ethanol was added di-*tert*-butyl dicarbonate (13 mL, 56.52 mmol) and (3,4-diaminophenyl)(phenyl)methanone **2** (4.0 g, 18.86 mmol). The reaction was monitored by thin layer chromatography (TLC) and upon completion, the solvent was removed by evaporation, residue was dissolved in 100 mL dichloromethane (DCM) and washed with water (2×30 mL). After separation and evaporation of the DCM, a light-yellow solid of **3** was obtained (6.5 g, yield 86%). Spectroscopic characterization of **3** perfectly matched with the reported in the literature.[16] M.P.: 137-138 ^{o}C, IR (cm^{-1}): 3303, 2983, 2938, 1730, 1703, 1641, 1516, 1244, 1145, 713. ^{1}H NMR (400 MHz, $CDCl_3$) δ ppm: 7.82 (br, s, 1H), 7.80 (d, *J* = 8.39 Hz, 1H), 7.72 (d, *J* = 7.61 Hz, 2H), 7.68 (t, *J* = 7.62 Hz, 2H), 7.56 (t, *J* = 7.61 Hz, 1H), 7.47 (dd, *J* = 8.4, 2 Hz, 1H), 7.19 (br. s, NH), 6.39 (br. s, NH), 1.45 (s, 9H), 1.43 (s, 9H). ^{13}C NMR (100 MHz, $CDCl_3$) δ ppm: 195.33, 154.25, 152.96, 137.61, 132.29, 129.92, 128.26, 81.46, 81.23, 28.24, 28.20.

4.7.3 Synthesis of 5-(1,2,2-triphenylvinyl)-1H-benzo[d]imidazol-2(3H)-one 1

Under an argon atmosphere, n-BuLi (1.6 M in hexane, 7.4 mL, 11.9 mmol) was added dropwise to a solution of diphenylmethane **4** (1.0 g, 5.95 mmol) in dry THF (50 mL) cooled to 0 ^{o}C. After stirring for 2 h at this temperature, *N,N'*-di-(*tert*-butoxycarbonyl)-3,4-diaminobenzophenone **3** (2.0 g, 4.51 mmol) in 8 mL of dry THF was added and the mixture was allowed slowly to warm at room temperature. The reaction was monitored by TLC and

quenched with 20 mL aqueous NH_4Cl solution after completion of the reaction.. Compound was extracted with DCM (3×25 mL), the solvent was removed by evaporation to give quantitative yield of compound **5**. Compound **5** (as received) was dissolved in toluene (20 mL), *p*-toluenesufonic acid (p-TSA, 0.8 g) was added and heated to 110 ^oC for 16 hr. The reaction was monitored by TLC and after complete conversion evaporated solvent to obtain crude product **6**, which was used in the next step without purification. The reaction mixture was dissolved in 10 mL DCM and added 1 mL trifluoroacetic acid dropwise at room temperature to produce 1.13 g of compound **1** (overall yield 60%). M.P. = 144 ^oC, ^1H NMR (400 MHz, DMSO-d_6) δ ppm: 7.05-7.13 (m, 9H), 6.92-6.96 (m, 6H), 6.68-6.70 (d, J = 6.48 Hz, 1H), 6.52-6.58 (m, 2H), 10.47 (s, 1H, N-H), 10.60 (s, 1H, N-H); ^{13}C NMR (100 MHz, DMSO-d_6): δ ppm:155.89, 144.05, 143.97, 143.89, 141.35, 140.18, 136.37, 131.09, 130.98, 129.54, 128.60, 128.30, 128.26, 128.23, 126.95, 126.85, 124.24, 111.39, 108.54; IR (cm^{-1}): 3641, 3125, 1711, 1602, 1508; MS-TOF Chemical Formula: $C_{27}H_{20}N_2NaO$, Exact Mass (cal.) : 411.1473, (Obs.): 411.3445. Anal. Calcd. For $C_{27}H_{20}N_2O$ C, 83.48; H, 5.19; N, 7.21; Found: C, 83.29; H, 5.21; N, 7.31.

4.7.4 UV-Vis absorption spectroscopy

The probe **1** (20 μM) was prepared in DMSO corresponding to the maximum of UV-Vis absorbance in range ~0.4 for the experiments. The solution of the probe was placed in a quartz cuvette (l = 1 cm, V_0 = 2 mL), and the various anions were added. All the UV-Vis measurements were performed at room temperature.

4.7.5 Fluorescence spectroscopy

For fluorescence emission studies, the molecule **1** was excited at 330 nm. The anion was added to a solution of probe **1** (20 μM) in DMSO. Emission spectra were recorded at room temperature, for each successful addition of anion. (slit width = 5 mm)

4.7.6 ^1H NMR spectroscopic experiments

Compound **1** (10 mg) was dissolved in DMSO-d_6 (0.4 mL) and the ^1H NMR spectrum was recorded. Thereafter, 1, 2, 3, 4 and 5 equiv. of fluoride (as its TBA salt prepared in DMSO-d_6) were added to separate solutions of **1** and the ^1H NMR spectrum recorded.

4.8 Result and Discussion

4.8.1 Synthesis of 5-(1,2,2-triphenylvinyl)-1H-benzo[d]imidazol-2(3H)-one 1

A straightforward and uncomplicated chemosensor has been successfully synthesized by

utilizing cyclic urea as a proton-transfer signaling unit for the selective detection of F^- ions. While attempting the synthesis of diamino-TPE **7** for possible purposes, the cyclic urea was accidentally discovered (**scheme 4.7**). The partly deprotected TPE derivative **6** was produced when lithium diphenylmethanide is combined with N,N'-di-(tert-butoxycarbonyl)-3,4-diamino benzophenone in presence of *p*-toluenesulfonic acid (p-TSA). Further when compound **6** was reacted with trifluoroacetic acid to complete the deprotection process, the anticipated diamino-TPE compound **7**, rather than the cyclic urea compound **1**, was produced instead.

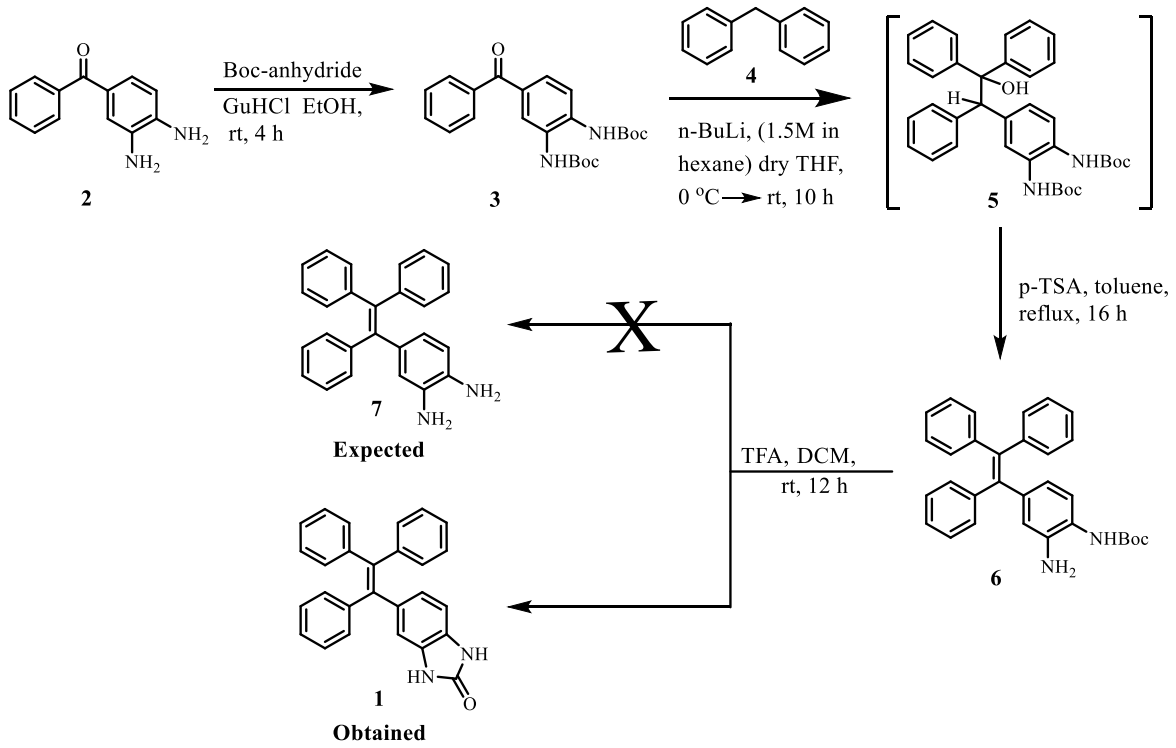

Scheme 4.7: Synthesis of the tetraphenylethylene-cyclic urea **1**.

4.8.2 Characterization of Synthesized compounds by IR, NMR and Mass spectroscopy

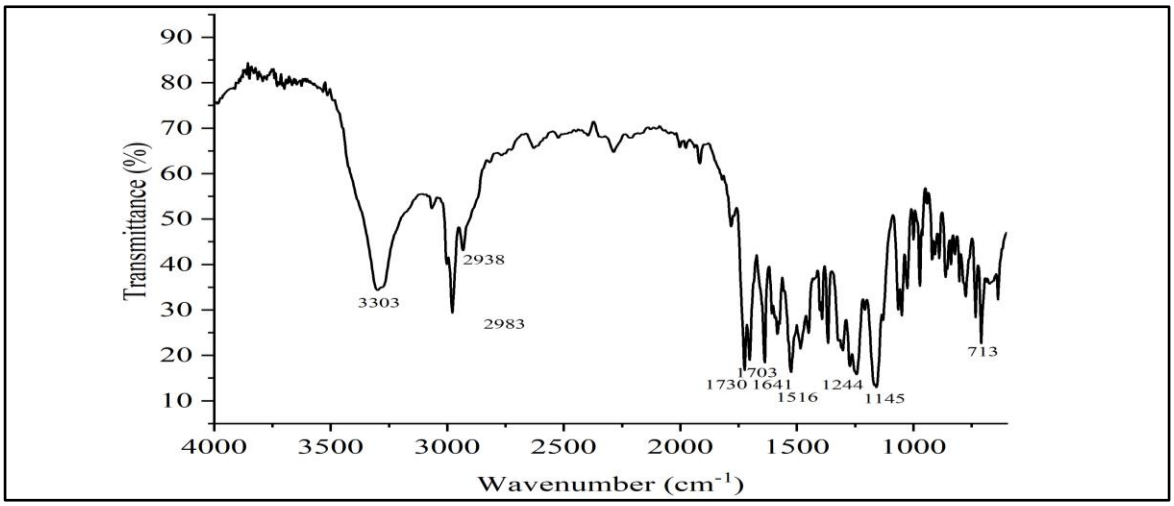

Figure 4.24: FT-IR of *N, N'*-di-(*tert*-Butoxycarbonyl)-3,4-diaminobenzophenone **3**

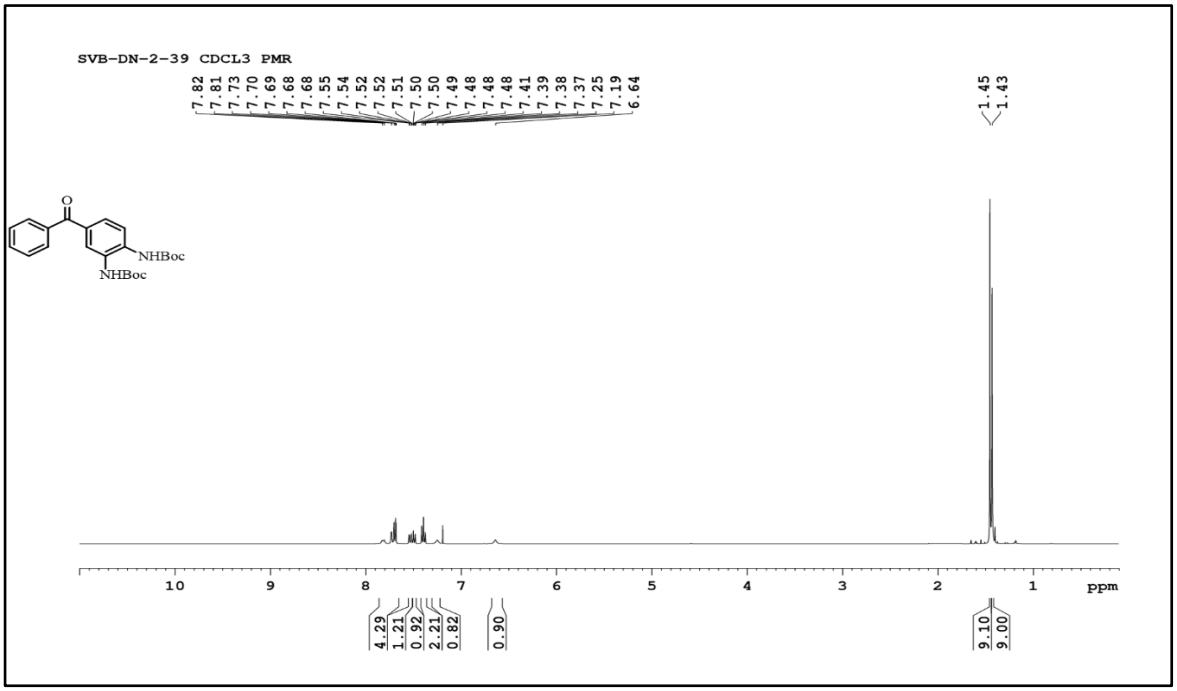

Figure 4.25: ^{1}H NMR spectrum of *N, N'*-di-(*tert*-Butoxycarbonyl)-3,4-diaminobenzophenone **3**

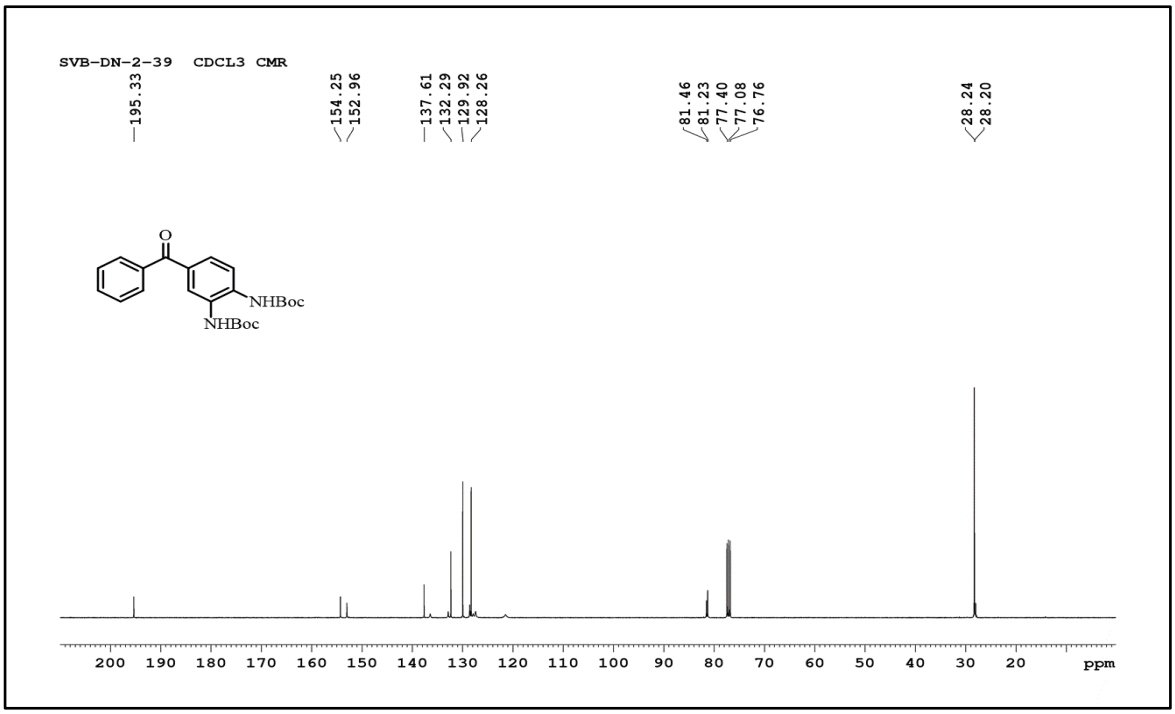

Figure 4.26: ^{13}C NMR of *N, N'*-di-(*tert*-Butoxycarbonyl)-3,4-diaminobenzophenone **3**

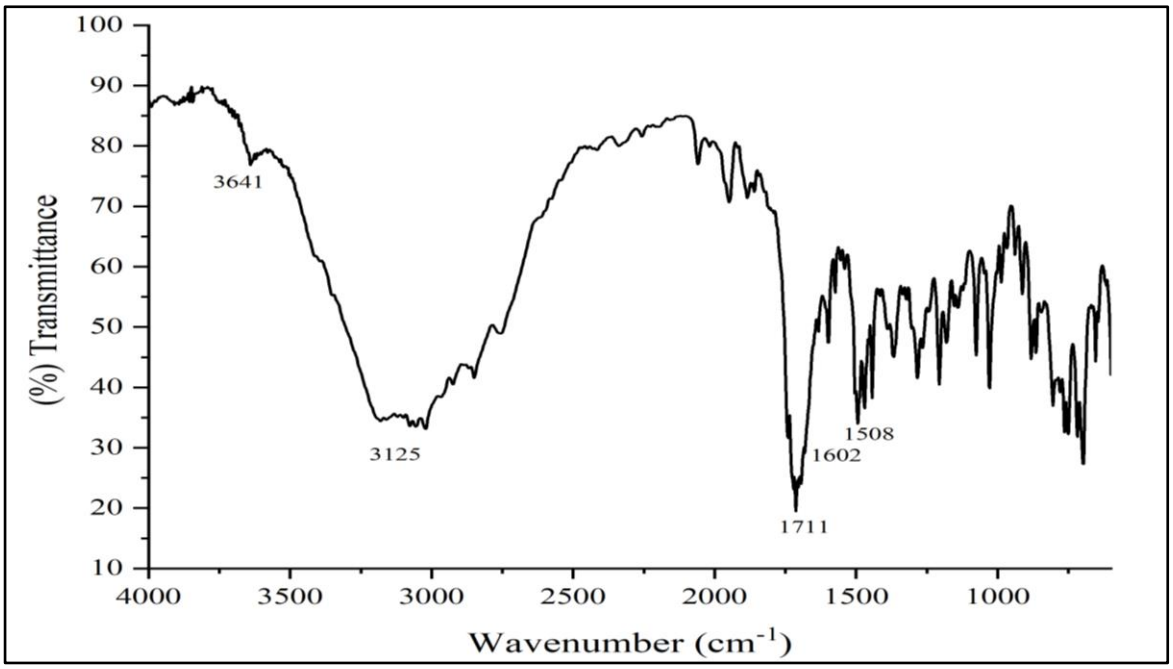

Figure 4.27: FT-IR of 5-(1,2,2-triphenylvinyl)-1H-benzo[d]imidazol-2(3H)-one **1**

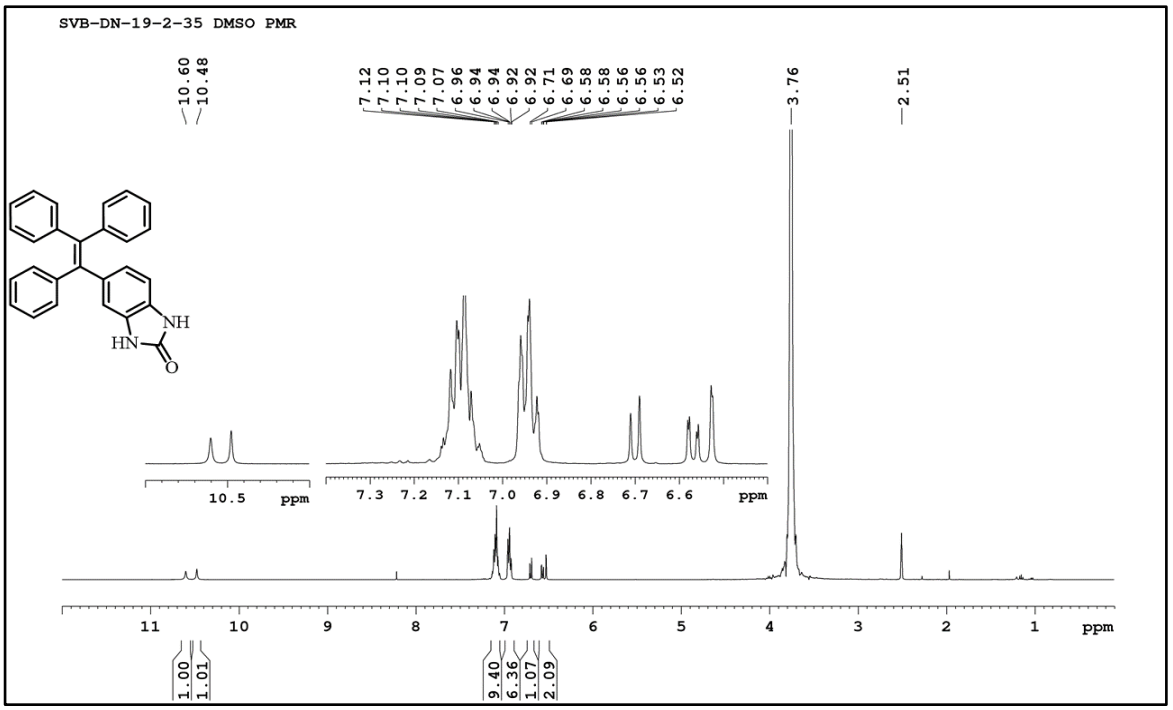

Figure 4.28: ^{1}H NMR of 5-(1,2,2-triphenylvinyl)-1H-benzo[d]imidazol-2(3H)-one **1**

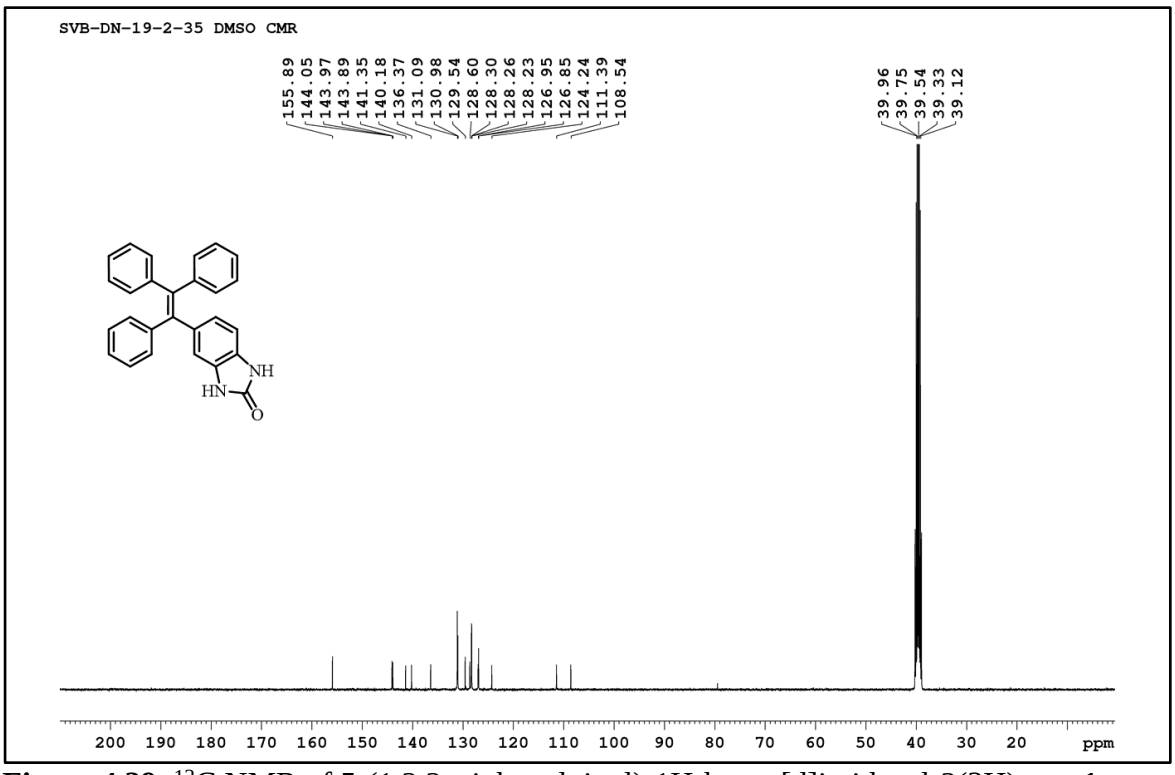

Figure 4.29: ^{13}C NMR of 5-(1,2,2-triphenylvinyl)-1H-benzo[d]imidazol-2(3H)-one **1**

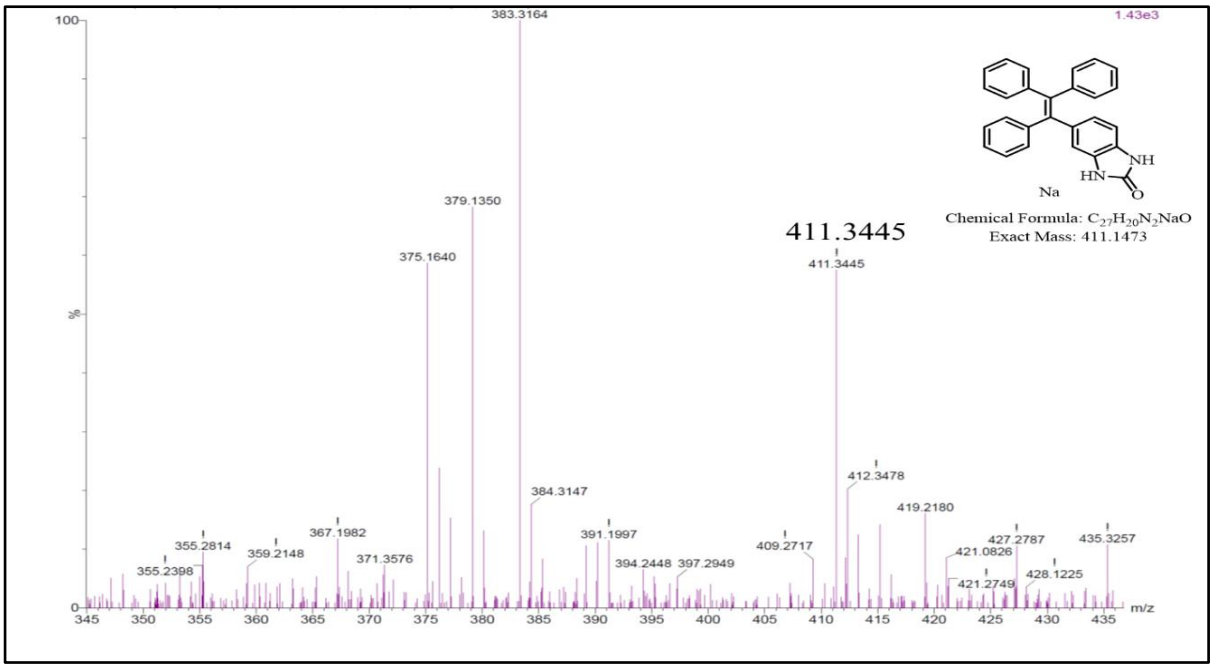

Figure 4.30: MS-TOF of 5-(1,2,2-triphenylvinyl)-1H-benzo[d]imidazol-2(3H)-one **1**

4.8.3. Mechanochromic and AIE studies of synthesized molecule 1

Compound **1** also exhibits mechanochromic luminescence with variety of colors. When **1** was in powder form, UV irradiation (365 nm) produced a sky-blue fluorescence that, after being ground with a pestle, changed to a bluish-green color. Fascinatingly, when the grounded mixture was fumed with the vapor of a polar solvent such methanol, as illustrated in **figure 4.31**, the original sky-blue colored fluorescence of **1** was regained.

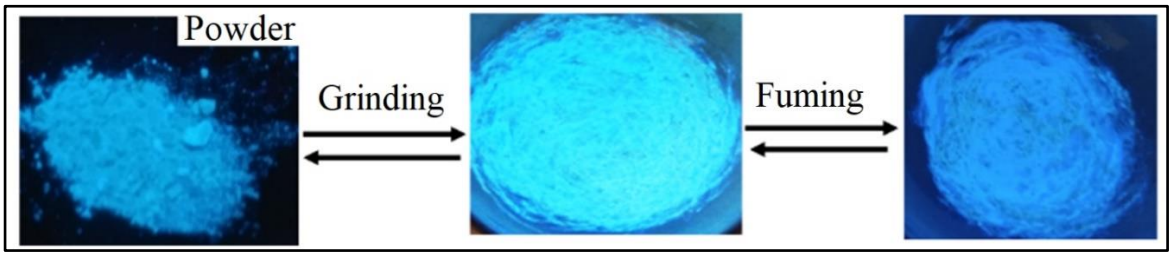

Figure 4.31: Fluorescence color changes of **1** upon grinding and fuming with methanol vapor. Images taken under UV excitation at 365 nm

4.8.4. Optical properties

Basically, receptor **1** is non-emissive in THF solution but after of addition of water resulted "turned on" in fluorescence. Therefore, Solvatochromism characteristics of receptor **1** were assessed at different water fractions (f_w). Molecule **1** is non-fluorescent at the initial water fractions from 10 to 70%, but intriguingly, it was shown to be quite emissive (λ_{max} 450 nm) at f_w = 80% (**Figure 4.32a**).

However, when f_w was raised to 99%, an emission at 465 nm with a 15 nm red-shift ensued, which is an improvement of 73 times over f_w = 0%. When estimated using Rhodamine B as a standard with Φ_F = 70% in ethanol, the quantum yield (Φ_F) of **1** in pure THF solution was 0.05%, which was increased 22-fold to 1.98 and 6.65% with f_w = 90 and 99%, respectively. Receptor **1** has lower solubility and exhibited enhanced molecular self-assembly with gradual increase in water fractions. This provided clear evidence for AIE activites of molecule **1**(**Figure. 4.32b & c**). **Figure 4.32c** illustrates how the AIE-activity of **1** may be observed with the naked eye at 365 nm when exposed to UV radiation. It is important to note that Receptor **1** partly aggregates in DMSO and emits fluorescence (Φ = 1.3%) which is equivalent to the emission generated by 90% water in THF. Molecule **1** is non-emissive in THF (Φ = 0.05%) due to its high solubility (**Figure. 4.32a**),because TPE and its derivatives are highly emissive in polar solvents, and the fluorescence emission intensity increases with increasing solvent polarity. This compound was found to be more emissive in DMSO than THF due to the relative polarity of DMSO being (0.444), which was found to be twice that of THF (0.207). The outcomes are comparable to those reported by Chen et al., who found that TPE derivatives fluoresced more strongly in DMSO than they did in DCM, ether, acetone, or DMF, respectively.[27]

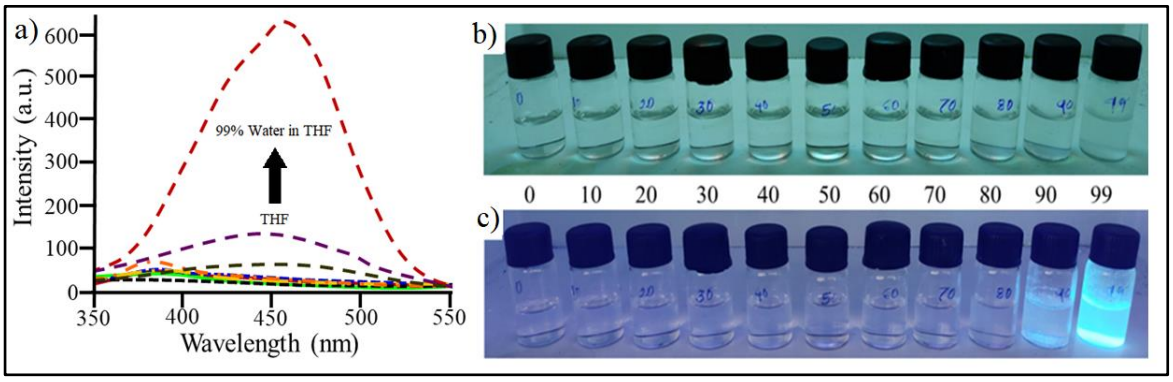

Figure 4.32: a) Fluorescence emission spectra of **1** (30 μM, λ_{ex} = 330 nm), after addition of water fraction 0-99% v/v in THF. Naked eye color changes of **1** (30 μM) after addition of water fraction 0-99% v/v in THF: b) under ambient light and c) under UV irradiation (365 nm)

Start by diluting **1** (20 μM) DMSO solutions with 5 equivalents of different anions. **Figure 4.33a** demonstrates that only the presence of the F^- ion had a notable effect on receptor **1**, causing the change in color of the solution colorless to yellow-green. None of the other anions examined had a discernible impact on the solution appearance. It is known that TPE is a AIE-active luminophores which can be observed under UV light (365 nm). Our TPE

based receptor **1** resulted decrease in fluorescence emission in the presence of F^- whereas the other anions did not exhibit any impact (**Fig. 4.33b**).

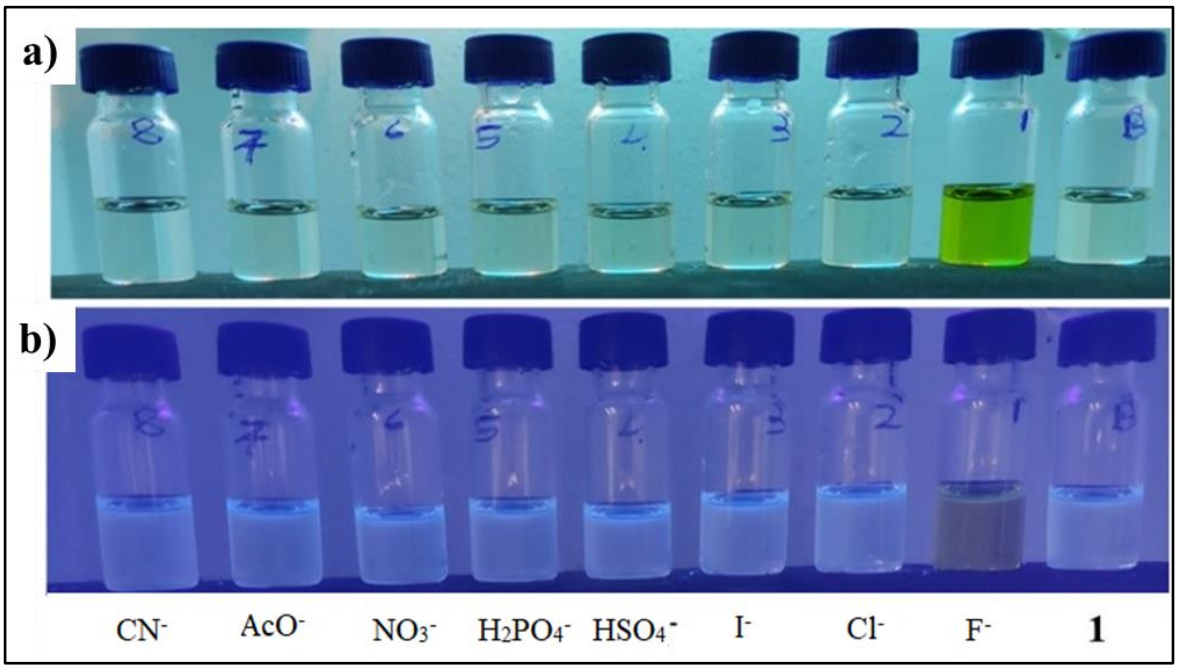

Figure 4.33: Solutions of **1** (20 μM) in DMSO upon addition of 5 equiv. of CN^-, AcO^-, NO_3^-, $H_2PO_4^-$, HSO_4^-, I^-, Cl^-, F^-, and only 1 without any anions: a) under ambient light and b) under UV light 365 nm.

Since, it was found that **1** was not highly soluble in several popular organic solvents, such as $CHCl_3$, CH_2Cl_2 and CH_3CN, DMSO was chosen for further investigation. During the process of analyzing receptor **1**, rapid color change was observed on addition of fluoride ions, these interesting results led us to carry out its further study Several anions were used in the form of their tetrabutylammonium (AcO^-, NO_3^-, $H_2PO_4^-$, HSO_4^-, I^-, Cl^- and F^-) or tetraethylammonium (CN^-) salts for the anion-detection studies of chemosensor **1**.

4.8.5. UV-Vis absorption and ^{1}H-NMR titration

The qualitative analysis for sensing properties of receptor **1** were demonstrated with UV-Vis absorption spectroscopy. **Figure 4.34a** represents the UV-Vis absorption spectra of a 20 μM solution of receptor **1** in DMSO, which typically showed a very high absorption band at 330 nm. Even at high concentrations of anion, the UV-Vis absorption spectra of **1** in the presence of CN^-, AcO^-, NO_3^-, $H_2PO_4^-$, HSO_4^-, I^- and Cl^- (as its TBA salts, with the exception of CN^- employed as TEA salt) did not show observable differences (up to 100 equiv.) A band at 385 nm and a new peak at 290 nm (presumably connected to intermolecular

hydrogen bond interactions) were first seen in the spectra of **1** following the addition of 5 equiv. of F- ion, which is an important red-shift of 55 nm for the peak maxima (as its TBA salt). The titration experiments were performed with recording UV-Vis. absorption spectra, to study the interaction of **1** (20 μM) in DMSO with the fluoride ion (**Fig 4.34b**). It can be observed that the absorbance of maximum absorption band was gradually decreasing with successive addition of fluoride ions from 0 to 2.0 equivalents and started reaching to maximum with increasing addition of F^-, ranging from 2.5 to 5.0 equivalents. At the same time new band was appearing at wavelength of 385 nm during addition of fluoride ions. . Accordingly, we proposed at first, the F^- ions bind to receptor **1** and disrupt the intermolecular H-bonding between nearby molecules. The band at 385 nm achieves a peak with a distinct isosbestic point at 355 nm upon subsequent addition of F^- ions, resulted in the appearance of new band at 385 nm. Similarly, PMR spectroscopic titrations were carried out in DMSO-d_6 solvent for verification of complex formation of receptor **1** with F^- ions. The two N-H protons of receptor **1** appeared at 10.52 and 10.61 ppm, as illustrated in **Figure 4.34c**. The resonance peaks observed to be broadened and became less powerful with the addition of 2.0 equiv. of F- ions, but continuous addition up to 5.0 equivalents resulted entire diminishing of N-H proton peaks

These results are in agreement with the UV-Vis absorption spectroscopic data wherein, the first equivalent of F^- ion forms H-bond with the N-H group in **1**·Furtheraddition of fluoride ions results in two hydrogen bifluoride ions forming complex with **1**. This proves that the formation of hydrogen bifluoride ion, $[FHF]^-$. In Addition to this broadening of the peaks and absence of the N-H resonances was observed with the appearance of a new broad peak at 16.46**(Fig. 4.35)**.[28,29]

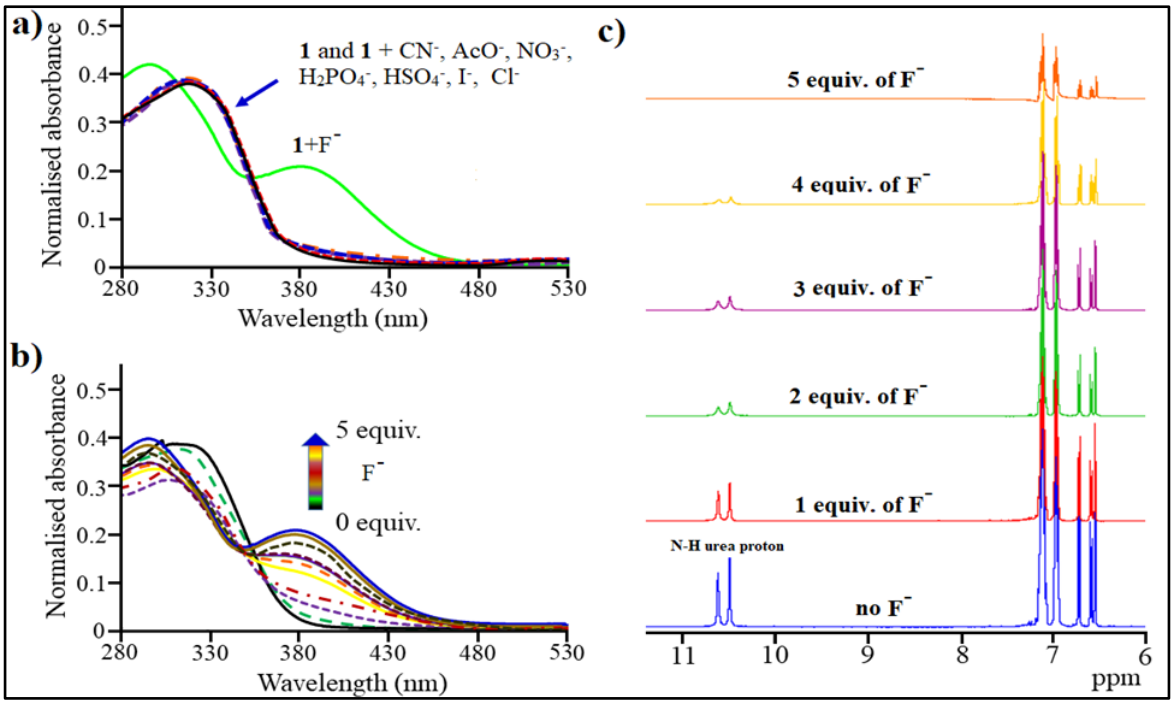

Figure 4.34: a) UV-Vis spectra of **1** (20 μM) in DMSO and addition of 5 equi. of various anions, such as CN^-, AcO^-, NO_3^-, $H_2PO_4^-$, HSO_4^-, I^-, Cl^- and F^- (as their TBA salts except for CN^-, which was a TEA salt). b) UV-Vis spectra of **1** (20 μM) in DMSO with gradual addition of 0-5 equiv. of fluoride ion and, c) ^1H NMR spectra of **1** in DMSO-$d_6$with successive addition of 0 to 5 equi. of fluoride ions, respectively.

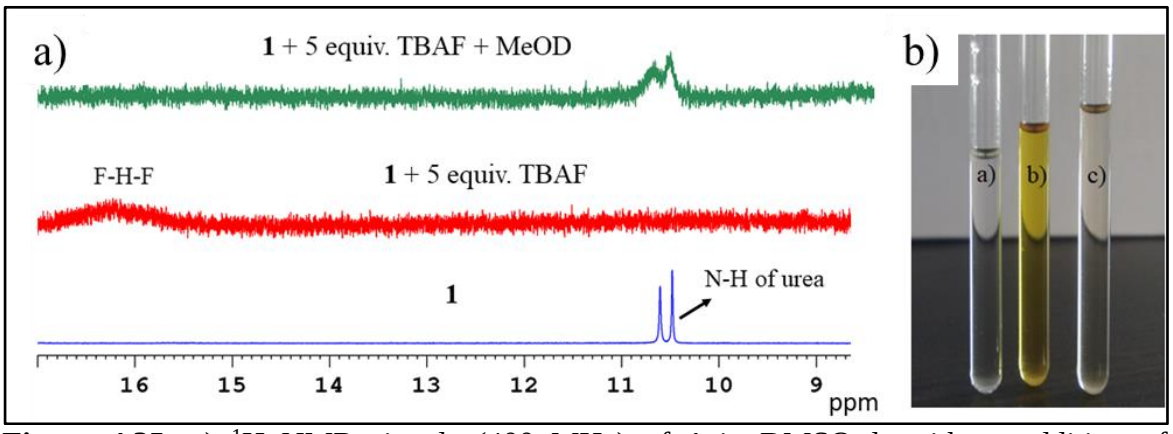

Figure 4.35: a) ^1H NMR signals (400 MHz) of **1** in DMSO-d_6 without addition of tetrabutylammonium fluoride (TBAF) (bottom) and with TBAF (middle) and upon addition of methanol (top) and b) shows respective images of NMR tube as: a) only compound **1** (30 μm) in DMSO-d_6, b) with addition of TBAF (5 equiv.) and c)with addition of MeOD, respectively.

The development of the hydrogen-bonding complex of the fluoride ion with urea, i.e. HF_2^-, was linked to the elimination of the N-H proton resonances in the ^1H NMR spectrum of the

cyclic urea. Interestingly, the addition of a polar solvent (methanol) to the complex of **1**-F^- resulted the confirmation of reversible anion sensing. Finally, in order to develop practical applications a strip test was carried out with the chemosensor **1** for selective sensing of fluoride ions.

4.8.6. Fluorescence properties

Fluorescence emission spectroscopy was used to get a detailed understanding of the optical characteristics of **1** in presence of different anions. **Figure 4.36** is representation of the fluorescence emission spectra of receptor **1** in DMSO solvent (20 μM) exhibited a prominent band at 445 nm (λ_{ex} = 330 nm, with quantum yield = Φ = 1.3), whose intensity was markedly reduced and red-shifted by 80 nm with the addition of fluoride ions (Φ = 0.07). On the other hand, the addition of CN^-, AcO^-, NO_3^-, $H_2PO_4^-$, HSO_4^-, I^-, Cl^-, OH^-, ClO_4^- and SCN^-, did not result in change of fluorescence intensity. The shift with rapid quenching of the fluorescence is clearly seen with progressive addition of F^- (0-5 equiv. λ_{ex} = 330 nm) in DMSO to assess the selectivity of receptor **1** for F- ion (**Fig. 4.36b**). The preferential interaction of receptor **1** to F^- via the strong hydrogen bonding with the urea N-H is determined from this experiment and confirmed by the UV-Vis measurements (**Fig. 4.34a&b**) and ^{1}H NMR spectroscopy (**Fig. 4.34c**).

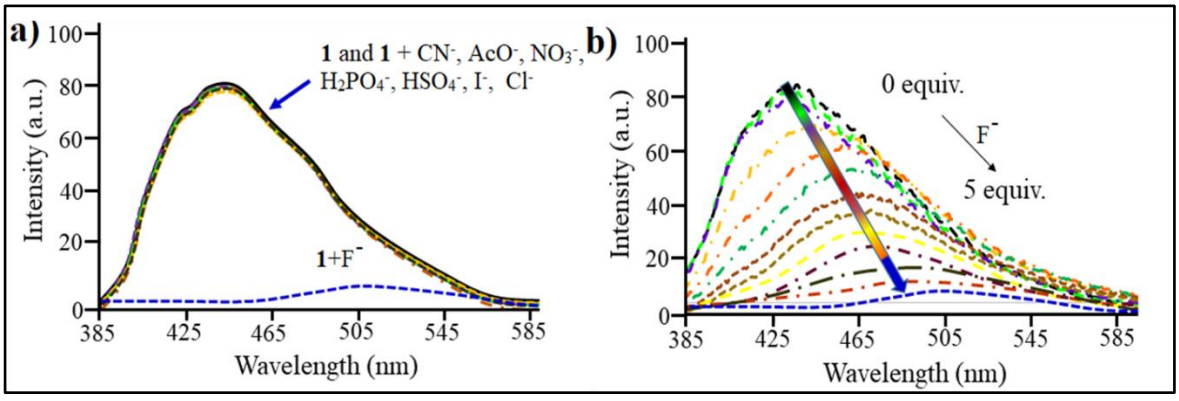

Figure 4.36: a) Fluorescence emission spectra of **1** in DMSO (20 μM, λ_{ex} = 330 nm) after addition of different anions (as TBA salts), and b) fluorescence titration spectra of **1** in DMSO (20 μM, λ_{ex} = 330 nm) with gradual addition of F^- (0-5 equiv.)

The polar protic solvent methanol was added to a solution of **1**-F^- to further demonstrate that the detection of fluoride ion by receptor **1** was accomplished by strong hydrogen bonding with N-H groups. The solution's rapid recovery to its former bluish hue and immediate recovery of the fluorescence (**Fig. 4.37a**) were evidence that the reverse situation protonation of **1**-F^- by methanol had taken place. The continuous variation approach of the

Job's plot was employed to estimate the binding stoichiometry of the final complex between **1** and F^- (**Fig. 4.37b**). With a constant increase in the molar fraction of receptor **1**, the final concentration of receptor **1** and F^- was maintained at 50 μM. With regard to receptor **1** and F^-, the strong peak confirms that the dominating species is the 1:2 complex, which is consistent with the titration results from the UV-Vis, ^1H NMR, and fluorescence spectroscopy techniques. In order to confirm the high selectivity of receptor **1** at low F^- concentrations in DMSO, the association constant (K) of receptor **1** for F^- ions was calculated from the fluorescence titration experiments and was to be 4.90×10^8 M^{-2} (**Fig. 4.36b** and **Fig. 4.38**), and the detection limit (LOD), calculated using 3/σ formula, was 30 μM.[30]

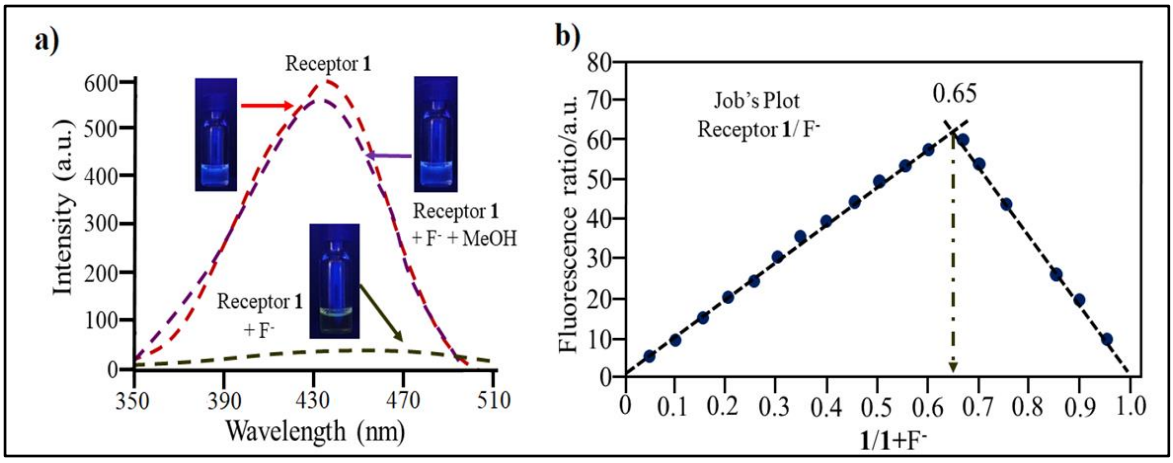

Figure 4.37: a) Fluorescence emission spectra of **1** (30 μM, λ_{ex} = 330 nm), after the addition of F^- (10 equiv.) and addition of methanol to complex **1**-F^- in DMSO, and b) Job′s plot for the association of **1** with F^- in DMSO.

4.8.7. The Benesi–Hildebrand analysis

$$\mathbf{1}/F\text{-}F_{min} = \mathbf{1}/K_a.(F_{max}\text{-}F_{min}).[F^-]^2 + \mathbf{1}/F_{max}\text{-}F_{min} \quad \text{---------- (1)}$$

Above equation (1) is used to calculate the binding strength based on the 1: 2 stoichiometry of **1** with F^-. The plot of $\mathbf{1}/[F\text{-}F_{min}]$ against $\mathbf{1}/[F^-]^2$ is found to be linear(**Figure 4.38**). From the Benesi–Hildebrand analysis, the association constant is determined to be $4.90\times10^8 M^{-2}$ where,F_{min} and F are the fluorescence intensity of receptor **1** in the absence and presence of fluoride anion, respectively. K_a is the association constant of the F^- complex of **1**, F_{max} the fluorescence intensity obtained with a large excess of F^-, and $[F^-]$ is the concentration of F^-.

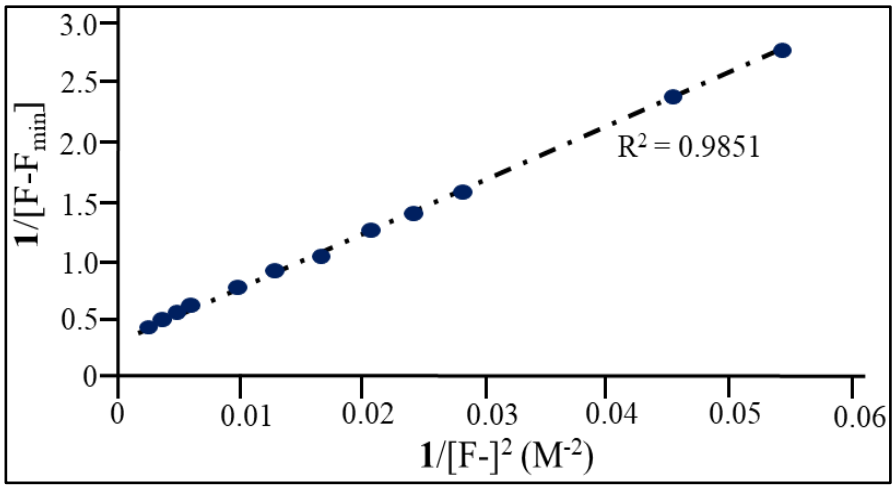

Figure 4.38: The Benesi-Hildebrand plot of **1**/[F-Fmin] against **1**/[F^-].

4.8.8 Acid-Base effect and strip-based sensing

When the deprotonation and protonation effects were examined in the presence of NaOH and HCl, it was found that the earlier happened with NaOH and the latter occurred with the acid, i.e. HCl (**Fig. 4.39**). Additionally, when confirmed by ^{1}H NMR, deprotonation was seen after the addition of NaOH (0.1 M) and that the addition of HCl restored the proton signal of N-H to its original position **1**. (**Fig. 4.40**). As anticipated, only minor alteration was seen in the UV-Vis and fluorescence spectra, leading us to believe that structurally TPE core is unaffected by the deprotonation of the N-H of urea with base. However, ^{1}H NMR (**Fig. 4.40**) demonstrated complete deprotonation in the presence of base and reverse with HCl.

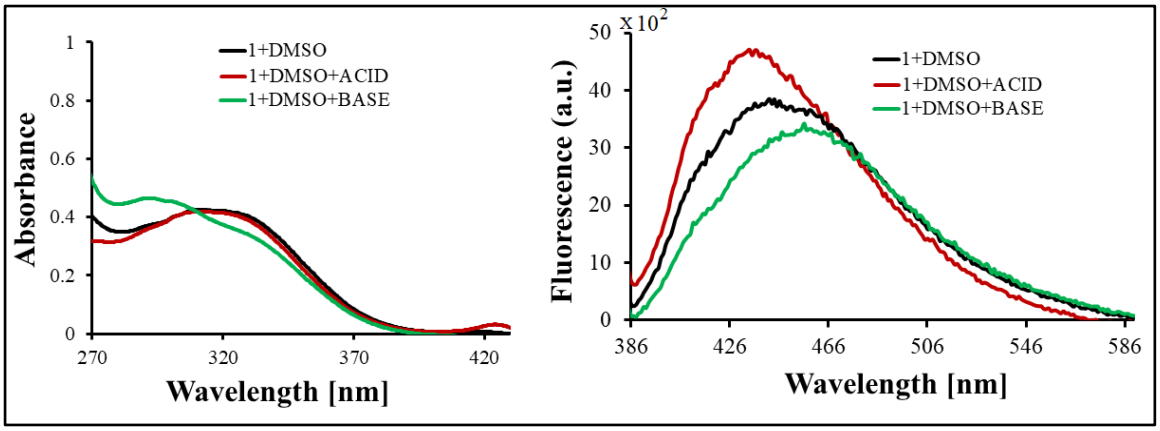

Figure 4.39: Molecule**1** (20 μm) in the presence of acid (HCl) and base (NaOH) showing deprotonation and protonation effect of the cyclic urea.

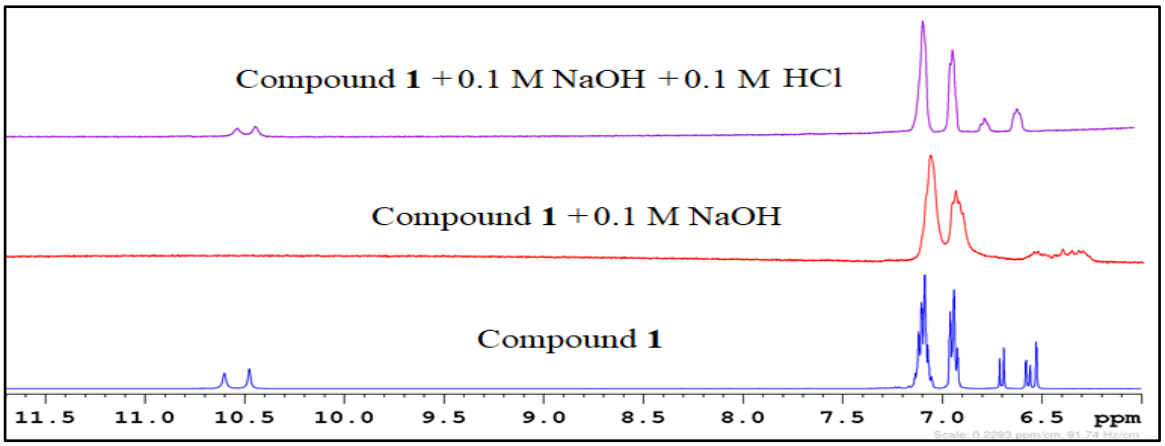

Figure 4.40: ^{1}H NMR of **c**ompound **1** (20 μm) in the presence of acid and base showing deprotonation and protonation effect of the cyclic urea.

Further, an easy strip-based sensor was built, as shown in **Figure 4.41,** which clearly illustrates that, when the strip is submerged in fluoride solution, the fluorescence emission of receptor **1** is quenched under UV irradiation (365 nm), whereas solutions of other anions have no impact. As a result, this experiment unequivocally shows how useful receptor **1** is for the specific detection of fluoride anion.

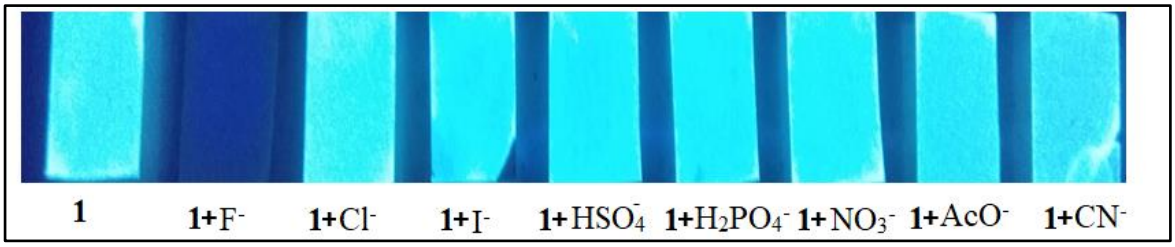

Figure 4.41: Strip based selective detection of fluoride anion, over other anions.

4.9 Conclusion

In conclusion, the novel cyclic-urea-based receptor **1** was designed and synthesized, and its potential for use in AIE activity and anion sensing was studied. It has been demonstrated that Receptor 1 is very selective for the detection of fluoride anions. UV-Vis absorption spectroscopy, a drop in fluorescence, and strip-based sensing were used to establish the selective and sensitive detection of fluorides anion over other anions, such as CN^-, AcO^-, NO_3^-, $H_2PO_4^-$, HSO_4^-, I^-, OH^-, ClO_4^-, SCN^- and Cl^-. As a result, this give new idea that these particular cyclic urea derivatives may have useful practical uses in both sensing and the development of solid-state fluorescence devices. Therefore, believe that, this particular type of cyclic urea receptor and others like it may have useful applications in the future.

References

(1) Martínez-Máñez, R.; Sancenón, F. *Fluorogenic and Chromogenic Chemosensors and Reagents for Anions*; 2003; Vol. 103. https://doi.org/10.1021/cr010421e.

(2) Gale, P. A.; Caltagirone, C. Anion Sensing by Small Molecules and Molecular Ensembles. *Chem. Soc. Rev.* **2015**, *44* (13), 4212–4227. https://doi.org/10.1039/c4cs00179f.

(3) Jose, D. A.; Kumar, D. K.; Ganguly, B.; Das, A. Efficient and Simple Colorimetric Fluoride Ion Sensor Based on Receptors Having Urea and Thiourea Binding Sites. *Org. Lett.* **2004**, *6* (20), 3445–3448. https://doi.org/10.1021/ol048829w.

(4) Esteban-Gómez, D.; Fabbrizzi, L.; Licchelli, M. Urea Fra Oversigt. *J. Org. Chem.* **2005**, *70*, 5717–5720.

(5) Kassl, C. J.; Christopher Pigge, F. Anion Detection by Aggregation-Induced Enhanced Emission (AIEE) of Urea-Functionalized Tetraphenylethylenes. *Tetrahedron Lett.* **2014**, *55* (34), 4810–4813. https://doi.org/10.1016/j.tetlet.2014.06.115.

(6) Sahu, S.; Sikdar, Y.; Bag, R.; Maiti, D. K.; Cerón-Carrasco, J. P.; Goswami, S. Visual Detection of Fluoride Ion Based on ICT Mechanism. *Spectrochim. Acta - Part A Mol. Biomol. Spectrosc.* **2019**, *213*, 354–360. https://doi.org/10.1016/j.saa.2019.01.073.

(7) Samanta, S.; Manna, U.; Ray, T.; Das, G. An Aggregation-Induced Emission (AIE) Active Probe for Multiple Targets: A Fluorescent Sensor for Zn2+ and Al3+ & a Colorimetric Sensor for Cu2+ and F-. *Dalt. Trans.* **2015**, *44* (43), 18902–18910. https://doi.org/10.1039/c5dt03186a.

(8) Gale, P. A.; Camiolo, S.; Chapman, C. P.; Light, M. E.; Hursthouse, M. B. Hydrogen-Bonding Pyrrolic Amide Cleft Anion Receptors. *Tetrahedron Lett.* **2001**, *42* (30), 5095–5097. https://doi.org/10.1016/S0040-4039(01)00896-6.

(9) Aiken, K.; Bunn, J.; Sutton, S.; Christianson, M.; Winder, D.; Freeman, C.; Padgett, C.; McMillen, C.; Ghosh, D.; Landge, S. Nuclear Magnetic Resonance Spectroscopy Investigations of Naphthalene-Based 1,2,3-Triazole Systems for Anion Sensing. *Magnetochemistry* **2018**, *4* (1), 1–18. https://doi.org/10.3390/magnetochemistry4010015.

(10) Schramm, A. D. S.; Nicoleti, C. R.; Stock, R. I.; Heying, R. S.; Bortoluzzi, A. J.; Machado, V. G. Anionic Optical Devices Based on 4-(Nitrostyryl)Phenols for the

Selective Detection of Fluoride in Acetonitrile and Cyanide in Water. *Sensors Actuators, B Chem.* **2017**, *240*, 1036–1048. https://doi.org/10.1016/j.snb.2016.09.052.

(11) Wang, Q.; Xie, Y.; Ding, Y.; Li, X.; Zhu, W. Colorimetric Fluoride Sensors Based on Deprotonation of Pyrrole-Hemiquinone Compounds. *Chem. Commun.* **2010**, *46* (21), 3669–3671. https://doi.org/10.1039/c001509a.

(12) Ghule, N. V.; Bhosale, S. V.; Bhosele, S. V. Dipyrrolyl-Bis-Sulfonamide Chromophore Based Probe for Anion Recognition. *RSC Adv.* **2014**, *4* (52), 27112–27115. https://doi.org/10.1039/c4ra04000g.

(13) Chahal, M. K.; Dar, T. A.; Sankar, M. Facile Synthesis of Functionalized Urea, Imidazolium Salt, Azide, and Triazole from a 2-Amino-5,7-Dimethyl-1,8-Naphthyridine Scaffold and Their Utilization in Fluoride Ion Sensing. *New J. Chem.* **2018**, *42* (12), 10059–10066. https://doi.org/10.1039/c8nj00503f.

(14) Dey, S. K.; Al Kobaisi, M.; Bhosale, S. V. Functionalized Quinoxaline for Chromogenic and Fluorogenic Anion Sensing. *ChemistryOpen* **2018**, *7* (12), 934–952. https://doi.org/10.1002/open.201800163.

(15) Gold, M. R. Biochemistry Of. **1994**, *55* (CaF 2), 1–12.

(16) Kirk, K. L. Biochemistry of Inorganic Fluoride. *Biochem. Elem. Halogens Inorg. Halides* **1991**, *3* (CaF 2), 19–68. https://doi.org/10.1007/978-1-4684-5817-6_2.

(17) Zhou, Y.; Zhang, J. F.; Yoon, J. Fluorescence and Colorimetric Chemosensors for Fluoride-Ion Detection. *Chem. Rev.* **2014**, *114* (10), 5511–5571. https://doi.org/10.1021/cr400352m.

(18) Rivadehi, S.; Reid, E. F.; Hogan, C. F.; Bhosale, S. V.; Langford, S. J. Fluoride-Selective Optical Sensor Based on the Dipyrrolyl- Tetrathiafulvalene Chromophore. *Org. Biomol. Chem.* **2012**, *10* (4), 705–709. https://doi.org/10.1039/c1ob06459b.

(19) Bhosale, S. V.; Bhosale, S. V.; Kalyankar, M. B.; Langford, S. J. A Core-Substituted Naphthalene Diimide Fluoride Sensor. *Org. Lett.* **2009**, *11* (23), 5418–5421. https://doi.org/10.1021/ol9022722.

(20) Li, Y.; Zhuang, Z.; Lin, G.; Wang, Z.; Shen, P.; Xiong, Y.; Wang, B.; Chen, S.; Zhao, Z.; Tang, B. Z. A New Blue AIEgen Based on Tetraphenylethene with Multiple Potential Applications in Fluorine Ion Sensors, Mechanochromism, and Organic Light-Emitting Diodes. *New J. Chem.* **2018**, *42* (6), 4089–4094. https://doi.org/10.1039/c7nj04742h.

(21) Jiang, G.; Liu, X.; Wu, Y.; Wang, J.; Dong, X.; Zhang, G.; Li, Y.; Fan, X. An AIE

Based Tetraphenylethylene Derivative for Highly Selective and Light-up Sensing of Fluoride Ions in Aqueous Solution and in Living Cells. *RSC Adv.* **2016**, *6* (64), 59400–59404. https://doi.org/10.1039/c6ra10878d.

(22) Bineci, M.; Baɨlan, M.; Atilgan, S. AIE Active Pyridinium Fused Tetraphenylethene: Rapid and Selective Fluorescent "Turn-on" Sensor for Fluoride Ion in Aqueous Media. *Sensors Actuators, B Chem.* **2016**, *222*, 315–319. https://doi.org/10.1016/j.snb.2015.08.087.

(23) Dhanunjayarao, K.; Mukundam, V.; Venkatasubbaiah, K. A Highly Selective Ratiometric Detection of F-Based on Excited-State Intramolecular Proton-Transfer (Imidazole) Materials. *J. Mater. Chem. C* **2014**, *2* (40), 8599–8606. https://doi.org/10.1039/c4tc01711k.

(24) Du, M.; Huo, B.; Li, M.; Shen, A.; Bai, X.; Lai, Y.; Liu, J.; Yang, Y. A "Turn-On" Fluorescent Probe for Sensitive and Selective Detection of Fluoride Ions Based on Aggregation-Induced Emission. *RSC Adv.* **2018**, *8* (57), 32497–32505. https://doi.org/10.1039/c8ra06774k.

(25) La, D. D.; Bhosale, S. V.; Jones, L. A.; Bhosale, S. V. Tetraphenylethylene-Based AIE-Active Probes for Sensing Applications. *ACS Appl. Mater. Interfaces* **2018**, *10* (15), 12189–12216. https://doi.org/10.1021/acsami.7b12320.

(26) Simsek Turan, I.; Pir Cakmak, F.; Sozmen, F. Highly Selective Fluoride Sensing via Chromogenic Aggregation of a Silyloxy-Functionalized Tetraphenylethylene (TPE) Derivative. *Tetrahedron Lett.* **2014**, *55* (2), 456–459. https://doi.org/10.1016/j.tetlet.2013.11.059.

(27) Chen, Q.; Jia, C.; Zhang, Y.; Du, W.; Wang, Y.; Huang, Y.; Yang, Q.; Zhang, Q. A Novel Fluorophore Based on the Coupling of AIE and ESIPT Mechanisms and Its Application in Biothiol Imaging. *J. Mater. Chem. B* **2017**, *5* (37), 7736–7742. https://doi.org/10.1039/c7tb02076g.

(28) Christe, K. O.; Wilson, W. W. Reaction of the Fluoride Anion with Acetonitrile. Chloroform and Methylene Chloride. *J. Fluor. Chem.* **1990**, *47* (1), 117–120. https://doi.org/10.1016/S0022-1139(00)80453-4.

(29) Fujiwara, F. Y.; Martin, J. S. The Heterobihalide Ions. Nuclear Magnetic Resonance Spectroscopy of Strong Hydrogen Bonds. *J. Am. Chem. Soc.* **1974**, *96* (25), 7625–7631. https://doi.org/10.1021/ja00832a005.

(30) Ma, Q. J.; Zhang, X. B.; Zhao, X. H.; Jin, Z.; Mao, G. J.; Shen, G. L.; Yu, R. Q. A Highly Selective Fluorescent Probe for Hg2+ Based on a Rhodamine-Coumarin

Conjugate. *Anal. Chim. Acta* **2010**, *663* (1), 85–90. https://doi.org/10.1016/j.aca.2010.01.029.

Section III: Study of tetraphenylethylene derivative bearing thiophenylbipyridine moiety for sensing of copper (II) ion

4.10 Introduction

One of the most significant metals used in both domestic and commercial applications is copper.[1] Copper is the third most prevalent metal ion in all living things among transition metals.[2] Through the copper cycle, elemental copper plays a critical role in the basic physiological processes in biological, environmental, and chemical systems.[3,4] Additionally, copper is a critical component of vital biological functions including respiration,[5] DNA synthesis, and metabolism at ideal concentrations. But both an abundance and a lack of copper can cause a number of illnesses, including neurological problems, Wilson disease (WD), Menkes disease (MD), haematological manifestations, kidney and liver damage, among others.[6–12] The World Health Organization (WHO) recommends a 2-ppm upper limit for Cu^{2+} ions in drinking water.[13,14] Therefore, it is relatively challenging to create a highly effective and straightforward technique of preference for Cu^{2+} ion detection with high selectivity and sensitivity in environmental and biological materials. Over time, a number of analytical methods for the detection of Cu^{2+} metal ions were developed, including atomic absorption spectroscopy(AAS),[15] cathodic stripping voltammetry(CSV),[16] inductively coupled plasma-mass microscopy(ICP-MS),[17] surface enhanced Raman spectroscopy(SERS),[18] liquid chromatographic mass spectrometry(LCMS),[19] and nuclear quadrupole resonance(NQR),[20] and energy dispersive X-ray diffraction(EDS).[21] These techniques have a number of flaws, including the need for handling expensive devices, transportation, and inability to be applied to real-world live monitoring scenarios. Researchers have designed fluorescent chemosensors that can be turned on or off to get around these constraints.[22] Due to their great selectivity, sensitivity, and operational simplicity, these approaches are simple to use, affordable, and allow for immediate reaction. Therefore, researchers are interested in developing colorimetric and fluorescent techniques with excellent selectivity and sensitivity for the detection of Cu^{2+} ions. According to a review of the literature, several small organic molecules have been successfully developed into colorimetric and fluorescence sensors, including pyrene,[23] anthracene,[24] 1,8-naphthalimide,[25] rhodamine B,[26] amino-functionalized zirconium MOF,[27] bis(N-methylindolyl)methane,[28] triarylamine-based dendrimer,[29] coumarin derivative,[30,31] 1,3,5-triphenylbenzene,[32] and princer type.[33] A significant issue still exists in the availability of

such synthesised fluorophores and their selectivity towards the Cu^{2+} ion in the presence of other interfering metal ions with poor detection limits.[34] Due to their superior selectivity, sensitivity, and ease of analysis, aggregation induced emission (AIE) properties of tetraphenylethylene (TPE) based sensor materials have attracted significant interest in recent years for the detection of metal ions in biological and environmental systems. Due to their AIE properties,[35–41] TPE derivatives are the most common chromophore to investigate for the complexation with metal ions.[38,42] An elegant method to create new chromophores for metal ions detection is to functionalize the TPE molecular structure with pendent coordinating sites for metal ions.[38,42] The interaction between the receptor sites for the chromophore and the analytes determines the detection effectiveness of the TPE, which is reliant on its AIE features.[43] TPE and other AIE derivatives, for instance, have been shown to be used for the detection of Cu^{2+} ions.[44–46] It's noteworthy to note that because chromophores attached to terpyridine have strong binding affinities for transition metal ions, they have attracted a lot of interest.[47–51] For metal ion sensors, it surprises us that bithiophenepyridine and thiophenylbipyridine attached chromophores are rarely studied.[52,53] With all of these details in mind, the primary objective of our research was to examine the association between transition metal ions and TPE sensors with thiophenylbipyridine attached.

The synthesis and characterization of TPE **1**, which has a pendant thiophenylbipyridine receptor site, are discussed in this part with the goal of examining a highly effective, sensitive, and selective chemosensor for the detection of the Cu^{2+} ion. The sensing mechanism of **1** towards the Cu^{2+} ion is based on the photo induced electron transfer (PET) "off-on," in contrast to the reported chemosensors. The capacity of TPE-subunit to donate electrons is improved when probe **1** coordinates with Cu^{2+} ions, leading to a considerable reduction in absorption peak intensity and enabling the colorimetric detection of Cu^{2+} with the naked eye. Cu^{2+} ion complexation with **1** causes fluorescence quenching concurrently, making **1** a PET Cu^{2+} "turn-off" sensor.

4.11 Experimental

4.11.1 Material and Methods

Compounds **4** and **6** were prepared using methods described in the literature,[54] while compound **1** was synthesized via the reaction of compound **8** with the pyrindine salt **9** in the presence of acetate of ammonium. Different metal ions and Acetonitrile were acquired from Spectrochem and TCI. Copper perchlorate salt is made from Cu^{2+}, while Zn^{2+} Pb^{2+}, Ni^{2+},

Mg^{2+} and Ag^{+} were obtained from nitrate salts and Fe^{3+}, Cd^{2+}, Mn^{2+}, Al^{3+}, Hg^{2+}, Co^{2+}, $Ba^{2+}$and K^{+} were obtained from chloride salts. ^{13}C NMR was done using a Bruker spectrometer operating at 100 MHz, while ^{1}H NMR was done at 400 MHz. The internal standard utilized was tetramethylsilane (TMS). Both $CDCl_3$ and DMSO-d_6 were deuterated solvents. Using an Agilent Technologies 1100 Series (Agilent Chemistation Software) mass spectrometer, positive electron spray ionization (ESI-MS) was used to collect mass spectrometric data. The UV-Vis-1800 Shimadzu spectrophotometer was employed to record UV-Vis absorption spectra, while the Agilent Carry Eclipse spectrophotometer was utilized to analyze fluorescence.

4.11.2 Synthesis of 1-(4-bromophenyl)-1,2,2-triphenylethene 4

This molecule was synthesized using a method described in the literature.[54] Dropwise additions of n-butyl-lithium (1.6 M in hexane, 18.5 mL) were added to a solution of diphenylmethane **2** (5.0 g, 29.7 mmol) in dry THF (200 mL) at 0 °C while nitrogen was maintained. The mixture was then kept at the ambient temperature for two hours. Then, 5.79 g, (22.2 mmol) of (4-bromophenyl)(phenyl)methanone **3**, was added in 30 ml of THF. TLC was employed to maintain a check on the mixture as it was stirred at room temperature. After the reaction was confirmed to be complete, it was quenched with NH_4Cl, extracted with DCM (3×50ml), dried with Na_2SO_4, and evaporated to dryness.After obtaining the crude alcohol, it was dissolved in toluene (80ml), pTSA (1.5gm) was added, and the solution was then refluxed for 16 hours. After the toluene was evaporated, the crude product was purified with column chromatography using n-hexane to obtain analytical pure compound **4** as a white solid with an 80% yield (9.7 g), IR (cm^{-1}): 3072, 3019, 1605, 1485, 1444, 1391, 1065, 1012, 811, 753, 704. ^{1}H NMR (400 MHz, $CDCl_3$) δ: 7.24-7.19 (m, 2H), 7.15-7.08 (m, 9H), 7.04-6.99 (m, 6H), 6.91-6.88 (m, 2H); ^{13}C NMR (100 MHz, CDCl3) δ :143.43, 143.34, 143.24, 142.71, 141.59, 139.65, 133.01, 131.32, 131.27, 131.25, 130.87, 127.90, 127.80, 127.70, 126.72, 126.67, 126.62, 120.46

4.11.3. Synthesis of 5-(4-(1,2,2-triphenylvinyl)phenyl)thiophene-2-carbaldehyde 6

Under an argon atmosphere, compound **4** (1.0 g, 2.4 mmol) was added to a solution of dimethyloxyethane (DME):2 M Na_2CO_3 (3:1, 40 mL). Subsequently, compound 5 (5-formylthiophen-2-yl)boronic acid 5 was added (0.49 g, 3.16 mmol). Using argon, the resultant reaction mixture was degassed for 15 to 20 minutes. The mixture was then heated to reflux for 24 hours at 150 °C by adding $Pd(PPh_3)_4$ (0.085 g). TLC analysis was used to

examine the completion of the reactions. After the reaction was finished, it was extracted with DCM (3×50 mL) and quenched with water. The mixed organic layer rinsed with water, then dried over anhydrous sodium sulphate before being evaporated. The crude product was purified using column chromatography, and **6** was obtained as a yellow solid with a 60% yield after the column was eluted with 8:92 ethyl acetate and hexane (0.65 g). IR (cm^{-1}):3075, 3017, 2922, 2848, 1668, 1455, 1225, 1070, 806. ^{1}H NMR (400 MHz, $CDCl_3$) δ: 9.88-9.87 (m, 1H), 7.72 (d, *J*=4.0 Hz, 1H), 7.45-7.42 (m, 2H), 7.35 (d, *J*=3.9 Hz, 1H), 7.17-7.10 (m, 10H), 7.10-7.02 (m, 7H). ^{13}C NMR (100 MHz, $CDCl_3$) δ : 182.80, 154.23, 145.31, 143.42, 143.40, 143.29, 142.07, 141.98, 139.93, 137.52, 132.16,131.37, 131.33, 131.31, 130.85, 127.93, 127.85, 127.71, 126.82, 126.72, 126.68, 125.64, 123.88.

4.11.4. Synthesis of 1-(thiophen-2-yl)-3-(5-(4-(1,2,2-triphenylvinyl) phenyl) thio-phen-2-yl)prop-2-en-1-one 8

A solution of potassium hydroxide (5%, 25mL) was gradually added to a mixture of 5-(4-(1,2,2-triphenylvinyl)phenyl)thiophene-2-carbaldehyde **6** (0.50 g, 1.13mmol) and 1-(thiophen-2-yl)ethanone **7** (0.17 g, 1.36mmol) in ethanol (25mL). For 24 hours, the mixture was mixed. After being filtered, washed with water, dried, and recrystallized from ethanol, the precipitated product yielded 8 (0.57 g, 89%), a yellow solid. IR (cm^{-1}):3082, 3022, 2924, 2854, 1670, 1639, 1575, 1411, 1239, 807, 661. ^{1}H NMR (400 MHz, $CDCl_3$) δ: 7.92 (d, *J*=16.4 Hz, 1H), 7.84 (d, *J*=4.4 Hz, 1H), 7.69 - 7.66 (m, 1H), 7.57(m, 1H), 7.38 (d, *J*=7.6 Hz, 2H), 7.30 (dd, *J*=3.6, 10.0 Hz, 1H), 7.24 (d, *J*=5.2 Hz, 1H), 7.20 - 7.16 (m, 1H), 7.16 - 7.02 (m, 17H). ^{13}C NMR(100 MHz, CDCl3) δ :181.50, 147.82, 147.68, 147.61, 147.09, 145.66, 144.31, 143.52, 143.40, 141.71, 140.11, 139.07, 138.55, 138.45, 136.58, 133.80, 133.74, 132.05, 131.55, 131.39, 131.33, 131.32,128.24, 127.88, 127.80, 127.68, 126.72, 126.65, 126.59, 125.18, 124.47, 124.10, 123.99, 119.83, 119.11, Elemental Analysis: $C_{37}H_{26}OS_2$: Cal. C, 80.69; H, 4.76; Obs. C, 80.73; H, 4.70.

4.11.5. Synthesis of 6-(thiophen-2-yl)-4-(5-(4-(1,2,2-triphenylvinyl)phenyl)thiophen-2-yl)-2,2'-bipyridine 1

Ammonium hydroxide (25%) (5 gm), glacial acetic acid(15 mL), and a stirring solution of compound **8** (0.5 g, 0.91 mmol) and 1-(2-oxo-2-(pyridin-2-yl)ethyl)pyridin-1-ium **9** (0.36 g, 1.81 mmol) were heated under reflux conditions for 12 hours. After the reaction was complete (confirmed by TLC), ice cold water (30 mL) was added, and the precipitate that resulted was filtered, water washed, dried, and purified by column chromatography to get the yellow solid **1** (0.27g, 45%). IR(cm^{-1}): 3082, 3027, 2915, 2854, 1639, 1569, 1415, 1244,

968, 853, 698. ^{1}H NMR (400 MHz, DMSO) δ :8.22 (d, *J*=3.8 Hz, 1H), 8.05 - 8.02 (m, 1H), 7.85 (d, *J*=15.2 Hz, 1H), 7.66 (d, *J*=3.6 Hz 1H), 7.55 (d, *J*=5.8 Hz, 1H), 7.53 - 7.48 (m, 3H), 7.31 - 7.27 (m, 1H), 7.19-7.09 (m, 11H), 7.05-6.95 (m, 10H). ^{13}C NMR(100 MHz, DMSO) δ: 147.25, 145.79, 144.09, 143.49, 143.31, 141.68, 140.29, 139.14, 136.27, 135.88, 135.20, 133.78, 132.05, 131.46, 131.20, 131.13, 131.09, 129.44, 128.46, 128.41,128.30, 127.29, 127.20, 127.13, 125.68, 125.47, 120.46. Elemental Analysis: $C_{44}H_{30}N_2S_2$: Cal. C, 81.20; H, 4.65; N, 4.30; Obs. C, 81.23; H, 4.63; N, 4.35. ESI (M/z) $C_{44}H_{30}N_2S_2$, Calc. 650.1850 [M^+]., Found. 651 [M^+].

4.11.6 General sensing procedure

Fluorescent probe 1 prepared in a stock solution (10^{-4} M in CH_3CN). UV-Vis absorption and fluorescence emission were measured in a quartz cuvette (path length = 1 cm), and the results were then titrated with different cations and their corresponding salts. The minerals Zn^{2+} Pb^{2+}, Ni^{2+}, Mg^{2+} and Ag^{+} were derived from nitrate salts, whereas Fe^{3+}, Cd^{2+}, Mn^{2+}, Al^{3+}, Hg^{2+}, Co^{2+}, $Ba^{2+}$and K^{+} were obtained from chloride salts. Copper is the source of copper perchlorate salt.

4.11.7 Determination of LOD

The following equation was used to determine the limit of detection based on the fluorescence titration: where **k** is the slope between the fluorescence intensity vs. Cu^{2+} conc. and **σ** is the standard deviation of blank data.

Limit of detection **= 3 σ/k**

Titration was carried out by adding 20 μL of the **1** in 2 mL acetonitrile in a quartz cell and scanned fluorescence (λ_{ex}= 410) to evaluate the sensitivity of the sensor **1** to various concentration of Cu^{2+}. The emission was then measured while the ion concentration was changed by the addition of 10 μL dilutions. It was discovered that the chemosensor 1's Cu^{2+} binding association constant (K_a) was $2.34x10^{-5}$ M. A comparable linear response was seen, and the detection limit was shown to be as low as 7.83 nM. (**Fig. 4.62**)

4.11.8 Determination of Stoichiometry by Job's plot

A 20 μL of Cu^{2+} ion was gradually added to the solution of **1** in order to understand the ratio of Cu^{2+} with chemosensor, and fluorescence emission was recorded and assessed using Job's plot. According to **Fig. 4.61**, which indicates that the coordination ratio of the **1** and Cu^{2+} ion was 2:1, the fluorescence intensity at 630 nm was plotted as a function of molar ratio (Cu^{2+}/[Cu^{2+}+**1**]), and a point of intersection was found at the molar ratio = 0.31.

4.12 Results and Discussion

4.12.1 Synthesis of Compound 1

Synthesis of the receptor 6-(thiophen-2-yl)-4-(5-(4-(1,2,2-triphenylvinyl)phenyl)thiophen-2-yl)-2,2'-bipyridine **1** was obtained *via* multistep synthetic reaction strategy. In the first step 2-(4-bromophenyl)ethene-1,1,2-triyl)tribenzene **4** was prepared by reacting diphenylmethane and (4-bromophenyl)(phenyl) methanone in presence of n-BuLi followed by reflux the with *p*-tolunesulfonic acid (PTSA) in dry toluene to obtain compound **4**. Then formation of 5-(4-(1,2,2-triphenylvinyl)phenyl)thiophene-2-carbaldehyde (**6**) was achieved by Suzuki coupling reaction between **4** and (5-formylthiophen-2-yl)boronic acid. In the next step formation of chalcone **8** by treating with acetyl thiophene in presence of KOH, in final step the synthesis of receptor **1** reaction between compound **8** and pyrindine salt **9** in presence of ammonium acetate to gives compound **1**. The structure of compound **1** was confirmed by ^{1}H NMR, ^{13}C NMR, elemental analysis and mass spectroscopy.

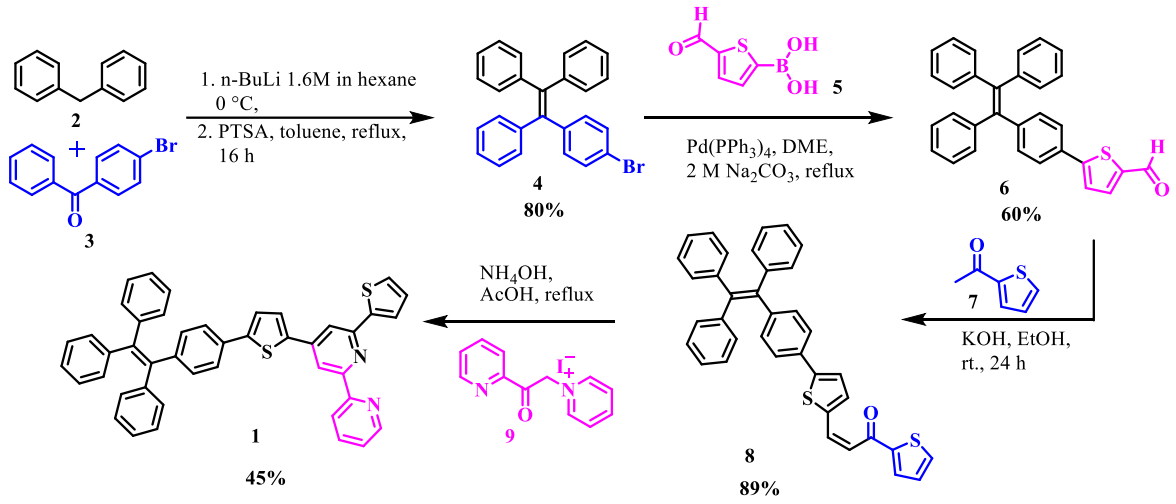

Scheme 4.8: Synthesis of Compound **1**.

4.12.2 Characterization of synthesized compounds by IR, NMR, and Mass spectroscopy

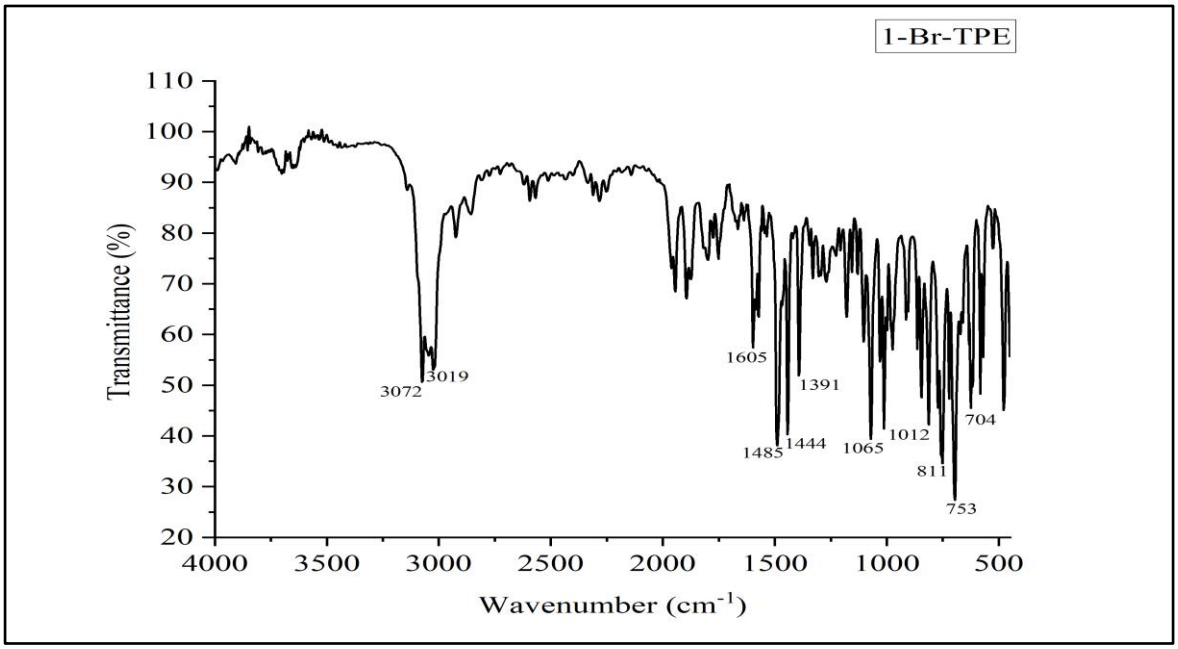

Figure 4.42: FT-IR spectrum of (2-(4-bromophenyl) ethene-1, 1, 2-triyl) tribenzene **4**

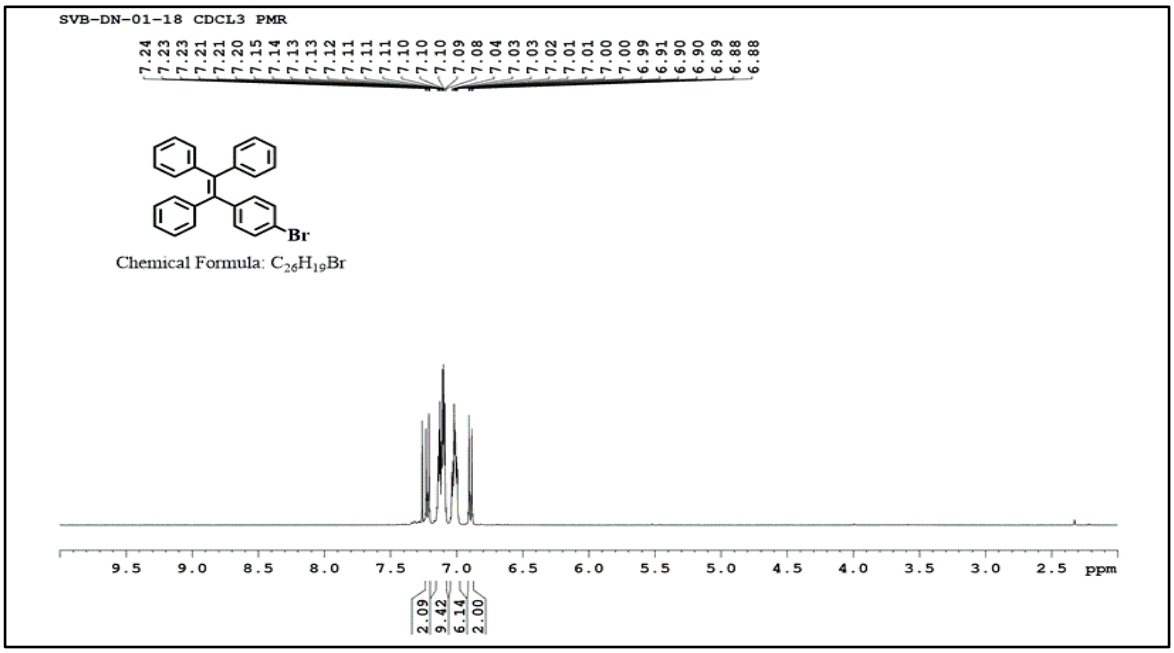

Figure 4.43: ^{1}H NMR spectrum of (2-(4-bromophenyl) ethene-1, 1, 2-triyl) tribenzene **4**

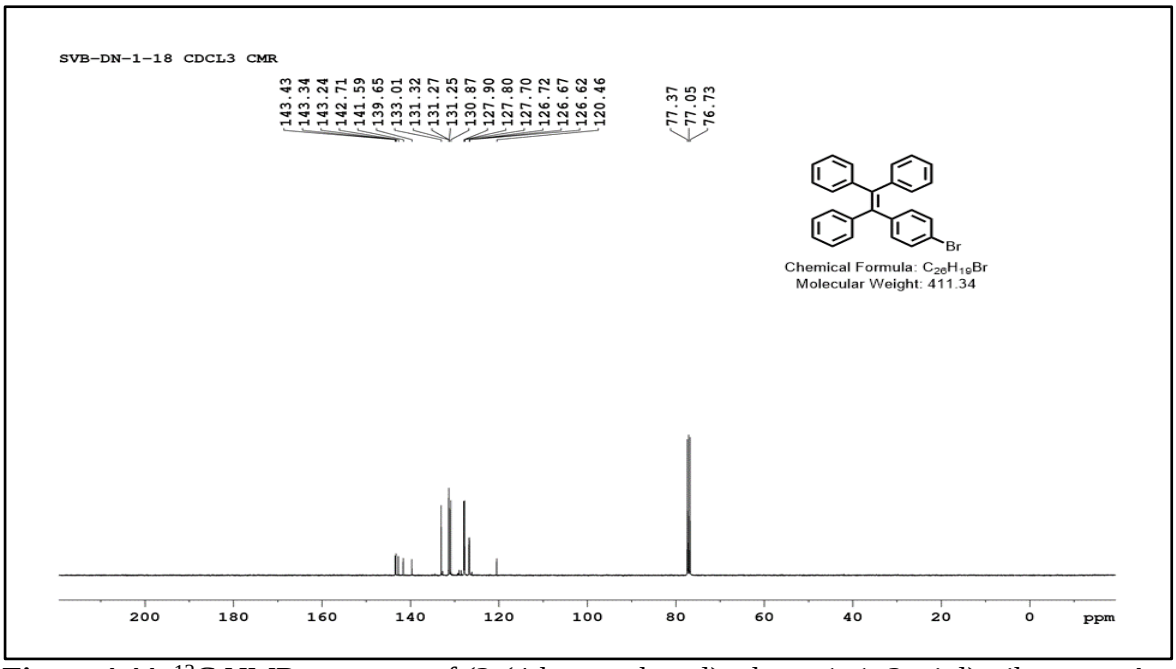

Figure 4.44: ^{13}C NMR spectrum of (2-(4-bromophenyl) ethene-1, 1, 2-triyl) tribenzene **4**

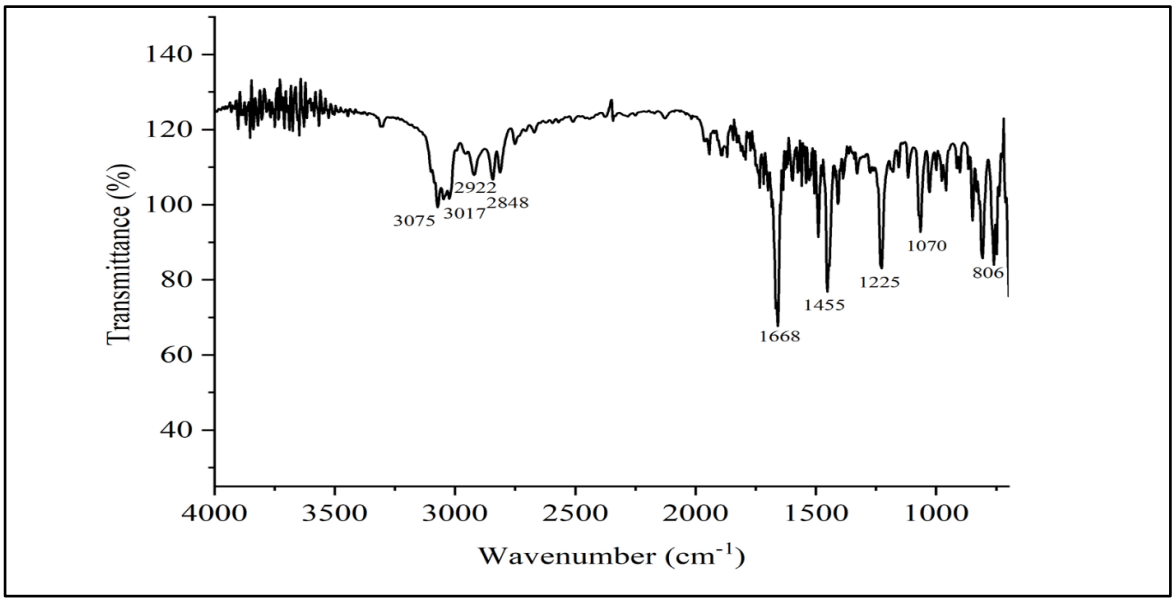

Figure 4.45: FT-IR spectrum of 5-(4-(1,2,2-triphenylvinyl)phenyl)thiophene-2-carbaldehyde **6**

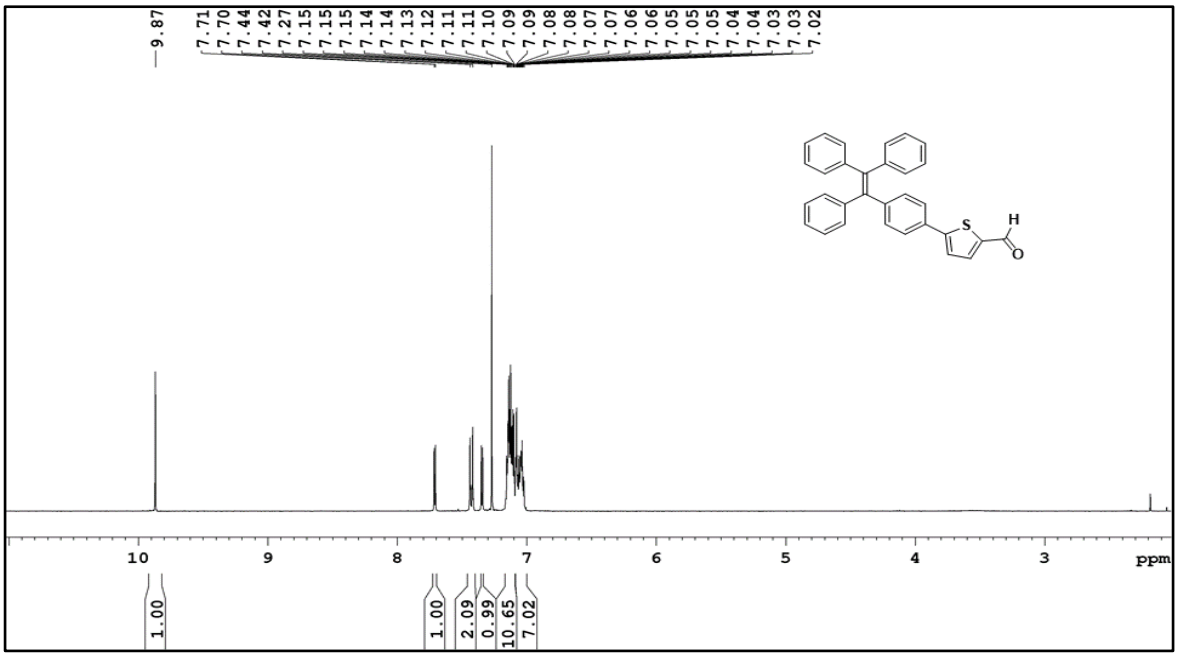

Figure 4.46: ^{1}H NMR spectrum of 5-(4-(1,2,2-triphenylvinyl)phenyl)thiophene-2-carbaldehyde **6**

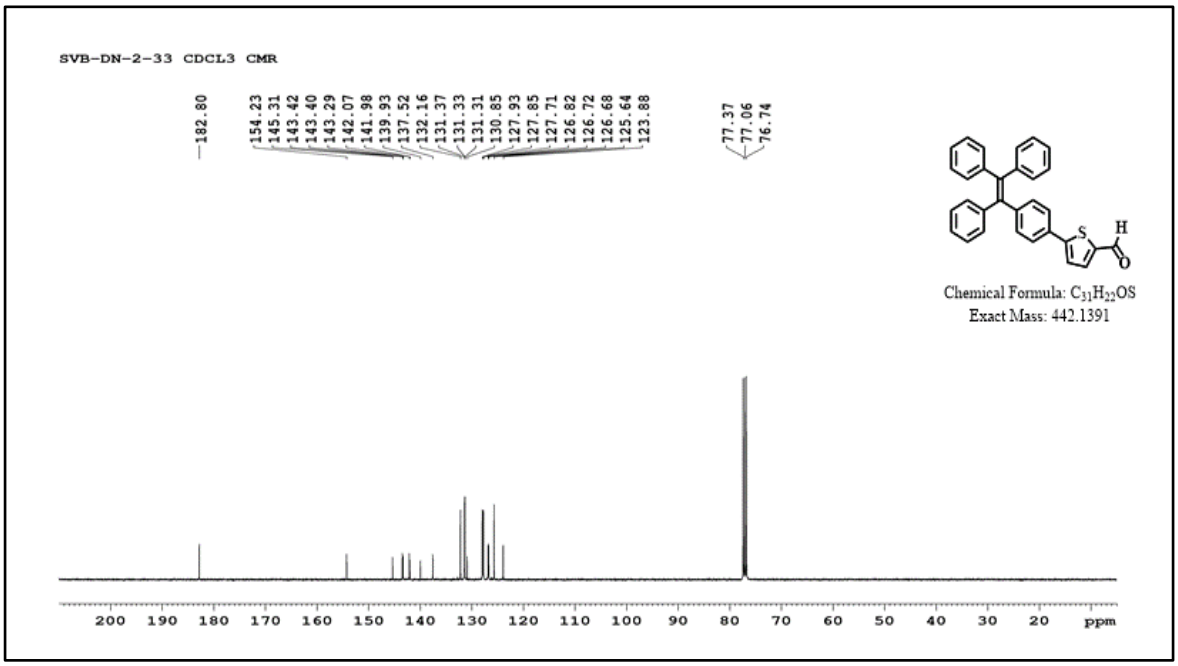

Figure 4.47: ^{13}C NMR spectrum of 5-(4-(1,2,2-triphenylvinyl)phenyl)thiophene-2-carbaldehyde **6**

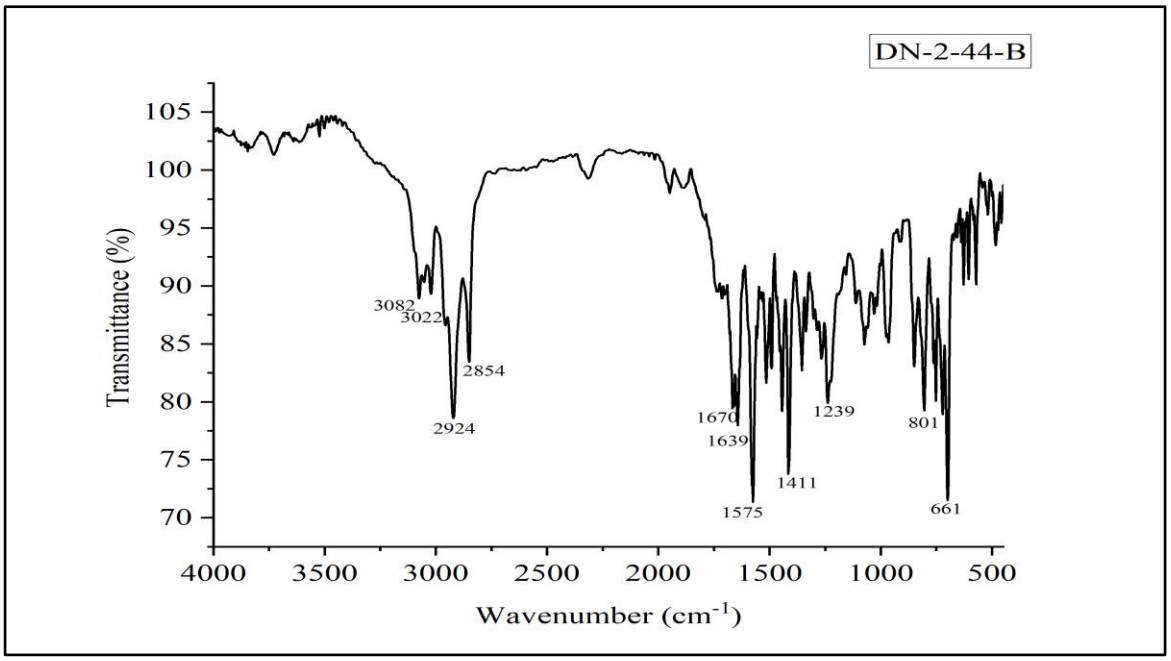

Figure 4.48: FT-IR spectrum of 1-(thiophen-2-yl)-3-(5-(4-(1,2,2-triphenylvinyl) phenyl)thiophen-2-yl)prop-2-en-1-one **8**

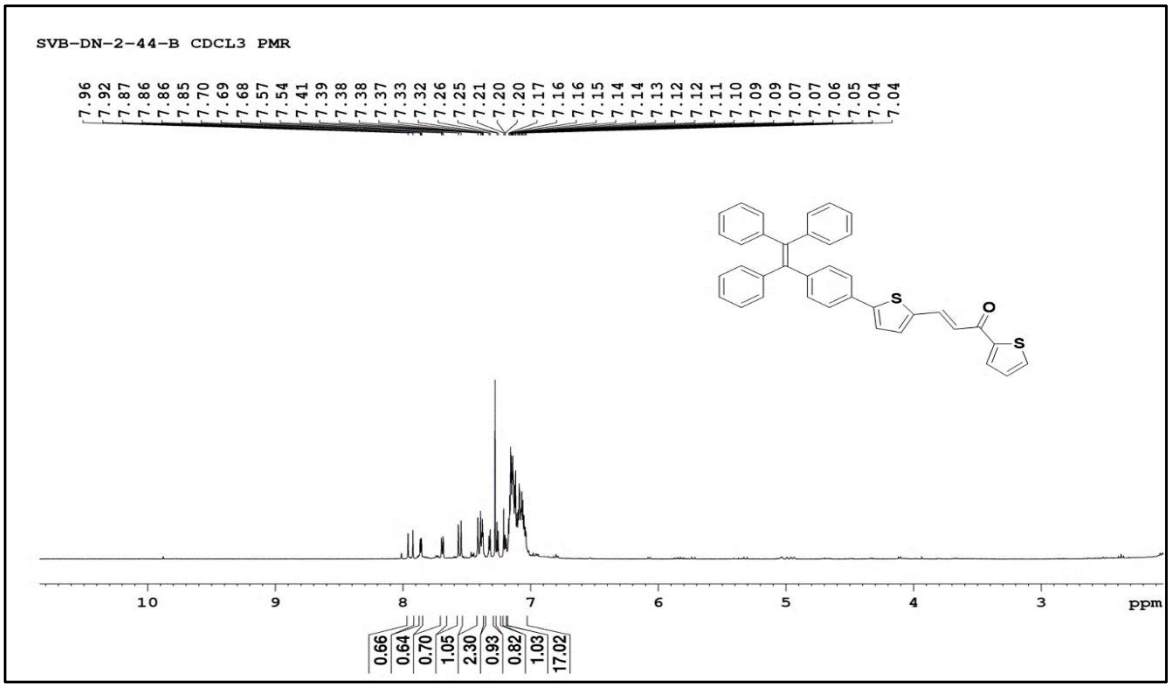

Figure 4.49: ^{1}H NMR spectrum of 1-(thiophen-2-yl)-3-(5-(4-(1,2,2-triphenylvinyl)phenyl) thiophen-2-yl)prop-2-en-1-one **8**

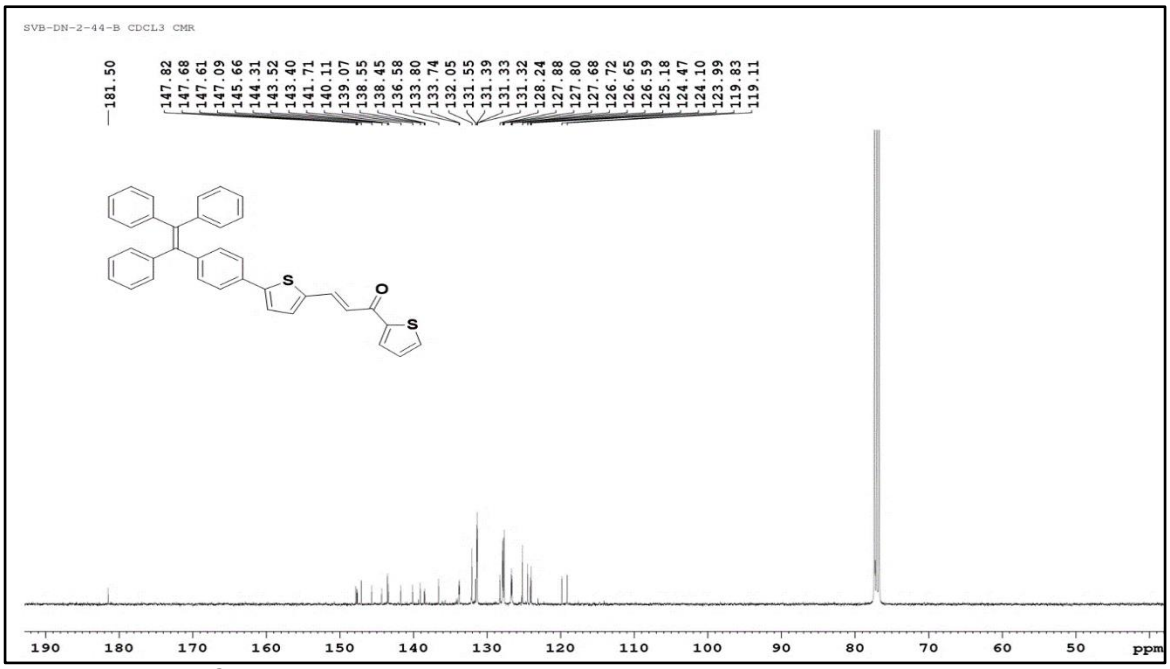

Figure 4.50: ^{13}C NMR spectrum of 1-(thiophen-2-yl)-3-(5-(4-(1,2,2-triphenylvinyl) phenyl)thiophen-2-yl)prop-2-en-1-one **8**

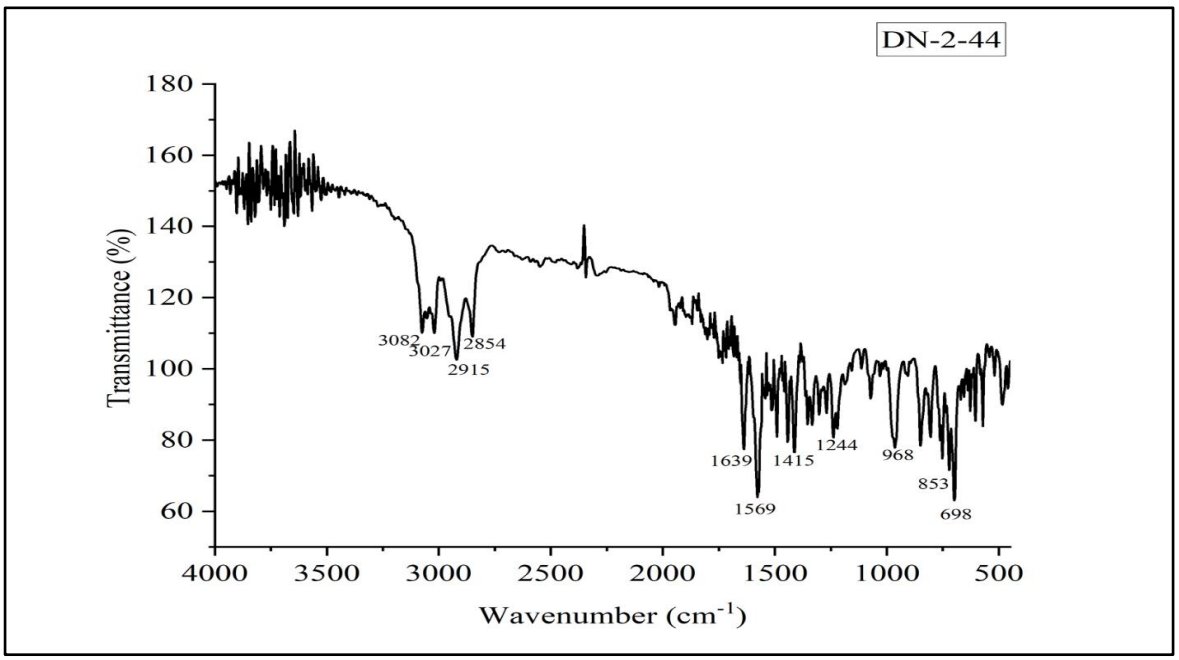

Figure 4.51: FT-IR spectrum of Synthesis of 6-(thiophen-2-yl)-4-(5-(4-(1,2,2-triphenyl vinyl)phenyl)thiophen-2-yl)-2,2'-bipyridine **1**

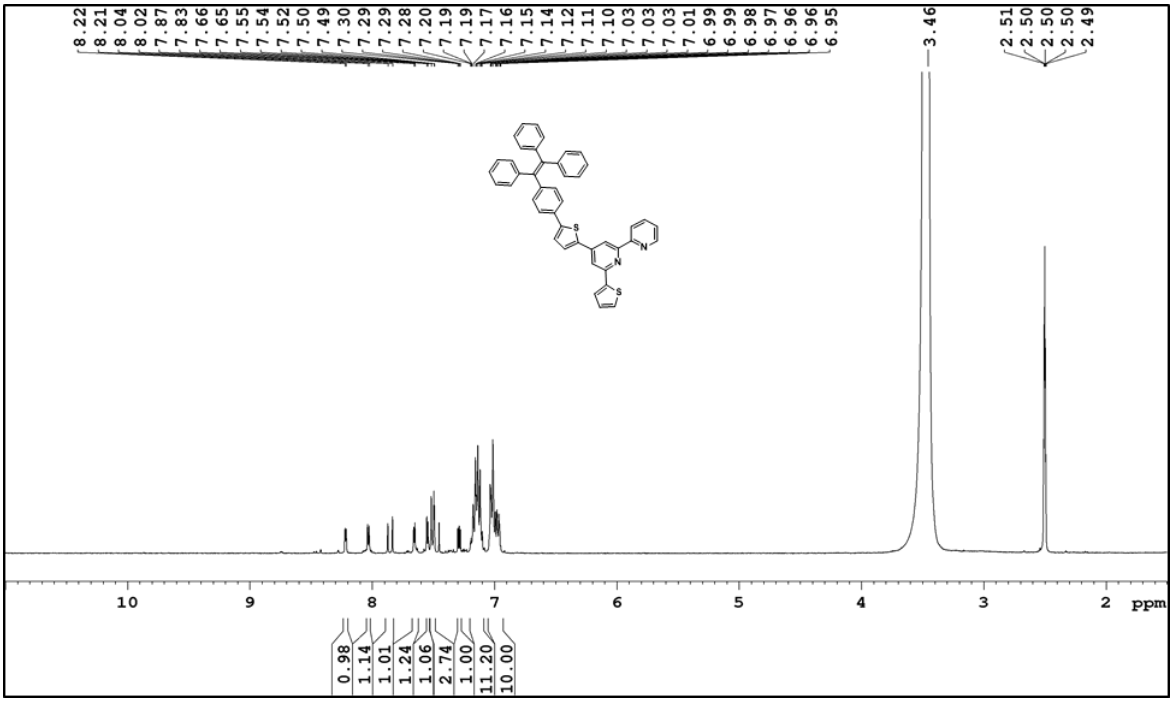

Figure 4.52:[1]H NMR spectrum of Synthesis of 6-(thiophen-2-yl)-4-(5-(4-(1,2,2-triphenyl vinyl)phenyl)thiophen-2-yl)-2,2'-bipyridine **1**.

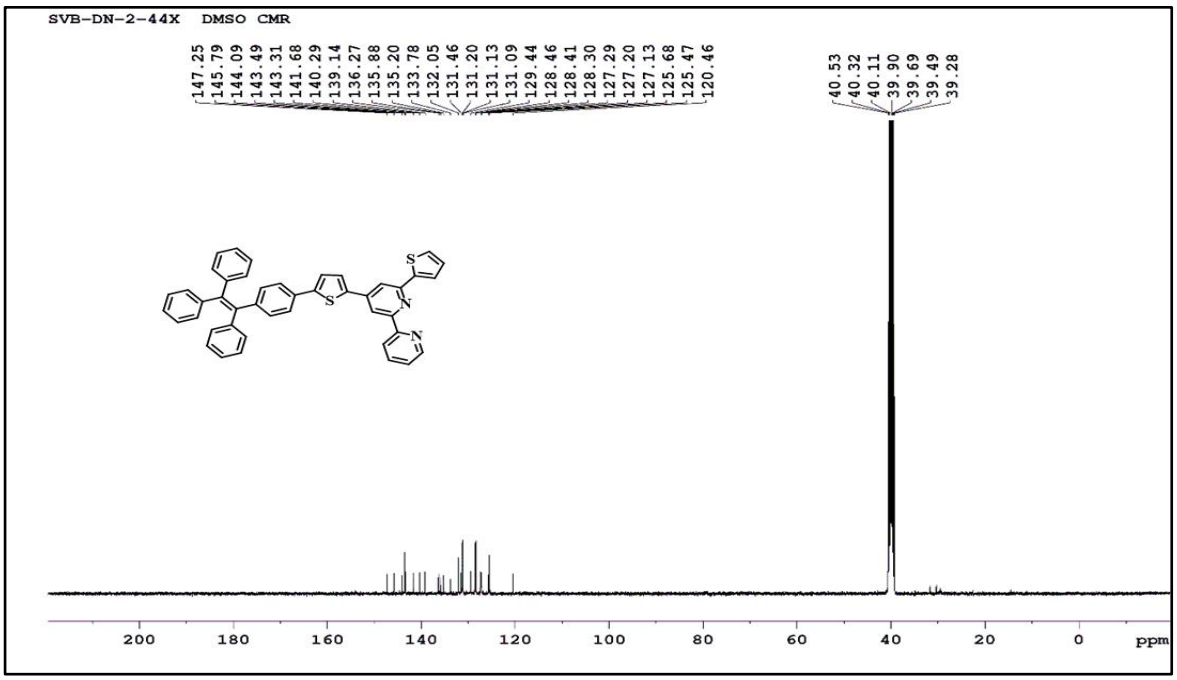

Figure 4.53: [13]C NMR spectrum of Synthesis of 6-(thiophen-2-yl)-4-(5-(4-(1,2,2-triphenyl vinyl)phenyl)thiophen-2-yl)-2,2'-bipyridine **1**.

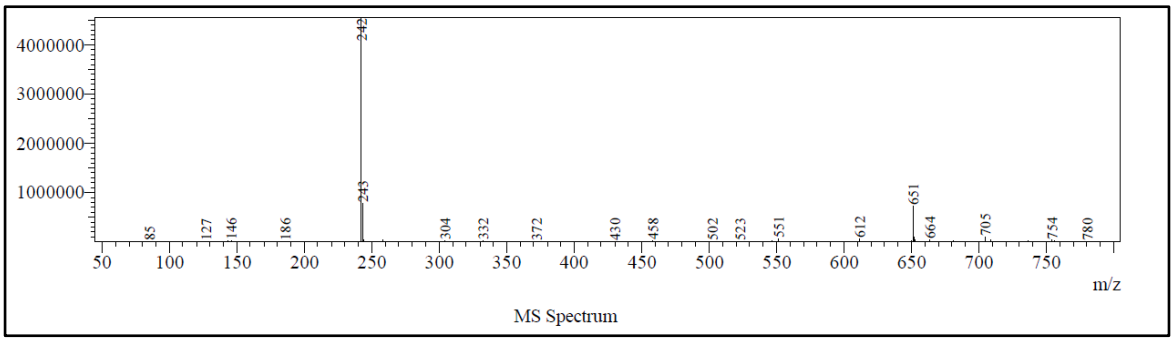

Figure 4.54: ESI-Mass spectrum of Synthesis of 6-(thiophen-2-yl)-4-(5-(4-(1,2,2-triphenyl vinyl)phenyl)thiophen-2-yl)-2,2'-bipyridine **1**

4.12.3 Absorbance and emission spectra of 1 in different solvents

The UV-Vis absorption and fluorescence spectroscopy employed to characterise **1** absorption and fluorescence properties were recorded in different organic solvents, as shown in **Figures 4.55a and b**, respectively. The sensor **1**'s absorption spectra in hexane show a prominent peak with a maximum absorption wavelength of 400 nm and an extinction coefficient of 2.600×10^3 $M^{-1}cm^{-1}$. It was determined that the π-transition in the molecular architecture was the cause of the relatively high extinction coefficient ($\sim10^3$ $M^{-1}cm^{-1}$) in all of the solvents. When the solvent's polarity was increased, the form of the absorption peak remained unchanged (**Fig. 4.55a**). Additionally, the results of a study on the emission characteristics of sensor **1** upon excitation at (λ_{ex} = 370 nm) are shown in **Figure 4.55b**. The probe **1** (25 μM) was excited (λ_{ex} = 370 nm) in various solvents, and the emission spectra were observed at various wavelengths with a change in intensity. In various solvents, the probe **1**'s band location and shape are unchanged by the excitation wavelength. With a quantum yield (Φ = 1.51), the emission peak in a less polar solvent, such as hexane, emerged at 488 nm. Inversely, as shown in **Table 4.4**, the emission band of sensor 1 in DMSO occurred at 570 nm with a quantum yield (Φ = 3.73). This demonstrates that the fluorescence peak of **1** is blue-shifted in a less polar solvent (**Fig. 4.55b**). In various solvents, **1**, the fluorescence quantum yield is variable. As a result, the polarity of the solvents affects the emission peak position and quantum yield of **1**, and the fluorescence quantum yield of the probe was calculated using Rhodamine B as the reference substance.[55]

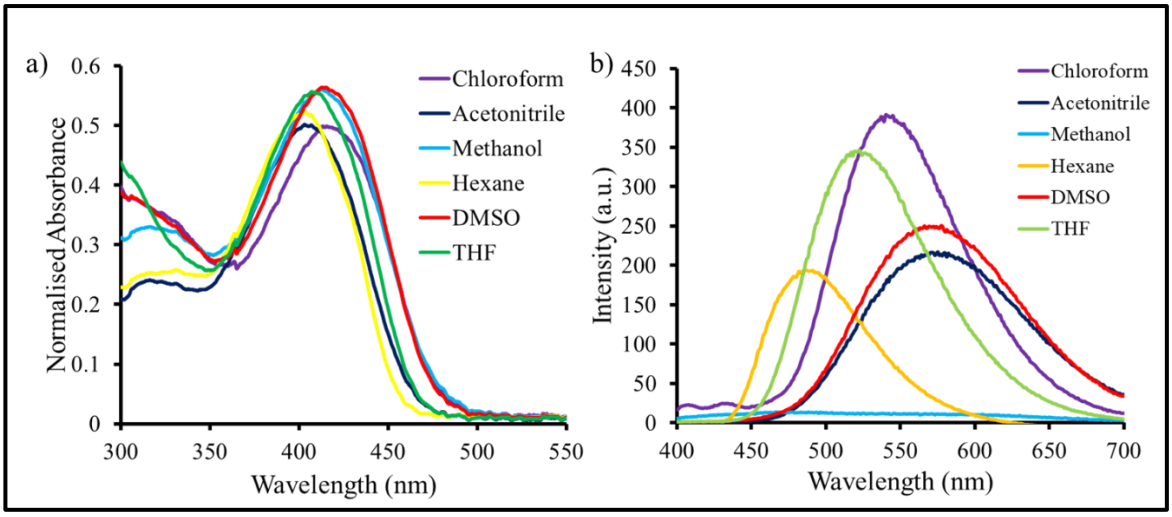

Figure 4.55: a) UV-Vis and b) Fluorescence emission spectra of sensor **1** ($2.5x10^{-4}$ M) in different solvents

Table 4.4: UV-Vis absorption and fluorescence emission data of **1** in different solvents

Solvent	**Maximum wavelength/nm**		**Quantum yield (Φ)**
	Absorption (ε/$M^{-1}cm^{-1}$)	**Emission**	
Hexane	404 (2.600×10^3)	488	1.51
Chloroform	417 (2.485×10^3)	542	4.73
THF	410 (2.770×10^3)	521	4.54
Acetonitrile	406 (2.495×10^3)	577	3.47
MeOH	413 (2.800×10^3)	------	N/A
DMSO	417 (2.795×10^3)	570	3.73

Additionally, the spectra of **1**'s emission and absorption when dissolved in THF with 99% water were investigated. Figures **4.56a** and **4.56b**, respectively, show the emission and UV-Vis spectral data. The peak of **1**'s absorption in THF was visible at 410 nm ($\varepsilon = 2.600\times10^{-3}$ $M^{-1}cm^{-1}$). When water was added, the absorption peak acquired a bathochromic shift, and a band at 430 nm ($\varepsilon = 1.980\times10^{-3}$ $M^{-1}cm^{-1}$) was observed. When polar solvent (H_2O) is added, the shape of the absorption spectra broadens and a noticeable red shift (17 nm) of the absorption peak (**Fig. 4.56a**). The emission spectra of **1** in THF were visible at 521 nm ($\Phi = 4.54$) after excitation (λ_{ex} = 370 nm) (**Fig. 4.56b**). In the presence of 99% H_2O in a THF solution, the shape and emission band region at 542 nm with $\Phi = 1.29$ are changed. This is due to the sensor **1**'s aggregation induced quenching (ACQ) in THF:H_2O (1:99%, *v/v* ratio). This suggests that ACQ effect rather than AIE phenomena is being displayed by probe **1**.

This is not immediately apparent due to the fact that TPE AIEgen has a polar receptor site (containing a pendant thiophenylbipyridine receptor), which causes the molecule to dissolve in a THF/water solution at high water content and result in an ACQ effect rather than an AIE event.

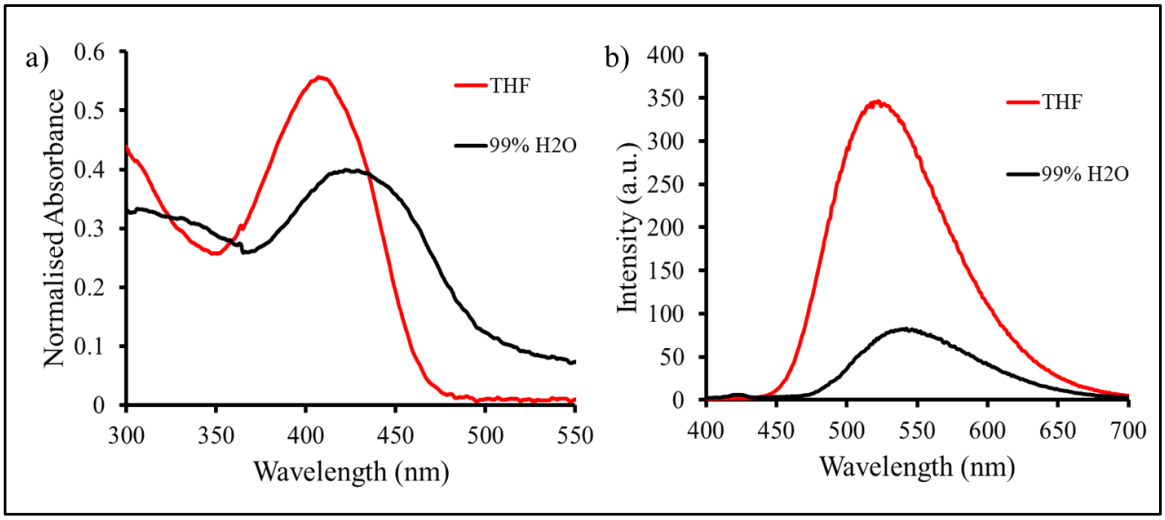

Figure 4.56: a) UV-Vis and b) Fluorescence emission spectra of receptor **1** ($2x10^{-4}$ M) in THF and THF:H_2O solvent mixtures

4.12.4 Mechanochromic properties of 1

As TPE exhibits aggregation-induced emission (AIE), its mechanochromic properties were examined in their solid form. Compound **1** displays a green fluorescent colour in solid form. The emissive colour of the probe **1** solid immediately changes from green to bright yellow after being ground in a mortar and pestle. Furthermore, annealing and fuming with solvent vapours affected the colour of **1**'s solid state. Chromophore **1** changes from bright yellow to dark rocky green and back to bright yellow after annealing at 200 ^{o}C and fuming with acetone, respectively. Here, we found that acetone fuming and annealing at 200 ^{o}C did not return the material to its natural colour. **(Fig. 4.57)**.

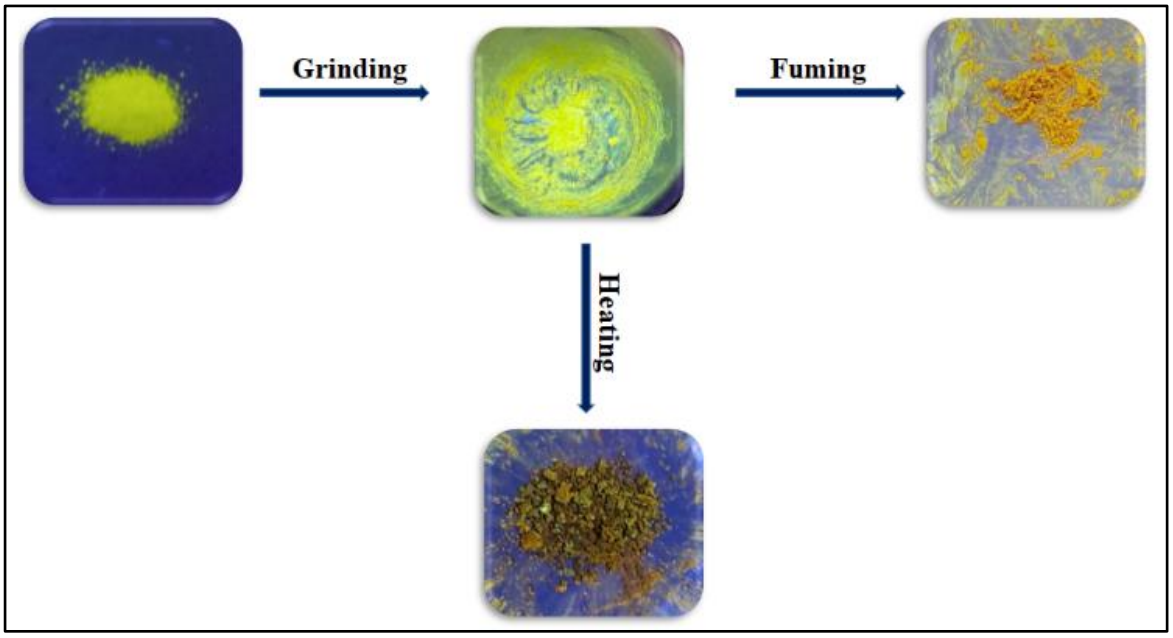

Figure 4.57: The mechanochromic properties of sensor **1** displaying the luminescence changing of it after grinding, fuming and heating.

4.12.5 Sensing performance of probe 1

Through tests in colorimetry, UV-Vis absorption, fluorescence emission, and ^{1}H NMR titration, the sensing behaviour of receptor **1** for various metal ions was investigated. A simple and appealing method is to investigate the selectivity of sensor molecules towards specific ion colorimetric sensing. Therefore, visual colorimetric changes were used to test the probe **1**'s colorimetric sensing capability toward various metal ions, including Cu^{2+}, Zn^{2+}, Pb^{2+}, Ni^{2+}, Fe^{3+}, Cd^{2+}, Mg^{2+}, Mn^{2+}, Al^{3+}, Hg^{2+}, Co^{2+}, Ba^{2+}, Ag^{+} and K^{+}. In acetonitrile, Sensor **1** displays a yellow colour. It was discovered that the yellow solution in a solution of receptor **1** transforms to a green solution when Cu^{2+} ions are added, as shown in **Figure 4.58a.** Other ions such as Zn^{2+}, Pb^{2+}, Ni^{2+}, Fe^{3+}, Cd^{2+}, Mg^{2+}, Mn^{2+}, Al^{3+}, Hg^{2+}, Co^{2+}, Ba^{2+}, Ag^{+} and K^{+} do not, however, cause any visible colour changes in the solution of receptor **1** under the same circumstances. As a result, one of the most efficient approaches to demonstrate the selectivity of receptor **1** towards the Cu^{2+} ion is through naked-eye tests. Additionally, when copper ion was added to the receptor **1** that was fluorescing in acetonitrile, the fluorescence was quenched as a result of the photoinduced electron transfer action (**Fig. 4.58b**).

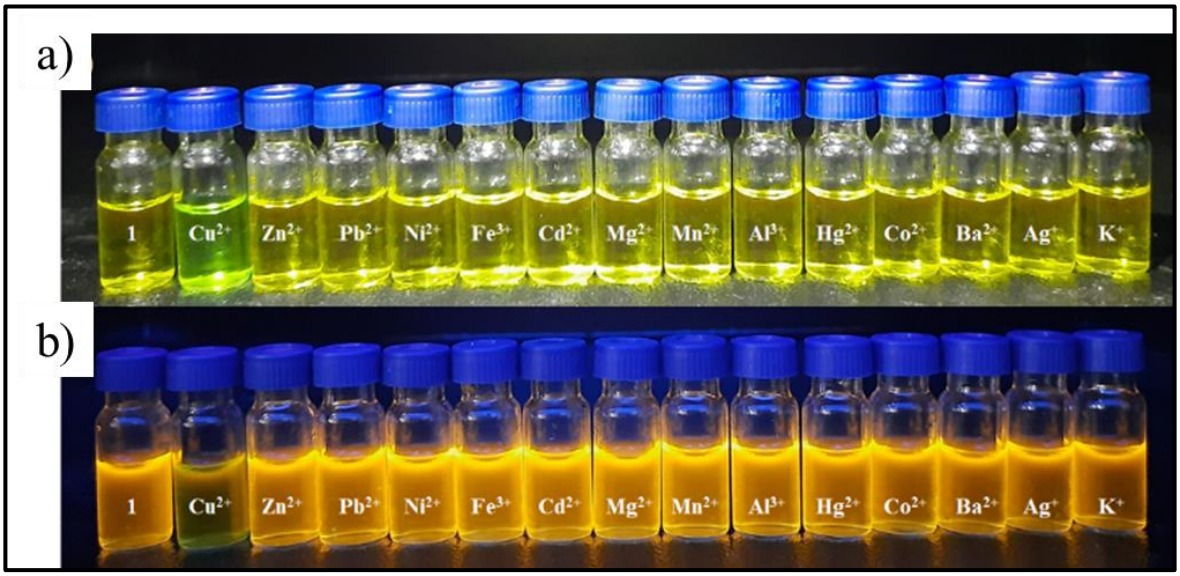

Figure 4.58: Colorimetric behaviour of solution of receptor **1** ($2.0x10^{-4}$ M) in acetonitrile upon interaction with various metal salts (10 equiv.) salts, a) under visible light and b) under UV light 365 nm at 25 °C.

4.12.6 Absorption study

The extent of the interaction, as well as the selectivity and sensitivity of the probe towards the cations, were also investigated using UV-Vis absorption spectroscopy techniques. The outcomes of the UV-Vis experiment in acetonitrile at room temperature are illustrated in **Fig. 4.59a** and **b**. At 406 nm ($\varepsilon = 2.495\times10^3$), the receptor **1** ($2.0x10^{-4}$ M) displays high absorption maxima. The characteristic peak of the $\pi\rightarrow\pi^*$ transition is the absorption peak at 406 nm. To explore the receptor 1's capacity for selective sensing, several metal ions, including Zn^{2+}, Pb^{2+}, Ni^{2+}, Fe^{3+}, Cd^{2+}, Mg^{2+}, Mn^{2+}, Al^{3+}, Hg^{2+}, Co^{2+}, Ba^{2+}, Ag^{+} and K^{+} were used to alter the position and intensity of this absorption band. Only with the addition of Cu^{2+} ions did receptor **1**'s UV-Vis absorption spectra show a noticeable alteration (10 equiv.). Under the same research conditions, the UV-Vis absorption spectra of the other cations, including Zn^{2+}, Pb^{2+}, Ni^{2+}, Fe^{3+}, Cd^{2+}, Mg^{2+}, Mn^{2+}, Al^{3+}, Hg^{2+}, Co^{2+}, Ba^{2+}, Ag^{+} and K^{+} did not significantly differ from those of the free receptor **1**. Cu^{2+} ion addition significantly altered the absorption spectra of receptor **1**, which suggests a complex has formed between the receptor and the ion. To look into how adding Cu^{2+} ions causes a consistent shift in absorption spectra, UV-Vis titration experiments were conducted. The absorption peak intensity at 406 nm gradually decreased with the addition of copper ions

(0–10 equiv.) to a 4.5×10^{-4} M solution of **1** in acetonitrile, and it totally disappeared at 10 equiv. of Cu^{2+} ion addition. As a result, receptor **1** has been proven a selective sensor for the detection of Cu^{2+} ions by both UV-Vis absorption investigations and the naked eye.

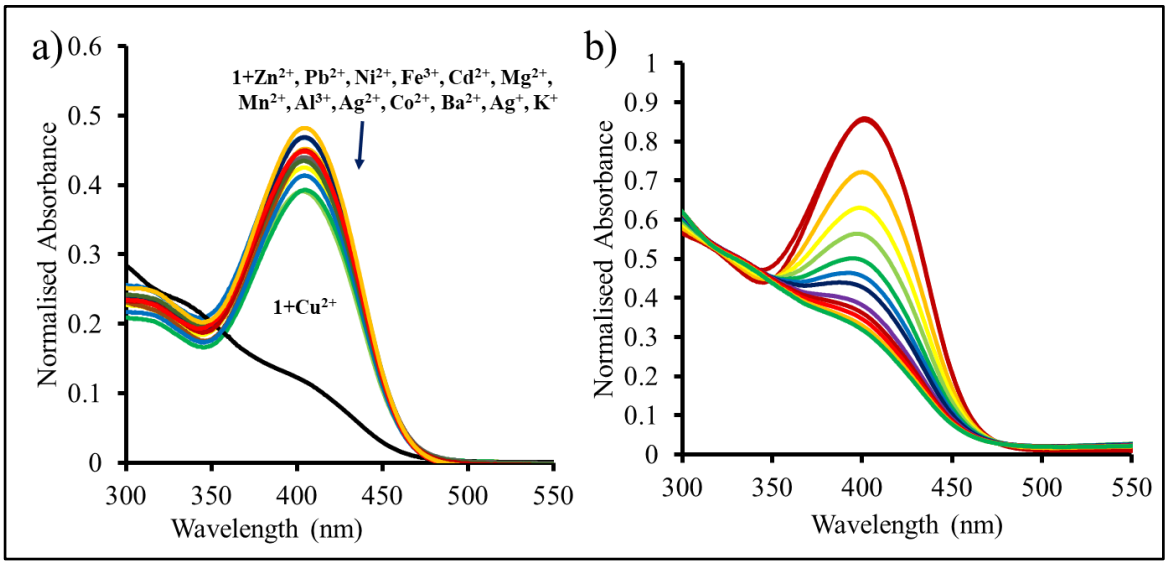

Figure 4.59: a) UV of sensor **1** ($2.0\text{x}10^{-4}$ M) with the addition of various metal salts (10 equiv.) in acetonitrile and b) UV titration of sensor **1** ($4.5\text{x}10^{-4}$ M) with the addition of Cu^{2+} (0 to 10 equiv.) in acetonitrile.

4.12.7 Fluorescence emission study

The binding interactions of receptor **1** with Cu^{2+} ions in acetonitrile were examined using fluorescence emission spectroscopy. **Fig. 4.60a** and **b** shows the emission spectrum data of sensor **1** and their interactions with various metal ions. The receptor **1** has a strong emission peak at 577 nm in response to stimulation at λ_{ex} = 370 nm. In response to stimulation at λ_{ex} = 370 nm, the receptor **1** emits with a prominent peak at 577 nm. With the addition of several metal ions (10 equiv.), including Cu^{2+}, Zn^{2+}, Pb^{2+}, Ni^{2+}, Fe^{3+}, Cd^{2+}, Mg^{2+}, Mn^{2+}, Al^{3+}, Hg^{2+}, Co^{2+}, Ba^{2+}, Ag^{+} and K^{+} the first fluorescence emission spectra of receptor **1** were captured. Metal ions Zn^{2+}, Pb^{2+}, Ni^{2+}, Fe^{3+}, Cd^{2+}, Mg^{2+}, Mn^{2+}, Al^{3+}, Hg^{2+}, Co^{2+}, Ba^{2+}, Ag^{+} and K^{+} were added to a solution of receptor **1**, however it was determined that there were no appreciable changes in the emission spectrum intensity (**Fig. 4.60a**). The fluorescence emission peak intensity significantly decreased with the addition of Cu^{2+} ion (10 equiv.). Furthermore, the fluorescence titration studies were carried out by gradually adding Cu^{2+} ions (0-10 equiv.) to the acetonitrile solution of receptor **1** in order to gain a thorough understanding of the binding capability of sensor 1 towards Cu^{2+} ions. It was discovered that adding 10 equivalent Cu^{2+} ions reduced the emission peak intensity at 577 nm. The

reversible PET 'on' process that results from the complexation of receptor **1** with the Cu^{2+} ion is responsible for the fluorescence quenching effect. From the TPE core moiety to the thiophenylbipyridine ligand's interaction with Cu^{2+} ions, the "PET on" step occurs. As a result, the probe **1**'s fluorescence behaviour demonstrates the PET "off-on" process after interacting with copper.

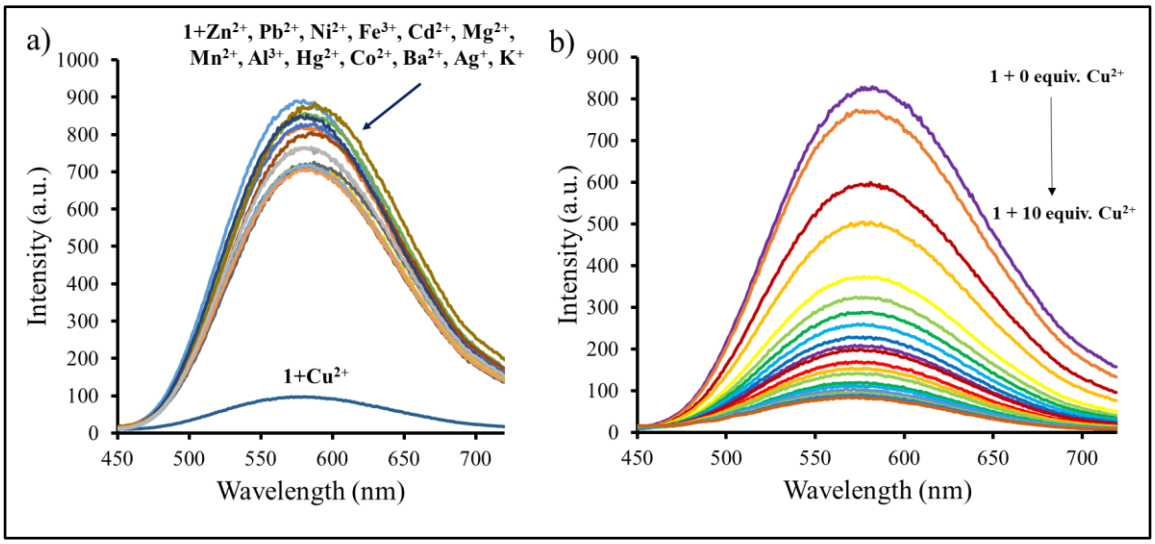

Figure 4.60: Emission spectra of sensor **1** ($5.0x10^{-4}$ M) upon excitation at 370 nm wavelength. a) PL of **1** with the addition of various metal salts (10 equiv.) in acetonitrile and b) PL titration of **1** with the addition of Cu^{2+} (0 equiv. to 10 equiv.) in acetonitrile.

4.12.8 Stoichiometry of complexation

To evaluate the stoichiometry of the complex 1:Cu^{2+} produced by the receptor **1** and Cu^{2+} ion, Job's plot from the emission titration experiments was used. The fluorescence emission bands for the 1:Cu^{2+} complex indicated a maximum around 0.31 mole fraction of Cu^{2+} to the receptor **1**, as shown by the Job's plot in Figure **4.61a**. The Job's plot result for showed that the complex stoichiometry was 2:1. Benesi-Hildebrand plot of **1** with acetonitrile-containing Cu^{2+} (**Fig. 4.61b**). The measured wavelength was 577 nm, while the excitation wavelength was 370 nm. When the Cu^{2+} ion was bound to receptor **1**, the binding constant was $2.34x10^{-5}$ M.

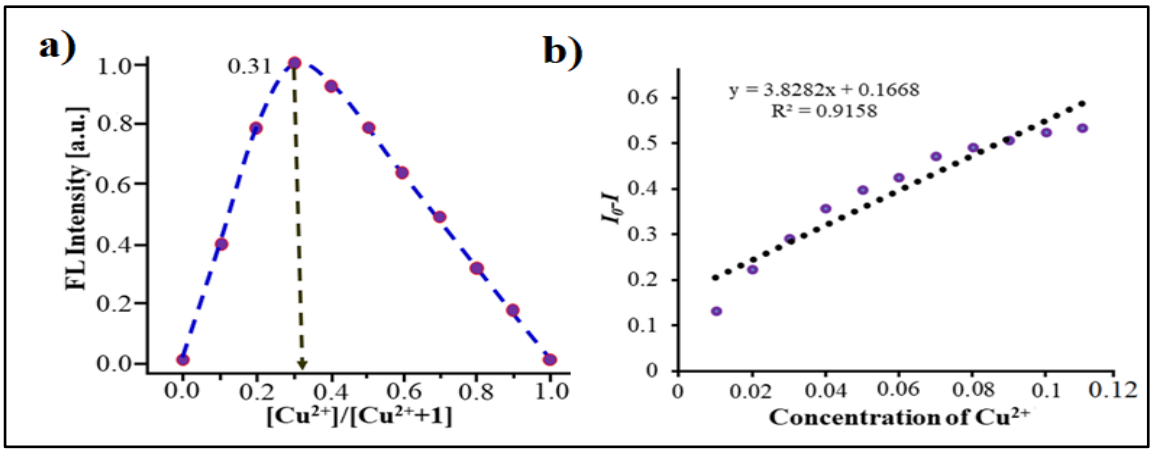

Figure 4.61: **a)** Job's plot for sensor **1**:Cu^{2+} in the ratio 2:1 complexation in acetonitrile. b) Benesi–Hildebrand plot of **1** with Cu^{2+} in acetonitrile.

4.12.9 Limit of detection

The limit of detection was estimated using the formula 3σ/slope, where slope is the slope from the linear plot and is the standard deviation of blank probe samples. The detection limit of probe **1** for Cu^{2+} was determined from the fluorescence titrations (**Fig. 4.62**), and it was discovered to be as low as 7.93 nM. This clearly illustrates that probe **1** has a significant deal of potential to detect copper ions selectively and precisely.

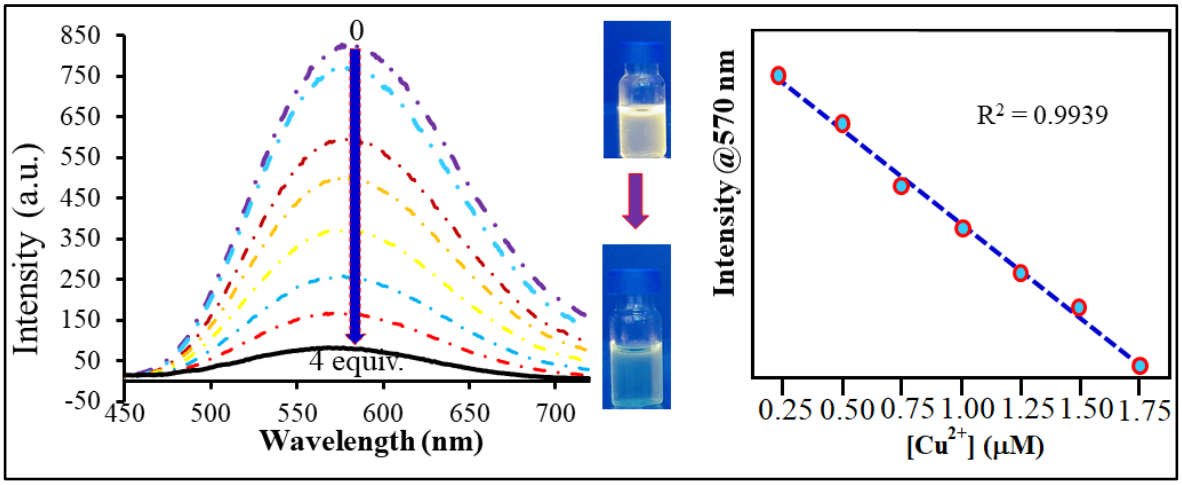

Figure 4.62: Emission spectra of **1** (2.0×10^{-4} M) in acetonitrile presence with the addition of Cu^{2+} (0-4 equiv.) and detection limit.

4.12.10 Competitive binding study

The results of the fluorescence studies, which were carried out to investigate the selectivity of the receptor **1** towards Cu^{2+} in the presence of competing cations, are shown in **Figure 4.63**. The competitive binding studies for receptor **1** were conducted using a variety of

cations, including Cu^{2+}, Zn^{2+}, Pb^{2+}, Ni^{2+}, Fe^{3+}, Cd^{2+}, Mg^{2+}, Mn^{2+}, Al^{3+}, Hg^{2+}, Co^{2+}, Ba^{2+}, Ag^{+} and K^{+} (10 equiv.). Similar to what the Cu^{2+} ion alone does, the interfering ions have an impact on the emission properties. With the addition of the Cu^{2+} ion in the presence of the investigated cations, it was observed that the fluorescence emission intensity of **1** was dramatically reduced. As a result, it is seen that the other metal ions have no effect on how Cu^{2+} binds to receptor **1**. In view of this, the results demonstrated that sensor **1** is a selective fluorescence sensor capable of detecting Cu^{2+} ions even when the majority of competing metal ions are present.

4.12.11 ^{1}H NMR spectra of 1 and 1 plus Cu^{2+}

The ^{1}H NMR spectra of **1** and **1+Cu^{2+}** in deuterated DMSO-d6 were collected. When ^{1}H NMR spectra of **1** and **1+Cu^{2+}** are compared, the peaks in **1** look well-defined but all of the peaks in **1+Cu^{2+}** are moved towards the up field (**Fig. 4.64**). This shows that copper ion binds to receptor **1**, and copper ion's paramagnetic properties affect the peaks.[56]

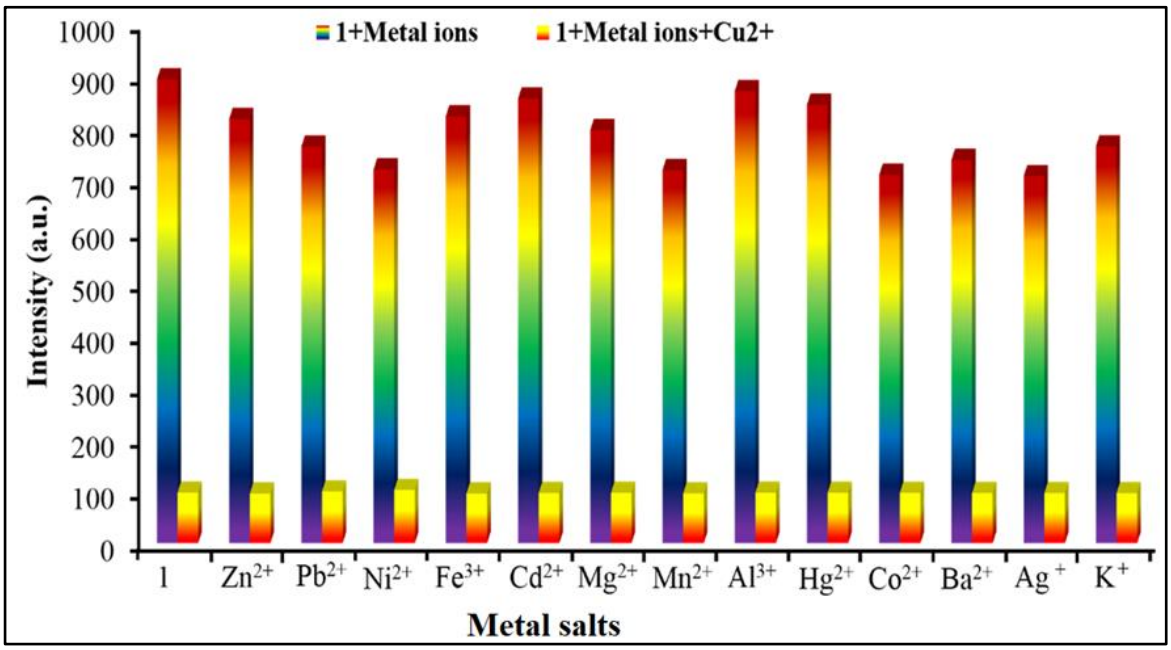

Figure 4.63: Pictogram fluorescence spectra of **1** ($2.0x10^{-4}$ M) exposed to 10 equiv. various metal ions and to the mixture of **1** and 10 equiv. Cu^{2+} with in ACN solution.

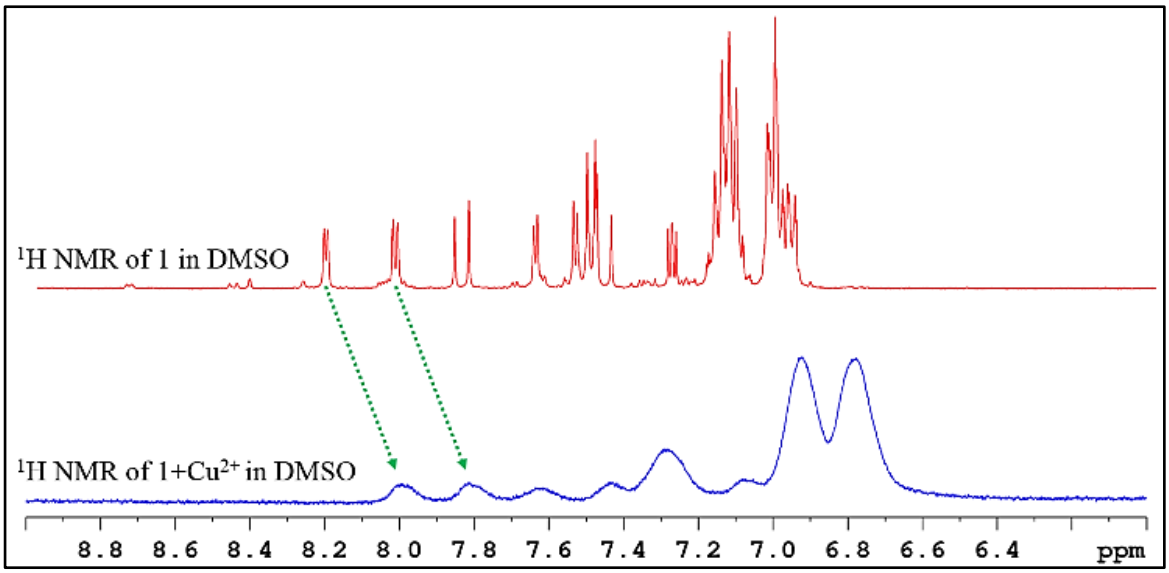

Figure 4.64: ^{1}H NMR spectral changes of **1** (a) in DMSO-d_6 and (b) upon addition of 1 equiv. Cu^{2+} ions.

4.12.12 Test strip for Cu^{2+} detection by sensor 1

The utilization of receptor 1's strip-based sensing for real world application as well. **Figure 4.65** shows the dark yellow fluorescence that was produced during the production of the paper strip in acetonitrile solution under UV illumination (365 nm). This fluorescence is suppressed when receptor **1** binds to copper ions. However, other metals have little impact on receptor **1** that may be seen in fluorescence.

Figure 4.65: Paper strip (prepared in acetonitrile solvent of **1**: 3.5 mM) as a shown in left strip, and detection of copper metal ions (strip is shown in right) upon dipping strip in copper solution (10 mM), picture is taken under UV light 365 nm.

4.12.13 Sensing mechanism

The compound **1** initially not showing PET in acetonitrile at λ_{ex}= 370 nm emitted fluorescence while the compound **1** were bind with Cu^{2+} ion shows the PET effect therefore fluorescence quenching observed as illustrated in **Figure 4.66.**

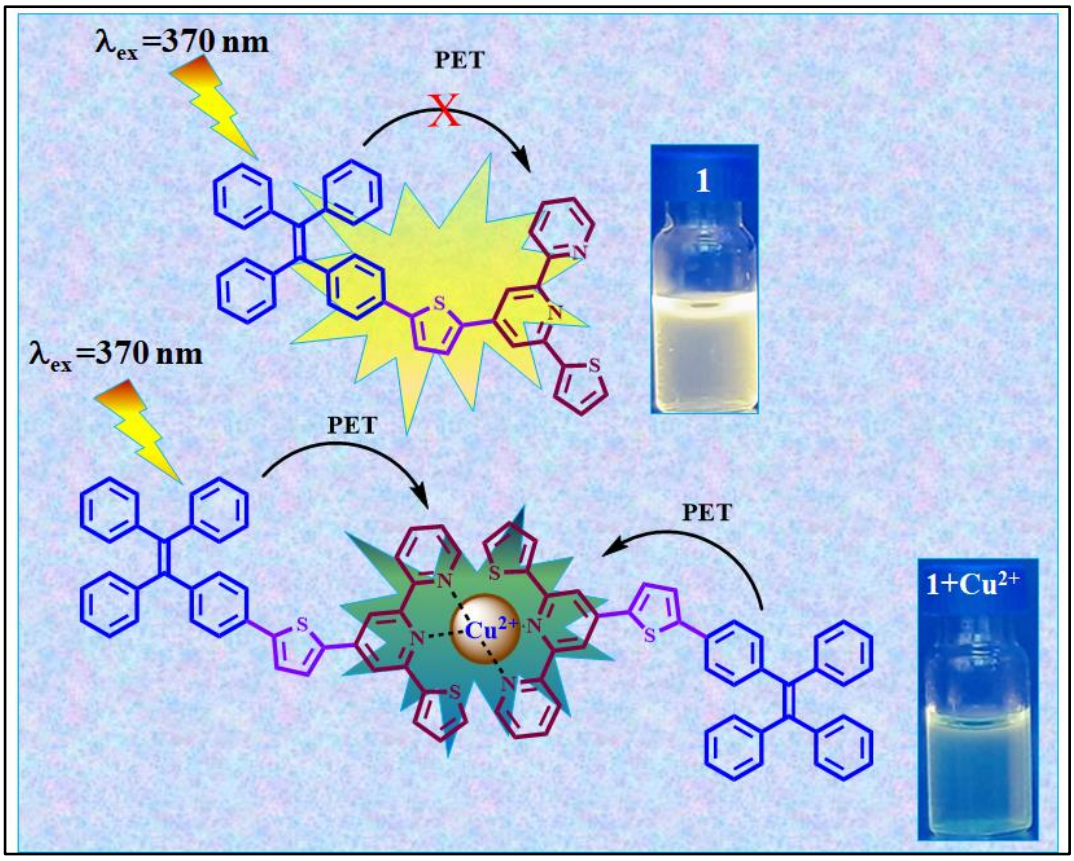

Figure 4.66: Sensing mechanism of **1** towards Cu^{2+} ion.

4.13 Conclusions

In conclusion, novel AIE-active receptor **1** was synthesized, and its mechanochromic characteristics were investigated. Receptor **1** displays different quantum yields in various solvents. However, receptor **1** is helpful in metal ion sensing owing to its AIE-active characteristics. Colorimetric, visual, and fluorescence detection of the Cu^{2+} metal ion are all demonstrated by receptor **1**. The limit of detection (LOD) for **1** with Cu^{2+} was found to be as low as 7.93 nM and the binding constant was 2.34×10^{-5} M.

UV-Vis absorption and fluorescence emission spectroscopy, as well as paper strip-based sensing, were used to study the extremely selective for the Cu^{2+} metal ions over other metal anions, such as Zn^{2+}, Pb^{2+}, Ni^{2+}, Fe^{3+}, Cd^{2+}, Mg^{2+}, Mn^{2+}, Al^{3+}, Hg^{2+}, Co^{2+}, Ba^{2+}, Ag^{+} and K^{+}. In addition, investigated the chromophore **1** as a paper strip sensor for Cu^{2+} in response to the binding constant in order to build kits for future use in the real world.

References

(1) Gupta, V. K.; Ali, I.; Aboul-Enein, H. Y. Chapter 3 Metal Ions Speciation in the Environment: Distribution, Toxicities and Analyses. *Dev. Environ. Sci.* **2007**, *5* (07), 33–56. https://doi.org/10.1016/S1474-8177(07)05003-6.

(2) Vella, F. Principles of Bioinorganic Chemistry. *Biochem. Educ.* **1995**, *23* (2), 115. https://doi.org/10.1016/0307-4412(95)90685-1.

(3) Stillman, M. Biological Inorganic Chemistry. Structure and Reactivity. Edited by Ivano Bertini, Harry B. Gray, Edward I. Stiefel and Joan S. Valentine. *Angew. Chemie Int. Ed.* **2007**, *46* (46), 8741–8742. https://doi.org/10.1002/anie.200785504.

(4) Kozlowski, H.; Janicka-Klos, A.; Brasun, J.; Gaggelli, E.; Valensin, D.; Valensin, G. Copper, Iron, and Zinc Ions Homeostasis and Their Role in Neurodegenerative Disorders (Metal Uptake, Transport, Distribution and Regulation). *Coord. Chem. Rev.* **2009**, *253* (21–22), 2665–2685. https://doi.org/10.1016/j.ccr.2009.05.011.

(5) Ashish, B.; Neeti, K.; Himanshu, K. Copper Toxicity: A Comprehensive Study. *Res. J. Recent Sci.* **2013**, *2* (ISC-2012), 58–67.

(6) Brown, T. Deisign Thinking. *Harv. Bus. Rev.* **2008**, *86* (6), 84–92. https://doi.org/10.1002/med.

(7) Kuhn, D. J.; Wang, Y.; Minic, V.; Coates, C.; Reddy, G. S. K.; Daniel, K. G.; Shim, J.; Chen, D.; Landis-piwowar, K. R.; Miller, F. R.; Turos, E.; Dou, Q. P. The Prevention Program, Barbara Ann Karmanos Cancer Institute, and Department of Pathology, School of Medicine, Wayne State University, Detroit, Michigan, USA, 2 Department of Chemistry, College of Arts and Sciences, University of South Florida, Tampa, Fl. **2004**, No. 1, 2605–2617.

(8) Takiyama, Y. .; Nishizawa, M. .; Tanaka, H. .; Kawashima, S. .; Sakamoto, H. .; Karube, Y. .; Shimazaki, H. .; Soutome, M. .; Endo, K. .; Ohta, S. © 199 3 Nature Publishing Group Http://Www.Nature.Com/Naturegenetics. *Nat. Genet.* **1993**, *3*, 73–96.

(9) O'Dell, B. L. Biochemistry of Copper. *Med. Clin. North Am.* **1976**, *60* (4), 687–703. https://doi.org/10.1016/S0025-7125(16)31853-3.

(10) Desai, V.; Kaler, S. G. Role of Copper in Human Neurological Disorders. *Am. J. Clin. Nutr.* **2008**, *88* (3), 855–858. https://doi.org/10.1093/ajcn/88.3.855s.

(11) Barnham, K. J.; Masters, C. L.; Bush, A. I. Neurodegenerative Diseases and Oxidatives Stress. *Nat. Rev. Drug Discov.* **2004**, *3* (3), 205–214.

https://doi.org/10.1038/nrd1330.

(12) Que, E. L.; Domaille, D. W.; Chang, C. J. Erratum: Metals in Neurobiology: Probing Their Chemistry and Biology with Molecular Imaging (Chemical Reviews (2008) Vol. 108 (1517)). *Chem. Rev.* **2008**, *108* (10), 4328. https://doi.org/10.1021/cr800447y.

(13) Kumar, M.; Puri, A. A Review of Permissible Limits of Drinking Water. *Indian J. Occup. Environ. Med.* **2012**, *16* (1), 40–44. https://doi.org/10.4103/0019-5278.99696.

(14) Herschy, R. W. Water Quality for Drinking: WHO Guidelines. *Encycl. Earth Sci. Ser.* **2012**, 876–883. https://doi.org/10.1007/978-1-4020-4410-6_184.

(15) Noroozifar, M.; Khorasani-Motlagh, M.; Hosseini, S. N. Flow Injection Analysis-Flame Atomic Absorption Spectrometry System for Indirect Determination of Cyanide Using Cadmium Carbonate as a New Solid-Phase Reactor. *Anal. Chim. Acta* **2005**, *528* (2), 269–273. https://doi.org/10.1016/j.aca.2004.10.056.

(16) Ensafi, A. A.; Khayamian, T.; Benvidi, A.; Mirmomtaz, E. Simultaneous Determination of Copper, Lead and Cadmium by Cathodic Adsorptive Stripping Voltammetry Using Artificial Neural Network. *Anal. Chim. Acta* **2006**, *561* (1–2), 225–232. https://doi.org/10.1016/j.aca.2006.01.015.

(17) Skrzydlewska, E.; Balcerzak, M.; Vanhaecke, F. Determination of Chromium, Cadmium and Lead in Food-Packaging Materials by Axial Inductively Coupled Plasma Time-of-Flight Mass Spectrometry. *Anal. Chim. Acta* **2003**, *479* (2), 191–202. https://doi.org/10.1016/S0003-2670(02)01527-1.

(18) Schlücker, S. Surface-Enhanced Raman Spectroscopy: Concepts and Chemical Applications. *Angew. Chemie - Int. Ed.* **2014**, *53* (19), 4756–4795. https://doi.org/10.1002/anie.201205748.

(19) Klejdus, B.; Zehnálek, J.; Adam, V.; Petřek, J.; Kizek, R.; Vacek, J.; Trnková, L.; Rozik, R.; Havel, L.; Kubáň, V. Sub-Picomole High-Performance Liquid Chromatographic/Mass Spectrometric Determination of Glutathione in the Maize (Zea Mays L.) Kernels Exposed to Cadmium. *Anal. Chim. Acta* **2004**, *520* (1–2), 117–124. https://doi.org/10.1016/j.aca.2004.02.060.

(20) Anferov, V. P.; Mozjoukhine, G. V.; Fisher, R. Pulsed Spectrometer for Nuclear Quadrupole Resonance for Remote Detection of Nitrogen in Explosives. *Rev. Sci. Instrum.* **2000**, *71* (4), 1656–1659. https://doi.org/10.1063/1.1150514.

(21) Luggar, R. D.; Farquharson, M. J.; Horrocks, J. A.; Lacey, R. J. Multivariate Analysis

of Statistically Poor EDXRD Spectra for the Detection of Concealed Explosives. *X-Ray Spectrom.* **1998**, *27* (2), 87–94. https://doi.org/10.1002/(SICI)1097-4539(199803/04)27:2<87::AID-XRS256>3.0.CO;2-0.

(22) Cotruvo, J. A.; Aron, A. T.; Ramos-Torres, K. M.; Chang, C. J. Synthetic Fluorescent Probes for Studying Copper in Biological Systems. *Chem. Soc. Rev.* **2015**, *44* (13), 4400–4414. https://doi.org/10.1039/c4cs00346b.

(23) Sarkar, S.; Roy, S.; Sikdar, A.; Saha, R. N.; Panja, S. S. A Pyrene-Based Simple but Highly Selective Fluorescence Sensor for Cu 2+ Ions via a Static Excimer Mechanism. *Analyst* **2013**, *138* (23), 7119–7126. https://doi.org/10.1039/c3an00928a.

(24) Shellaiah, M.; Wu, Y. H.; Singh, A.; Ramakrishnam Raju, M. V.; Lin, H. C. Novel Pyrene- and Anthracene-Based Schiff Base Derivatives as Cu 2+ and Fe3+ Fluorescence Turn-on Sensors and for Aggregation Induced Emissions. *J. Mater. Chem. A* **2013**, *1* (4), 1310–1318. https://doi.org/10.1039/c2ta00574c.

(25) Wang, W.; Wen, Q.; Zhang, Y.; Fei, X.; Li, Y.; Yang, Q.; Xu, X. Simple Naphthalimide-Based Fluorescent Sensor for Highly Sensitive and Selective Detection of Cd2+ and Cu2+ in Aqueous Solution and Living Cells. *Dalt. Trans.* **2013**, *42* (5), 1827–1833. https://doi.org/10.1039/c2dt32279j.

(26) Guo, D.; Dong, Z.; Luo, C.; Zan, W.; Yan, S.; Yao, X. A Rhodamine B-Based "Turn-on" Fluorescent Sensor for Detecting Cu2+ and Sulfur Anions in Aqueous Media. *RSC Adv.* **2014**, *4* (11), 5718–5725. https://doi.org/10.1039/c3ra45931d.

(27) Wu, L.; Zhang, X. F.; Li, Z. Q.; Wu, F. A New Sensor Based on Amino-Functionalized Zirconium Metal-Organic Framework for Detection of Cu2 + in Aqueous Solution. *Inorg. Chem. Commun.* **2016**, *74*, 22–25. https://doi.org/10.1016/j.inoche.2016.10.031.

(28) Kaur, P.; Kaur, S.; Singh, K. Bis(N-Methylindolyl)Methane-Based Chemical Probes for Hg 2+ and Cu 2+ and Molecular IMPLICATION Gate Operating in Fluorescence Mode. *Org. Biomol. Chem.* **2012**, *10* (8), 1497–1501. https://doi.org/10.1039/c2ob06793e.

(29) Shellaiah, M.; Rajan, Y. C.; Lin, H. C. Synthesis of Novel Triarylamine-Based Dendrimers with N 4,N 6-Dibutyl-1,3,5-Triazine-4,6-Diamine Probe for Electron/Energy Transfers in H-Bonded Donor-Acceptor-Donor Triads and as Efficient Cu 2+ Sensors. *J. Mater. Chem.* **2012**, *22* (18), 8976–8987. https://doi.org/10.1039/c2jm00112h.

(30) Padhan, S. K.; Murmu, N.; Mahapatra, S.; Dalai, M. K.; Sahu, S. N. Ultrasensitive Detection of Aqueous Cu2+ Ions by a Coumarin-Salicylidene Based AIEgen. *Mater. Chem. Front.* **2019**, *3* (11), 2437–2447. https://doi.org/10.1039/c9qm00394k.

(31) Jung, H. S.; Kwon, P. S.; Lee, J. W.; Kim, J. I. I.; Hong, C. S.; Kim, J. W.; Yan, S.; Lee, J. Y.; Lee, J. H.; Joo, T.; Kim, J. S. Coumarin-Derived Cu2+-Selective Fluorescence Sensor: Synthesis, Mechanisms, and Applications in Living Cells. *J. Am. Chem. Soc.* **2009**, *131* (5), 2008–2012. https://doi.org/10.1021/ja808611d.

(32) Sirilaksanapong, S.; Sukwattanasinitt, M.; Rashatasakhon, P. 1,3,5-Triphenylbenzene Fluorophore as a Selective Cu2+ Sensor in Aqueous Media. *Chem. Commun.* **2012**, *48* (2), 293–295. https://doi.org/10.1039/c1cc16148b.

(33) Tavallali, H.; Deilamy-Rad, G.; Moaddeli, A.; Asghari, K. A New Pincer-Type "Naked-Eye" Colorimetric Probe for Cu2+ Determination in 80% Water Media and Its Application as a Solid State Sensor and an Efficient Antibacterial Product. *Sensors Actuators, B Chem.* **2017**, *244*, 1121–1128. https://doi.org/10.1016/j.snb.2016.11.114.

(34) La, D. D.; Bhosale, S. V.; Jones, L. A.; Bhosale, S. V. Tetraphenylethylene-Based AIE-Active Probes for Sensing Applications. *ACS Appl. Mater. Interfaces* **2018**, *10* (15), 12189–12216. https://doi.org/10.1021/acsami.7b12320.

(35) Gao, M.; Tang, B. Z. Fluorescent Sensors Based on Aggregation-Induced Emission: Recent Advances and Perspectives. *ACS Sensors* **2017**, *2* (10), 1382–1399. https://doi.org/10.1021/acssensors.7b00551.

(36) Hiremath, S. D.; Gawas, R. U.; Mascarenhas, S. C.; Ganguly, A.; Banerjee, M.; Chatterjee, A. A Water-Soluble AIE-Gen for Organic-Solvent-Free Detection and Wash-Free Imaging of Al3+ Ions and Subsequent Sensing of F− Ions and DNA Tracking. *New J. Chem.* **2019**, *43* (13), 5219–5227. https://doi.org/10.1039/c9nj00418a.

(37) Wang, D.; Tang, B. Z. Aggregation-Induced Emission Luminogens for Activity-Based Sensing. *Acc. Chem. Res.* **2019**, *52* (9), 2559–2570. https://doi.org/10.1021/acs.accounts.9b00305.

(38) Li, Y.; Zhong, H.; Huang, Y.; Zhao, R. Recent Advances in AIEgens for Metal Ion Biosensing and Bioimaging. *Molecules* **2019**, *24* (24), 1–18. https://doi.org/10.3390/molecules24244593.

(39) Marandi, P.; Kumar, P. P. P.; Venugopalan, P.; Neelakandan, P. P. Selective Metal-Ion Detection and Activatable Photosensitization Properties of a

Tetraphenylethylene-Based Salicylideneimine. *ChemistrySelect* **2019**, *4* (19), 5707–5713. https://doi.org/10.1002/slct.201901035.

(40) Li, Y.; Yu, H.; Shao, G.; Gan, F. A Tetraphenylethylene-Based "Turn on" Fluorescent Sensor for the Rapid Detection of Ag+ Ions with High Selectivity. *J. Photochem. Photobiol. A Chem.* **2015**, *301* (3), 14–19. https://doi.org/10.1016/j.jphotochem.2014.12.013.

(41) Bian, N.; Chen, Q.; Qiu, X. L.; Qi, A. Di; Han, B. H. Imidazole-Bearing Tetraphenylethylene: Fluorescent Probe for Metal Ions Based on AIE Feature. *New J. Chem.* **2011**, *35* (8), 1667–1671. https://doi.org/10.1039/c1nj20122k.

(42) Luo, J.; Xie, Z.; Xie, Z.; Lam, J. W. Y.; Cheng, L.; Chen, H.; Qiu, C.; Kwok, H. S.; Zhan, X.; Liu, Y.; Zhu, D.; Tang, B. Z. Aggregation-Induced Emission of 1-Methyl-1,2,3,4,5-Pentaphenylsilole. *Chem. Commun.* **2001**, *18*, 1740–1741. https://doi.org/10.1039/b105159h.

(43) Mei, J.; Leung, N. L. C.; Kwok, R. T. K.; Lam, J. W. Y.; Tang, B. Z. Aggregation-Induced Emission: Together We Shine, United We Soar! *Chem. Rev.* **2015**, *115* (21), 11718–11940. https://doi.org/10.1021/acs.chemrev.5b00263.

(44) Li, D.; Li, J.; Duan, Y.; Zhao, B.; Ji, B. A Highly Efficient Aggregation-Induced Emission Fluorescent Sensor for Copper(II) in Aqueous Media. *Anal. Methods* **2016**, *8* (31), 6013–6016. https://doi.org/10.1039/c6ay01300g.

(45) Assiri, M. A.; Al-Sehemi, A. G.; Pannipara, M. AIE Based "on-off" Fluorescence Probe for the Detection of Cu2+ Ions in Aqueous Media. *Inorg. Chem. Commun.* **2019**, *99*, 11–15. https://doi.org/10.1016/j.inoche.2018.11.001.

(46) Geng, L. Y.; Zhao, Y.; Kamya, E.; Guo, J. T.; Sun, B.; Feng, Y. K.; Zhu, M. F.; Ren, X. K. Turn-off/on Fluorescent Sensors for Cu 2+ and ATP in Aqueous Solution Based on a Tetraphenylethylene Derivative. *J. Mater. Chem. C* **2019**, *7* (9), 2640–2645. https://doi.org/10.1039/c8tc06075d.

(47) Sil, A.; Maity, A.; Giri, D.; Patra, S. K. A Phenylene-Vinylene Terpyridine Conjugate Fluorescent Probe for Distinguishing Cd2+ from Zn2+ with High Sensitivity and Selectivity. *Sensors Actuators, B Chem.* **2016**, *226*, 403–411. https://doi.org/10.1016/j.snb.2015.11.106.

(48) Purohit, A. K.; Padhan, S. K.; Mohanty, J. R.; Kar, P. K. Chromo-Luminescent Selective Detection of Fluoride Ions by a Copper(Ii) Bis(Terpyridine) Complex Solution: Via a Displacement Approach. *Photochem. Photobiol. Sci.* **2018**, *17* (6), 815–821. https://doi.org/10.1039/c8pp00108a.

(49) Abdalrahman, M. A.; Abebe, F.; Briggs, J.; Kassel, W. S.; Burdette, S. C.; Seitz, W. R.; Planalp, R. P. A Bifunctional 2,2′:6′,2″-Terpyridine-Based Ligand for Ratiometric Cu(II) Sensing. *J. Coord. Chem.* **2017**, *70* (7), 1123–1136. https://doi.org/10.1080/00958972.2017.1300660.

(50) Johnson, A. D.; Curtis, R. M.; Wallace, K. J. Low Molecular Weight Fluorescent Probes (LMFPs) to Detect the Group 12 Metal Triad. *Chemosensors* **2019**, *7* (2). https://doi.org/10.3390/chemosensors7020022.

(51) Hofmeier, H.; Schubert, U. S. Recent Developments in the Supramolecular Chemistry of Terpyridine-Metal Complexes. *Chem. Soc. Rev.* **2004**, *33* (6), 373–399. https://doi.org/10.1039/b400653b.

(52) Nurkkala, L. J.; Steen, R. O.; Friberg, H. K. J.; Häggström, J. A.; Bernhardt, P. V.; Riley, M. J.; Dunne, S. J. The Effects of Pendant vs. Fused Thiophene Attachment upon the Luminescence Lifetimes and Electrochemistry of Tris(2,2′-Bipyridine)Ruthenium(II) Complexes. *Eur. J. Inorg. Chem.* **2008**, No. 26, 4101–4110. https://doi.org/10.1002/ejic.200800456.

(53) Nandre, K. P.; Puyad, A. L.; Bhosale, S. V.; Bhosale, S. V. A Novel Donor-Acceptor Receptor for Selective Detection of Pb 2+and Fe3+ Ions. *Talanta* **2014**, *130*, 103–107. https://doi.org/10.1016/j.talanta.2014.06.064.

(54) Rananaware, A.; Bhosale, R. S.; Ohkubo, K.; Patil, H.; Jones, L. A.; Jackson, S. L.; Fukuzumi, S.; Bhosale, S. V.; Bhosale, S. V. Tetraphenylethene-Based Star Shaped Porphyrins: Synthesis, Self-Assembly, and Optical and Photophysical Study. *J. Org. Chem.* **2015**, *80* (8), 3832–3840. https://doi.org/10.1021/jo502760e.

(55) Li, Z.; Xu, Y.; Xu, H.; Cui, M.; Liu, T.; Ren, X.; Sun, J.; Deng, D.; Gu, Y.; Wang, P. A Dicyanomethylene-4H-Pyran-Based Fluorescence Probe with High Selectivity and Sensitivity for Detecting Copper (II) and Its Bioimaging in Living Cells and Tissue. *Spectrochim. Acta - Part A Mol. Biomol. Spectrosc.* **2021**, *244*, 118819. https://doi.org/10.1016/j.saa.2020.118819.

(56) Li, H.; Zhang, R.; Li, C.; Huang, B.; Yu, T.; Huang, X.; Zhang, X.; Li, F.; Zhou, H.; Tian, Y. Real-Time Detection and Imaging of Copper(Ii) in Cellular Mitochondria. *Org. Biomol. Chem.* **2017**, *15* (3), 598–604. https://doi.org/10.1039/c6ob02384c.

Chapter V

Conclusion

In this chapter, we conclude all thesis work, by studying scope of self-assembly and chemosensor of TPE and NDI derivatives. We choose this topic and focus on novel organic photoluminescence materials based on TPE and NDI. For better understanding, we were carry out a detailed literature survey on tuning achiral molecule to chiral superstructures and chemosensor.

In first chapter divided into two sections, in that one literature survey on chiral assembly and another on chemosensor. In first section, we discussed general strategies for supramolecular chiral molecules, including the synthesis and self-assembly of an achiral molecule to controlled chiral supramolecular superstructure with their photo luminescent properties. These strategies may also be used for sensitive, selective, and quick analyte detection. Different small compounds for achiral to chiral conversion, chirality induction, and controlled chiral helical structures were all addressed. In second section, we discussed the use of photo luminescent molecules, such as TPE, NDI, Porphyrin, Schiff's bases, conjugate polymers, different COFs, and MOFs, has recently caught the eye of the majority of researchers for a wide range of applications, including chemosensors, host-guest, and biological probes. Additionally, attention was given to recently developed photo luminous molecules for cations, anions, and neutral guests' chemosensors. Moreover, a general process underlying chemosensing was addressed. The most typical chemosensor consists of three components: a binding site, a spacer, and a signalling unit. When the substance binds at the binding site, the signaling unit responds. Excited State Intramolecular Proton Transfer (ESIPT), Photo induced Electron Transfer (PET), Fluorescence Resonance Energy Transfer (FRET), Intramolecular Charge Transfer (ICT), Chelation Enhanced Fluorescence (CHEF), and other mechanisms contributed to the majority of the detection mechanism. These all mechanisms with one example were discussed in this section.

In Second chapter, we have successfully designed, synthesized achiral **TPE-BTA** molecule for chiral assembly. The synthesized all compounds were characterized by various spectroscopic techniques like IR, NMR and Mass spectroscopy. **TPE-BTA** having amide functional group with C3 symmetry. Furthermore, a molecule that exhibited comparable fluorescence features in various states led to a mechanochromic analysis of **TPE-BTA**. According to the findings of an absorption and emission, study in various solvents, aggregation and self-assembly were seen in THF/Water and $CHCl_3$/MCH. In SEM, flower-like and helical structures were seen in $CHCl_3$ and $CHCl_3$/MCH. From CD spectra, it expose

the formation of chiral assembly of **TPE-BTA** in used solvent system. Based on this, it is clearly suggesting that solvent induced chiral assembly is formed by using achiral molecule. In third chapter, we have designed, synthesized, and characterized NDI-R/S-BINOL molecules. And synthesized novel and known molecules were confirmed by IR, NMR, and Mass spectroscopy. Further, we examined absorption and emission spectra of both isomers NDI-R-BINOL and NDI-S-BINOL, and showed comparable absorption spectra. Afterword, we performed absorption and emission analysis **NDI-R/S-BINOL** in various solvents such as tetrahydrofuran, toluene, methyl cyclohexane, methanol, acetonitrile, tetrachloroethane, and the results possess that charge transfer band. Moreover, we performed the self-assembly study of NDI-R/S-BINOL in tetrachloroethane (TCE) and methyl cyclohexane (MCH) solvents by using UV-Vis. and fluorescence study. **NDI-R-BINOL** and **NDI-S-BINOL** exhibited positive and negative cotton effects, respectively in TCE: MCH solvent system. From DLS data resulted aggregation occurred in 01% TCE in MCH. Finally, concluded that chiral BINOL molecules were induced and controlled chirality in planar, achiral NDI molecule in TCE and MCH solvent system.

In forth chapter, we mainly focused on sensing study by using TPE derivatives. This chapter divided into three sections. In section first, we designed, synthesized TPE-based azobenzene **1** photoswitchable molecule, and characterized by IR, NMR, and Mass spectroscopic techniques. Further, we described TPE-based azobenzene possess structural conversion of the structure upon E→Z Photoisomerization. In addition, compound shown complementary cavity (host) for the housing of the C60 guest molecule. We employed various spectroscopic techniques examined a host-guest interaction with both the *E* and the *Z* isomers of TPE-based azobenzene and the C60 molecule. Whereas, we found that the ***Z*-1.C60** association was prominent as compared to the isomer ***E*-1.C60.** However, we also explored Job's plot for stoichiometry of host-guest was observed 1:1. Further, we studied release of C60 from ***Z*-1.C60** association by the irradiation with visible light that converts the ***Z*-1** form to the ***E*-1** form. Therefore, this one of the best example which demonstrated of the stimuli-responsive host system that may be utilized for light-induced association and dissociation of a C60 molecule. In section second, we have designed and synthesized tetraphenylethylene cyclic-urea-based receptor. Characterized by various spectroscopic techniques. Receptor was exhibited to be highly selective and sensitive for fluoride anion. We confirmed detection of fluoride ion by UV-Vis. and emission spectroscopy, over other anions, such as CN^-, AcO^-, NO_3^-, $H_2PO_4^-$, OH^-, ClO_4^-, SCN^-, HSO_4^-, I^- and Cl^-. We also employed ^1H NMR analysis to find the binding site of analyte, from this it reveals that the disappearance of the N_2H

proton resonances in the cyclic urea was attributed to the formation of a (HF_2^-) hydrogen bonding complex of fluoride ion with urea. We calculate the the stoichiometry of the receptor was by using Job's plot and it showed 1:2. And a using for limit of detection (LOD) was calculated 30μM. We also studied reversible anion sensing by adding of methanol. Finally, we developed test-strips for fluoride anion sensing on the real world application. In last section, where we have designed, synthesized, and characterized new AIE-active receptor for copper (II) ion. Initially we studied mechanochromic properties of receptor. Receptor exposed various quantum yields in different solvents. Receptor displays colorimetric, naked eyes, and fluorescent sensing of Cu^{2+} metal ions. Further we calculate association constant of with Cu^{2+} was shown be $2.34x10^{-5}$ M. and also we investigated stoichiometry of receptor by using Job's plot, receptor shown with Cu^{2+} 2:1 and limit of detection (LOD) found as low as 7.93 nM by using 3δ/S formula. To find selectivity of receptor we used other metal anions, such as Zn^{2+}, Pb^{2+}, Mg^{2+}, Mn^{2+}, Al^{3+}, Hg^{2+}, Co^{2+}, Ba^{2+}, Ni^{2+}, Fe^{3+}, Cd^{2+}, $Ag^{+,}$ and K^+. we employed UV-Vis absorption and fluorescence emission spectroscopy for sensing confirmation. And finally we also developed strip-based sensing for copper (II) ion.

Finally, we conclude from this thesis work, the design and synthesis of novel organic photo-luminescent materials based on TPE and NDI systems exhibits a promising potential for its applications in self-assembly and chemosensor. We believe that this type of photo-luminescent material will beneficial to scientific world for enhanced applications.

List of publications:

Appended to thesis:

1. M. Samanta, A. Rananaware, **D. N. Nadimetla**, S. A. Rahaman, M. Saha, R. W. Jadhav, S. V. Bhosale and S. Bandyopadhyay, Light triggered encapsulation and release of C60 with a photoswitchable TPE-based supramolecular tweezers, *Sci. Rep.*, 2019, **9**, 1-7.
2. **D. N. Nadimetla**, G. A. Zalmi and S. V. Bhosale, An AIE-Active Tetraphenylethylene-Based Cyclic Urea as a Selective and Efficient Optical and Colorimetric Chemosensor for Fluoride Ions, *ChemistrySelect*, 2020, **5**, 8566-8571.
3. **D. N. Nadimetla**, M. Al Kobaisi, S. T. Bugde and S. V. Bhosale, Tuning Achiral to Chiral Supramolecular Helical Superstructures, *Chem. Rec.*, 2020, **20**, 793-819. **This work also been highlighted for the Journal's front cover.**
4. **D. N. Nadimetla** and S. V. Bhosale, Tetraphenylethylene AIEgen bearing thiophenylbipyridine receptor for selective detection of copper(ii) ion, *New J. Chem.*, 2021, **45**, 7614-7621.

Other contribution publications:

1. S. V. Gaikwad, **D. N. Nadimetla**, M. Al Kobaisi, M. Devkate, R. Joshi, R. G. Shinde, M. V. Gaikwad, M. D. Nikalje, S. V. Bhosale and P. D. Lokhande, Iodine-DMSO-Catalyzed Chemoselective Biomimetic Aromatization of Tetrahydro-β-carbolines-3-carboxylic Acid: Mechanism Study with DFT-Calculation, *ChemistrySelect*, 2019, **4**, 10054–10059.
2. A. D. Jangale, R. W. Jadhav, **D. N. Nadimetla**, M. D. Burud, V. G. More and S. V. Bhosale, Meet the Board of ChemistryOpen: Sheshanath V. Bhosale, *ChemistryOpen*, 2019, **8**, 403–405.
3. S. M. Wagalgave, A. C. Mendhe, **D. N. Nadimetla**, M. Al Kobaisi, B. R. Sankapal, S. V. Bhosale and S. V. Bhosale, Aggregation induced emission (AIE) materials based on diketopyrrolopyrrole chromophore for CdS nanowire solar cell applications, *J. Electroanal. Chem.*, 2021, **895**, 115451.
4. D. B. Shaikh, M. D. Aljabri, **D. N. Nadimetla**, S. S. Birajdar, M. Al Kobaisi, R. S. Bhosale, F. Antolasic, S. V. Bhosale and S. V. Bhosale, pH-Controlled Supramolecular Self-Assembly of Naphthalenediimide Appended l-Alanine and Ethylenediamine Asymmetric Bolaamphiphile, *Helv. Chim. Acta*, 2021, **104**, e2100011

5. S. P. Goskulwad, **D. N. Nadimetla**, D. B. Shaikh, D. D. La, M. Al Kobaisi, R. S. Bhosale, S. V. Bhosale and S. V. Bhosale, Supramolecular self-assembly of naphthalene diimide bolaamphiphile with biologically important amines: Cyclam, spermine and melamine, *J. Mol. Struct.*, 2020, **1206**, 127743.

6. G. A. Zalmi, **D. N. Nadimetla**, P. Kotharkar, A. L. Puyad, M. Kowshik and S. V. Bhosale, Aggregation-Induced Emission-Based Material for Selective and Sensitive Recognition of Cyanide Anions in Solution and Biological Assays, *ACS Omega*, 2021, **6**, 16704–16713.

7. S. P. Pandey, P. Jha, **D. N. Nadimetla**, S. V. Bhosale and P. K. Singh, A tetracationic aggregation induced emission-based probe for efficient and improved detection of Heparin, *Sensors Actuators B Chem.*, 2022, **353**, 131016.

8. D. I. Bhusanur, **D. N. Nadimetla**, S. S. Harmalkar, R. S. Bhosale, A. L. Puyad, S. M. Wagalgave, S. V. Bhosale and S. V. Bhosale, Synthesis, crystal structure and supramolecular self-assembly of tetraphenylethylene subunit appended isoindigo derivatives, *J. Mol. Struct.*, 2022, **1255**, 132452.

9. P. Gupta, D. Ojha, **D. N. Nadimetla**, S. V. Bhosale and A. B. RODE, Tetraphenylethene Derivatives Modulate the RNA Hairpin-G-quadruplex Conformational Equilibria in Proto-Oncogenes, *ChemBioChem*, 2022, **69**, 1377–1409.

10. J. Kaur, **D. N. Nadimetla**, S. V Bhosale and P. K. Singh, Polyanionic Cyclodextrin-Induced Supramolecular Assembly of a Cationic Tetraphenylethylene Derivative with Aggregation-Induced Emission, *J. Phys. Chem. B*, 2022, **126**, 1147–1155.

11. V. G. More, **D. N. Nadimetla**, G. A. Zalmi, V. K. Gawade, R. W. Jadhav, Y. D. Mane and S. V. Bhosale, A New 'Off–On' System Based on Core-Substituted Naphthalene Diimide with Dimethylamine for Reversible Acid–Base Sensing, *ChemistryOpen*, 2022, **11**, 12–15.

12. V. G. More, **D. N. Nadimetla**, D. B. Shaikh, A. L. Puyad, S. V Bhosale and S. V Bhosale, Naphthalenediimide-Benzothiazole-Based Chemodosimeter for Selective and Sensitive Chromogenic for Cyanide Ion, *ChemistrySelect*, 2022, **7**, e202201537.

13. G. A. Zalmi, V. K. Gawade, **D. N. Nadimetla** and S. V. Bhosale, Aggregation Induced Emissive Luminogens for Sensing of Toxic Elements, *ChemistryOpen*, 2021, **10**, 681–696.

14. R. W. Jadhav, **D. N. Nadimetla**, V. K. Gawade and L. A. Jones, Mimicking the Natural World with Nanoarchitectonics for Self-Assembled Superstructures. *Chem. Rec.* 2022, e202200180.

15. G. A. Zalmi, **D. N. Nadimetla**, S. S. Harmalkar, K. U. Narvekar and S. V Bhosale, A Receptor Based on Diphenylaniline Donor Connected with Difuran and Pyridine as Acceptors : Synthesis , Crystal Structure and Selective Detection of Iron Ion, *ChemistrySelect* 2022, **7**, e202202276

Manuscript under preparation:

1. **D. N. Nadimetla and S. V. Bhosale ***, Solvent induced self-assembly of a TPE-derivatives

2. **D. N. Nadimetla and S. V. Bhosale ***, Induce and controlled chirality of naphthalene diimide derivative by using R/S-BINOL

Participation and presentation at National & International conferences/webinar/seminar/workshop:

1. **D. N. Nadimetla and S. V. Bhosale*** "Controlled supramolecular helical assembly from achiral molecule triggered by solvent" the international symposium on "***Exploring New Horizons in Chemical Sciences***" (ENHCS-2019) organized by the Department of Chemistry, Deogiri College, Aurangabad, on 10th -12th January 2019.
2. **D. N. Nadimetla** participated in the One Day National Seminar on **"*Recent Advances in Chemical and Physical Sciences*"** organized on 31st January 2019, by the Dept. of Chemistry, Physics & Electronics Sangameshwar College, Solapur in association with Solapur University, Solapur.
3. **D. N. Nadimetla and S. V. Bhosale*** "Controlled supramolecular helical assembly from achiral molecule triggered by solvent" National Level Conference on "***Recent Advances in Material Science***" held on 5th February 2019 organized by the Department of Chemistry, Field marshal K. M. Cariappa College Madikeri. ***(First Prize** for best poster presentation)*
4. **D. N. Nadimetla** attended one day seminar on the theme "***Recent Trends in Structural Chemistry***" organized by department of chemistry, Goa University, Goa on 16th February 2019.
5. **D. N. Nadimetla and S. V. Bhosale*, "**Supramolecular chiral superstructures from AIE-active tetraphenylethene achiral molecule" National Conference on "***New Horizons in Green Chemistry and Toxicology***" organized on 2nd April, 2019 by Department of Chemistry at D.P. Bhosale College, Koregaon.
6. **D. N. Nadimetla and S. V. Bhosale*** "Controlled supramolecular helical assembly from achiral molecule triggered by solvent" Two- day workshop on "***Material Science***" between University of Coimbra, University of Porto and Goa University on 18th and 19th November 2019 at School of Chemical Sciences Goa University.
7. **D. N. Nadimetla** and Sheshanath V. Bhosale* "Light triggered encapsulation and release of C60 with a photoswitchable TPE-based supramolecular tweezers" National

Conference on ***"New Frontiers in Chemistry-from Fundamentals to Applications***" Organized by Department of Chemistry, BITs Goa, 20th -22nd, December 2019.

8. **D. N. Nadimetla** participated in the webinar on "***Use of Elsevier Tools for developing Research Workflow and Academic Writing***" organized by the Directorate of Higher Education, Goa in collaboration with ELSEVIER on 18th May 2020.
9. **D. N. Nadimetla** participated in the two day International Webinar on **"*Role of Nanotechnology in Health Management*"** organized by the Department of Chemistry, St. Ann's College For Women, Mehdipatnam, Hyderabad-28, India, on 10th-11th July 2020
10. **D. N. Nadimetla** participated in the 1st Virtual Internation Symposium on "***C-H activation*"** held on 27th-30th July, 2020, Georg-August-Universitat Gottingen, Germany.
11. **D. N. Nadimetla** participated in the John Wiley and Sons research webinar on **"*Managing Research Overload*"** held on 02nd February 2021, organised by wiley.
12. **D. N. Nadimetla** attended RSC Desktop Seminar Lectureship Series with "***Natural Products Reports*"** held on 15th March 2021, organised by RSC Publishing Webinars.
13. **D. N. Nadimetla** attended RSC Desktop Seminar Lectureship Series with "***Energy and Environmental Science" (Joseph Hupp and Yana Vaynzof)*** held on 31th March 2021, organised by RSC Publishing Webinars.
14. **D. N. Nadimetla** participated in the National Webinar on **"*Synthetic Chemists and Our Society and Concept Transfer From Nature*"** on 11th September 2021, organized by Department of Chemistry under the Aegis of ACS international student chapter, Dr. Ambedkar College, Deekshabhoomi, Nagpur.
15. **D. N. Nadimetla** participated in the TWO-DAY **Industry-Academia** international Symposium (Virtual) on *"**Fuels for Environmental Sustainability**"* held by Department of Chemistry, Government College of Arts, Science and Commerce, Khandola, Goa on 8th-9th October 2021.
16. **D. N. Nadimetla** participated in the webinar entitled '***Mending academic talent for industrial applications'*** held on 28th February, 2022 in celebration of National Science Day at School of Chemical Sciences, Goa University.
17. **D. N. Nadimetla** participated in One Day Virtual National Conference on "***Role of Women Chemists and Technologists for Sustainable Future***" held on 8th March 2022 on the occasion of International Women's Day, organized by The Department of Chemistry (Research Centre) in association with Rotary Club of Miramar, Panjim, Goa.

18. **D. N. Nadimetla** participated in the Two-day online "***International Conference on Advances in Sciences and Technology***" organized by Rajashri Chhatrapati Shahu College, Kohlapur during 9th -10th March 2022.
19. **D. N. Nadimetla** attended National Webinar on "***Emerging Trends in Heavy Metal Detection Sensors and C-H Functionalization*****"** organized by the Dept. of Chemistry, DCT's Dhempe College of Art's and Science, Miramar-Goa on 22nd April 2022.
20. **D. N. Nadimetla** participated in three days workshop "X-ray Crystallography" held on 21st - 23rd July 2022 organized by School of Chemical Sciences and School of Physical & Applied Sciences, Goa University, Goa.